Effect of Lightweight Aggregate on Early-Age Cracking of Mass Concrete

by

Aravind Tankasala

A dissertation submitted to the Graduate Faculty of
Auburn University
in partial fulfillment of the
requirements for the Degree of
Doctor of Philosophy

Auburn, Alabama
December 16, 2017

Keywords: Coefficient of thermal expansion, creep, cracking tendency, internal curing, restraint, shrinkage, temperature, thermal stress

Approved by

Anton K. Schindler, Chair, Professor and Director of the Highway Research Center
Robert W. Barnes, Associate Professor of Civil Engineering
Andrzej Nowak, Professor and Department Chair of Civil Engineering
Mary Hughes, Lecturer and Assistant Chair for Undergraduate Studies
Steven Taylor, Dean of Research for College of Engineering

Abstract

Early-age cracking in mass concrete structures is a severe problem which could lead to long-term serviceability related problems in the structure. In this dissertation, the effect of using lightweight aggregates (LWAs) on the early-age cracking tendency of mass concrete was evaluated.

Concretes were made with 30% Class F fly ash to be representative of mass concrete and the following concrete types were made at water-to-cementitious materials (*w/cm*) ratios of 0.45 and 0.38: 1) normalweight concrete, 2) internally cured concrete, 3) inverse sand-lightweight (ISLW) concrete, 4) sand-lightweight (SLW) concrete, and 5) all-lightweight (ALW) concrete. Rigid cracking frames were used to measure from the time of setting until the onset of cracking the development of concrete stresses caused by autogenous and thermal shrinkage effects. Rigid cracking frame specimens were tested under isothermal and match-cured temperature conditions. The match-cured temperature condition simulated the edge of an 8 × 8 ft mass concrete column.

In addition, three concrete cross-section sizes, (4×4, 8×8, and 12×12 ft) were modeled using ConcreteWorks for four different concrete mixtures to determine the maximum concrete temperatures, maximum concrete temperature differences, stresses, and cracking risk.

The results indicate that the maximum in-place concrete temperatures increase as more lightweight aggregates were used in each mixture; therefore, care should be taken

when using LWA concrete in mass concrete to make sure that the delayed Ettringite formation (DEF) temperature threshold is not exceeded. The use of LWAs in concrete with low *w/cm* is beneficial to control early-age cracking, because it helps to mitigate autogenous shrinkage and lower the modulus of elasticity of the higher strength concrete. The presence of LWAs in concrete delayed the time to cracking, with SLW concrete providing the best overall resistance to early-age cracking. Although an increasing amount of LWA in the concrete will increase the maximum concrete temperature in mass concrete applications, the increasing use of LWA will reduce the modulus of elasticity, reduce the coefficient of thermal expansion, and eliminate autogenous shrinkage effects, which all contribute to improve the resistance to early-age cracking.

The commonly used maximum temperature difference limit of 35°F in mass concrete applications is inappropriate for concretes containing lightweight aggregates. A simplified version for computing the maximum concrete temperature difference limit for all concretes is proposed.

Acknowledgments

I like to sincerely thank Dr. Anton Schindler for his technical guidance, time, and support throughout my stay at Auburn, without whom the research performed in this dissertation would not have been possible. I am grateful to Dr. Schindler for having faith and trust in my abilities even during difficult times, during the course of research. Working under his supervision, has been a fulfilling experience, serving as a stepping stone to my future. I would also like to thank Dr. Robert Barnes, for playing a major role in my academic development as well as helping me out with questions related to research. Special Thanks to Dr. Andy Nowak, for taking time out of his busy schedule and reviewing this dissertation. Particular Thanks to Dr. Mary Hughes for providing assistance, friendship, and council throughout my stay at Auburn. I would also like to thank Dr. Steven Taylor for agreeing to serve on my dissertation committee. Billy Wilson deserves special thanks for assisting me with lab related work during the course of this project.

I would also like to thank members of the Expanded Shale, Clay, and Slate Research Institute for their financial support. I would like to specifically thank Dr. Reid Castrodale and Ken Harmon for their timely guidance and support during the initial stages of this dissertation study. Donations in support of the laboratory portion of this program from BASF Corporation Inc., Cemex and Shermann Industries is acknowledged.

I would like to thank Walt Waltoz for providing the fellowship for me to attend graduate school.

The research work performed in this dissertation was supported by a group of research assistants. Contributions from Yalin Liu, Eric Gross and Drew Eiland are acknowledged. It was a pleasure to work with student helpers and graduate students - Michael Harris, Drew Graves, Charlie Johnson, Yohance Stringfield, Jackson Adams, Rob Crosby and Christopher Kerner and their assistance is acknowledged.

I had a great time at Auburn and this was because of the special friendships I had during the course of study, which relieved a great deal of stress during the trying times of my PhD study. While it is not possible to acknowledge everyone, I would like to thank Yalin Liu, my research colleague who helped me with my research as well cooking great food during weekends. Eric Gross, for helping me with my lab experiments and helping me with field tests, those long drives to workplaces were fun. I would thank HongYang Wu, and Anjan Babu for their eagerness to help whenever possible. Particular Thanks to Dave Mante for providing counsel with selection of concrete materials, and support, inspiration during the final stages of my PhD.

The encouragement and kindness provided by my uncle, aunt and cousins during my stay in the United States are gratefully acknowledged. Being away from immediate family, they provided me a home to go for thanksgiving visits and were there for me when I needed them.

I would like to express my most sincere appreciation and gratitude to Han Chen, who supported me emotionally and tolerated my eccentric behavior during the final stages of my research.

I would like to thank my family for their encouragement and support throughout my stay in the United States. The countless phone calls, video chats and emails, especially in trying times kept me encouraged, refreshed and motivated me to complete my research. I am grateful to my maternal uncles for instilling the sense of hard work and persistence in whatever work I do. I am thankful to my younger brother for encouraging me throughout my studies. I am thankful to my dad for his logical advice and to my mom for her unending love. Without the love and continual support of my family, the pursuit of my PhD would not have been possible. It is to them I owe this accomplishment.

This dissertation is dedicated to Amma, Appa and Chini. All of this is made possible because of you. Thank you, for everything!.

TABLE OF CONTENTS

LIST OF TABLES

LIST OF FIGURES

Chapter 1

1.1 BACKGROUND

Cracking in concrete occurs when the concrete stresses exceeds the tensile strength of the concrete. Concrete stress development is dependent on many factors such as coefficient of thermal expansion, temperature history, and creep-adjusted modulus of elasticity of the hardening concrete (Emborg and Bernander 1994). The tensile strength of the concrete is affected by the cement type, supplementary cementious materials type, water-to-cementious-materials ratio (*w/cm*), and the temperature history of the concrete (Neville 2011). The strength of concrete increases with the progression of the hydration reaction of the concrete. Assessing the stresses and strength at early-ages for concrete is thus a complex process due to the various material interactions taking place in the concrete. Mass concrete structures face additional issues with regard to cracking due to their size and temperature issues.

Mass concrete is defined as “any volume of concrete with dimensions large enough to require that measures be taken to cope with generation of heat from hydration of the cement and attendant volume changes to minimize cracking” (ACI 207 2012). With regard to size, the least dimension of the concrete element is important in deciding if the element can be categorized as mass concrete (Gajda and Vangeem 2002). Most states and agencies designate mass concrete as elements with least dimension equal to or greater than 4 feet (Jahren et al. 2014). While mass concrete structures are commonly associated with dams, in recent years, bridge columns such as those shown in Figure 1-

1, and footings are also included in the category of mass concrete. During the process of hydration, considerable heat is generated in the concrete structure. The heat generation will result in a significant rise in temperature (subsequent fall as well) leading to high temperature differentials within the concrete element. In the presence of restraint, early-age temperature differentials lead to high early-age stresses. When the stresses exceed the strength of the element, it leads to early-age cracking of the concrete. Early-age cracking of the concrete element is an important concern to the construction industry, both for aesthetic reasons as well as durability issues developing in the concrete, leading to a potential decrease in service life of the structure (Bentz and Weiss 2011). By minimizing early-age cracking the durability of mass concrete structures can be improved.

Figure 1-1: Mass concrete column under construction (Courtesy: PCA 2007)

Two unique types of distresses can develop due to the high early-age temperatures that develop in mass concrete. The first of these—known as thermal cracking—is primarily attributed to a large difference between the concrete temperature at the core and edge of the element. If the concrete member is subjected to differential heating and cooling, stresses are induced in the concrete and as a result, it can lead to early-age thermal cracking of the concrete member (Emborg 1989). Figure 1-2 is an example of thermal cracking in a bridge column in Texas.

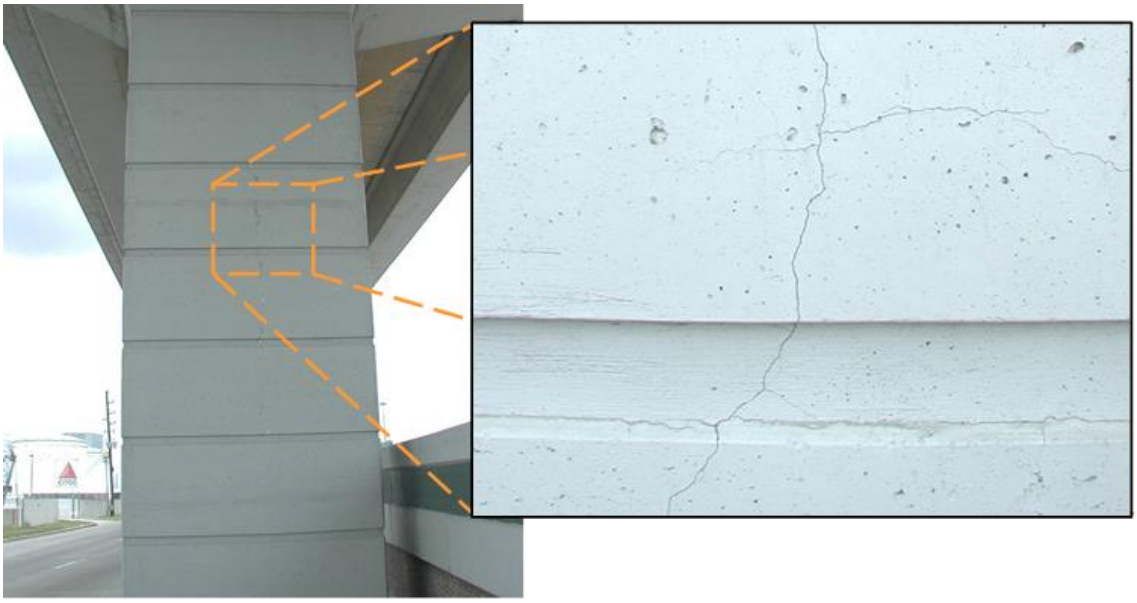

Figure 1-2: Thermal cracking of a bridge column in Texas (Photo courtesy of Dr. J.C. Liu)

The second type of distress of potential concern in mass concrete is known as delayed ettringite formation (DEF). DEF is a form of internal concrete sulfate attack, which is triggered by high early-age temperatures, the availability of moisture, and the availability of sulfate that is internally present in the concrete (Taylor et al. 2001). DEF causes an expansion in the concrete and this can lead to cracking, as shown in Figure 1-3.

Research surveys conducted in 2014, concluded that seven of the states with mass concrete specifications limit the maximum concrete temperature difference to 20 °C (35 °F), and two states limit the maximum in-place temperature to 71 °C (160 °F) (Jahren et al. 2014). The reasons behind these restrictions on maximum core temperatures and temperature differences are to avoid DEF and early age thermal cracking respectively. While many measures can be used to minimize early-age cracking there is scarce literature available which focuses on the use of internal curing on using lightweight aggregate in mass concrete applications to minimize early-age cracking.

Figure 1-3: Cracking due to DEF at the San Antonio Y overpass (Thomas et al. 2008)

Internal curing is defined as “supplying water throughout a freshly placed cementitious mixture using reservoirs, via pre-wetted materials, that readily release water as needed for hydration or to replace moisture lost through evaporation or self-desiccation” (ACI CT 2016). The pre-wetted materials in concrete act like internal reservoirs and aid in relieving early-age capillary stresses caused by self-desiccation in the concrete (Holt 2001). Decreasing capillary stresses reduces the stresses developed as a result of autogenous shrinkage (Holt 2001).

1.2 LIGHTWEIGHT AGGREGATES

Lightweight aggregates have been used over the past 100 years from building ships to bridge structures. Though found in nature, industry made LWA is increasingly popular in the United States. Rotary kilns are used to produce LWA from shale, slate, and clay rocks (Bremner and Ries 2009). While addition of LWA to concrete reduces its density, an additional and valuable property is its ability to absorb large quantities of water. The additional water act as internal reservoirs and supplies water to the concrete, hence the term “internal curing of concrete” (Bentz and Weiss 2010). Internal curing water can provide additional water for hydration purposes, thus eliminating autogenous shrinkage stresses and improves the strength of the concrete (Byard and Schindler 2010). Limited work has been done to determine the cracking tendency of mass concrete structures when incorporating with lightweight aggregates. Thus, it is necessary to determine the effects of lightweight aggregate on the cracking tendency of mass concrete structures.

Lightweight aggregates have an increased insulation ability and thus mass concretes containing lightweight aggregates tend to have a higher maximum core temperature and temperature difference when compared to normalweight concretes (Maggenti 2007).

Maggenti (2007) reported an increased core concrete temperature and temperature difference in concrete columns containing lightweight aggregates. Due to increased temperature differences, concerns were raised regarding the cracking risk of concretes containing lightweight aggregates. However, increased temperature difference does not necessarily translate to an increased cracking risk of concrete (Byard and Schindler 2010). The temperature difference limit for mass concrete is usually restricted to 35°F, however, this limit may be inappropriate for concrete containing LWA (Bamforth 2007). Since, thermal cracking risk is a combination of many factors such as concrete strength, modulus of elasticity, coefficient of thermal expansion (CTE), creep adjusted modulus of elasticity, and temperature difference of the concrete, the temperature difference limit for concretes containing LWA may have to be adjusted. Also, concretes containing lightweight aggregate are known to have a reduced modulus of elasticity, lower CTE, and similar splitting tensile strength in comparison to reference concrete, which in turn reduces the cracking tendency of concretes at early-ages (Byard and Schindler 2010). Thus, it may be beneficial to introduce lightweight aggregate in mass concrete structures, thereby reducing the early-age concrete cracking risk.

1.3 RESEARCH APPROACH

This study comprises of two parts, Part I and Part II. In Part I, the effect of lightweight aggregates on the effect of early-age temperature and stress development of mass concrete structures is assessed by cracking frame testing techniques. Rigid cracking frames as developed by Dr. Rupert Sprinenschmid at the Technical University Munich, Germany was used in this research study. Cracking frames at Auburn University as illustrated in Figure 1-4, can measure the development of early-age stresses due to

thermal and autogenous shrinkage stresses. The cracking tenedency of concretes was measured in the RCF, using a temperature profile to simulate mass concrete placement.

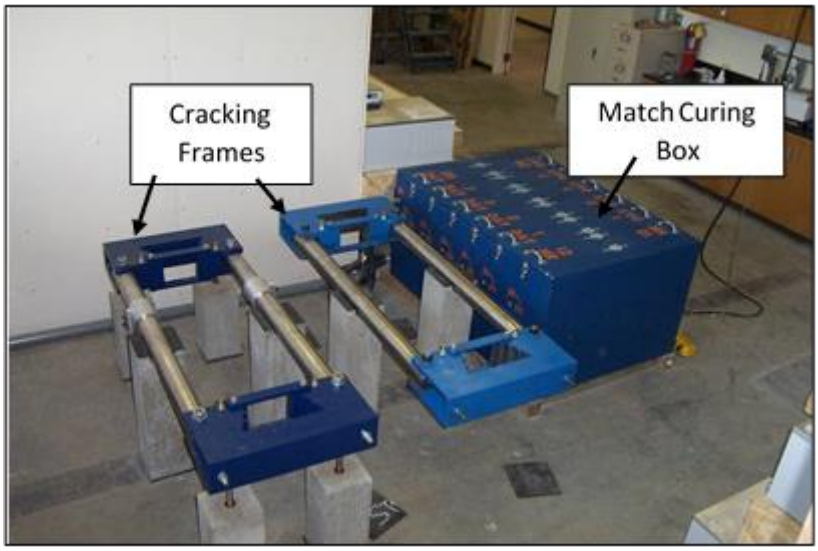

Figure 1-4: Test equipment to evaluate the cracking potential of concrete mixtures (Byard and Schindler 2010)

This was achieved by assessing the early-age stress development and cracking tendency of concrete of varying densities. The concretes were divided into two groups with different water-to-cementious-materials-ratio (*w/cm*), and each group contained concretes with different densities. In order to be representative of mass concrete, Class F fly ash at a 30% (by mass) cement replacement level was used in all mixtures. In addition to the cracking behavior of concrete specimens, the unrestrained free shrinkage was also determined using free-shrinkage frames (FSF), as shown in Figure 1-5. The time-dependent development of mechanical properties were determined by performing compressive, splitting tensile, and modulus of elasticity tests at various ages as per ASTM

C39 (2014), ASTM C496 (2014), and ASTM C469 (2014), respectively. The coefficient of thermal expansion of each concrete was determined as per AASHTO T336 (2009).

Figure 1-5: Free-shrinkage frame used to evaluate the unrestrained free shrinkage of concretes (Byard and Schindler 2010)

In Part II, the effect of lightweight aggregates on the effect of early-age temperature and stress development of mass concrete structures is assessed by a numerical study─ supplemented with data from experimental work─ to evaluate the effects of incorporating LWA in mass concrete structures. Three column sizes were evaluated in ConcreteWorks software, each with varying amount of LWA, placed under similar environmental conditions and their respective temperatures, stresses, critical stress locations and risk of cracking were analysed. The effectiveness of the 35°F maximum temperature difference limit was evaluated and a modified temperature difference limit, derived using a mechanistic approach, was proposed.

1.4 RESEARCH OBJECTIVES

The primary objective of this research is to assess the early-age behavior of mass concrete made with LWA. This was achieved by assessing the early-age stress development and cracking tendency of concrete of varying densities. The concretes were divided into two groups with different water-to-cementious-ratio (*w/cm*), and each group contained concretes with different densities. In order to be representative of mass concrete, Class F fly ash at a 30% (by mass) cement replacement level was used in all mixtures. The Also, the effectiveness of the 35°F maximum temperature differential limit was evaluated and a modified temperature difference limit was proposed.

The research presented in this dissertation is divided into two stand-alone parts. The research described in Part I has the following objectives:

1. Evaluate the effect of using lightweight aggregate on the development of concrete temperatures in mass concrete applications,
2. Evaluate the compressive strength, splitting tensile strength, modulus of elasticity, coefficient of thermal expansion, and thermal diffusivity and determine their effect on the early-age cracking tendency of mass concrete,
3. Evaluate the effect of water-to-cementitious-materials ratio (*w/cm*) in concrete containing lightweight aggregates on the cracking tendency of mass concrete,
4. Compare the measured modulus of elasticity values to estimates from ACI 318 (2014) and AASHTO LRFD Bridge Design Specifications (2016) expressions, and
5. Compare the measured splitting tensile strength values to estimates from ACI 207.2R (2007) and ACI 207.1R (2012) expressions, and evaluate the applicability

of lightweight modification (λ) factor to estimate the splitting tensile strength recommended by Green and Graybeal (2013).

Part II focuses on the maximum concrete temperature differences, concrete stresses, and cracking risk. The research described in Part II has the following objectives:

- Evaluate the maximum concrete temperature differences, early-age stresses, early-age cracking-risk of normalweight concrete and concrete containing LWAs.
- Develop a simplified and improved model to calculate allowable temperature-difference limits to minimize thermal cracking in concretes containing LWAs.

1.5 DISSERTATION OUTLINE

This dissertation is divided into two parts. Part I focuses on the cracking tendency of various concretes made with LWAs in mass concrete applications, Part II addresses the development of a simplified equation to assess the maximum concrete temperature difference limit. Each part focused on different aspects of early-age concrete behavior, hence each part was written to be a stand-alone document.

The first part evaluates the cracking tendency of concrete containing lightweight aggregates. Shale lightweight aggregates were shipped from North-eastern United States and were assessed in internal-curing, sand-lightweight, inverse-sand lightweight, all-lightweight mixtures. Two groups of *w/cm*, 0.38 and 0.45 mixtures were chosen. Each group contained five different types of concretes mentioned including reference concrete. The mixtures were tested in rigid cracking frames which were match-cured to modeled fall placement scenarios. The early-age stresses of each mixture was measured from the time of placement till cracking. Additionally, the stresses due to autogenous shrinkage was assessed separately in another rigid cracking frame. In addition, a free shrinkage

frame was match cured with the rigid cracking frame and the free shrinkage strains due to autogenous and thermal effects were measured. Match-cured concrete cylinders were used to determine the concrete compressive, splitting tensile strengths, and the modulus of elasticity. The coefficient of thermal expansion was measured for hardened concrete specimens. The mechanical properties were then assessed with standard estimation equations to evaluate their applicability for use in lightweight aggregates.

Part II is a numerical investigation which utilized the concrete mixtures developed in Part I, namely reference concrete, internally-cured concrete, sand-lightweight concrete, and all-lightweight concrete. ConcreteWorks software was used to compute the maximum core temperature, temperature differences, early-age stresses, cracking risk of three different column cross-section sizes. The maximum temperature difference limit for concretes containing lightweight aggregates were evaluated using a mechanistic model and compared with the cracking risk from ConcreteWorks.

PART 1:

CRACKING TENDENCY OF CONCRETE INCORPORATING LIGHTWEIGHT AGGREGATES FOR MASS CONCRETE APPLICATIONS

Chapter 2

PART I: INTRODUCTION

2.1 BACKGROUND

Mass concrete is defined by ACI 207.1R (2012) as “any volume of concrete with dimensions large enough to require that measures be taken to cope with the generation of heat from hydration of the cement and attendant volume change to minimize cracking”. Mass concrete construction began in the United States with the construction of large scale concrete structures such as dams and foundations. In 1930, the ACI committee 207 was formed to examine and solve problems related to cracking of dams. Today, mass concrete includes dams, bridge elements as shown in Figure 2-1, mat foundations, etc.

With regard to size, the least dimension of the concrete element is important in deciding if the element can be categorized as mass concrete (Gajda and VanGeem 2002). Most states and agencies designate mass concrete as elements with least dimension equal to or greater than 4 feet (Jahren et al. 2014).

Hydration of cementitious materials in concrete is an exothermic process, and a considerable quantity of heat is generated during the early stages of concrete construction (Neville 2011). The result is a significant rise in temperature at the core of element, and a temperature difference between the interior and exterior of the element due to the heat transfer at the edge with the environment. Two unique types of distresses can develop due to the high early-age temperatures that develop in mass concrete. The first of these—known as thermal cracking—is primarily attributed to a large difference

between the concrete temperature at the core and edge of the element. Cracking occurs in the concrete when stresses in the concrete exceed the tensile strength of the concrete (Mehta and Monteiro 2013). If the concrete member is subjected to differential heating and cooling, stresses are induced in the concrete and as a result, it can lead to early-age thermal cracking of the concrete member (Emborg 1989). Concrete stresses are dependent on many factors such as the tensile strength, coefficient of thermal expansion, restraint conditions, modulus of elasticity, creep (relaxation), and temperature history (Emborg 1989). Effective control of early-age cracking can result in reduced cracking at later ages, more durable concrete with lower overall porosity, and extended service life of the structure (Bentz and Weiss 2011). Figure 2-2 is an example of thermal cracking in a bridge column in Texas.

Figure 2-1: Bridge column wrapped with insulating blankets (Jahren et al. 2014)

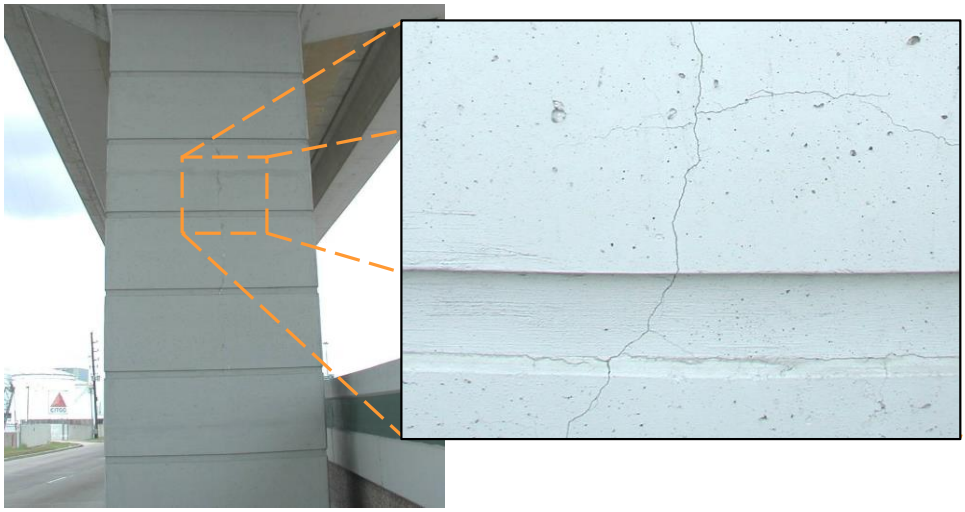

Figure 2-2: Thermal cracking of a bridge column in Texas (Photo courtesy of Dr. J.C. Liu)

The second type of distress of potential concern in mass concrete is known as delayed ettringite formation (DEF). DEF is a form of internal concrete sulfate attack, which is triggered by high early-age temperatures, the availability of moisture, and the availability of sulfate that is internally present in the concrete (Taylor et al. 2001). DEF causes an expansion in the concrete and this can lead to cracking, as shown in Figure 2-3.

Figure 2-3: Cracking due to DEF at the San Antonio Y overpass (Thomas et al. 2008)

2.2 LIGHTWEIGHT AGGREGATES

Lightweight aggregates (LWAs) have been used over the past 100 years from building ships to various structures. Though found in nature, manufactured LWAs are becoming increasingly popular in the concrete industry. Rotary kilns are used to produce lightweight aggregate (LWA) from shale, slate, and clay rocks under controlled conditions (Bremner and Ries 2009). While the addition of LWAs reduces the density of concrete, an additional and valuable property is its ability to absorb large quantities of water. The high internal

pore volume of the LWAs acts as internal water reservoirs and when saturated the LWAs can supply water to the concrete to promote hydration of the cementitious materials, hence the term “internal curing of concrete” (Bentz and Weiss 2011).

Different classifications of concrete are obtained when adding LWA to concrete, and the commonly used ones include sand-lightweight concrete (SLWC), all-lightweight concrete (ALWC), and “internally cured” concrete (ICC). SLWC contains coarse LWA and normalweight fine aggregate, while ALWC contains both coarse and fine LWA. ICC generally involves replacing a portion of fine aggregate with fine LWA. Internal curing takes place in all concretes containing pre-wetted LWAs.

Lightweight aggregate has a higher insulating ability when compared to normalweight aggregate (Maggenti 2007) and concretes containing LWA have been found to reach higher maximum in-place temperatures due to hydration, as shown in Figure 2-4 (Tankasala et al. 2017). Early-age cracking and the associated cracking risk of concrete are affected by several factors; therefore, a higher temperature difference alone does not render the concrete as more prone to early-age cracking (Byard and Schindler 2010). An earlier study concluded that the use of LWAs in bridge deck applications resulted in a significant improvement in resistance to early-age cracking when compared to normalweight concrete (Byard and Schindler 2010). This improved behavior was observed in internally cured (IC), sand-lightweight (SLW), and all-lightweight (ALW) concretes, and was attributed to an increase in tensile strength and a decrease in modulus of elasticity, coefficient of thermal expansion (CTE), and autogenous shrinkage. The study further concluded that although SLW and ALW concretes experienced higher peak temperatures, this did not translate to an increase in early-age

cracking in bridge deck applications, and the reduction in CTE and elasticity modulus led to a significant overall delay of early-age cracking in bridge deck applications. Hence from an initial assessment, it would appear that the compounded benefits associated with LWA could be beneficial to mass concrete placements; however, verification of this concept by laboratory and field tests or by more sophisticated analysis has not yet been conducted.

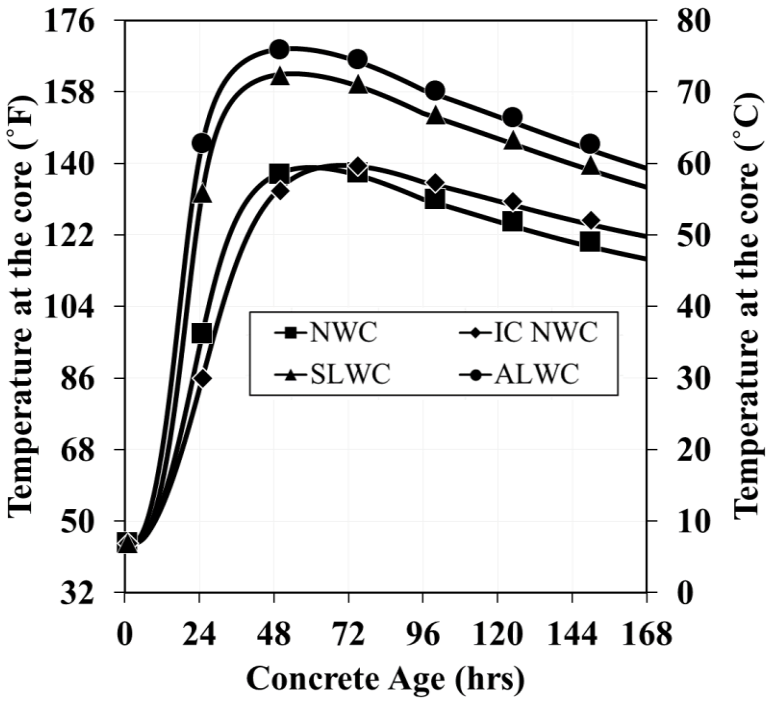

Figure 2-4: Comparison of simulated core concrete temperatures for normalweight concrete (NWC), internally cured normalweight concrete (IC NWC), sand-lightweight concrete (SLWC), and all-lightweight concrete (ALWC) for an 8×8 ft cross-section size column (Tankasala et al. 2017)

2.3 OBJECTIVES

The primary objective of Part I is to assess the effect of using lightweight aggregate on the early-age cracking tendency of mass concrete. The impact of using ICC, inverse sand-lightweight concrete (ISLWC), SLWC, and ALWC on the early-age cracking of mass concrete relative to normalweight concrete will be quantified. The secondary objectives of this study are as follows:

1. Evaluate the effect of using lightweight aggregate on the development of concrete temperatures in mass concrete applications,
2. Evaluate the compressive strength, splitting tensile strength, modulus of elasticity, coefficient of thermal expansion, and thermal diffusivity and determine their effect on the early-age cracking tendency of mass concrete,
3. Evaluate the effect of water-to-cementitious-materials ratio (*w/cm*) in concrete containing lightweight aggregates on the cracking tendency of mass concrete,
4. Compare the measured modulus of elasticity values to estimates from ACI 318 (2014) and AASHTO LRFD Bridge Design Specifications (2016) expressions, and
5. Compare the measured splitting tensile strength values to estimates from ACI 207.2R (2007) and ACI 207.1R (2012) expressions, and evaluate the applicability of lightweight modification (λ) factor to estimate the splitting tensile strength recommended by Green and Graybeal (2013).

2.4 RESEARCH APPROACH

Rigid cracking frames (RCF), as shown in Figure 2-5, were used to evaluate the development of early-age concrete stresses from the time of initial set to cracking

(Mangold 1998). Rigid cracking frames can measure the early-age development of thermal and autogenous stresses in hardening concrete. The cracking frames can be programmed to simulate a unique temperature history, thereby allowing researchers to gain detailed information about the combined effect of the heat of hydration, modulus of elasticity, creep (relaxation), coefficient of thermal expansion, tensile strength, and restraint on the cracking tendency of concrete. In this study, the cracking tendency of concretes was measured in the RCF, using a temperature profile to simulate mass concrete placement. A detailed discussion of the rigid cracking frame is provided in Section 4.4.3.

In addition to the cracking behavior of concrete specimens, the unrestrained free shrinkage was also determined using free-shrinkage frames (FSF), as shown in Figure 2-6. A detailed discussion of the free-shrinkage frame is provided in Section 4.4.4.

The time-depended development of mechanical properties were determined by performing compressive, splitting tensile, and modulus of elasticity tests at various ages as per ASTM C39 (2014), ASTM C496 (2014), and ASTM C469 (2014), respectively. The cylinders used to test the time-depended development of mechanical properties were match cured to the temperature of the RCF specimens. Semi-adiabatic calorimetry was used to characterize the heat of hydration and thermal diffusivity of each concrete as discussed in Sections 4.4.1 and 4.4.2, respectively. The coefficient of thermal expansion of each concrete was determined as per AASHTO T336 (2009).

Two groups of concretes, each with a *w/cm* of 0.38 and 0.45 were tested. Each group of concretes contained five mixtures: a reference normalweight concrete, internally cured concrete, inverse sand-lightweight concrete, sand-lightweight concrete, and all-

lightweight concrete. Ten concretes were thus produced under laboratory conditions and evaluated in this study. The use of two different *w/cm* concretes allows one to assess the effect of *w/cm* on the cracking tendency and stress development of the lightweight aggregate and reference concrete mixtures. For the lower *w/cm* concrete mixtures, the development of stress due to autogenous shrinkage were recorded under isothermal conditions. In order to be representative of mass concrete, Class F fly ash at a 30% (by mass) cement replacement level was used in all mixtures.

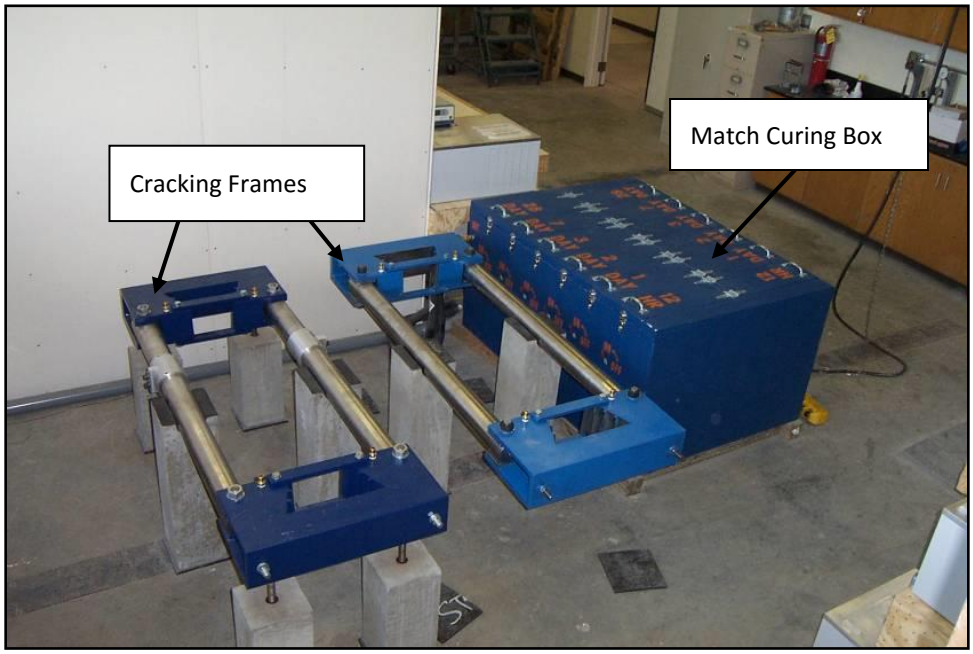

Figure 2-5: Rigid cracking frames used to evaluate the cracking potential of concretes (Byard and Schindler 2010)

Figure 2-6: Free-shrinkage frame used to evaluate the unrestrained free shrinkage of concretes (Byard and Schindler 2010)

2.5 PART I OUTLINE

Part I contains six chapters. A literature review regarding early-age cracking, unique mass concrete issues, internal curing, lightweight aggregates, properties of lightweight aggregate, and the beneficial effects of lightweight aggregate in concrete is presented in Chapter 3. The experimental testing program to evaluate the early-age stress development of concrete and properties is covered in Chapter 4. In addition, the methods to assess the early-age stress development of concrete, temperature modeling of concrete, and properties of the materials used in the study are covered in Chapter 4. The results of the experimental work performed for this study are presented in Chapter 5. A discussion and synthesis of results are presented in Chapter 6. The summary, conclusions, and recommendations of Part I are presented in Chapter 7.

Chapter 3

PART I: LITERATURE REVIEW

A summary of the available research literature relevant to this study is provided in this chapter. The review includes a review of the factors responsible for early-age cracking, an overview of mass concrete structures and their associated temperature issues, lightweight aggregates, and the effects of internal curing on chemical and autogenous shrinkage along with its potential benefits for mass concrete applications.

3.1 EARLY-AGE CRACKING

Early-age cracking is primarily affected by the following factors (Emborg and Bernander 1994):

- Temperature development in the structure,
- Autogenous shrinkage associated with low *w/c* ratios,
- Early-age creep effects,
- Mechanical properties of the young concrete, and
- Restraint of the structure.

The effect of these factors on early-age cracking will be discussed in the remainder of this section.

3.1.1 Temperature and Thermal Stress Development

The thermal stresses can be computed from Equation 3-1 (Emborg and Bernander 1994). Creep (or relaxation) effects at early ages need to be accounted for to obtain an accurate estimate of the stress developments (Emborg 1989).

$$\text{Thermal Stress} = \sigma_T = \Delta T \times CTE \times K_r \times E_c \qquad \text{(Equation 3-1)}$$

where,

ΔT = temperature change = $T_{zero\text{-}stress}$ - T_{min} (˚F),

CTE = coefficient of thermal expansion (strain/˚F),

K_r = degree of restraint factor,

E_c = creep adjusted elasticity of modulus (psi),

$T_{zero\text{-}stress}$ = concrete zero-stress temperature (˚F), and

T_{min} = minimum concrete temperature (˚F).

In order to gain an understanding of the evolution of early-age thermal stresses and how it is impacted by concrete temperatures and mechanical properties, a fully restrained element with an uniaxial stress state is considered in Figure 3-1. The concrete is placed in its fresh state under hot summer field conditions. Initially the concrete is in a plastic state and hence no stresses are present. However, after final set is achieved, represented by time t_{fs}, stresses begin to develop in the concrete. The concrete hydration process is an exothermal reaction, and hence the concrete temperature begins to rise rapidly, starting from temperature at final set $T_{final\text{-}set}$ to a maximum temperature T_{max} (line B). The continued rise in temperature initially induces compressive stresses in the concrete; however, due to early-age relaxation effects the compressive stresses are

reduced in magnitude (Emborg 1989; Westman 1999). When a concrete specimen is subjected to constant strain, creep manifests itself in the form of a progressive decrease in stress over time, and this phenomenon is known as relaxation (Neville 2011). The mechanical properties such as the strength and stiffness of the concrete starts to develop at final set, t_{fs}, and develops rapidly thereafter. After the maximum temperature is reached, the temperature begins to drop and the concrete begins to contract as a result. This results in the decrease of compressive stresses which eventually reaches a zero value at time t_{zs}. The corresponding temperature is known as zero-stress temperature T_{zs}. The zero-stress temperature is often considerably higher than the final set temperature T_{fs}. Beginning from time t_{zs} the stresses in concrete change from compression to tension for the first time. After further cooling, the stresses begin to increase (tensile), and once the stresses exceed the tensile strength of the concrete, cracking occurs and the time of cracking is denoted as t_c (Springenschmidt, Breitbucher and Mangold 1994). Therefore, only the portion of tensile stresses, which develop after the zero-stress temperature is unfavorable and results in thermal cracks.

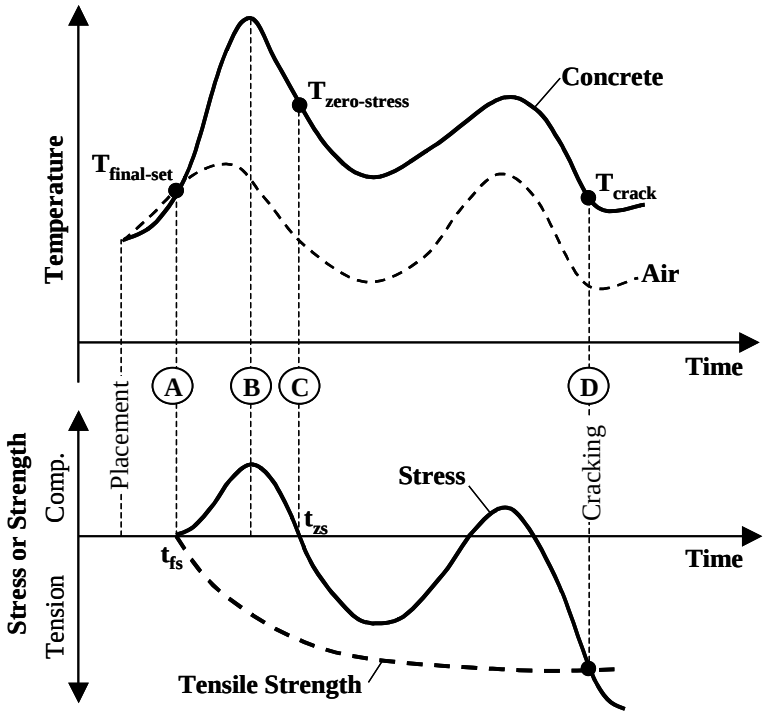

Figure 3-1: Evolution of early-age thermal stresses (Schindler and McCullough 2002)

3.1.2 Autogenous Shrinkage

The phenomena wherein the absolute volume of cement plus water decreases progressively with hydration is known as chemical shrinkage (Tazawa 1998; Holt 2001). Before setting, this phenomenon results in volumetric change, however, no stresses are generated since the concrete is still in a plastic state (Holt 2001). At setting, enough hydration products have formed to provide a self-supporting skeletal framework in the paste matrix. Water filled capillary voids are present in between the framework of solids. As water is consumed by the ongoing hydration process, the voids empty and capillary tensile stresses are generated, resulting in volumetric shrinkage (Tazawa 1998; Lura et al. 2003). The concrete volume change that occurs without mass loss, temperature

variation, external force application, or restraint is called autogenous shrinkage (Tazawa 1998). At early concrete ages, viscous behavior is quite pronounced and the smallest stresses make way for large deformations (Lura et al. 2003). Stresses related to autogenous shrinkage may contribute significantly to early-age cracking (Tazawa 1998). For higher *w/c*m, generally above 0.42, autogenous shrinkage and related stresses are not a major concern (Holt 2001). A graphical illustration of the relationship between chemical and autogenous shrinkage (horizontal direction) is shown in Figure 3-2, where *C* is the cement volume, *W* is the volume of water, H_y is the volume of hydration products, and *V* is the volume of voids.

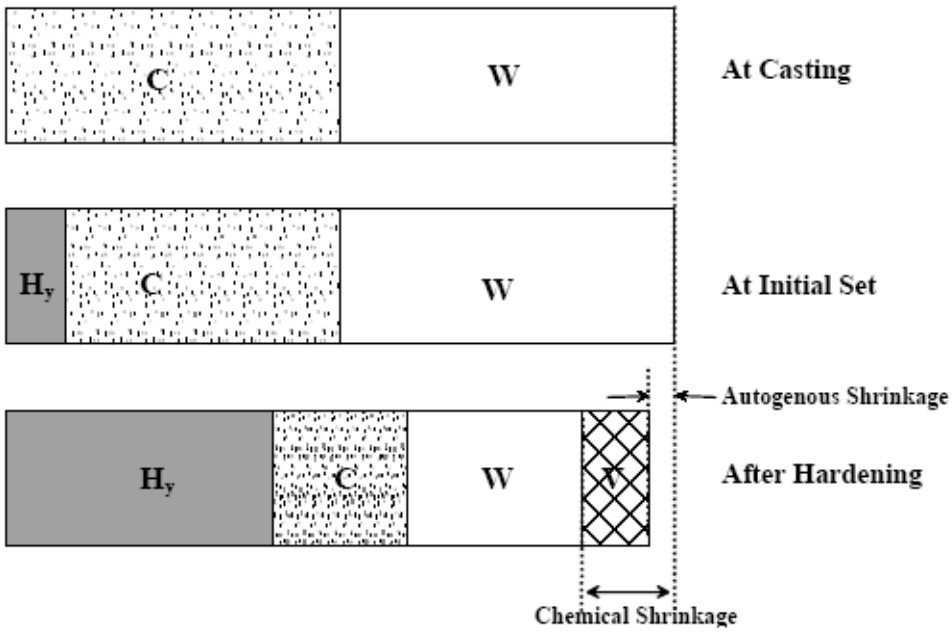

Figure 3-2: Volume reduction because of autogenous shrinkage (Tazawa 1998)

3.1.3 Early-age Creep or Relaxation

Creep can be defined as a gradual increase in strain with time under loading, i.e., an increase in strain under a sustained stress. Alternatively, if the concrete is restrained in such a manner that it is subjected only to a constant strain, then creep manifests itself in the form of a gradual decrease in stress over a period and this phenomenon is known as relaxation (Neville 2011). Early-age creep or relaxation is generally beneficial in reducing early-age stresses and consequently cracking in concrete (Atrushi 2003).

Creep tends to be influenced by a mixture of intrinsic and extensive factors. Intrinsic factors include the strength, modulus of elasticity of aggregate, fraction of aggregate in the concrete mixture, and the aggregate size. An increase in any of these factors results in a decrease in creep (Bažant 1982). Extensive factors include temperature, pore water

content, age at loading, etc. and their influence on creep is complicated (Bažant 1982). Early-age creep data are scarce in literature owing to the complexity of testing concrete creep at early ages. Compressive and tensile creep tends to increase with a rise in temperature; however, this is offset by an increase in hydration rate, which in turn reduces creep (Umehara et al. 1994; Bažant 1982).

3.1.4 Mechanical Properties of Concrete

3.1.4.1 Compressive Strength

The compressive strength of concrete depends on many factors: the water-to-cementitious materials-ratio (*w/cm*), curing conditions, total air content, aggregate type, aggregate size, and rate of loading to name a few (Mehta and Monteiro 2013). Numerous expressions exist for modeling the compressive strength of concrete (Hedlund 2000); however, for this study the exponential equation, Equation 3-2, developed by Freiesleben Hansen and Pederson (1977) is used.

$$f_c(t_e) = f_{cult} \times exp\left(-\left(\frac{\tau_s}{t_e}\right)^{\beta_s}\right) \qquad \text{(Equation 3-2)}$$

where,

$f_c(t_e)$ = compressive strength at equivalent age t_e (psi),

f_{cult} = ultimate compressive strength parameter (psi),

τ_s = strength development time parameter (hrs),

β_s = strength development slope parameter (unitless), and

t_e = equivalent age (hrs).

3.1.4.2 Splitting Tensile Strength

The tensile strength depends on similar factors as compressive strength; however, it is more sensitive to the quality of bond between the aggregate and paste. Higher tensile strength values at early ages are desired to improve resistance to early-age cracking. Splitting tensile strength can be estimated by Equation 3-3 (ACI 207.2R 2007), provided the compressive strength is known. ACI 207.1R (2012) adopted an expression from Raphael (1984), which is shown in Equation 3-4 for estimating the splitting tensile strength for mass concrete structures from a known compressive strength.

$$f_{st}=6.7 \times (f_c)^{0.5} \quad \text{(Equation 3-3)}$$

$$f_{st}=1.7 \times (f_c)^{\frac{2}{3}} \quad \text{(Equation 3-4)}$$

where,

f_{st} = splitting tensile strength (psi), and

f_c = concrete compressive strength (psi).

Greene and Graybeal (2013) also developed an expression, shown in Equation 3-5, to estimate the splitting tensile strength from known compressive strength values using a lightweight modification factor (λ). The lambda modification factor is determined from the concrete density, as shown in Equation 3-6.

$$f_{st}'' = 0.212 \times \lambda \times (f''_c)^{0.5} \quad \text{(Equation 3-5)}$$

$$0.75 \leq \lambda = 7.5 \times w_c'' \leq 1.0 \quad \text{(Equation 3-6)}$$

where,

w''_c = density of normalweight concrete or equilibrium density of lightweight concrete (kcf),

f''_{ct} = splitting tensile strength (ksi),

f''_c = concrete compressive strength (ksi), and

λ = lightweight modification factor (unitless).

3.1.4.3 Modulus of Elasticity

The modulus of elasticity is affected by the type of aggregate and the volume proportion of aggregate in the concrete (Neville 2011). Equation 3-7 from ACI 318 (2014) is used to estimate the modulus of elasticity from the known density and compressive strength. Recently, AASHTO (2016) adopted a new expression for determining the modulus of elasticity of concrete from known density and compressive strength values, and this expression is shown in Equation 3-8. From both these equations, it can be seen that a decrease in concrete density results in a decrease in modulus of elasticity. Lower modulus of elasticity of concrete will reduce early-age stresses and contribute to reduced cracking at early ages (Bentz and Weiss 2011; Byard et al. 2012).

$$E_c = 33\,(w_c)^{1.5}(f_c)^{0.5} \qquad \text{(Equation 3-7)}$$

$$E_c'' = 120{,}000\,K_1\left(w_c''\right)^{2.0}\left(f_c''\right)^{0.33} \qquad \text{(Equation 3-8)}$$

where,

E_c = modulus of elasticity (psi),

E''_c = modulus of elasticity (ksi),

f_c = concrete compressive strength (psi),

w_c = density of normalweight concrete or equilibrium density of lightweight concrete (lb/ft^3),

f''_c = concrete compressive strength (ksi),

w_c'' = density of normalweight concrete or equilibrium density of lightweight concrete (kips/ft^3), and

K_1 = aggregate correction factor (unitless)

3.1.5 Degree of Restraint

Degree of restraint is the ratio of the actual stress resulting from volume change to the stress that would be present if full restraint was present. All concrete elements are restrained to a certain degree either by supporting elements or by different parts of the element itself (ACI 207.2R 2007). Restraint of an element is impacted by many factors, with the important ones being its own modulus of elasticity, the modulus of elasticity of the restraining element, and the geometry of the structure (usually the cross-sectional area) (ACI 207.2R 2007). While restrained volume change may induce a tensile, compressive or flexural state of stresses in concrete elements, those restraint conditions leading to a tensile state of stress in concrete are of concern due to their contribution to concrete cracking (ACI 207.2R 2007). Lower restraint leads to lower stresses and various models for modeling of restraint are available in literature (Larson 2003; ACI 207.2R 2007).

3.2 UNIQUE MASS CONCRETE ISSUES

Thermal stresses arising because of temperature differences between the zero-stress temperature and the temperature at cracking were discussed in the previous section. However, unique temperature issues related to mass concrete exist. An important distinction between normal concrete elements and mass concrete elements is their size and the thermal behavior. Mass concrete sectionis defined by ACI (ACI 207.2R 2007) as "any volume of concrete with dimensions large enough to require that measures be taken to cope with the generation of heat and attendant volume change to minimize cracking". The minimum dimension for a structure to be defined as mass concrete varies across state agencies, but according to ACI 301 (2016), if the least dimension of the concrete structure is greater than 4 ft, it can be considered a mass concrete structure. Because of their size, high temperatures develop at the core of the mass concrete element which leads to increased risk of: 1) delayed ettringite formation (DEF), and 2) thermal cracking.

3.2.1 Delayed Ettringite Formation

Delayed ettringite formation (DEF) can be described as the formation of ettringite after the concrete hardening process is completed and in which none of the sulfate which causes the ettringite formation comes from external sources (Taylor, Famy, and Scrivener 2001). It is a form of internal concrete sulfate attack, which is triggered by high temperatures and availability of sulfate, which is internally present in the concrete. Owing to their large size and high heat of hydration, mass concrete with only plain portland cement, that experiences temperatures more than 158˚F (70°C), are generally susceptible to DEF formation (Sylla 1988; Folliard et al. 2006; Livingston et al. 2006). Distresses due to DEF may include map cracking, fracture of surfaces, and deterioration

of strength in the concrete due to formation of ettringite crystals (Livingston et al. 2006). Figure 3-3 shows a column of the San Antonio Overpass damaged because of DEF (Folliard et al. 2006). Various state agencies place a restriction on the maximum concrete temperature, generally 160˚F, to prevent DEF (Jahren et al. 2014). Incorporation of sufficient amounts of various supplementary cementitious materials (SCMs) helps in preventing DEF and the maximum temperature regulations may be relaxed in such cases (ACI 301 2016). For example, if the cementitious content includes 25 percent (by mass) of cement replacement with Class F fly ash, then the concrete maximum temperature limit may be increased to 185°F to mitigate DEF (ACI 301 2016).

Figure 3-3: Cracking observed in a mass concrete column due to DEF (Folliard et al. 2006)

3.2.2 Thermal Cracking

Thermal gradient can be defined as a temperature change along a specific path through the concrete structure (ACI 207.2R 2007). There are two types of thermal gradients, mass and surface gradients. The mass gradient refers to the long-term maximum internal temperature change of a large concrete mass as it cools from an internal peak temperature to a stable temperature equal to approximately the average ambient temperature. Surface gradients refers to the temperature differences between the core and the surface of the concrete member (ACI 207.2R 2007). Due to their large size, and other factors such as thermal conductivity, specific heat, and density, the heat generated in the interior of a mass concrete member is not easily transferred through the concrete and thus high temperatures are sustained in the core for extended durations (ACI 207.1R 2012). Also, heat generated at the surface can quickly be dissipated to the surroundings resulting in a lower surface temperature. This difference in temperature between the surface and the core can cause large thermal gradients leading to severe cracks, which may reduce the long-term durability of the mass concrete element (ACI 207.1R 2012). An example of thermal cracking is provided in Figure 3-4.

Figure 3-4: Thermal cracking observed in a thick slab (Gajda 2007)

Most state agencies limit the thermal gradients to 35˚F, and it is the most commonly used temperature differential limit in mass concrete projects (Jahren et al. 2014). This approach was resorted to as a precautionary measure to prevent thermal cracking after early research projects involving dams in Europe used this 35°F limit (FitzGibbon 1976; Bamforth 1981). Nonetheless, no readily available laboratory or field research evidence confirms the suitability of a maximum temperature differential of 35˚F for all concretes. The use of supplementary cementitious materials, reduced concrete placement temperatures, and favorable ambient temperature are some of the factors which can reduce thermal gradients in a mass concrete structure.

3.3 LIGHTWEIGHT AGGREGATES

Lightweight aggregate (LWA) occurs in nature and is found as pumice and scoria and have been used in lightweight concrete for over 100 years (Bremner and Ries 2009). Modern LWA is manufactured from special deposits of shale, clay, or slate. The diagram shown in Figure 3-5, taken from ESCSI Reference Manual (Holm and Ries 2007), details the LWA production process. The raw materials for LWA are mined from deposits of clay, shale, slate, etc. They are then crushed and sized (stored if necessary) and sent via a conveyor belt into a rotary kiln. They are produced by heating graded particles into the high end of the rotary kiln, to a temperature of 2100˚F. The rotary kiln is generally 60 to 225 ft in length with diameters varying between 6 to 12 ft. The LWA spends 30 to 60 minutes in the kiln, with gradual heating occurring in the first 2/3rd of the kiln length and rapid heating in the final 1/3rd of the kiln length. Upon heating the pyroplastic mass, gases are liberated which cause expansion, and the expansion is retained upon cooling. After cooling the expanded particles have a unique vesicular structure and contain pores that have a size range of approximately 5 to 300 μm developed in a continuous, crack-free, high-strength vitreous phase. After the cooling process the aggregates are crushed to appropriate gradations and shipped to concrete production plants (Holm and Ries 2007; ACI 213R 2013).

Pores close to the surface are readily permeable and rapidly absorb water within the first few hours of exposure to moisture; however, interior pores fill extremely slowly. Non-interconnected interior pores, which form a small fraction of the total pores, are never filled even after years of immersion in water (Holm and Ries 2007).

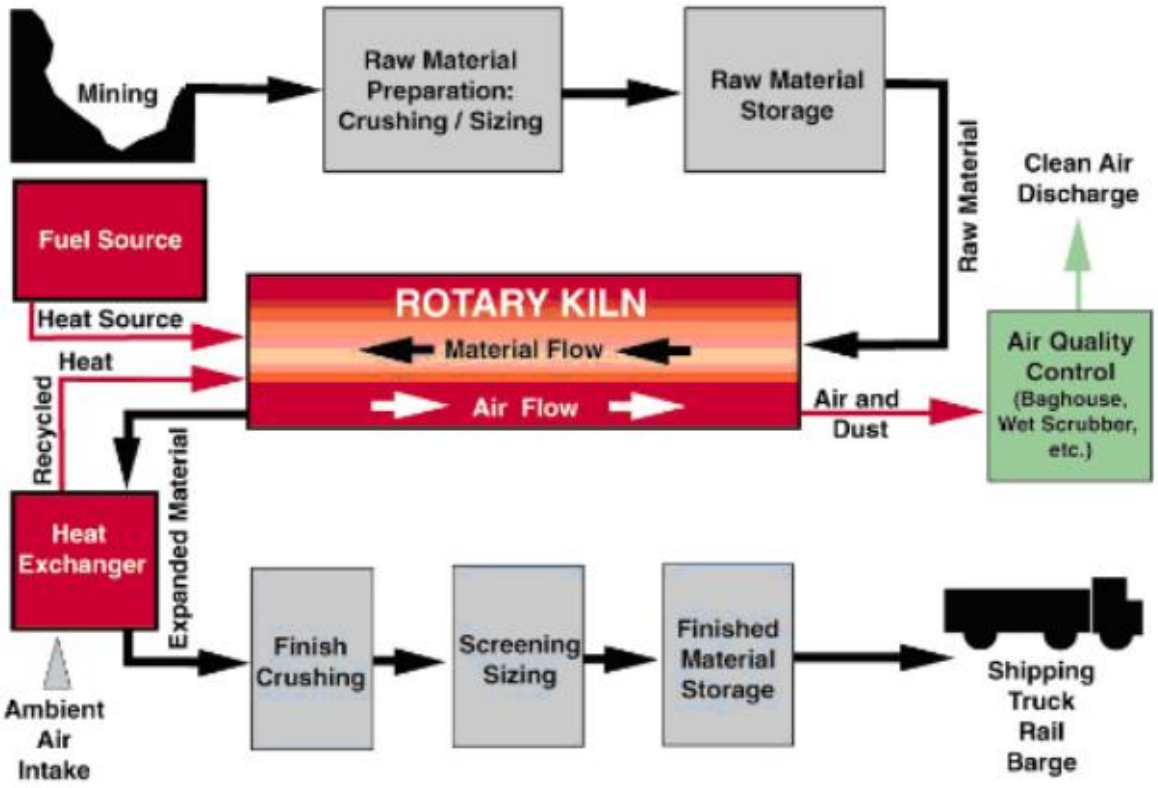

Figure 3-5: Production of rotary kiln lightweight aggregate (Holm and Ries 2007)

3.4 INTERNAL CURING

Internal curing is defined as “supplying water throughout a freshly placed cementitious mixture using reservoirs, via pre-wetted lightweight aggregates, that readily release water as needed for hydration or to replace moisture lost through evaporation or self-desiccation” (ACI CT 2016). The first published acknowledgement of internal curing dates to 1957, when LWA was used in production of concrete (Klieger 1957).

During the hydration of cementitious materials, capillary pores are created. Water present in the capillary pores continues to deplete as a result of hydration or due to external drying. This results in the formation of partially-filled pores within the

microstructure, leading to the development of air-water menisci. Capillary pressure is induced as a result, and concurrently a measurable stress is present. These stresses are usually of concern when the *w/cm* is low (Lura et al. 2003). LWA due to its high-water absorption capacity when pre-wetted and introduced in the concrete, can desorb water into the cement paste and as a result can relieve the concrete from autogenous shrinkage stresses (Bentz et al. 2005; Byard et al. 2012).

The addition of pre-wetted LWA to concrete has been shown to enhance hydration, improve internal water movement, and mitigate autogenous deformation due to the availability of moisture provided by the aggregates (Bentz and Weiss 2011; RILEM TC 196 2007; Byard et al. 2012). While other materials such as wood pulp fibers, perlite, and super absorbent polymer (SAP) may be used for internal curing, LWA also contributes to the load carrying capacity of the structure and its availability in the U.S. market makes it an attractive option to provide internal curing in concrete (Delatte et al. 2008).

Different classifications of concrete are obtained when adding LWA to concrete, and the commonly used ones are sand-lightweight concrete (SLWC), all-lightweight concrete (ALWC), and “internally cured” (IC) concrete. The latter generally involves replacing a portion of fine aggregate with fine LWA. This name is commonly used in literature (RILEM TC 196 2007) even though internal curing takes place in all concrete containing pre-wetted lightweight aggregates. For the sake of clarity, the term normalweight concrete (NWC) is used herein for concrete that does not contain any lightweight aggregate.

It is estimated that the desorbed water can travel 0.07 in. into the paste from (around) each aggregate particle (Henkensiefken et al. 2011). Therefore the use of fine

LWA is preferred for internal curing when compared to coarse LWA, as it allows for an improved spatial distribution of moisture throughout the microstructure of the concrete.

Proportioning of concrete for internal curing requires that an adequate amount of internal water be provided to overcome the effects of autogenous shrinkage. A simplified method to determine the amount of LWA needed to provide internal curing is provided with Equation 3-9 (Bentz et al. 2005). The quantity of internal curing water required to achieve total saturation within the hydrating cement paste, is estimated as the amount required to compensate for chemical shrinkage occurring at the maximum expected degree of hydration. While the goal of the method is to provide sufficient moisture to prevent autogenous shrinkage (self-desiccation), it actually provides enough internal curing water to mitigate chemical shrinkage, because it is difficult to only estimate the amount of autogenous shrinkage. Hence, this method is conservative, since autogenous shrinkage is always less than chemical shrinkage (Tazawa 1998).

$$M_{LWA} = \frac{C_f \times CS \times \alpha_{max}}{S \times \phi_{LWA}} \qquad \text{(Equation 3-9)}$$

where,

M_{LWA} = oven-dry weight of LWA (lb),

C_f = cement content (lb/yd^3),

CS = chemical shrinkage (lb of water/lb of cement),

α_{max} = maximum degree of cement hydration (0 to 1),

S = degree of saturation of aggregate (0 to 1), and

Φ_{LWA} = absorption of LWA (lb water / lb dry LWA).

Chemical shrinkage can be computed by determining the mass composition of the Bogue components within the cement (generally provided by manufacturer) and the chemical shrinkage coefficients provided in Table 3-1 (Bentz et al. 2005). For *w/cm* less than 0.36, the maximum degree of hydration can determined as (*w/cm)*/0.36. When the *w/cm* is greater than 0.36, it is assumed that the maximum degree of hydration is unity (Bentz et al. 2005).

Table 3-1: Coefficients for chemical shrinkage (Bentz et al. 2005)

Bogue Compounds	**Coefficient (lb of water/ lb of solid cement phase)**
C_2S	0.0704
C_3S	0.0724
C_3A	0.115*
C_4AF	0.086*

Note: * Denotes assuming total conversion of the aluminate phases to monosulfate.

An important consideration when using LWA is the amount of water that can be readily desorbed into the cement paste at high relative humidity values (i.e., ≥ 93% RH) (Castro et al. 2011). When pre-soaked LWA is added to the concrete mixture, the extra water is initially drawn from the larger pores in the LWA and subsequently from the relatively smaller pores (Lura et al. 2003). Various commercially available LWAs desorb between 85 to 98% of the absorbed water at 93% relative humidity (Castro et al. 2011). Desorption of water depends on the aggregate pore size distribution, the porous nature of the paste, and the internal relative humidity (RILEM TC 196 2007). Table 3-2 provides the absorption values and desorption coefficient values for the LWA used in this study. Desirable LWAs for internal curing generally have high absorption capacities, usually 10 to 30 percent by weight and high desorption capacities (Castro et al. 2011).

Table 3-2: LWA absorption and desorption coefficients (Castro et al. 2011)

Item	**Lightweight Aggregate - Shale**
Supplier Source	Norlite (Albany, NY)
Desorption coefficient at 93% relative humidity	0.955
Absorption capacity at 24 h (%)	18.1
Absorption capacity after vacuum (%)	21.2

3.5 EFFECT OF LWA ON CONCRETE PROPERTIES

3.5.1 Autogenous Shrinkage

Numerous studies have concluded that incorporation of LWA in concrete can lead to increased availability of moisture in the concrete leading to minimal or zero autogenous shrinkage and related stresses (RILEM TC 196 2007; Weiss and Bentz 2010; Byard et al. 2012). Replacement of fine aggregate with levels ranging from 7 to 33% (on a volume basis) of fine LWA has been shown to reduce or eliminate autogenous shrinkage (Henkensiefken et al. 2009). In the case of sand-lightweight and all-lightweight concretes, autogenous shrinkage stresses were insignificant (close to zero), thus relieving a major component of early-age stresses for the concrete (Byard et al. 2012).

3.5.2 Coefficient of Thermal Expansion

Lightweight aggregates in general have lower coefficient of thermal expansion when compared to normal- weight aggregates (Neville 2011). A major reason is the phase transformation undergone by lightweight aggregates in their manufacturing process (Chandra and Berntsson 2003). Concrete containing larger proportion of lightweight aggregates, including internally cured concrete, have lower coefficient of thermal

expansion values (Byard et al. 2012). A reduction in coefficient of thermal expansion is beneficial in reducing stresses due to thermal effects (Byard et al. 2012).

3.5.3 Mechanical Properties

The effects of internal curing on the mechanical properties of the concrete depend on mixture proportions, curing conditions, and testing age. In IC concrete, due to increased availability of moisture, the degree of hydration is higher than normalweight concrete (NWC) (Byard et al. 2012). However, some LWAs are inherently weaker than their natural gravel or limestone counterparts owing to their porous structure (Mehta and Monteiro 2013.) Thus, there are two competing effects which affect the mechanical properties of concretes made with LWA.

Schittler et al. (2010) found that when the replacement levels of sand with fine LWA is at 11 and 24 percent (volume basis) in IC concretes, the 28-day compressive strengths were similar when compared with NWC. Whereas they found, the tensile strengths of the IC concretes with a 20 percent (weight basis) replacement with LWA is higher than NWC by nearly 10 percent. Sand-lightweight concrete was found to have enhanced compressive and tensile strengths than NWC at 28 days (Byard et al. 2012). One of the reasons is the densification of the interfacial transition zone (ITZ), wherein water from the local LWA promotes hydration thus resulting in a stronger bond between the aggregate and the paste matrix (Neville 2011). There have also been studies (Raoufi 2011) which indicate that increasing replacement levels of LWA lead to an overall reduction in tensile strength. This can be attributed to the different types of LWA available in the market. All-lightweight concrete generally has lower compressive and tensile strengths due to a larger proportion of LWAs used in this concrete type (Byard et al. 2012).

The modulus of elasticity of concretes containing LWAs is significantly lower than NWC. The decrease in modulus of elasticity with concrete density can be estimated with either Equation 3-7 or 3-8. This is primarily because lightweight aggregates are less dense and have a porous structure (Neville 2011; Chandra and Berntsson 2003). Therefore, concretes containing large amounts of LWAs, specifically sand-lightweight and all-lightweight concrete, show a marked decrease in modulus of elasticity when compared with NWC (Raoufi 2011; Byard et al. 2012). This reduction in modulus of elasticity is beneficial in reducing concrete stresses due to restraint, thermal, drying, and autogenous shrinkage effects (Byard et al. 2012).

3.5.4 Creep

While many factors affect creep, the water content and the effect of aggregates are most important (Neville 2011). LWA being softer aggregates impose reduced restraint to cement paste movements, so creep is expected to increase (Byard 2011). The compliance with normalized elastic response of normalweight and slate lightweight mixtures with w/c of 0.42 loaded at 0.5 day is shown in Figure 3-6. It can be observed that the compliance (i.e. creep) is higher for the SLW and ALW concretes that contains large amounts of LWA (Byard 2011). On average, lightweight concrete (LWC) experiences higher creep than NWC (Clarke 2002). This may be attributed to the lower modulus of elasticity in LWA concrete. High creep (or relaxation) will reduce early-age stresses (Mehta and Monteiro 2013).

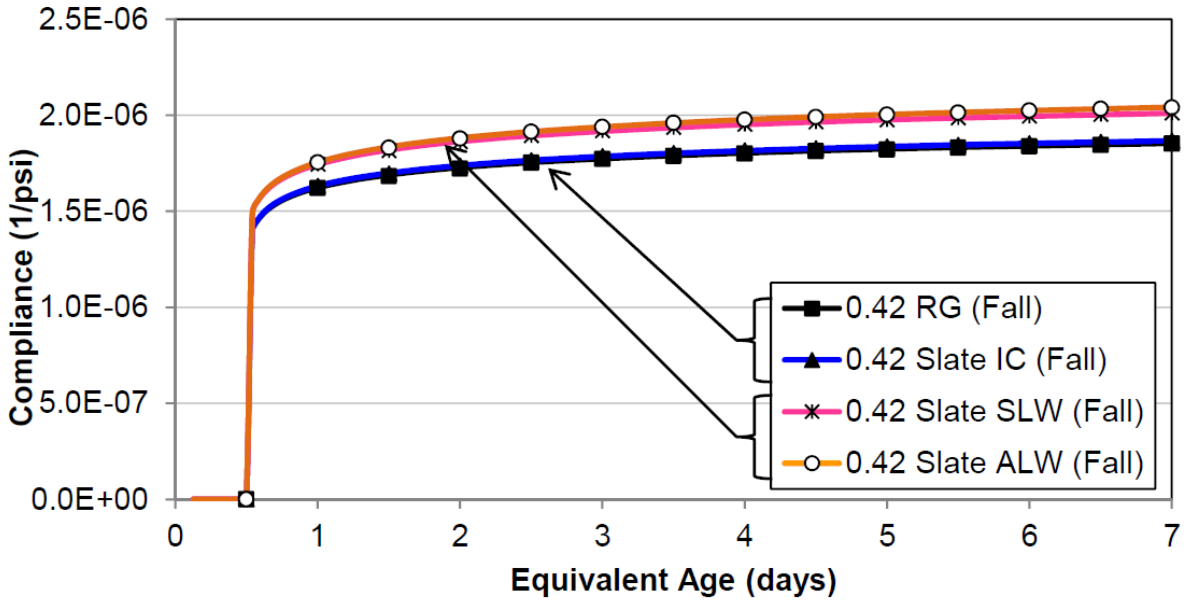

Figure 3-6: Compliance with normalized elastic response of normalweight and slate lightweight concretes with *w/c* of 0.42 loaded at 0.5 days (Byard 2011)

3.5.5 Thermal Conductivity

Thermal conductivity refers to the ability of the material to conduct heat. The mineralogical composition of the aggregate significantly affects the thermal conductivity of the concrete. For example, the higher the crystalline content, the higher its thermal conductivity (Neville 2011). LWA has a porous structure, is less crystalline, and hence has a lower thermal conductivity than its normalweight counterparts (Neville 2011; Chandra and Berntsson 2003). During the pours for mass concrete piers, Maggenti (2007) reported a higher temperature rise throughout the hydration process for concrete containing LWA when compared to concrete containing normalweight aggregates with identical cementitious and fine aggregate content. This higher temperature rise can be

attributed to a lower thermal conductivity and due to a lower density of concrete containing LWA (Chandra and Berntsson 2003).

Chapter 4

PART I: EXPERIMENTAL WORK

4.1 EXPERIMENTAL PROGRAM

Concrete containing various amounts of lightweight aggregate and cured under conditions simulating mass concrete were tested to assess their early-age cracking behavior. These results were then compared to the response of a normalweight concrete made with river gravel and river sand as coarse and fine aggregate, respectively. This mixture will be referred to as the reference mixture and did not contain any lightweight aggregates.

Two rigid cracking frames (RCF) and one free-shrinkage frame (FSF) were used for evaluating the cracking tendency and cylinders were match-cured simultaneously to test the time-dependent development of mechanical properties. A schematic of the test equipment and procedure is shown in Figures 4-1 and 4-2. Figure 4-1 schematically shows the match-cured temperature conditions used to test all concretes. Concrete in the match-cured RCF was cured to mass concrete (column) conditions and the thermal and autogenous stresses were recorded. The concrete in the second RCF, as shown in Figure 4-2, was tested under isothermal conditions; therefore, only stresses developing because of autogenous shrinkage were recorded. The FSF recorded the free-shrinkage strains for the match-cured specimens, with the concrete cylinder specimens match-cured in a similar fashion.

The typical water-to- cementitious materials (*w/cm*) for mass concrete construction varies between 0.38 and 0.55, hence two groups of concrete mixtures with *w/cm* mixtures of 0.38 and 0.45 were tested. Autogenous shrinkage development is important only for the low *w/cm* mixtures because for higher *w/cm* mixtures autogenous shrinkage is not a concern (Weiss and Bentz 2010).

Class F fly ash is used increasingly in mass concrete mixtures since it decreases the heat of hydration (Schindler and Folliard 2005). In this study, Class F fly ash at a cement replacement level of 30 percent by mass was used, because a large amount of mass concrete construction used fly ash in the range of 25 to 30 percent and many state agencies have a minimum requirement of approximately 25 to 30 percent (by mass) of fly ash for mass concrete construction (Jahren et al. 2014).

Each group of *w/cm* mixtures contained five concrete mixtures, and they comprised of a reference concrete mixture and four concretes containing varying amounts of lightweight aggregate. The use of two different *w/cm* mixtures allows one to assess the effect of *w/cm* on the cracking tendency and stress evolution of the lightweight aggregate and control concrete mixtures. The ConcreteWorks program developed at UT Austin (Poole et al. 2006) was used to predict the concrete temperature development for each specific concrete mixture. Since ACI 301 (2016) recommends that an element with least dimension of 4ft or greater be designated as mass concrete, the 8×8 ft column modeled in this study is representative of mass concrete. The temperature development was modeled for an 8 × 8 ft size column for both *w/cm* concretes. The temperature modeling is discussed in detail in Section 4.5.

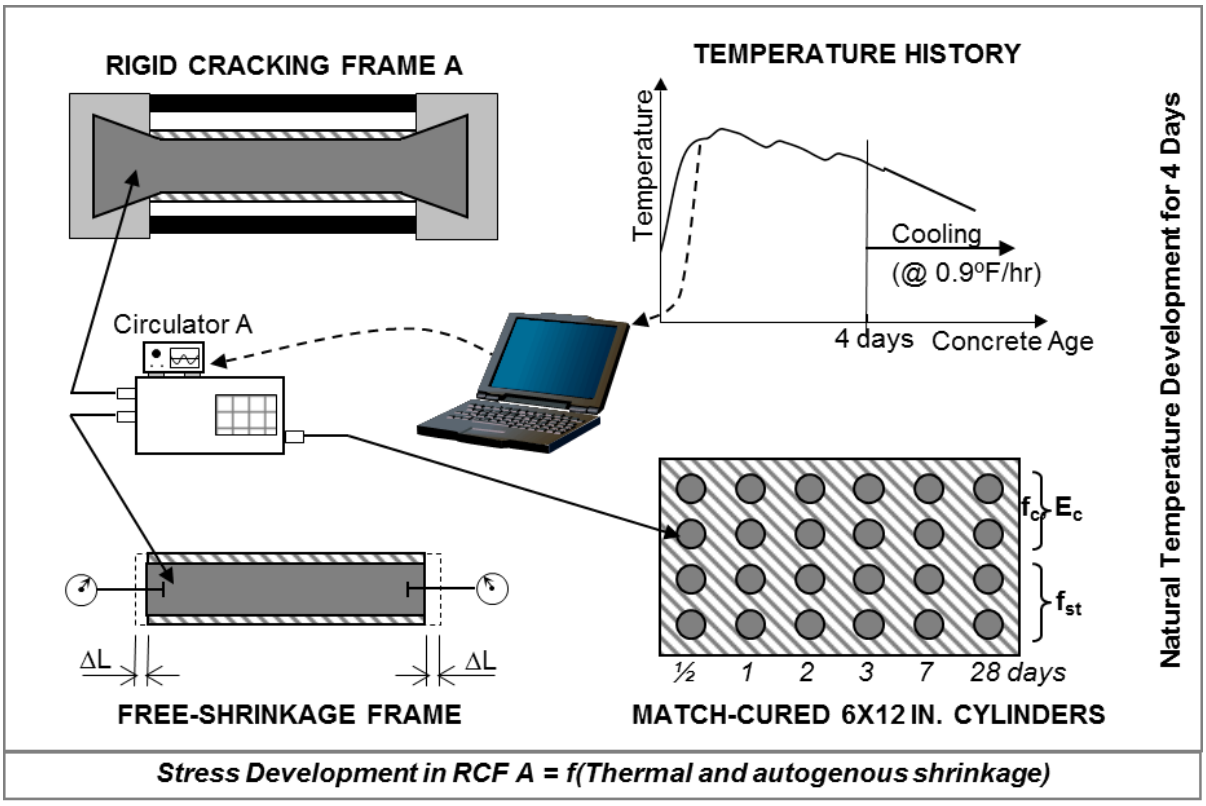

Figure 4-1: Mass-concrete curing test setup

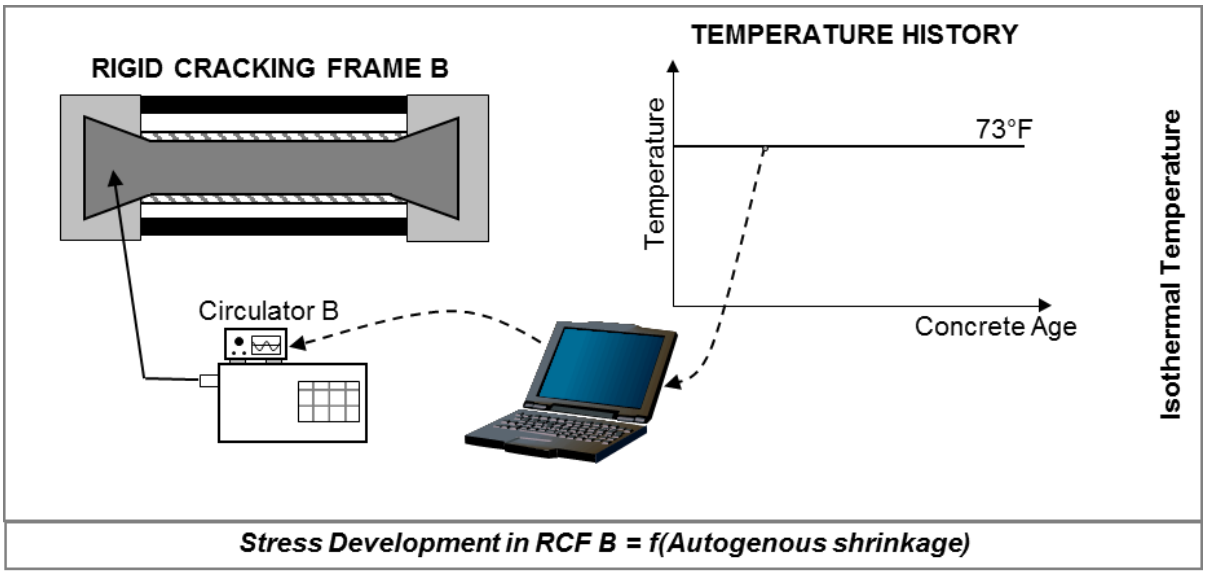

Figure 4-2: Isothermal curing test setup

4.2 LIGHTWEIGHT AGGREGATES

4.2.1 Source

Expanded shale was used in the production of all concretes containing lightweight aggregates. The type and source of the LWA is shown in Table 4-1. One fine and one coarse gradation of LWA was shipped directly from the supplier in super sacks to Auburn University's Concrete Materials Laboratory.

Table 4-1: Lightweight aggregate source, type, and properties

Item	**Shale Lightweight Aggregate**	
Source	Norlite Aggregates (Albany, NY)	
Type of LWA	Fine Aggregate	Coarse Aggregate
Particle size	0 to #4	#4 to ¾ in.
Relative density (SD[§])	1.67	1.35
Pre-wetted absorption *	20%	18%
Fineness modulus	3.3	NA

Note: * Measured water absorption after soaking in water for 7 days.
[§] Relative density at surface-dry state after 7 days of soaking in water.

4.2.2 Properties

The LWAs were sampled upon arrival and their gradations obtained by sieve analysis as per ASTM C136 (2014). The specific gravity and moisture content were obtained in accordance with ASTM C127 (2014) and ASTM C128 (2014). The samples were prewetted for a period of 7 days. In order to obtain the absorption of pre-wetted LWA, the

lightweight aggregates were sampled as per ASTM C1761 (2015). This method is usually known as the “paper towel method” and utilizes commercial grade paper towels to determine the surface-dry condition of the LWAs. The particle size, relative density, pre-wetted absorption, and fineness modulus results are shown in Table 4-1. The gradations are provided in Appendix A.

4.2.3 Lightweight Aggregate Preconditioning

The lightweight aggregates (LWA) were placed in water-filled 55-gallon plastic barrels for moisture preconditioning. The LWAs were submerged in plastic barrels for a period of 7 days, as shown in Figure 4-3. The presence of valves at the bottom of the barrel aided in draining the water. A 6 in. thick filter layer of normalweight aggregates were placed at the bottom of one of the barrels for filtering fine LWA. This layer facilitated draining of water without any clogging occurring in the valve. Water was slowly drained after prewetting to reduce the amount of fine LWA lost. Oval-shaped steel tanks with a design similar to the barrels were also used. After soaking for 7 days, the excess water was drained and the lightweight coarse and fine aggregate separately placed on a plastic sheet. The excess surface moisture was allowed to evaporate until the surface-dry condition was achieved. Following which, they were placed in sealed five- gallon buckets for batching. Prior to mixing the concrete, aggregate samples were sampled to determine their moisture content, which was used to make moisture corrections on the concrete proportions. The laboratory environment was maintained at a constant temperatur2e of 73°F; hence no temperature preconditioning was required.

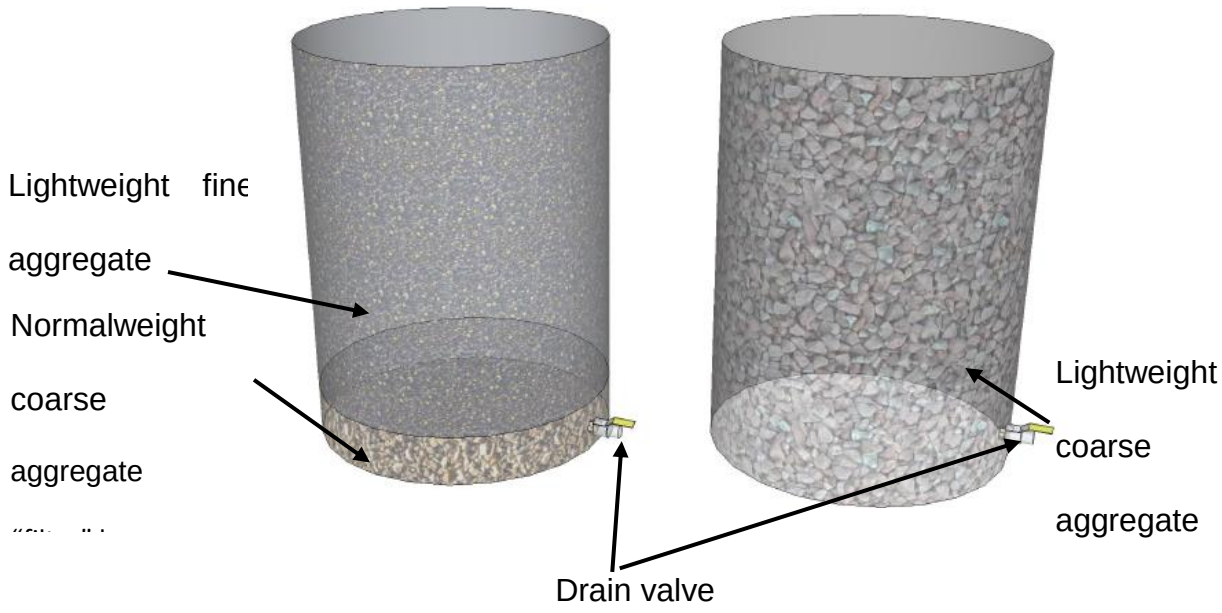

Figure 4-3: Illustration of barrel setup used for lightweight aggregate preconditioning (Byard and Schindler 2010)

4.3 MIXTURE PROPORTIONS

Five types of concrete mixtures were assessed at two different *w/cm*. They consisted of a reference normalweight concrete (REF), internally cured (IC) concrete, sand-lightweight (SLW) concrete, inverse sand-lightweight (ISLW) concrete, and all-lightweight (ALW) concrete.

For clarity, a mixture identification system is used in this study to refer to a specific concrete mixture containing a specific amount of LWA and *w/cm*. The identification system is as follows:

Mixture Type and ***w/cm***

REF	= Reference concrete	0.45
ICC	= Internally cured concrete	0.38
ISLWC	= Inverse sand-lightweight concrete	
SLWC	= Sand-lightweight concrete	
ALWC	= All-lightweight concrete	

Example: **ALWC 0.45,** represents the all-lightweight concrete with a *w/cm* of 0.45.

The mixture proportions for the two groups of concretes made at *w/cm* of 0.45 and 0.38 are shown in Tables 4-2 and Tables 4-3, respectively. LWAs may never reach a state of 100 percent saturation, hence the term saturated-surface dry is not used for them, and instead the term pre-wetted surface dry is used for LWAs. Therefore, the LWA batch weights are for pre-wetted surface-dry (SD) conditions.

Table 4-2: Proportions and properties for all *w/cm* = 0.45 mixtures

Item	**REF** **0.45**	**ICC** **0.45**	**ISLWC** **0.45**	**SLWC** **0.45**	**ALWC** **0.45**
Water Content (lb/yd^3)	263	263	263	263	263
Cement Content (lb/yd^3)	410	410	410	410	410
Class F Fly Ash Content (lb/yd^3)	175	175	175	175	175
SSD Normalweight Coarse Aggregate (lb/yd^3)	1740	1740	1425	0	0
SD Lightweight Coarse Aggregate (lb/yd^3)	0	0	0	910	857
SSD Normalweight Fine Aggregate (lb/yd^3)	1220	1000	0	1190	0
SD Lightweight Fine Aggregate (lb/yd^3)	0	140	975	0	820
Water-Reducing Admixture (oz/yd^3)	16.0	14.0	11.0	0.0	0.0
Mid-Range Water-Reducing Admixture (oz/yd^3)	0.0	0.0	3.0	22.0	18.0
Rheology-Controlling Admixture (oz/yd^3)	0.0	0.0	10.0	0.0	32.0
Air-Entraining Admixture (oz/yd^3)	1.0	1.0	1.0	3.5	3.5
Target Total Air Content (%)	5.0	5.0	5.0	5.0	5.0
Water-to-Cementitious Materials Ratio (*w/cm*)	0.45	0.45	0.45	0.45	0.45

Table 4-3: Proportions and properties for all *w/cm* = 0.38 mixtures

Item	**REF** **0.38**	**ICC** **0.38**	**ISLWC** **0.38**	**SLWC** **0.38**	**ALWC** **0.38**
Water Content (lb/yd^3)	243	243	243	243	243
Cement Content (lb/yd^3)	435	435	435	435	435
Class F Fly Ash Content (lb/yd^3)	195	195	195	195	195
SSD Normalweight Coarse Aggregate (lb/yd^3)	1740	1740	1425	0	0
SD Lightweight Coarse Aggregate (lb/yd^3)	0	0	0	910	857
SSD Normalweight Fine Aggregate (lb/yd^3)	1220	1000	0	1190	0
SD Lightweight Fine Aggregate (lb/yd^3)	0	140	975	0	820
Water-Reducing Admixture (oz/yd^3)	20.0	20.0	0.0	0.0	0.0
Mid-Range Water-Reducing Admixture (oz/yd^3)	0.0	0.0	22.0	28.0	26.0
Rheology-Controlling Admixture (oz/yd^3)	0.0	0.0	12.0	0.0	34.0
Air-Entraining Admixture (oz/yd^3)	1.0	1.0	1.0	3.5	3.5
Target Total Air Content (%)	5.0	5.0	5.0	5.0	5.0
Water-to-Cementitious Materials Ratio (*w/cm*)	0.38	0.38	0.38	0.38	0.38

The reference mixture as explained in previous sections was proportioned to represent mass concrete mixtures commonly used in the state of Alabama and meets the requirements of the Alabama Department of Transportation. In this study the ICC was proportioned to meet the requirements of normalweight concrete as per AASHTO LRFD Bridge Design Specifications (2016). Hence the amount of LWA was calculated so that the equilibrium density of the mixture was 135 pcf or greater. Therefore, the ICC mixtures contained less LWA than that required by the Bentz formula (Bentz et al. 2005).

The SLWC contained coarse LWA and normalweight fine aggregate, the ISLWC contained coarse normalweight aggregates and fine LWA, while ALWC contained both coarse and fine LWA. A slump of 4 ± 1 in. and total air content of 5.0 ±1.5% was targeted.

The measured densities were to be within ± 1 pcf of the calculated density for each concrete mixture. These values represent typical fresh concrete properties used in mass concrete production.

The amount of internal curing water required by the Bentz formula and the amount of internal curing water provided by each concrete, is presented in Table 4-4. The absorption values and the desorption coefficients were computed from values presented from Equation 3-9 (Bentz et al. 2005). As can be seen, the amount of internal curing water supplied by the LWA is less than the amount required by the Bentz formula. During the internal-curing process, it is assumed that the normalweight aggregate does not contribute to the process of internal curing, owing to its low absorption capacity in comparison to LWA. The data in Table 4-4 indicate that for ICC mixtures having *w/cm* of 0.45 and 0.38, the amount of internal curing water provided is 33 and 38 percent, respectively, less than the amount of water required by the Bentz formula. All SLW, ISLW, and ALW concretes supply more water than that required by the Bentz formula.

Table 4-4: Total absorbed water available from LWA and water required by Equation3-9

Concrete Type	**Internal Curing Water Available from LWA (lb/yd^3)**		**Water Required by Equation 3-9 (lb/yd^3)**	
	***w/cm* = 0.45**	***w/cm* = 0.38**	***w/cm* = 0.45**	***w/cm* = 0.38**
Internally cured concrete	27	27	41	44
Inverse sand-lightweight concrete	195	195	41	44
Sand-lightweight concrete	180	180	41	44
All-lightweight concrete	318	318	41	44

4.4 TEST METHODS

4.4.1 Heat of Hydration Characterization

The hydration reaction of portland cement and fly ash with water is an exothermic reaction, resulting in a temperature rise of the concrete specimen. Knowledge of this temperature rise during the hydration process helps in predicting the early-age temperature history of a concrete structure (Morabito 1998). The temperature rise over a period of time is unique for every concrete mixture proportion (Schindler and Folliard 2005). Semi-adiabatic calorimetry is employed in this study to characterize the temperature rise of each concrete.

Adiabatic calorimetry refers to a test method wherein a specimen is placed in an insulated chamber and no heat exchange (loss or gain) occurs with the surroundings. Semi-adiabatic calorimetry (SAC) is the condition in which, the rate of heat exchange is controlled from the concrete specimen with the help of insulating material and no external sources of heat are employed (Morabito 1998). Calibration of the SAC ensures that the heat loss is known and accounted for. This setup is convenient and provides accurate means of measuring the heat released during the hydration process (RILEM 119-TCE 1998).

In this study, a QDrum (iQuadrel) illustrated in Figure 4-4, was used as SAC. The laboratory equipment for performing the test was supplied by Digital Site Systems, Pittsburg, PA. No standard ASTM test procedure is available, therefore a draft RILEM procedure was used (RILEM 119-TCE 1998). The SAC setup comprised of an insulated 55-gallon drum, instrumented with sensors to measure the concrete temperature, ambient temperature, and the amount of heat lost through the calorimeter wall.

Prior to testing the heat of hydration of concrete, a calibration test must be performed to calculate the thermal losses of the SAC. Water of a known temperature was placed inside and the thermal losses of the calorimeter computed (Schindler and Folliard 2005). The thermal loss is a function of the insulating components and the differences between the sample and ambient temperature.

Trial batches were performed to establish whether the total air content, slump, and other fresh concrete properties met the required mixture design parameters. Following which, fresh concrete was consolidated in a 6×12 in. cylinder mold, that was weighed before being placed in the calorimeter. A temperature probe was fitted into the mold and the

drum was sealed. Data was recorded for a period of 5 days. The hydration parameters were then computed using the SAC data (Schindler and Folliard 2005).

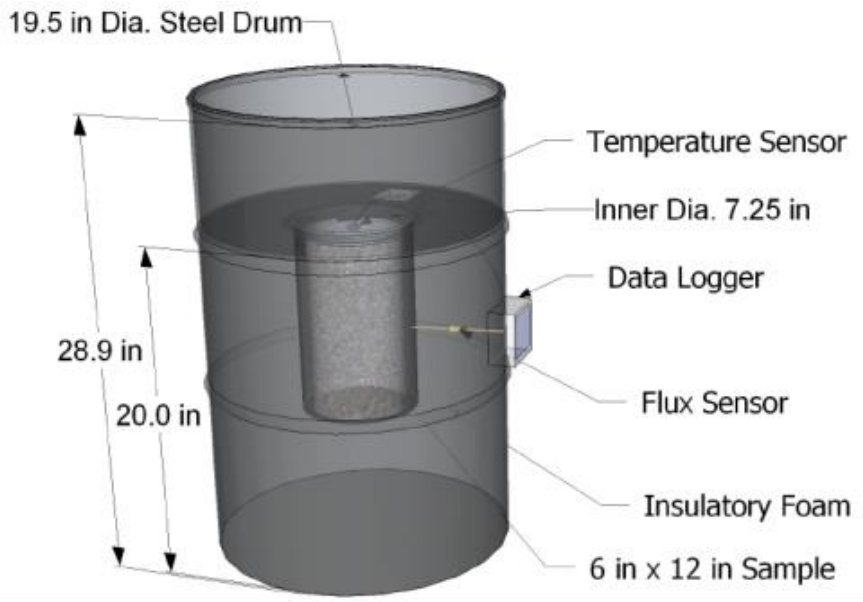

Figure 4-4: Semi-adiabatic calorimeter (adapted from Weakley 2009)

4.4.2 Thermal Diffusivity Evaluation

To assess the specific heat of the lightweight aggregates, the thermal diffusivity of the concrete was back-calculated using the SAC test apparatus. After casting, a 6×12 in. cylinder was moist cured for a period of 7 days. After 7 days, the concrete cylinder was sealed and heated to approximately 160˚F and then sealed in the SAC. The thermal decay was measured for a period of 5 days and the thermal diffusivity was back-calculated to fit the measured thermal decay curve. This allows one to determine the specific heat of the coarse LWA in the SLW concrete, since the specific heat of the remaining aggregates are established from published values, shown in Table 4-5 (Xu and

Chung 2000; Robertson 1988). The same procedure was repeated for the ALW concrete and the specific heat of the fine LWA was determined.

Table 4-5: Specific heat of concrete materials from published data

Concrete Raw Material	**Specific heat (Btu/lb per °F)**
Portland cement	0.17
Fly ash	0.17
River gravel coarse aggregate	0.20
Natural river fine aggregate	0.20
Water	1.00

With knowledge of the thermal and hydration parameters of the concrete, a temperature profile for mass concrete placement during fall season (placement temperature ~73˚F) was determined using the ConcreteWorks program (Poole et al. 2006). ConcreteWorks allows one to simulate the environmental conditions such as wind, temperature, humidity, etc. and other factors such as formwork, concrete placement time, etc. The temperature modeling conditions and other parameters used for the ConcreteWorks analysis are covered in detail in Section 3.5.

4.4.3 Restrained Stress Development

The rigid cracking frame (RCF) was initially developed by Dr. Springenschmidt in Germany in the 1970s for evaluating thermal stresses in concrete pavements (Springenschmidt et al. 1994). It comprises of a 6 × 6 × 49 in. prismatic specimen with

dogbone-shaped ends held in two mild-steel cross-heads as shown in Figure 4-5(a). The dogbone-shaped ends have steel teeth to help firmly grip the concrete. The specimen is restrained by two Invar side bars extending along both sides as shown in Figure 4-5(b). Strain gauges are mounted on the Invar bars that measure strains continuously during the test. The insulated and temperature controlled formwork is completely lined with plastic sheeting and is firmly supported by the Invar bars. The plastic sheeting prevents any moisture loss and reduces friction between the form surface and the concrete. The temperature profile simulated was for an 8 × 8 ft column placed in fall conditions. The temperature profile development is discussed in Section 4.5. After a period of 96 hours, if no cracking is observed in the concrete, it is cooled at a rate of 0.9˚F/hr until cracking occurs. The stress response was measured every five minutes with the help of a data acquisition system. In order to test autogenous stress development, the concrete was subjected to isothermal conditions (73˚F) and the stress response recorded.

a)

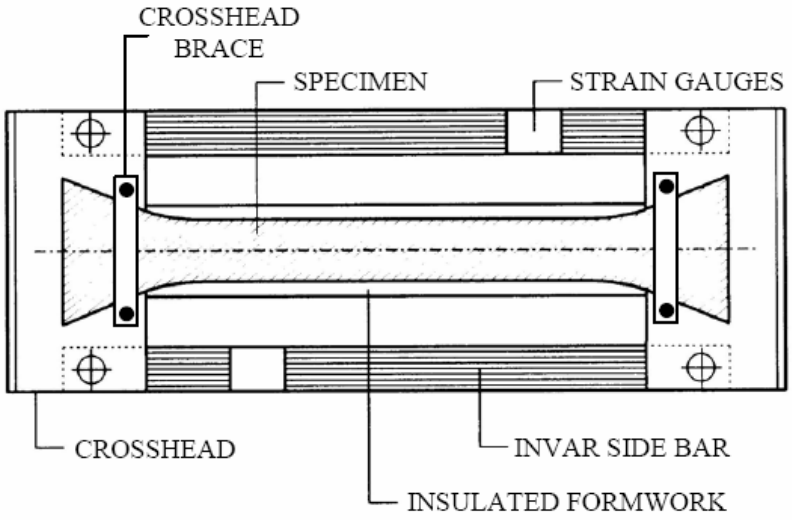

b)

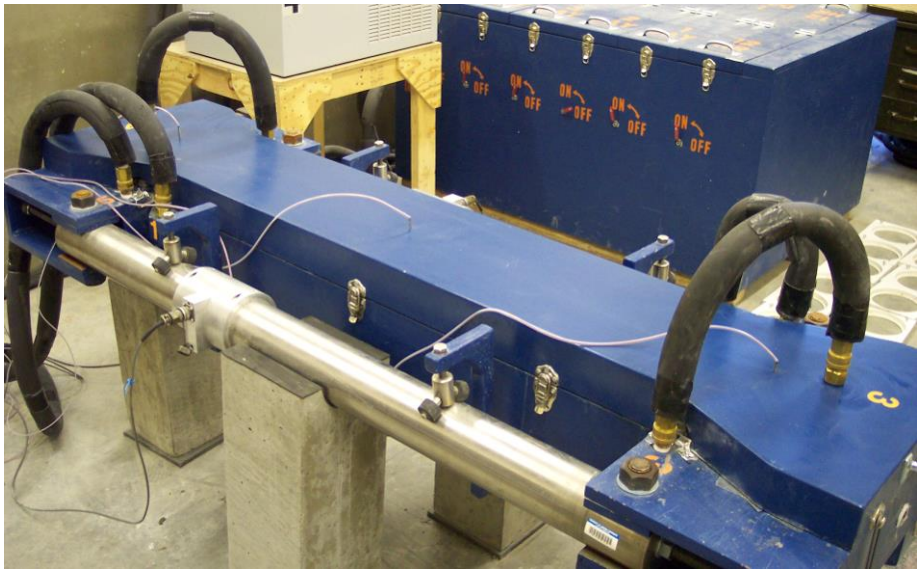

Figure 4-5: Rigid cracking frame test setup: a) Schematic of test setup (Mangold 1998)

and

b) Actual equipment used (Meadows 2007)

Fresh concrete is placed in two lifts and consolidated in the formwork using a needle vibrator. After finishing, a plastic sheet is placed on top of the concrete surface and taped to the formwork to prevent any moisture loss. Thus, drying shrinkage effects are not considered in this study. The formwork is closed from the top and connected via hoses to a circulator that circulates a mixture of water and ethylene glycol (50:50 ratio, by mass) through the formwork. The formwork contains 0.5 in. diameter copper tubes, which enables subjecting the concrete to any target temperature profile.

After final set, stresses start to develop due to autogenous and thermal shrinkage. The Invar bars provide restraint to the movement of the concrete, which results in the development of concrete stresses. Consequently, the strain gauges on the Invar bars

record the strains, which are converted to stresses using a computer-aided software program. Thermocouples are also inserted in the ends and center of the specimen to record the concrete temperature.

The stress observed at the time of cracking is less than the splitting tensile strength measured from match-cured concrete cylinders. This is because of differences in the loading rate, test specimen size, and type of loading of the concrete specimen (Riding et al. 2014). The rate of loading is lower in the case of the RCF and a lower rate of loading produces lower apparent strengths (Neville 1995). The splitting tensile strength specimens were loaded to failure in less than five minutes, whereas the duration of the RCF tests cover a period of approximately 4 to 6 days (Meadows 2007; Byard 2011). The tensile stresses are spread over a larger area (6 × 6 × 49 in.) in the RCF than in the cylinders (12 × 6 in.), hence there is a higher probability of finding flaws in the larger specimen, which makes it more susceptible to fail at a lower apparent strength (also known as size effects). In addition, the concrete cylinders undergo a splitting tension test, which is an *indirect* tensile strength test, whereas the concrete in the RCF is subjected to direct tension. The ratio of cracking frame stress at failure to the splitting tensile strength at the same time is generally between 40 and 80 percent (Riding et al. 2014).

4.4.3.1 Variability in RCF stresses for same concretes

The stress development in concretes using the RCF was measured for the same concrete in two trials. The stress development is shown in Figure 4-6. It can be observed that the differences in stress development, stress at cracking and time of cracking for the two trials are less than 5 percent.. Thus variability in the stress development for the concretes with similar temperature conditions is low.

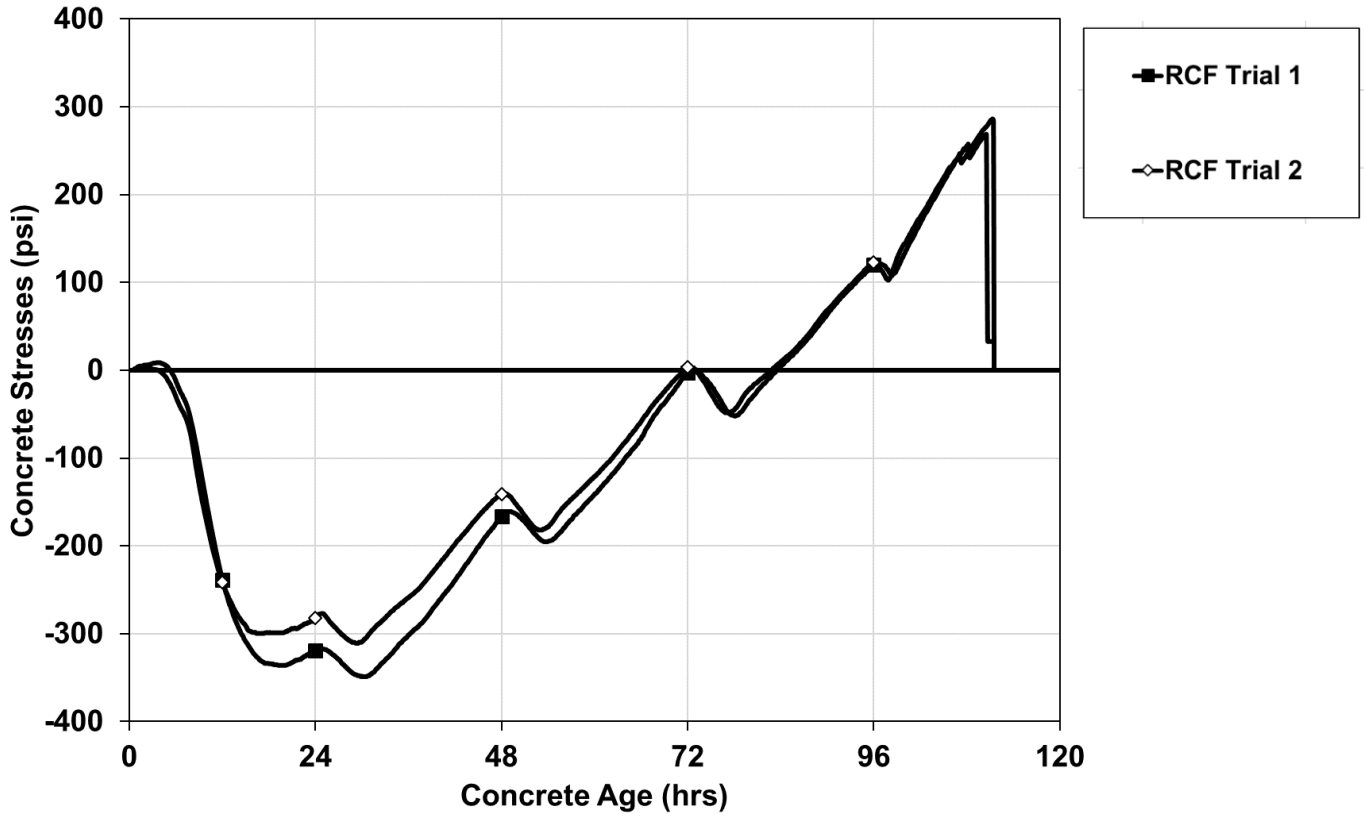

Figure 4-6: Variability in RCF stresses for the same concrete

4.4.4 Unrestrained Free Shrinkage

Free-shrinkage strain refers to the unrestrained uniaxial strain of the concrete. A free-shrinkage frame (FSF) was initially designed by Bjøntegaard (1999) in Norway to study autogenous shrinkage strains in concrete. A similar frame developed at Auburn University was used in this study and is shown in Figure 4-7(c).

The FSF used has dimensions of 6×6×24 in. and comprises of temperature-control formwork with two movable steel plates at its sides, with the whole setup supported on an Invar frame. The formwork has 0.5 in. copper tubes contained inside and is sealed to prevent any moisture loss. Two small holes on the top of the lid are present, which allow for temperature readings with the aid of thermocouples. The movable steel plates have

openings at their center, which allow for the insertion of an Invar rod at each end. One end of each Invar rod remains embedded in the concrete, while the other end is connected to a linear variable differential transformer (LVDT), which measures the expansion and contraction of the concrete. The formwork is connected via hoses to a circulator, which allows for the system to cure the concrete specimen to any desirable temperature profile. The formwork is lined with two layers of plastic sheeting, which prevents any adhesion between the frame and the concrete. A layer of oil lubrication separates the two plastic sheets, which allows for reduced friction and free movement of concrete. Fresh concrete is placed in the formwork, consolidated, and is sealed from the top with plastic to prevent any drying from taking place. Therefore, the effect of drying shrinkage is not considered in this test.

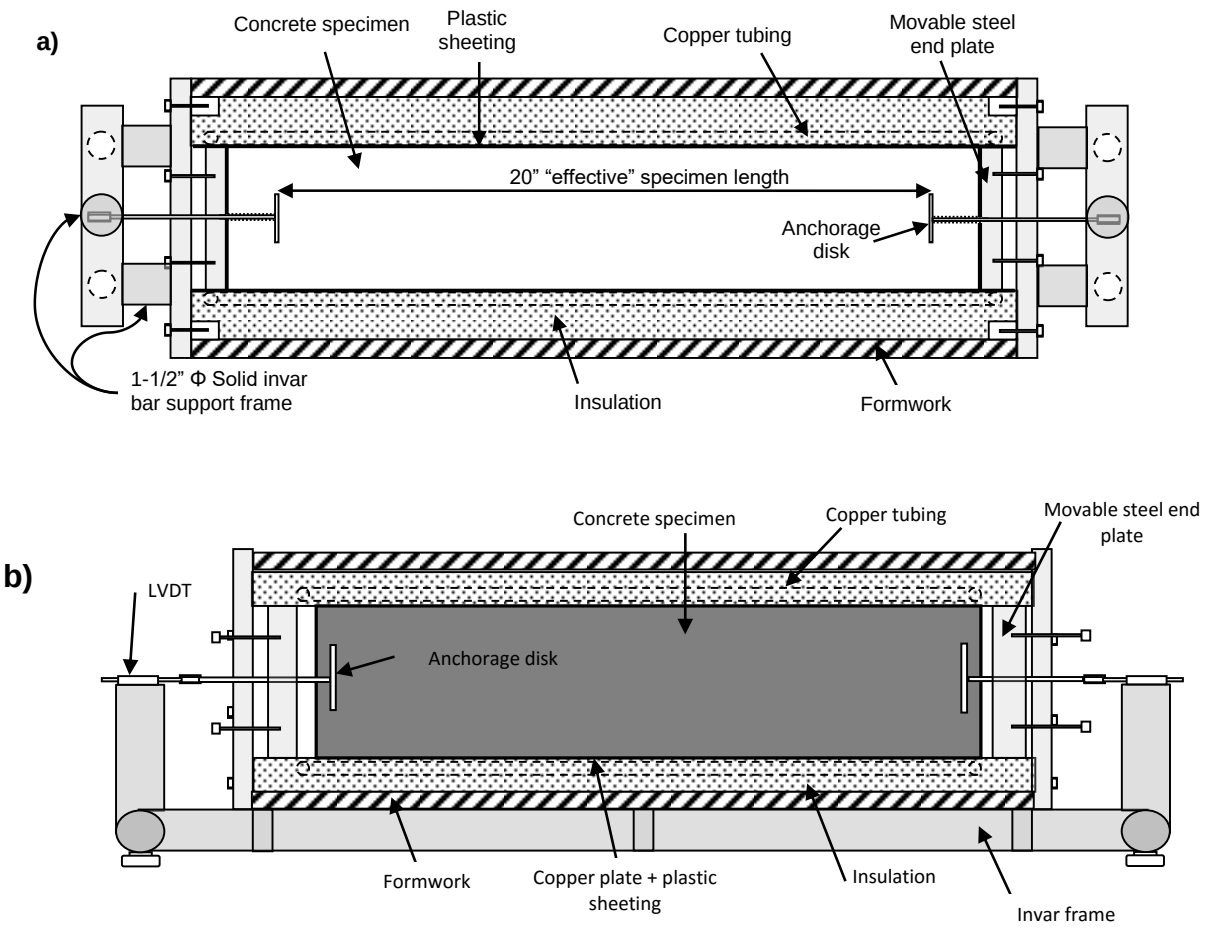

Figure 4-7: Free-shrinkage frame setup: a) Plan view schematic of test equipment, b) Section view schematic (Rao 2008), and c) Actual equipment used (Byard 2011)

The movable steel plates initially support the concrete ends; however, following initial set, the plates are moved back, which allows the concrete to move freely. Figures 4-7(a) and 4-7(b) indicate the position of the movable steel plates before and after initial set, respectively. Initial set is determined from penetration resistance as per ASTM C403 (2014), as discussed in Section 4.4.7. The unrestrained free shrinkage was recorded for all the concrete mixtures for a duration of 5 to 7 days. The temperature profile was match-cured to that of the RCF.

4.4.5 Concrete Mechanical Properties

The concrete mechanical properties were determined at 0.5, 1, 2, 3, 7, and 28 days by performing compressive, splitting tensile, and modulus of elasticity as per ASTM C39 (2014), ASTM C496 (2014), and ASTM C469 (2014), respectively.

A match-curing system was used to evaluate the mechanical properties and is shown in Figure 4-8. It comprises of a wooden box that can hold 24 6×12 in. cylinders, and is connected via hoses to a temperature control circulator. A mixture of water and ethylene glycol is circulated through a series of copper tubes running around each cylinder in the box, which allows the concrete cylinders to be simultaneously match-cured to the specimens in the RCF and FSF.

Figure 4-8: Cylinder match-curing system: a) Wooden box containing cylinders and b) A unit with two cylinders (Rao 2008)

4.4.6 Coefficient of Thermal Expansion

The coefficient of thermal expansion (CTE) of concrete is tested as per AASHTO T336 (2009). A 6×7 in. concrete cylinder is placed in a frame, shown in Figure 4-9, that is submerged in water. Mounted on the frame is a spring-loaded LVDT which is placed in contact with the concrete cylinder. The temperature of the water bath is varied between 50˚F to 122˚F, and the ensuing change in length of the concrete cylinder is measured. From the resulting displacements over the temperature changes, the coefficient of thermal expansion of the concrete can be calculated.

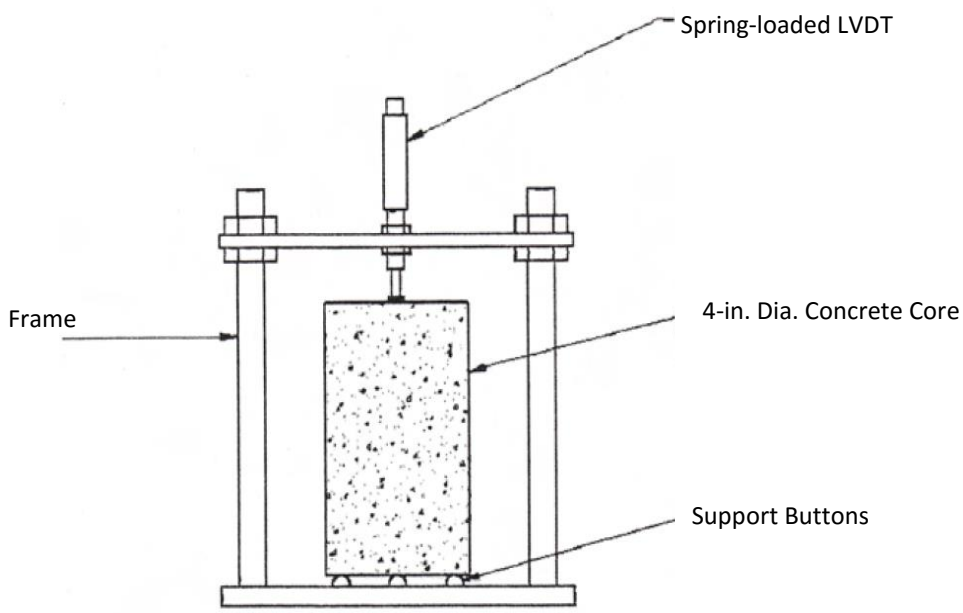

Figure 4-9: Schematic of the thermal expansion test setup (AASHTO T 336 2009)

For every concrete mixture, two 6 × 7 in. cylinders were cast and cured for a period of 28 days. Following which, they were tested in the CTE apparatus shown in Figure 4-10 as per AASHTO T336 (2009). Certain modifications were made to improve the repeatability of this test (Byard 2011). Specifically, ceramic inserts were added between the concrete specimen and the LVDT to mitigate any effects that temperature changes might have on the LVDT readings. Additionally, a small ceramic disk was used under the tip of the LVDT, along with a ceramic collar which was used to mount the LVDT onto the frame. The use of the ceramic collar was to ensure that temperature transfer was prevented from interfering with the LVDT through the mounting crossbar. Since the water levels in the temperature-controlled bath would fluctuate from time to time, an Invar spacer was employed and was placed on top of the concrete specimen. This provided additional height and ensured that the water fluctuations did not interfere with the LVDT readings.

The ceramic collar, disks, and other Invar spacer were present during the calibration procedure involving standard 6×7 in. steel specimens. Thus, the presence of these additions was accounted for in the calibration procedure and computations of the CTE.

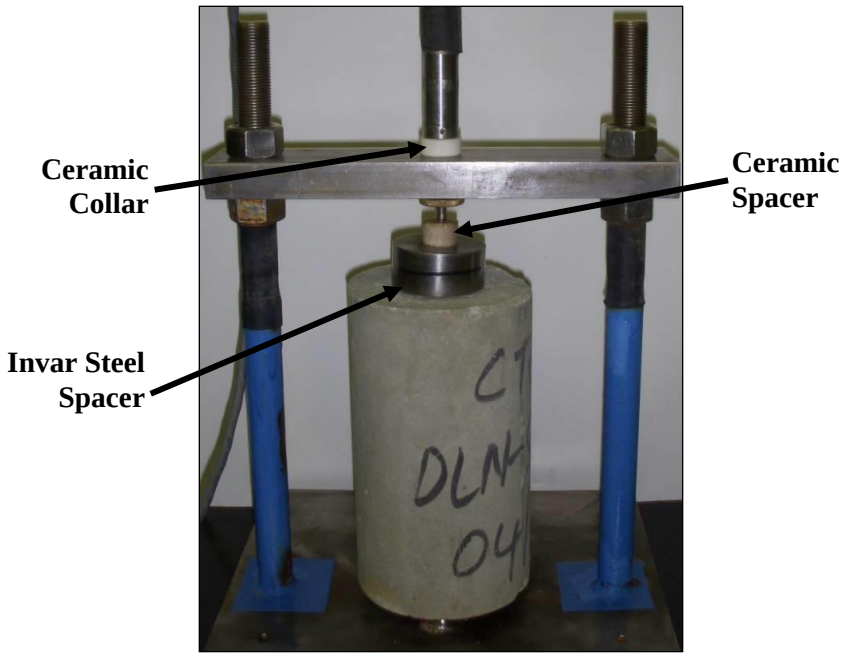

Figure 4-10: Modified AASHTO T336 setup used for CTE testing (Byard 2011)

4.4.7 Setting Test

The time of initial set is the time at which stresses in the concrete are discernable and can be recorded (Neville 2011). Initial set of concrete is established when the concrete reaches a penetration resistance of 500 psi, and final set is achieved when the penetration resistance reaches 4000 psi (ASTM C403 2014). To determine the time of initial set, each concrete mixture was sieved through a No. 4 sieve and the mortar was cast in a 6 × 8 in. cylindrical container and match-cured to the temperature in the RCF and FSF tests.

Penetration resistance tests were performed on the specimens as per ASTM C403 (2014).

4.4.8 Other Fresh Quality Control Tests

The concrete was mixed as per ASTM C192 (2014) under standard laboratory conditions. The slump, temperature, and the density were measured as per ASTM C143 (2014), ASTM C1064 (2014), and ASTM C138 (2014), respectively for every batch of concrete. The total air content was determined using the pressure method as per ASTM C231 (2014) for normalweight concretes. The volumetric method as per ASTM C173 (2014) was used to determine the total air content for concretes incorporating lightweight aggregates.

4.5 CONCRETE TEMPERATURE MODELING

The temperature modeling for the concrete mixtures was performed with the help of a software program called ConcreteWorks. It was developed at UT Austin and is utilized by TXDOT and some other states (Poole et al. 2006). ConcreteWorks can model the temperature history of a mass concrete element considering the geometry of the elements, type of aggregates used, chemical composition of cementitious materials, concrete mixture proportions, placement temperature, weather conditions (including humidity, solar radiations, and wind speeds), and type of formwork employed.

Initially semi-adiabatic calorimetry was performed on the concrete mixtures and the hydration parameters were determined (Schindler and Folliard 2005). Preliminary investigations were performed with ConcreteWorks to identify the appropriate mass

concrete element size for temperature modeling. The ALWC with a *w/cm* of 0.38, 30 percent Class F fly ash (substitution by mass), and Type I cement were chosen for preliminary modeling purposes, since it was expected that this mixture would experience the highest maximum concrete temperature (Byard and Schindler 2010). Three different mass concrete element sizes—4×4 ft, 8×8 ft, and 12×12 ft—were chosen for modeling purposes. These sizes are representative mass concrete element sizes for many transportation substructure components. The inputs used for modeling the temperature profile in ConcreteWorks were the hydration parameters along with the mixture proportion values and other factors including the placement date, type of formwork, etc. The results from ConcreteWorks include the maximum core and edge temperatures and are presented for the three mass concrete element sizes in Figures 4-10 and 4-11, respectively.

From Figures 4-11 and 4-12, it can be observed that the maximum core and edge temperatures for ALWC 0.38 are the highest for a 12×12 ft column. However, the differences between the maximum temperatures for 8×8 ft and 12×12 ft size column is minimal. Also, the maximum temperatures are below the critical DEF limit of 185°F (ACI 301 2016). Therefore, a 8×8 ft size column was chosen. From previous research (Tankasala et al. 2017), it was determined that thermal cracking is expected at the edge of cross-section when compared to the core, especially at early ages. All constituent materials were kept at room temperature (73˚F) prior to mixing. In order to ensure that all RCF tests are completed within a reasonable time frame, a duration of seven days was selected for temperature modeling and early-age concrete testing.

In this study, ConcreteWorks was used to model the edge temperature profile for a duration of four days (96 hours) for of 8 × 8 ft concrete column placed under fall placement conditions in Montgomery, Alabama on construction date of September 15th. The temperature profiles were modeled for both groups of *w/cm* concretes. After a period of four days (96 hours) if cracking has not occurred, the concrete was artificially cooled at a rate of 0.9˚F/hr until the onset of cracking. This approach is similar to the practice adopted by Breitenbucher and Mangold (1994) and Byard and Schindler (2010), except the cooling rate was halved. This gradual cooling rate ensured all the concrete specimens would fail within one week.

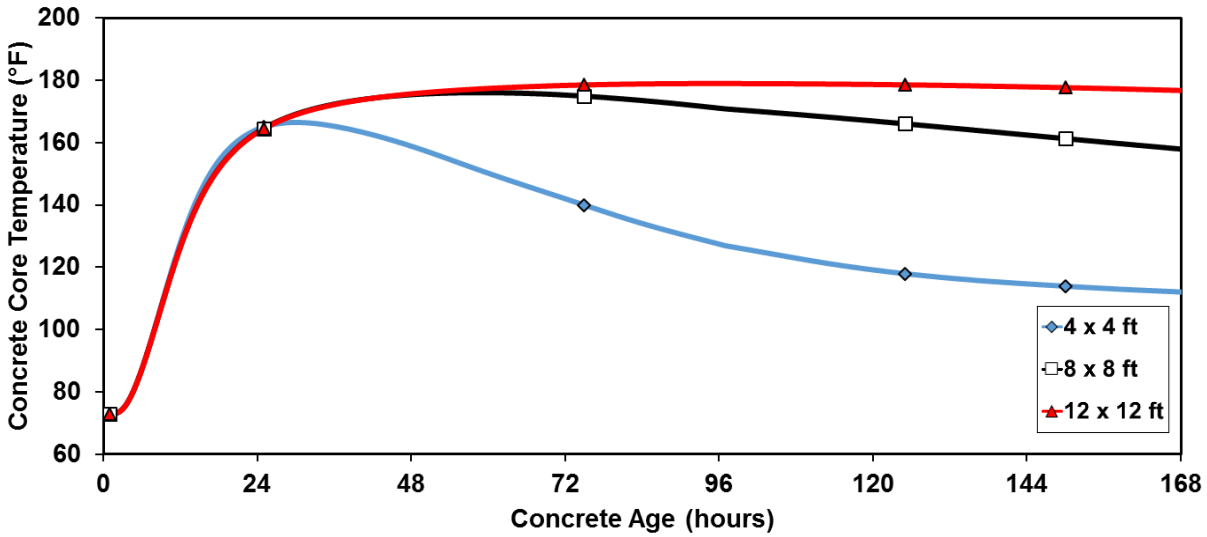

Figure 4-11: Concrete core temperature for various cross-section sizes (ALWC 0.38)

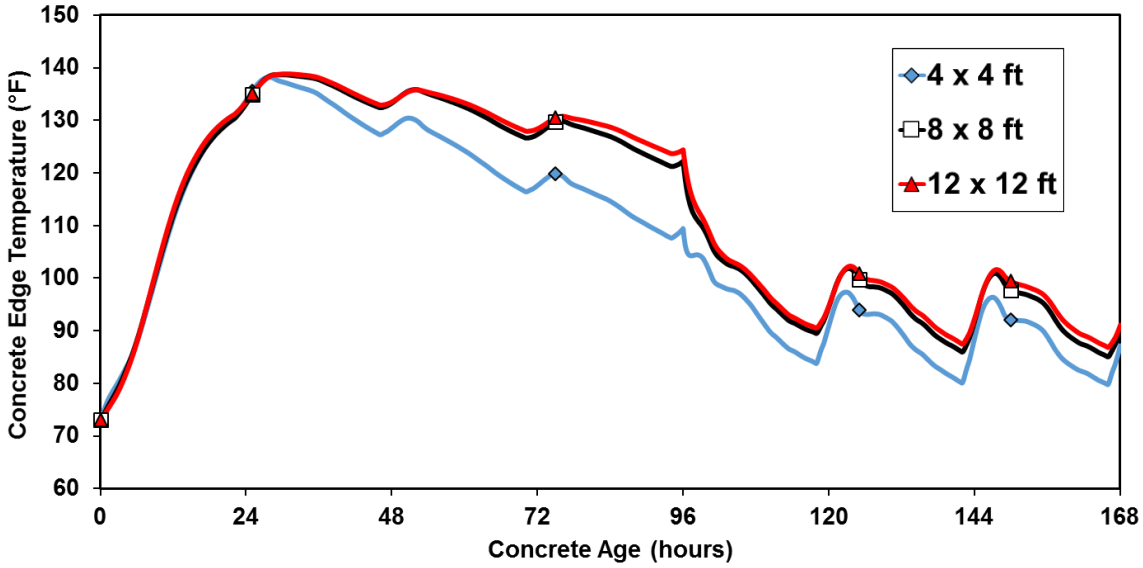

Figure 4-12: Concrete edge temperature for various cross-section sizes (ALWC 0.38)

4.6 OTHER RAW CONCRETE MATERIALS

4.6.1 Portland Cement

Type I cement was used in all concretes made in this study. The chemical composition and fineness of this cement are as shown in Table 4-6.

Table 4-6: Portland cement chemical composition and fineness

C_3S	C_2S	C_3A	C_4AF	Free CaO	SO_3	MgO	Blaine Fineness
60.3 %	18.2 %	5.4 %	11.3 %	0.9 %	2.6 %	1.3 %	351 (m^2/kg)

4.6.2 Fly Ash

The fly ash used for this study was Class F fly ash and was obtained from Boral Material Technologies. The chemical composition of this fly ash is listed in Table 4-7.

Table 4-7: Fly ash chemical composition

SiO_2	Al_2O_3	Fe_2O_3	CaO	MgO	SO_3	K_2O	Na_2O	Total Alkalis
55.7 %	27.9%	6.5 %	1.2 %	0.7 %	0.1 %	2.5%	0.3 %	2.0%

4.6.3 Normalweight Coarse and Fine Aggregates

The coarse aggregates used in this study were ASTM C33 (2014) No. 67 siliceous river gravel. The fine aggregate used was siliceous river sand. Both the aggregates were obtained from a concrete plant located in Auburn, Alabama which had stockpiles of the above aggregates. Sieve analysis was performed on sampled aggregates according to ASTM C136 (2014) and their gradations are shown in Appendix A. The specific gravity and absorption capacities of the aggregates were tested in accordance with ASTM C127 (2014) and ASTM C128 (2014), respectively. The properties of the normalweight aggregates are shown in Table 4-8.

Table 4-8: Properties of normalweight coarse and fine aggregate

Property	**Coarse Aggregate**	**Fine Aggregate**
Absorption Capacity (%)	0.16	0.34
Specific gravity	2.63	2.64
Fineness modulus	-	3.00

4.6.4 Chemical Admixtures

Chemical admixtures were used to obtain the desired slump and total air content for each concrete mixture. All chemical admixtures were supplied by the BASF Corporation. The dosages of all admixtures are provided in Tables 4-2 and 4-3.

MB AE90 was used as the air-entraining admixture (AEA) and it meets all the requirements of ASTM C260 (2014). The AEA dosage for each concrete mixture was determined with trial batches until the desired total air content was achieved.

The water-reducing admixture used was Pozzolith 322 N. A mid-range water-reducing admixture, (Polyheed 1025) was also used to achieve the desired slump for lower *w/cm* mixtures. Both these admixtures met all the requirements of ASTM C494 (2014). The dosages of the water-reducing admixtures were also determined using trial batches for each concrete mixture.

Due to the harsher nature and workability issues encountered for the ISLWC and ALWC, a rheology-controlling admixture (Navitas 33) was used. The rheology-controlling admixture helped to reduce the harshness of both the ISLWC and the ALWC and improve their workability. The rheology-controlling admixture met the requirements of ASTM C494 (2014) as a Type S Admixture.

Chapter 5

PART I: EXPERIMENTAL RESULTS

The results from the experimental work performed for this study are presented in this chapter. Discussions and analysis of results are presented in Chapter 5. The results contain herein include:

- Combined mixture gradations,
- Fresh concrete properties,
- Thermal properties,
- Concrete temperature histories,
- Restrained stress development,
- Unrestrained strain development, and
- Time-dependent development of mechanical properties.

5.1 CONCRETES WITH W/CM = 0.45

5.1.1 Combined Mixture Gradations

Five concrete mixtures with a *w/cm* of 0.45 and with four of them containing lightweight aggregates were produced and tested. The mixture proportions for these five concretes are presented in Table 4-2. In order to assess the impact of using lightweight aggregates on the fresh concrete properties, the combined gradations of these concretes are plotted on a 0.45-power curve and their workability factor determined. The 0.45-power curve in Figure 5-1 presents the particle packing of the combined aggregate gradation (Young,

Mindess and Darwin 2002). The workability factors (Shilstone 1990) for all 0.45 *w/cm* concretes are also presented in Figure 4-2.

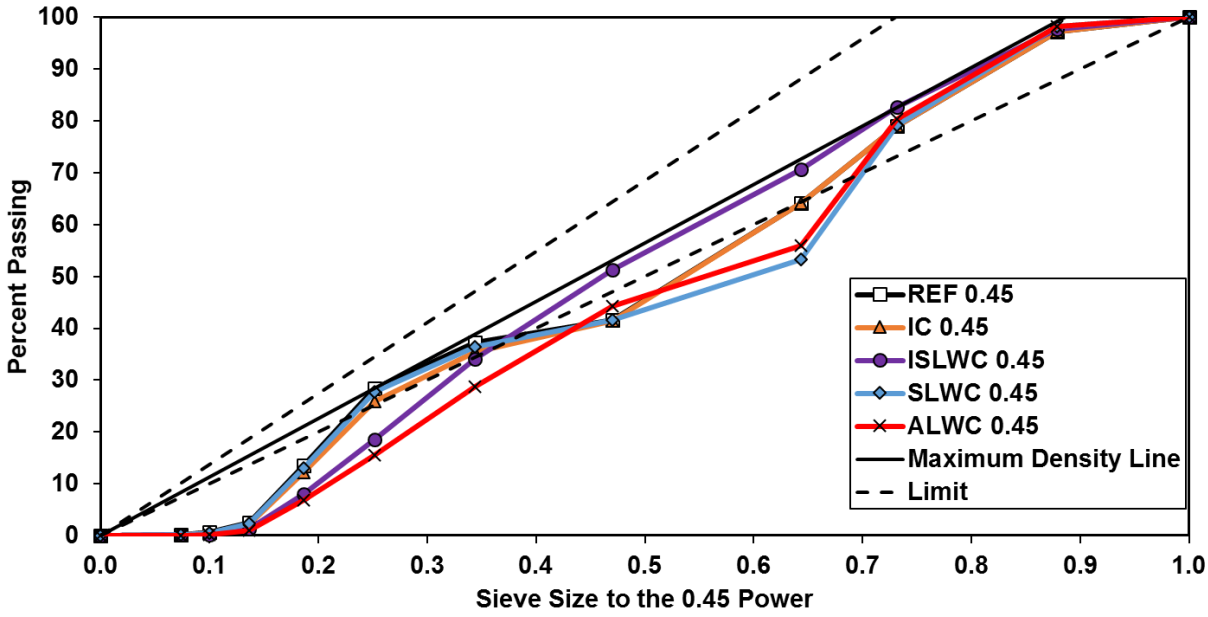

Figure 5-1: Combined gradation of all 0.45 *w/cm* concretes on the 0.45 power curve

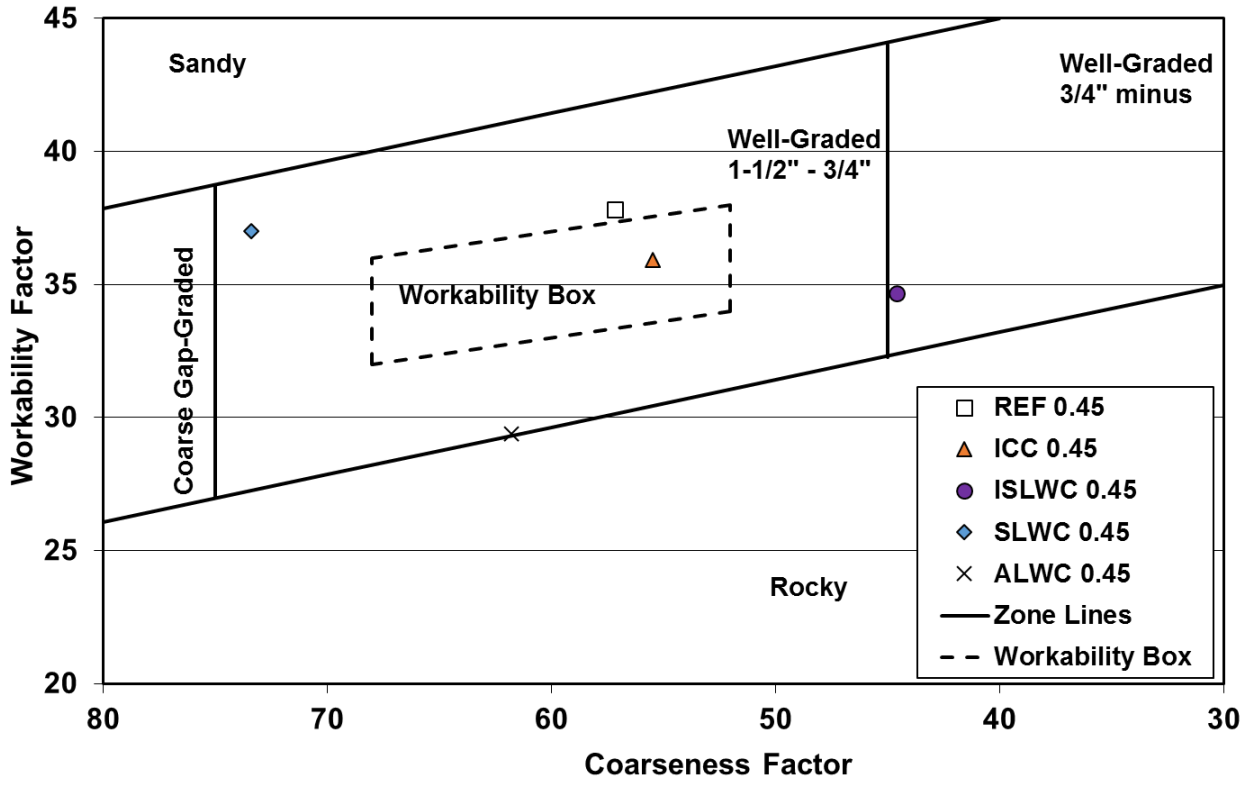

Figure 5-2: Workability factor versus coarseness factor for all 0.45 *w/cm* concretes

5.1.2 Fresh Concrete Properties

Trial batches were performed for each mixture until the desired slump and total air content were achieved. Following this, two batches of concrete were produced, with one batch being tested for mechanical properties of concrete and the other batch for RCF and FSF testing. The fresh properties of each mixture and batch are presented in Table 5-1. The "Δ density" column in Table 5-1 is the difference between the measured and designed densities after performing the corrections for measured total air content. A positive sign indicates that the measured density was higher than the calculated density and vice versa. The calculated equilibrium densities in accordance with ASTM C567 (2014) are also shown in Table 5-1. Only the slump of ISLWC 0.45 (Batch 1) was 0.5 in. below the

target slump range of 3 to 5 in.; however, the workability of this mixture was sufficient to allow it to be effectively consolidated.

Table 5-1: Measured fresh concrete properties for all 0.45 *w/cm* concretes

Concrete Mixture	Batch No.	Fresh Concrete Test Results				Calculated
		Slump (in.)	Temp. (°F)	Total Air (%)	Density (lb/ft^3)	Δ Density (lb/ft^3)
REF 0.45	1	3.5	74	5.0	141.5	0.5
	2	4.5	73	5.5	141.9	0.9
ICC 0.45	1	4.0	73	5.5	140.8	-0.7
	2	3.5	75	5.0	139.6	-1.0
ISLWC 0.45	1	2.5	73	4.0	120.6	0.1
	2	3.0	75	4.5	120.1	-0.4
SLWC 0.45	1	3.5	74	4.5	114.1	0.9
	2	3.5	73	5.0	114.2	1.0
ALWC 0.45	1	5.0	71	5.0	101.5	-0.6
	2	4.5	72	5.5	101.3	-0.8

5.1.3 Thermal Properties

The calculated equilibrium density, coefficient of thermal expansion, and thermal diffusivity are summarized in Table 5-2.

Table 5-2: Miscellaneous properties of all 0.45 *w/cm* concretes

Property	REF 0.45	ICC 0.45	ISLWC 0.45	SLWC 0.45	ALWC 0.45
Calculated Equilibrium Density (lb/ft^3)	139.0	135.5	115.4	110.6	95.6
Coefficient of Thermal Expansion (με/°F)	5.8	5.7	5.2	5.1	4.1
Thermal Diffusivity (ft^2/hr)	0.039	0.037	0.035	0.022	0.019

5.1.4 Peak Temperatures

The time-dependent development of temperatures at the core of an 8×8 ft column calculated from ConcreteWorks for the concretes with a *w/cm* of 0.45 are presented in Figure 5-3. The edge temperatures computed using ConcreteWorks were simulated in the rigid cracking frame, as mentioned in Section 5.5.

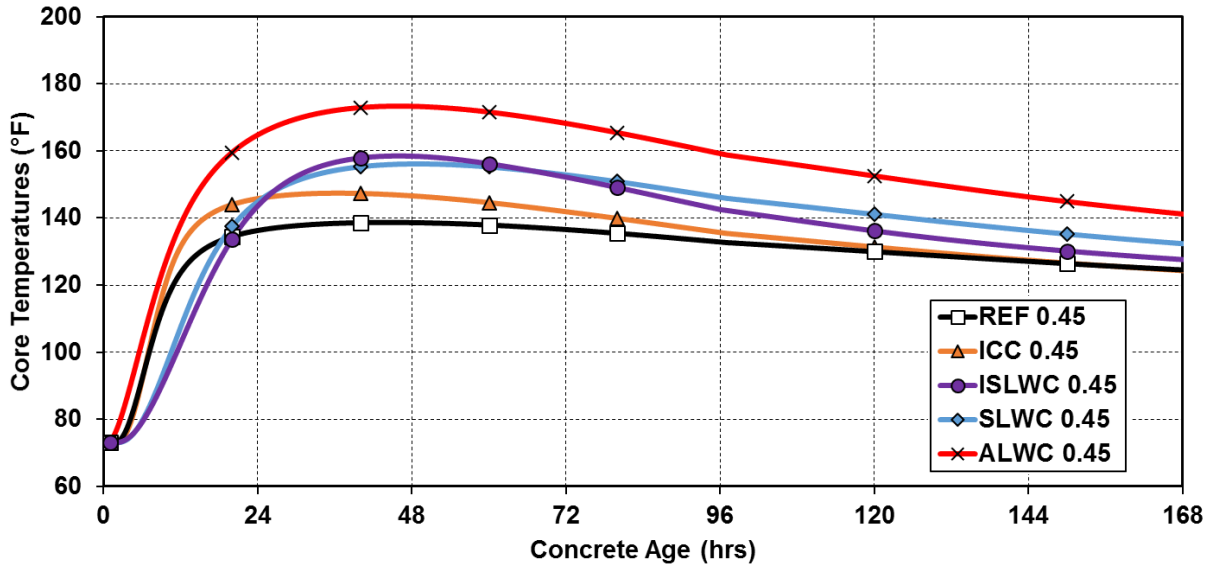

Figure 5-3: Temperature development in a 8×8 ft column for all 0.45 *w/cm* concretes

5.1.5 Restrained Stress Development

The restrained stress development measured with the RCF for all five concretes with *w/cm* of 0.45 and their curing temperatures are shown in Figures 5-4 and 5-5. The stresses are shown until the time of cracking, which is indicated by a sudden drop in stress. Isothermal stress development was not measured for any of the concretes with *w/cm* of 0.45, because their autogenous shrinkage is expected to be negligible (Weiss and Bentz 2010; Lura et al. 2003).

5.1.6 Unrestrained Strain Development

The unrestrained strain measurement measured with the FSF for all concrete specimens with a *w/cm* of 0.45 are shown in Figure 5-6. The concrete specimens were match-cured using the modeled temperature profiles of the RCF.

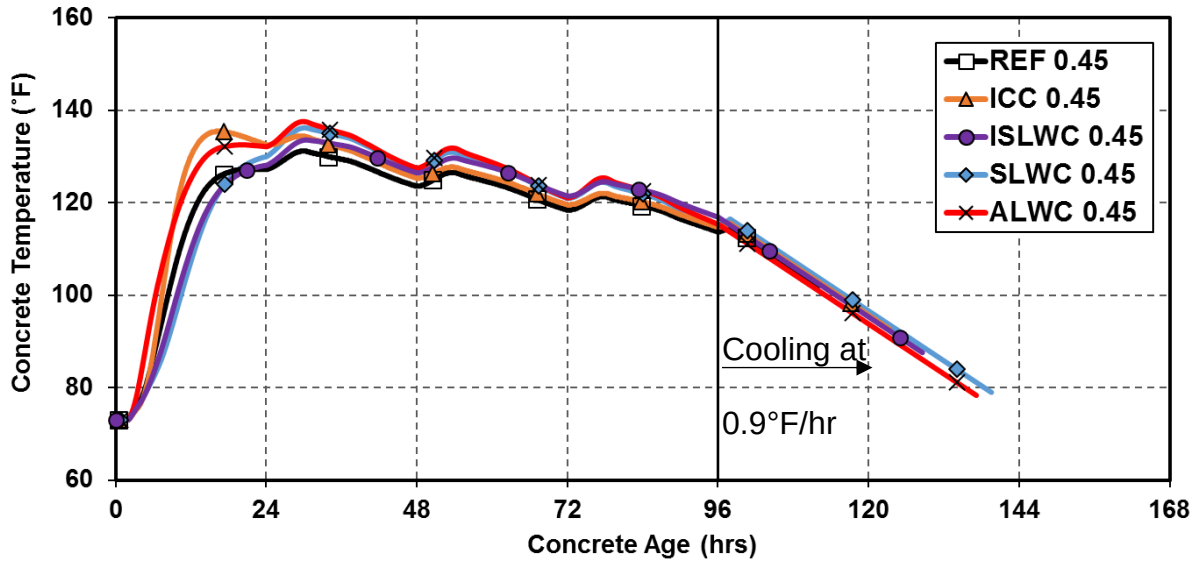

Figure 5-4: Concrete temperature profile for all 0.45 *w/cm* concretes

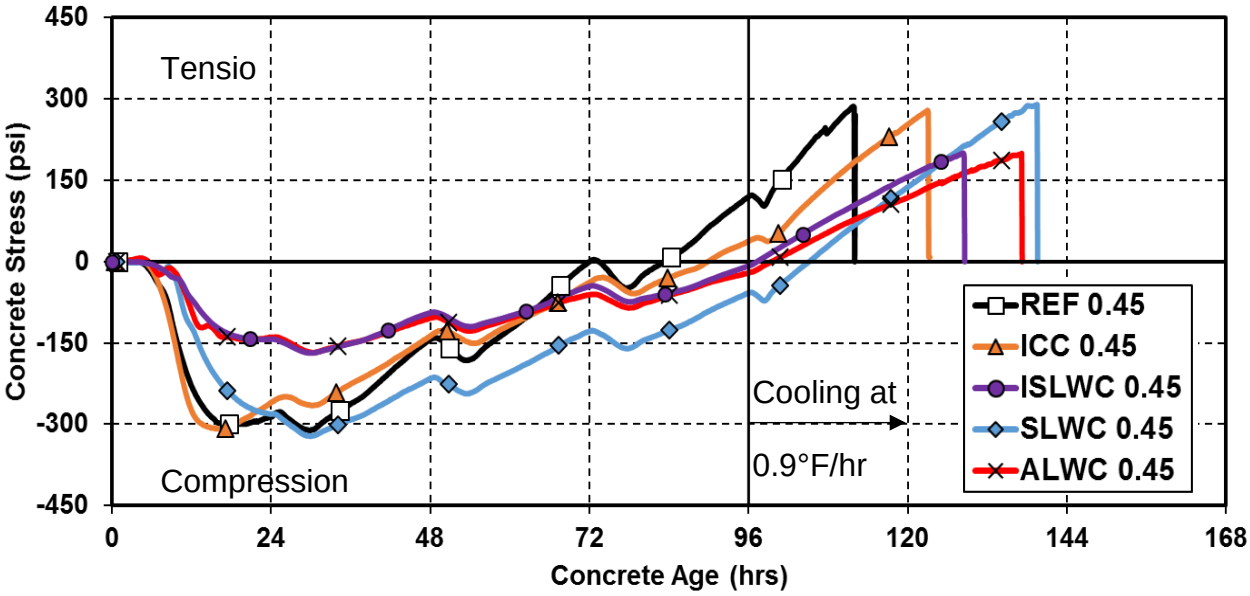

Figure 5-5: Restrained stress development for all 0.45 *w/cm* concretes

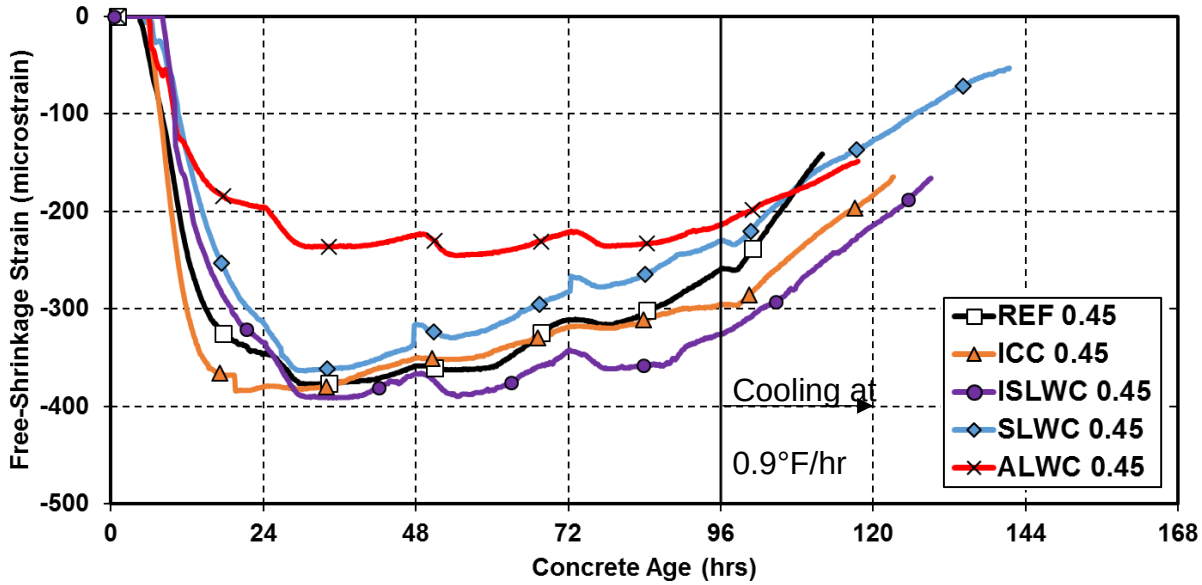

Figure 5-6: Unrestrained strain development for all 0.45 *w/cm* concretes

5.1.7 Summary of Rigid Cracking Frame Test Results

The maximum RCF temperature, time of cracking in the RCF, and the stresses at cracking are shown in Table 5-3 for all the concretes with *w/cm* of 0.45.

Table 5-3: Summary of RCF results for concrete with *w/cm* of 0.45

Item	***w/cm* = 0.45**				
	REF 0.45	**ICC 0.45**	**ISLWC 0.45**	**SLWC 0.45**	**ALWC 0.45**
Maximum RCF temperatures (°F)	130	135	135	136	139
Time of cracking (hrs)	110	123	128	139	137
Stress at cracking (psi)	290	290	200	290	200

5.1.8 Time-Dependent Development of Mechanical Properties

The time-dependent development of compressive strength, splitting tensile strength, and modulus of elasticity were tested for each concrete mixture. The measured values were averaged for two cylinders and are presented in Appendix B. Twenty-four cylinders were match-cured along with the RCF and FSF and were tested at varying ages. A regression analysis was performed according to ASTM C1074 (2014), which recommends the use of an exponential function. Best-fit curves were determined for the measured values and are plotted in Figures 5-7 to 5-9.

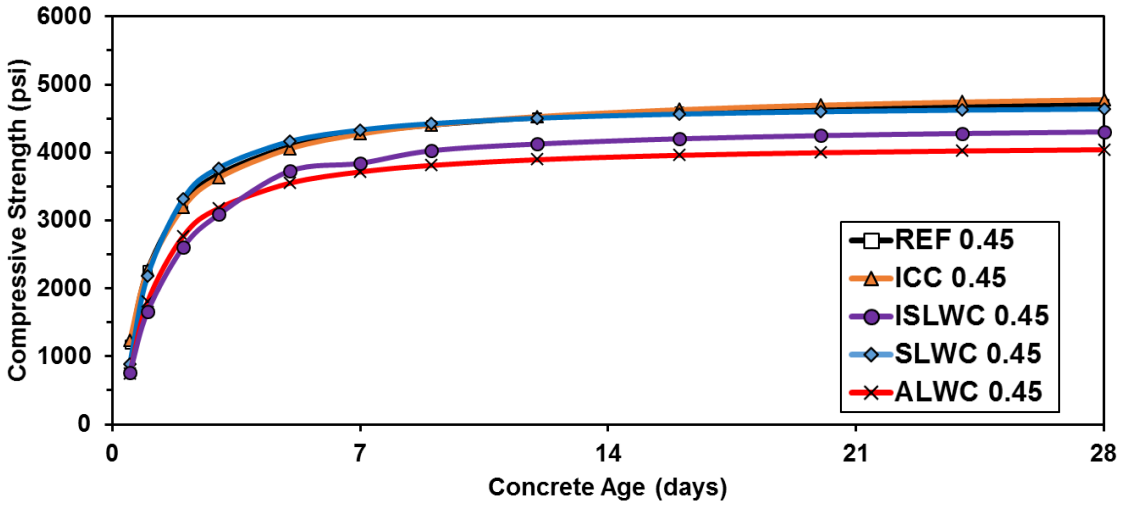

Figure 5-7: Compressive strength development for all 0.45 *w/cm* concretes

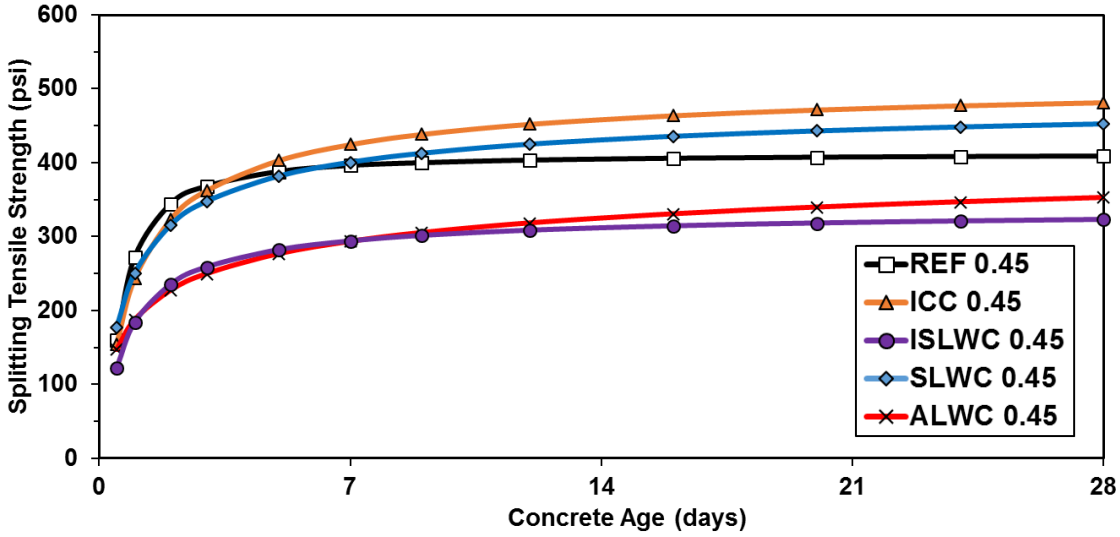

Figure 5-8: Splitting tensile strength development for all 0.45 *w/cm* concretes

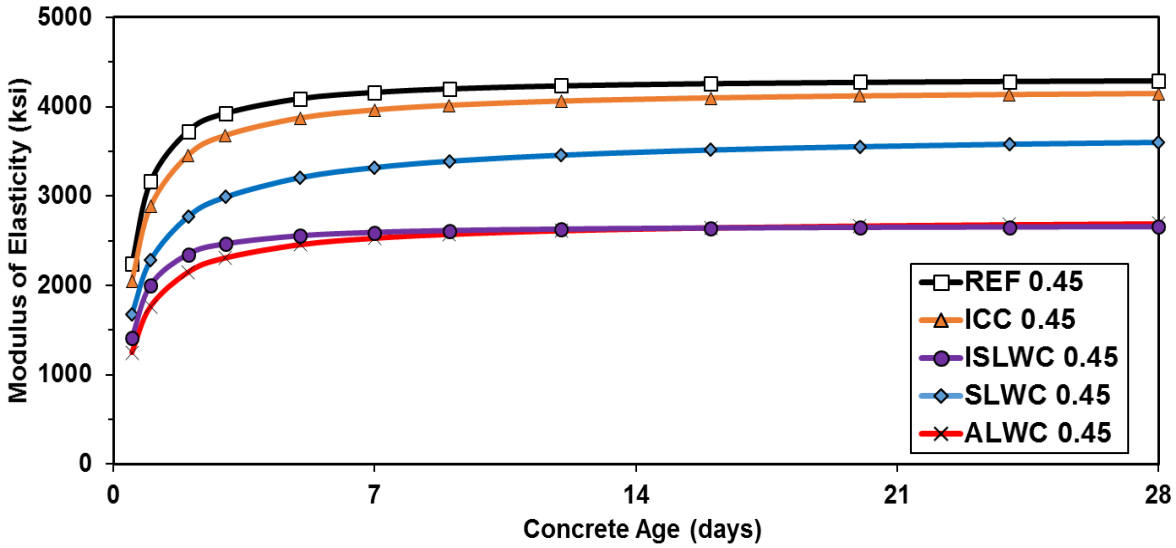

Figure 5-9: Modulus of elasticity development for all 0.45 *w/cm* concretes

5.2 CONCRETES WITH W/CM = 0.38

5.2.1 Combined Mixture Gradations

Five concrete mixtures with a *w/cm* of 0.38 and with four of them containing lightweight aggregates were produced and tested for fall conditions. The mixture proportions are, for these fine concretes are presented in Table 4-3. In order to assess the impact of using lightweight aggregates on the fresh concrete properties, the combined gradations of the concrete are plotted on a 0.45-power curve and their workability factor determined. The 0.45-power curve presented in Figure 4-10 presents the particle packing of the blended aggregate gradation (Young, Mindess and Darwin 2002). The workability factors (Shilstone 1990) for all 0.38 *w/cm* concretes are also presented in Figure 5-11.

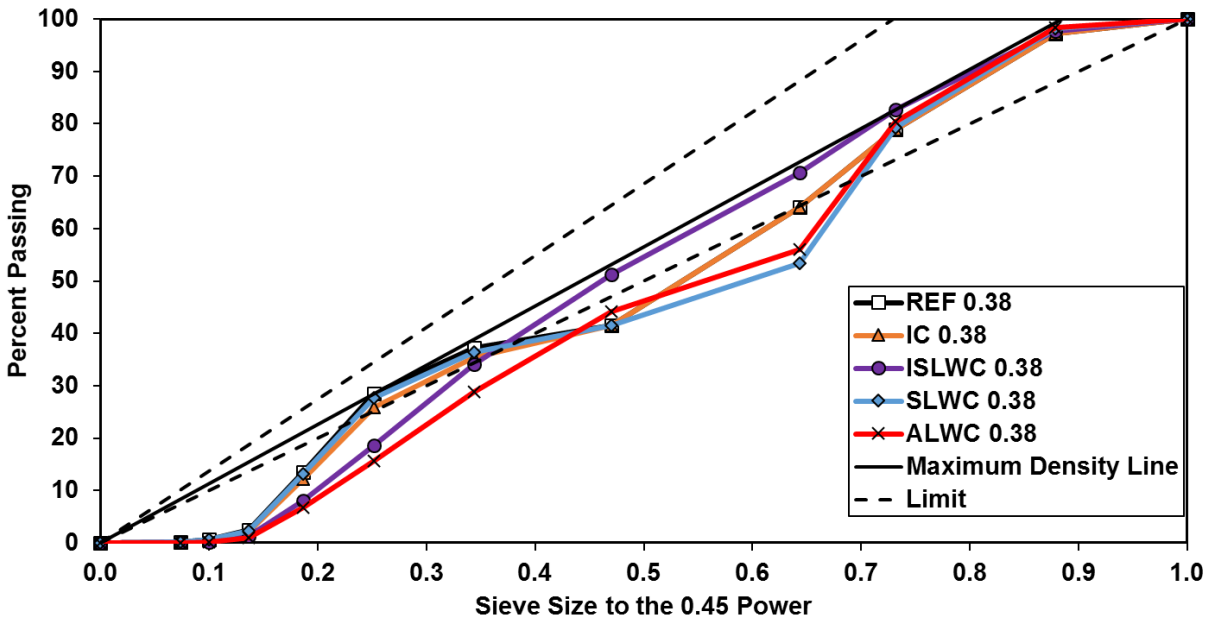

Figure 5-10: Combined gradation of all 0.38 *w/cm* concretes on the 0.45 power curve

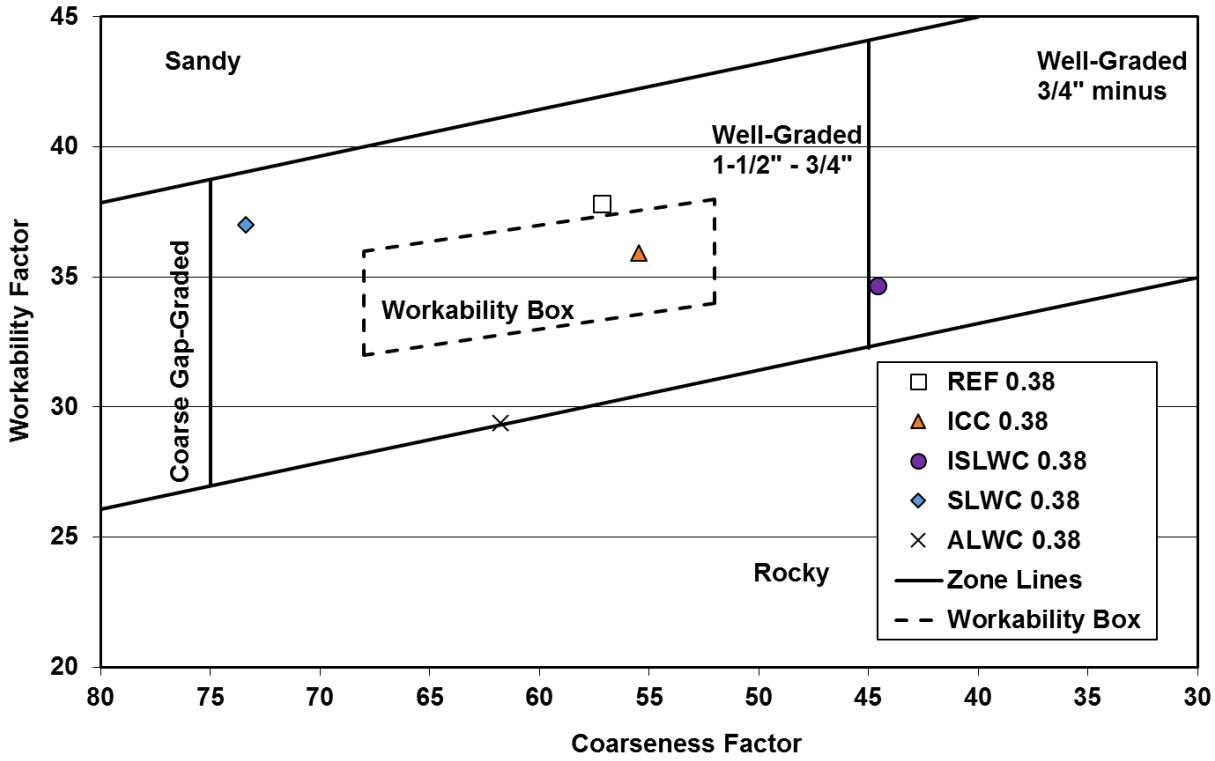

Figure 5-11: Workability factor versus coarseness factor for all 0.38 *w/cm* concretes

5.2.2 Fresh Concrete Properties

Trial batches were performed for each mixture until the desired slump and total air content were achieved. Following this, two batches of concrete were produced, with one batch being tested for mechanical properties of concrete and the other batch for RCF and FSF testing. The fresh properties of each mixture and batch are presented in Table 5-4. The "Δ density" column in Table 5-4 is the difference between the measured and designed densities after performing the corrections for measured total air content. A positive sign indicates that the measured density was higher than the calculated density and vice versa. The calculated equilibrium densities in accordance to ASTM C567 (2014) are also shown in Table 5-4. The slumps of SLWC 0.38 (Batch 1) and ALWC 0.38 (Batch 1) were

0.5 in. outside the target slump range of 3 to 5 in.; however, the workability of these concretes were sufficient to allow them to be effectively consolidated without any signs of segregation.

Table 5-4: Measured Fresh properties for all 0.38 *w/cm* concretes

Concrete Mixture	Batch No.	Fresh Concrete Test Results				Calculated
		Slump (in.)	Temp. (°F)	Total Air (%)	Density (lb/ft^3)	Δ Density (lb/ft^3)
REF 0.38	1	4.0	73	5.5	141.6	0.4
	2	3.0	73	5.0	141.9	0.7
ICC 0.38	1	3.5	72	4.5	141.2	0.6
	2	3.5	75	5.5	140.1	-0.5
ISLWC 0.38	1	3.5	73	4.0	120.8	0.3
	2	4.0	74	4.0	121.2	0.7
SLWC 0.38	1	2.5	73	5.5	115.0	1.2
	2	4.0	71	6.0	114.6	0.8
ALWC 0.38	1	5.5	74	6.0	101.3	-0.8
	2	4.0	73	5.5	101.8	-0.3

5.2.3 Thermal Properties

The calculated equilibrium density, coefficient of thermal expansion, and thermal diffusivity are summarized in Table 5-5.

Table 5-5: Miscellaneous properties of all 0.38 *w/cm* concretes

Property	REF 0.38	ICC 0.38	ISLWC 0.38	SLWC 0.38	ALWC 0.38
Calculated Equilibrium Density (lb/ft^3)	139.2	135.5	115.8	110.2	95.2
Coefficient of Thermal Expansion (με/°F)	6.1	5.9	5.3	5.3	4.1
Thermal Diffusivity (ft^2/hr)	0.039	0.038	0.037	0.021	0.014

5.2.4 Peak Temperatures

The time-dependent development of temperatures at the core of an 8×8 ft column calculated from ConcreteWorks for the concretes with a *w/cm* of 0.38 are presented in Figure 5-12. The edge temperatures computed using ConcreteWorks were simulated in the rigid cracking frame, as mentioned in Section 4.5.

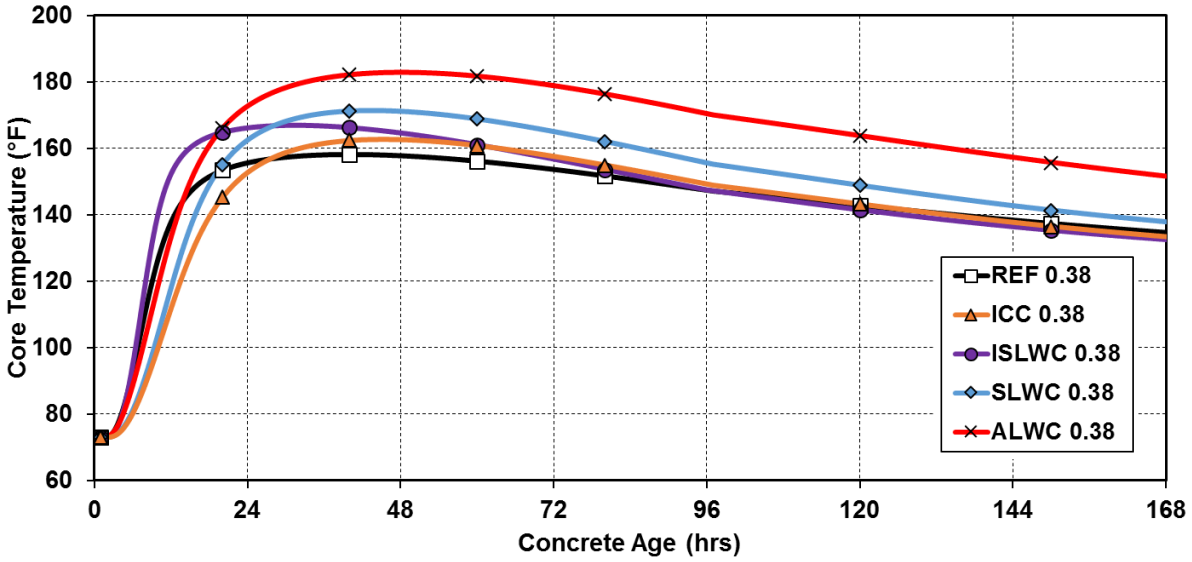

Figure 5-12: Temperature development in a 8×8 ft column for all 0.38 *w/cm* concretes

5.2.5 Restrained Stress Development

The restrained stress development measured with the RCF for all five concretes with *w/cm* of 0.38 and their curing temperature profiles are shown in Figures 5-13 and 5-14. The stresses are shown until the time of cracking, which is indicated by a sudden drop in stress.

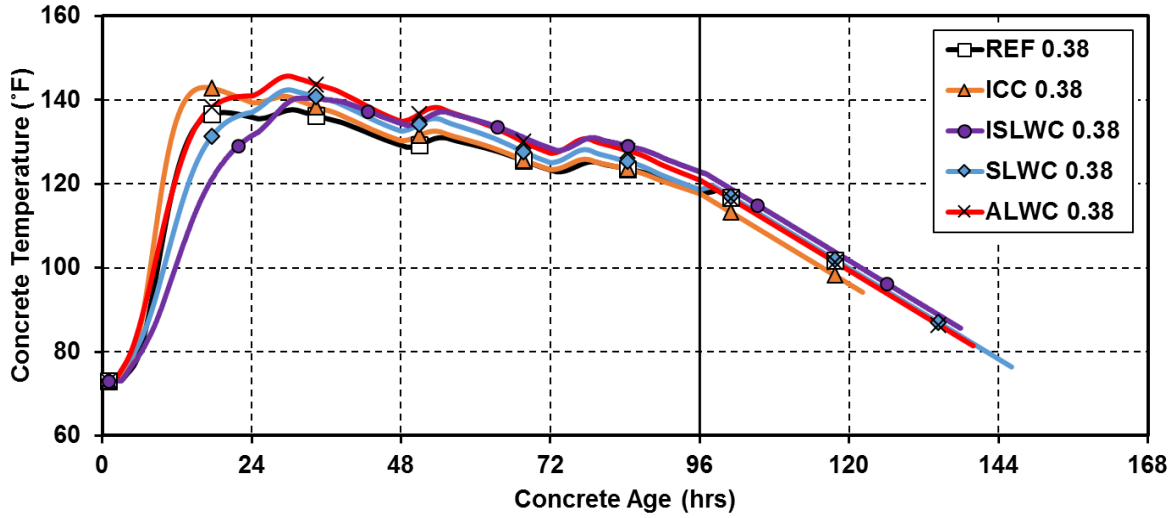

Figure 5-13: Concrete temperature profile for all 0.38 *w/cm* concretes

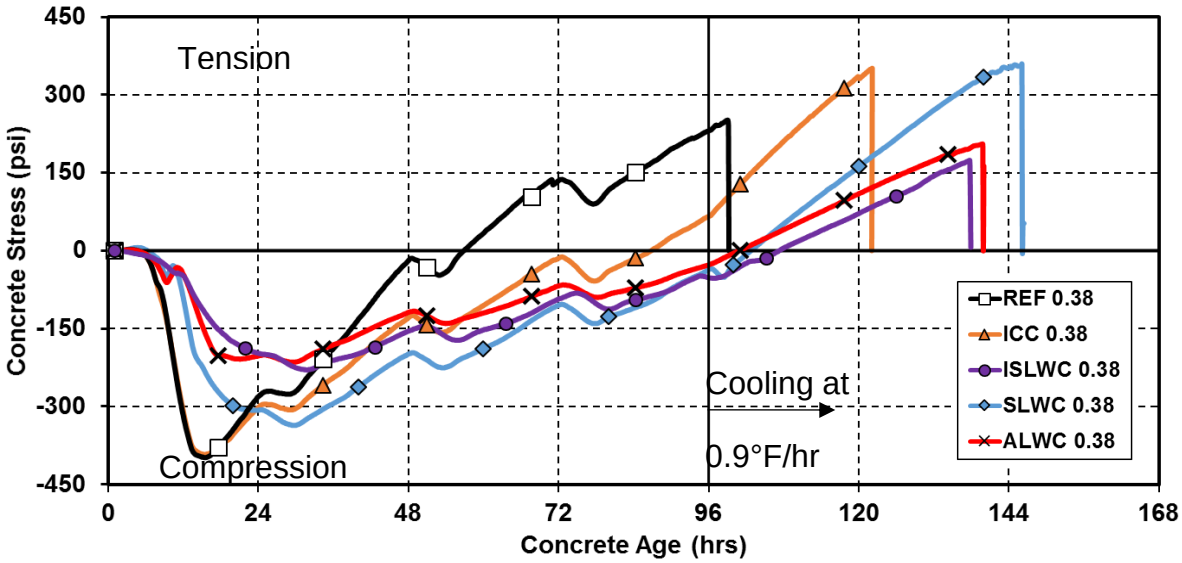

Figure 5-14: Restrained stress development for all 0.38 *w/cm* concretes

5.2.6 Unrestrained Strain Development

The unrestrained strain measurement measured with the FSF for all the concrete specimens with *w/cm* of 0.38 are shown in Figure 5-15. The concrete specimens were match-cured using the modeled temperature profiles of the RCF.

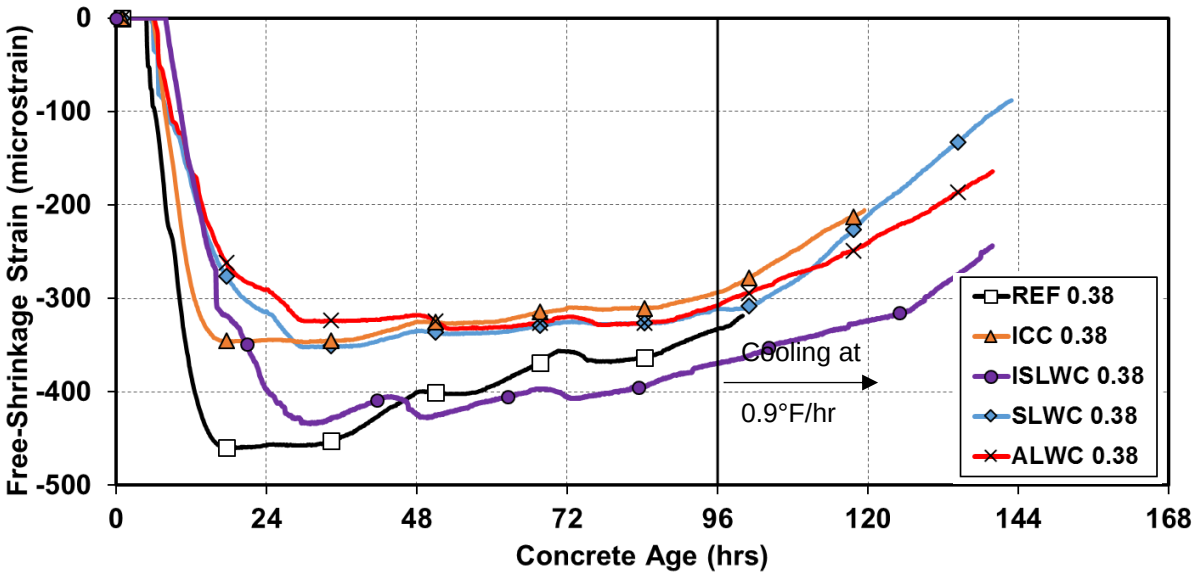

Figure 5-15: Unrestrained strain development for all 0.38 *w/cm* concretes

5.2.7 Isothermal Stress Development

The isothermal stress development measured with the RCF for all five low *w/cm* concretes are shown in Figure 5-16. The isothermal stresses refer to the concrete stresses when the specimen is subjected to a uniform temperature of 73°F, so in this setup these stresses only develop due to autogenous shrinkage.

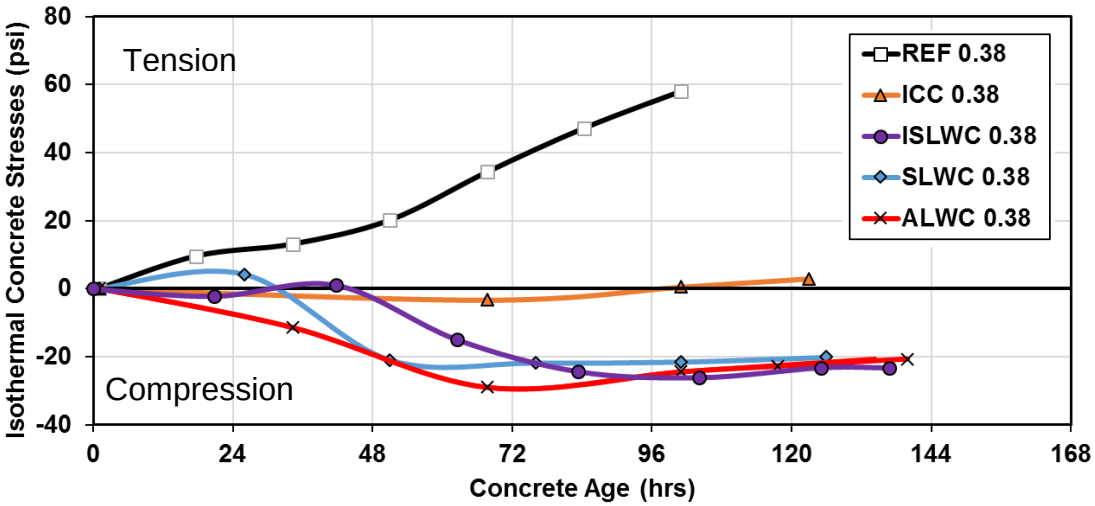

Figure 5-16: Isothermal stress development for all 0.38 *w/cm* concretes

5.2.8 Summary of Rigid Cracking Frame Test Results

The maximum RCF temperature, time of cracking in the RCF, and the stress at cracking are shown in Table 5-6 for all concrete with *w/cm* of 0.38.

Table 5-6: Summary of RCF results for concrete with *w/cm* of 0.38

Item	***w/cm* = 0.38**				
	REF 0.38	**ICC 0.38**	**ISLWC 0.38**	**SLWC 0.38**	**ALWC 0.38**
Maximum RCF temperatures (°F)	136	140	141	142	146
Time of cracking (hrs)	99	123	138	146	142
Stress at cracking (psi)	260	345	190	355	205
Maximum isothermal tensile stress (psi)	60	0	0	5	0

5.2.9 Time-Dependent Development of Mechanical Properties

The time-dependent development of compressive strength, splitting tensile strength, and modulus of elasticity were tested for each concrete mixture. Twenty-four cylinders were match-cured along with the RCF and FSF were tested at varying ages. The measured values were averaged for two cylinders and are presented in Appendix B. A regression analysis was performed as per ASTM C1074 (2014), which recommends the use of an exponential function. Best-fit curves were determined for the measured values and are plotted in Figures 5-17 to 5-19.

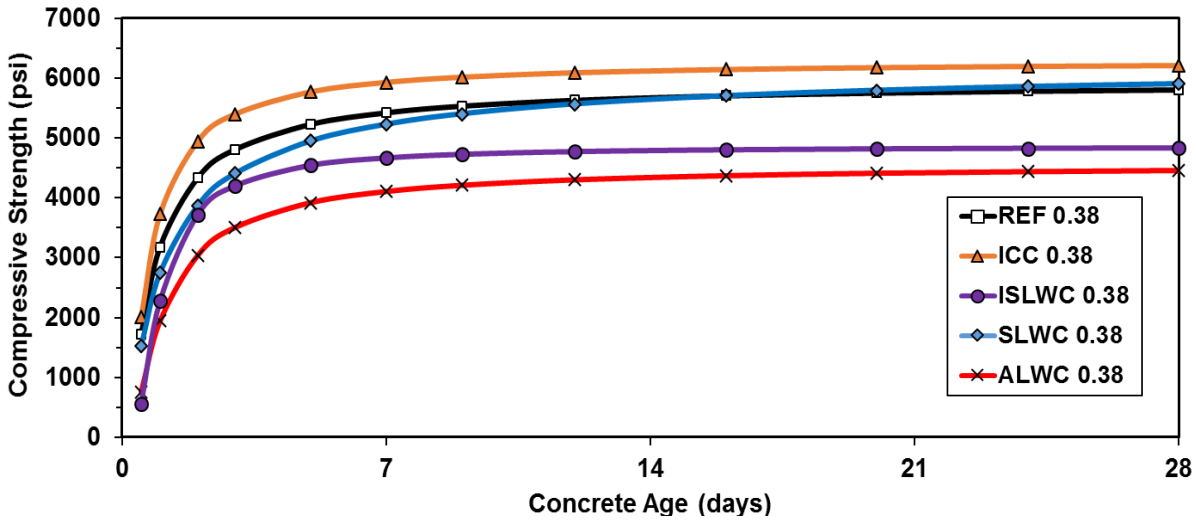

Figure 5-17: Compressive strength development for all 0.38 *w/cm* concretes

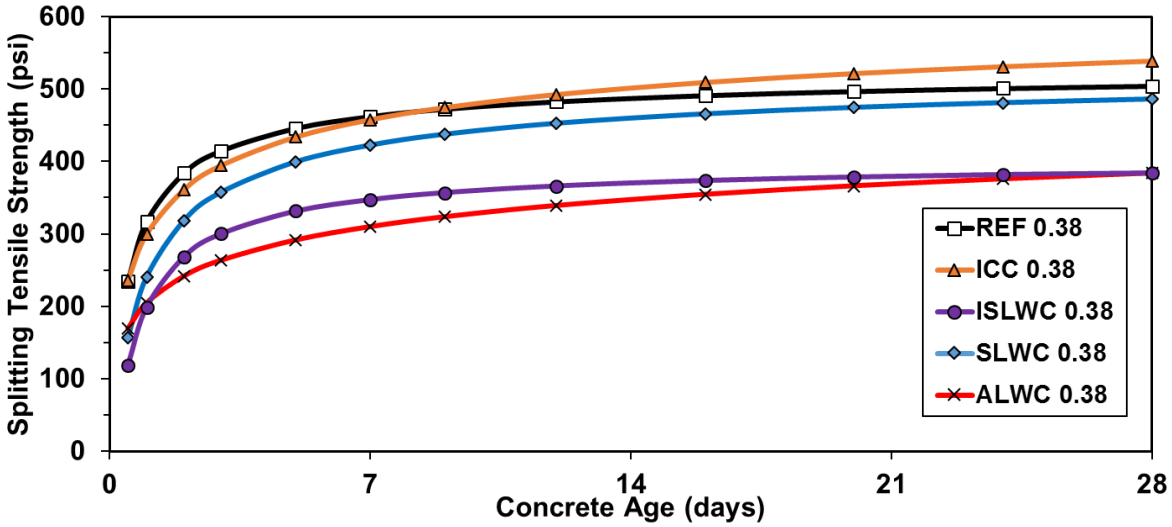

Figure 5-18: Splitting tensile strength development for all 0.38 *w/cm* concretes

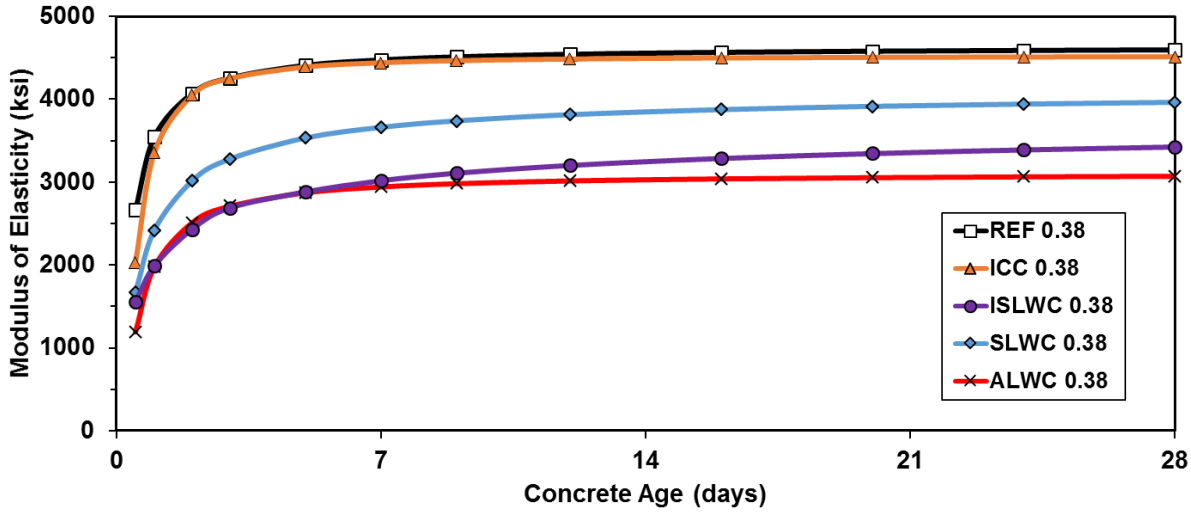

Figure 5-19: Modulus of elasticity development for all 0.38 *w/cm* concretes

Chapter 6

PART I: DISCUSSION OF RESULTS

A discussion of the collected results is presented in this chapter. The change in concrete properties due to the use of lightweight aggregates is assessed in Section 6.1. In Section 6.2, the effect of internal curing on autogenous stress development is covered. Next, the effects of lightweight aggregates on early-age concrete stresses are evaluated in Section 6.3. The cracking tendency, time to cracking, and peak hydration temperatures for all concretes are also compared and the reason for the observed behavior is discussed. Finally, the modulus of elasticity and splitting tensile strength results are compared to predictions from various expressions at the end of this chapter.

6.1 EFFECT OF LIGHTWEIGHT AGGREGATE ON CONCRETE PROPERTIES

6.1.1 Compressive Strength

Compressive strength developments for all concretes are presented in Figures 5-7 and 5-17. The 28-day design compressive strength for the reference concrete was 4,000 psi, and the experimental results indicate that the compressive strengths exceeded the design strength. When considering the with-in test variability, the compressive strength development for the reference, IC, and SLW concretes are similar for both groups of *w/cm* concretes. Similarly, ALW and ISLW concretes had approximately 10 % to 15 % lower compressive strengths compared to the reference concretes for both groups of *w/cm* concretes. This is most likely due to the use of large amount of fine LWA in both the ISLW and ALW concretes. It was unexpected that the ISLW concrete had a strength

much lower than the SLW concrete; however, the use of high volume of fine LWA could explain this result. When comparing the strengths achieved in Figures 5-7 and 5-17, it can be seen that both ISLW and ALW concretes are capable of higher strengths, if low *w/cm* concrete mixtures are used.

6.1.2 Splitting Tensile Strength

The splitting tensile strength developments for all concretes are presented in Figures 5-8 and 5-18. When considering the with-in test variability, the splitting tensile strength development for the reference, IC, and SLW concretes are similar for both groups of *w/cm* concretes. Whereas the ISLW and ALW concretes had approximately 20 % to 30 % lower splitting tensile strengths, when compared to the reference concretes for both groups of *w/cm* concretes. The most likely reasons for this result could be due to the higher proportion of fine LWA, poor particle packing of the ALW concretes, and the low coarseness factor of the ISLW concretes (Shilstone and Shilstone 1989) when compared to the reference concrete as shown in Figure 5-2 and 5-11.

6.1.3 Modulus of Elasticity

The modulus of elasticity development results for all concretes are presented in Figures 5-9 and 5-19. When considering the with-in test variability, the modulus of elasticity development for the reference and IC concretes are similar for both groups of *w/cm* concretes. The average modulus of elasticity values are lower by 12 %, 33 %, and 33 % for SLW, ISLW, and ALW concretes, respectively, when compared to the reference concretes for both groups of *w/cm* concretes. The primary factors contributing to this result are the lower stiffness of LWA and the reduced density of LWA concretes when compared to normalweight concretes. An unexpected result is the reduced modulus of

elasticity of the ISLW concrete when compared to SLW concrete. The SLW concrete has a slightly lower density (approximately 6 lb/ft^3) than ISLW concrete, but has a higher modulus of elasticity in comparison. A possible reason could be due to the much-reduced compressive strength of both ISLW concretes, as discussed in Section 6.1.1. Based on either Equation 3-7 or 3-8, a large decrease in strength will lead to a large decrease in modulus of elasticity. However, this large decrease in modulus of elasticity may be beneficial to reduce early-age concrete stresses.

6.1.4 Coefficient of Thermal Expansion

The coefficient of thermal expansion (CTE) values for all concretes are presented in Tables 5-2 and 5-5. As shown in Figure 6-1, the CTE values for both the *w/cm* concretes indicate that the concretes with an increasing amount of LWAs exhibit reduced CTE values, with an average CTE reduction of 5 % for IC, 10 % for ISLW, 10 % for SLW, and 30 % for ALW concretes when compared to the two reference concretes. The reduction in concrete CTE of concrete containing LWA is attributed to the lower CTE of LWA (Neville 2011). In accordance with Equation 3-1, a reduction in concrete CTE will result in a decrease in concrete thermal stress, which will lead to an improvement in resistance to thermal cracking.

6.1.5 Thermal Diffusivity

The thermal diffusivity for all the concretes are summarized in Tables 6-2 and 6-5. As shown in Figure 6-2, the thermal diffusivity values for both the *w/cm* concretes indicate that the concretes with increasing amount of LWAs exhibit reduced thermal diffusivity values, with an average thermal diffusivity reduction of 5 % for IC, 10 % for ISLW, 30 % for SLW, and 50 % for ALW concretes when compared to the two reference concretes. The lower diffusivity for concrete containing lightweight aggregates is due to its lower thermal conductivity and a lower density. The lower thermal diffusivity indicates that lightweight aggregate concretes will dissipate heat more slowly, which will lead to higher peak temperatures in mass concrete applications when compared to normalweight concrete.

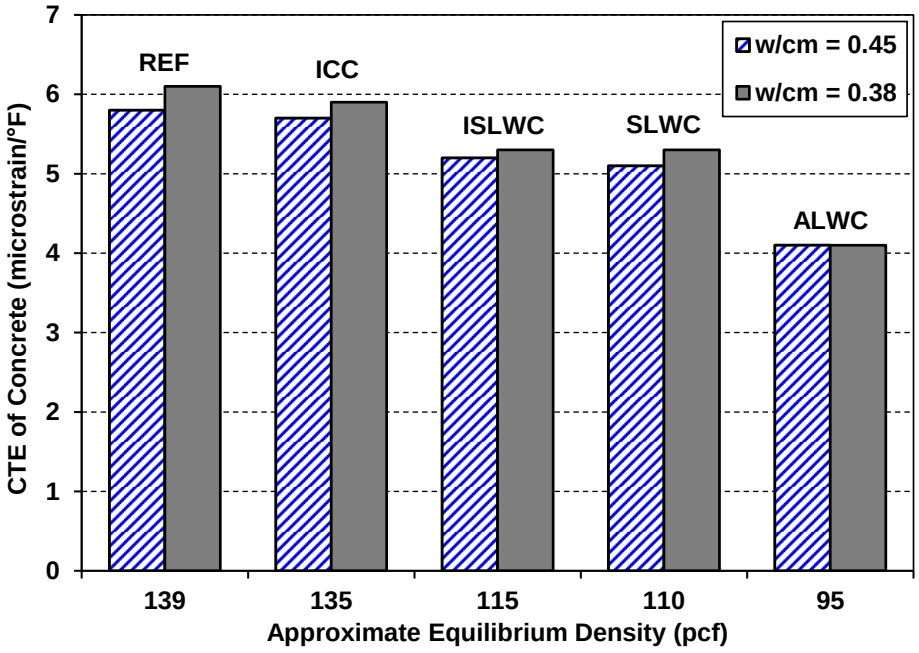

Figure 6-1: Measured CTE values for all concretes

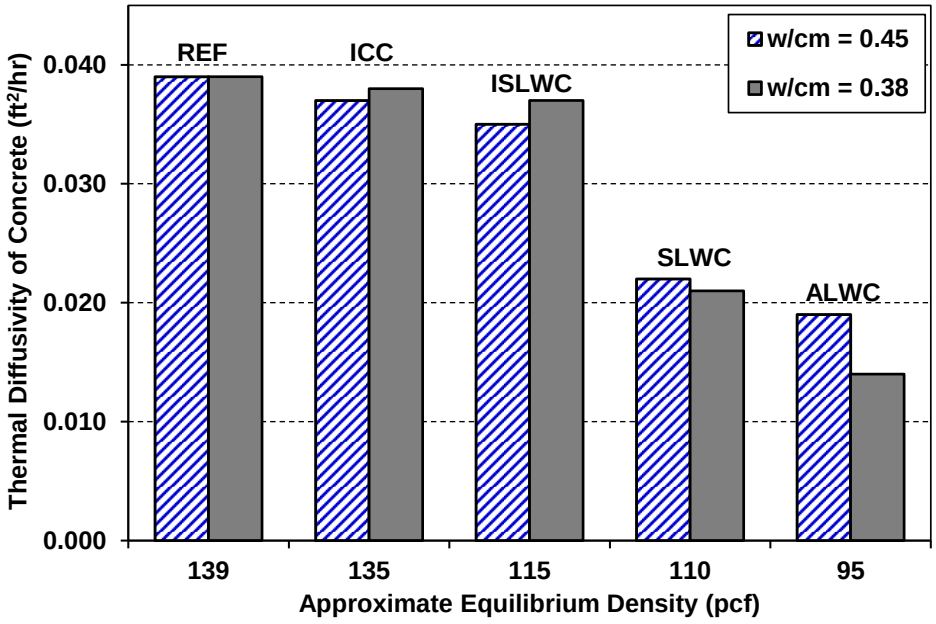

Figure 6-2: Measured thermal diffusivity values for all concretes

6.1.6 Peak Temperature

The development of peak temperatures at the core of an 8 × 8 ft cross-sectional mass concrete column are presented in Figures 5-3 and 5-12. These concrete temperatures were determined by using the ConcreteWorks software with the measured semi-adiabatic calorimeter and thermal diffusivity values for all concretes. As the *w/cm* of the concrete decreases, the peak concrete temperatures increase, which is due to the presence of more cementitious material in low *w/cm* concretes (Schindler and Folliard 2005).

It can be observed that the peak concrete temperatures are the highest for the ALW concretes, followed by the SLW and ISLW concretes that are higher than the peak temperatures of the IC and reference concretes. The reference concrete has the lowest maximum concrete temperature for all the concretes followed by the IC concrete. The major reason can be attributed to the systematically lower thermal diffusivity observed in

these lightweight aggregate concretes as compared to the normalweight concrete, as shown in Figure 6-2. The decrease in thermal diffusivity tends to have an insulating effect on the structure leading to a higher buildup of peak temperatures in concrete containing lightweight aggregates (Maggenti 2007; Byard and Schindler 2010). Another reason is due to the higher degree of hydration in lightweight aggregate concretes, due to internal curing provided by the pre-wetted LWAs in the concrete (Bentz and Weiss 2011). Since the maximum in-place concrete temperatures increased as more LWAs were used in the mixture, care should be taken when using LWA concrete in mass concrete to make sure not to exceed the in-place concrete temperature threshold for DEF.

6.2 EFFECT OF INTERNAL CURING ON AUTOGENOUS STRESS DEVELOPMENT

The internal curing water provided by lightweight aggregates for each concrete type is presented in Table 4-4. The availability of internal curing water is the highest in the ALW concrete, followed by SLW, ISLW, and IC concretes, because concrete containing higher proportion of the same LWA contains more internal curing water. The autogenous shrinkage stress development for all 0.38 *w/cm* concretes is presented in Figure 5-16. The autogenous shrinkage stresses are greatly reduced in all concretes containing LWA when compared to the reference concrete. The stress due to autogenous shrinkage is for all practical purposes zero in all concretes incorporating LWA. This decrease in autogenous shrinkage stresses has been documented in several research studies (Byard and Schindler 2010; Bentz and Weiss 2011; RILEM TC 196 2007). The internal curing water acts as internal water reservoirs, thus increasing the internal relative humidity inside

the concrete, and resulting in no autogenous shrinkage related stresses (RILEM TC 196 2007). This reduction or elimination of autogenous shrinkage related stresses point out that enough internal curing water is available to mitigate the effects of autogenous shrinkage.

It can be seen in Figure 5-5 and 5-14 that when compared to the reference concrete, the use of lightweight aggregates delays the occurrence of cracking in all concretes incorporating LWA. The lower *w/cm* reference concrete cracks at an earlier time when compared to the higher *w/cm* reference concrete. Although the 0.38 *w/cm* reference concrete has an increased splitting tensile strength, the earlier time to cracking in the 0.38 *w/cm* reference concrete is partly due to its higher modulus of elasticity and the contribution of autogenous shrinkage stresses which becomes more prominent at lower *w/cm*. The use of LWA in concrete with low *w/cm* will thus be more beneficial, because this is when the autogenous shrinkage will be at its highest, and the LWA will help to lower the modulus of elasticity of the low *w/cm* concrete.

6.3 EVALUATION OF THE BEHAVIOR OF VARIOUS TYPES OF LIGHTWEIGHT AGGREGATE CONCRETES

The early-age behavior of the concretes incorporating lightweight aggregates are compared with the behavior of the two reference concretes in this section.

6.3.1 Behavior of Internally Cured Concretes

The concrete temperature profiles and restrained stress development for the internally cured concretes for both *w/cm* concretes are compared to the response of the two reference concretes in Figures 6-3 and 6-4. For comparison, the modulus of elasticity

and splitting tensile strength development of all IC concretes and reference concretes are plotted in Figures 6-5 and 6-6. The concrete temperatures of the IC concretes are higher than their reference concrete counterparts. This is due to the increased availability of internal curing water and the reduced thermal diffusivity of the IC concretes.

The 0.45 *w/cm* IC concrete exhibit an increase in time to cracking, when compared to its reference concrete. This is mostly attributed to the reduced coefficient of thermal expansion observed in the 0.45 *w/cm* IC concrete, when compared its reference concrete, as discussed in Section 6.1.

For the low *w/cm* concrete mixture, a 30 % increase in stress at cracking and a 24-hour delay in time to cracking are observed in the IC concrete, when compared to the reference concrete. The improvement in cracking behavior of internally cured concretes of 0.38 *w/cm* is attributed to a combination of reduced coefficient of thermal expansion and autogenous shrinkage stress when compared to the reference concrete.

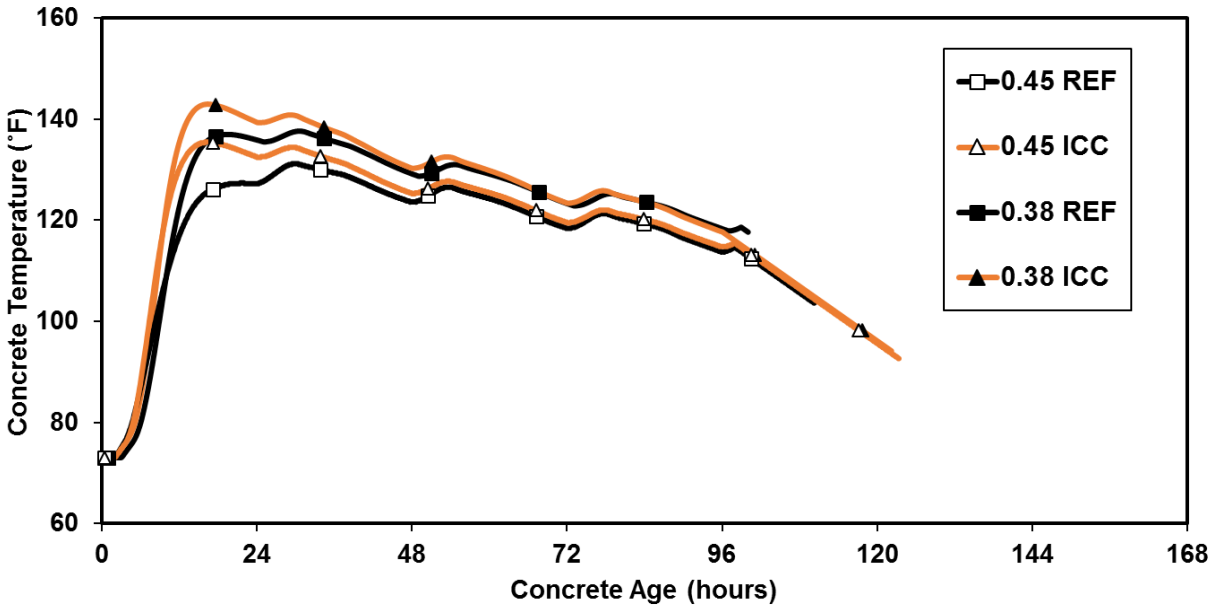

Figure 6-3: Concrete temperature profile of IC and reference concretes

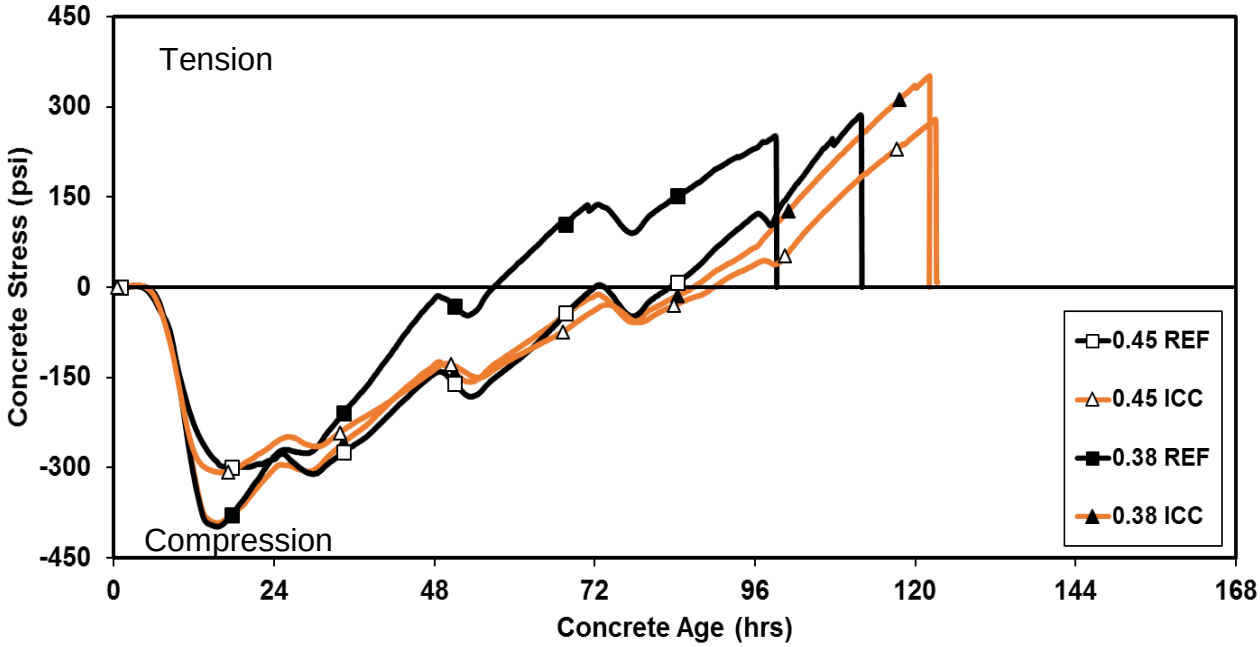

Figure 6-4: Measured restrained stress development of IC and reference concretes

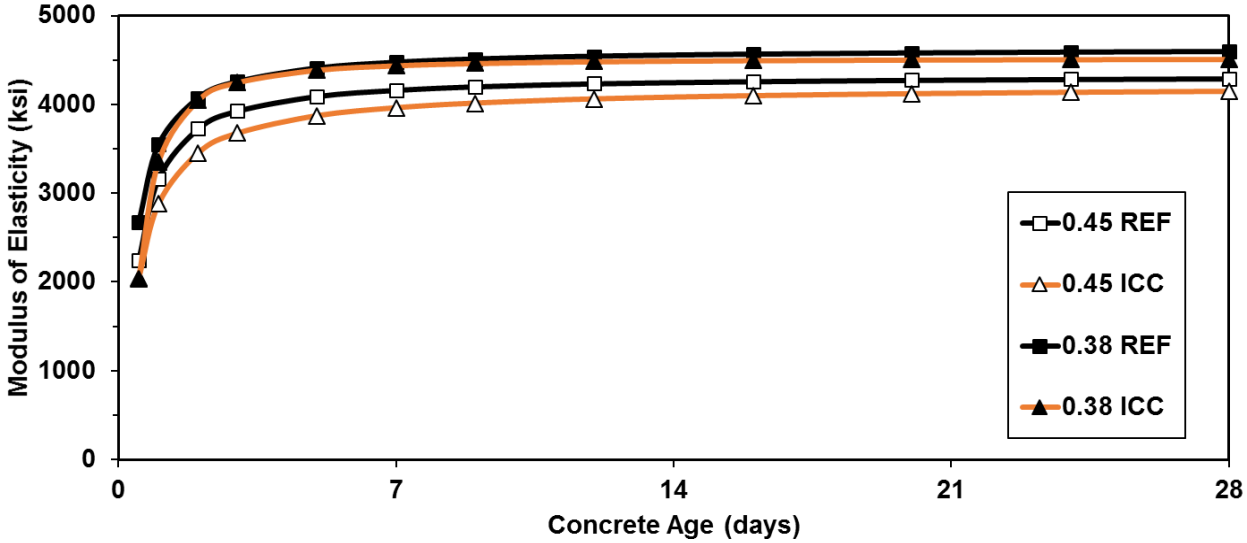

Figure 6-5: Measured modulus of elasticity of IC and reference concretes

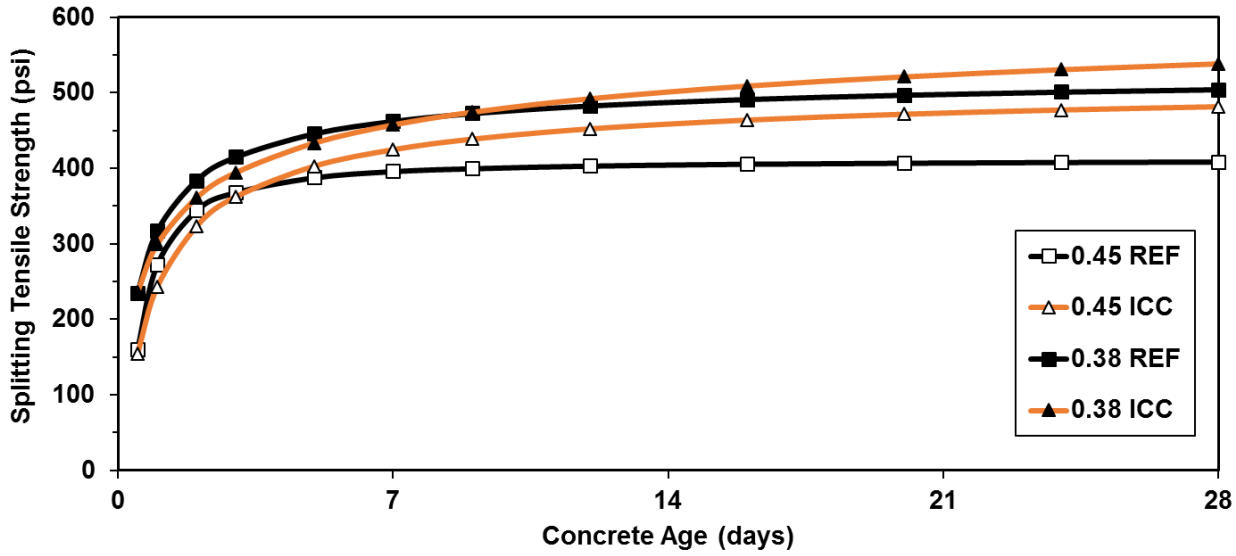

Figure 6-6: Measured splitting tensile strengths of IC and reference concretes

6.3.2 Behavior of Inverse Sand-Lightweight Concretes

The concrete temperature profiles and restrained stress development for the ISLW concretes for both *w/cm* concretes are compared to the response of the two reference concretes in Figures 6-7 and 6-8. For comparison, the modulus of elasticity and splitting tensile strength development of both ISLW and reference concretes are plotted in Figures 6-9 and 6-10.

The concrete temperatures of the ISLW concretes are higher than the reference concretes for both the *w/cm* concrete mixtures, due to a higher proportion of lightweight aggregates. This result is because of the decreased thermal diffusivity and increased heat of hydration due to internal curing, which causes higher temperatures in the ISLW concretes.

The time of cracking for ISLW concretes is increased by 18 and 39 hours for *w/cm* = 0.45 and *w/cm* = 0.38, respectively, in comparison to the reference concretes. Although

the ISLW concretes had much lower splitting tensile strengths when compared to the reference concretes (as shown in Figure 6-10), it still had an improved cracking tendency when compared to the reference concretes. An average reduction of 33% in modulus of elasticity for both *w/cm* concretes (as shown in Figure 5-9), complete elimination of autogenous shrinkage related stresses for the 0.38 *w/cm* ISLW concrete, and a lower coefficient of thermal expansion, all combine to delay the time to cracking for ISLW concretes when compared to the reference concretes.

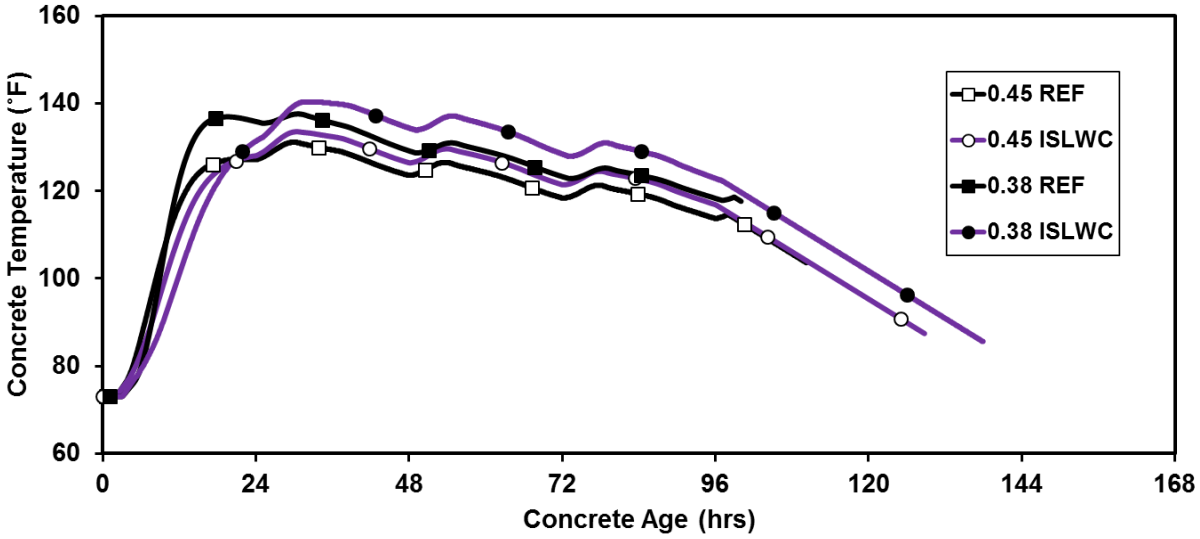

Figure 6-7: Concrete temperature profile of ISLW and reference concretes

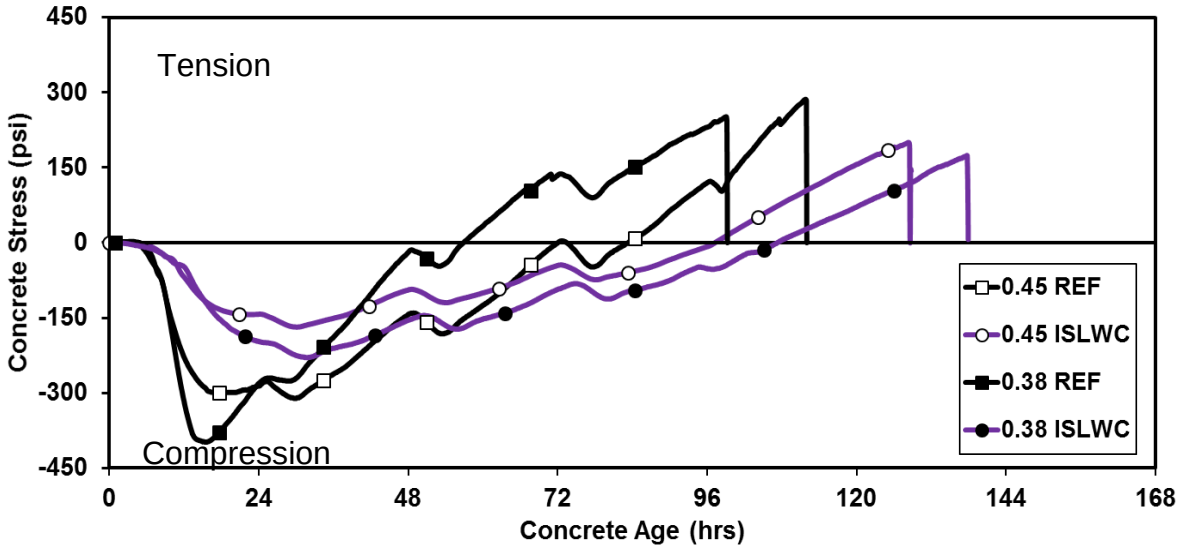

Figure 6-8: Measured restrained stress of ISLW and reference concretes

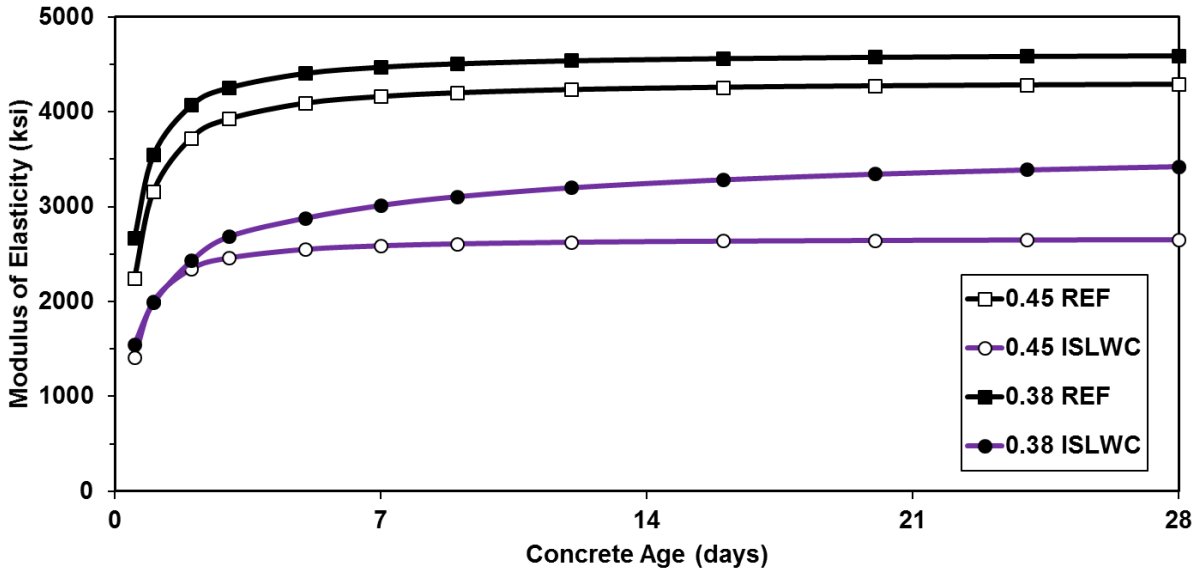

Figure 6-9: Measured modulus of elasticity of ISLW and reference concretes

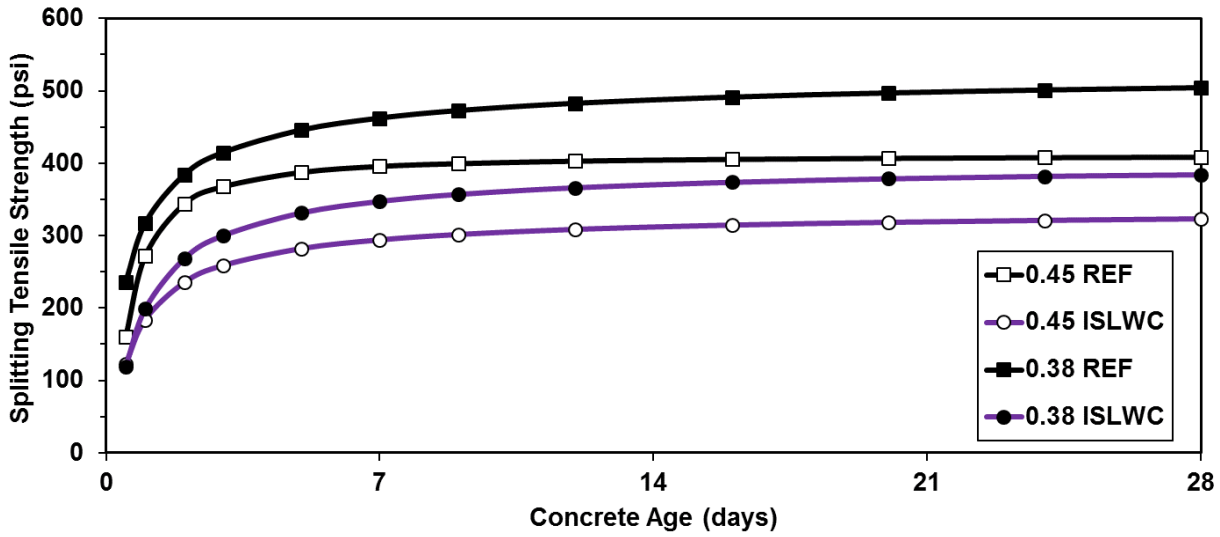

Figure 6-10: Measured splitting tensile strengths of ISLW and reference concretes

6.3.3 Behavior of Sand-Lightweight Concretes

The concrete temperature profiles and restrained stress development for the SLW concretes for both *w/cm* concretes are compared to the response of the two reference concretes in Figures 6-11 and 6-12. For comparison, the modulus of elasticity and splitting tensile strength development of both SLW and reference concretes are plotted in Figures 6-13 and 6-14.

The concrete temperatures of the SLW concretes are higher than the reference concretes, due to an increased proportion of lightweight aggregates. This result is because of the decreased thermal diffusivity and increased heat of hydration due to internal curing, which causes higher temperatures in the SLW concretes.

The time of cracking is increased by 24 hours (*w/cm* = 0.45) and 48 hours (*w/cm* =0.38) for the SLW concretes in comparison to the reference concretes. An average reduction of 12% in modulus of elasticity for both the *w/cm* concrete mixtures, (as shown

in Figure 6-13), elimination of autogenous shrinkage related stresses for the 0.38 *w/cm* SLW concretes, and a lower coefficient of thermal expansion, all combine to delay the time to cracking for SLW concretes when compared to reference concretes.

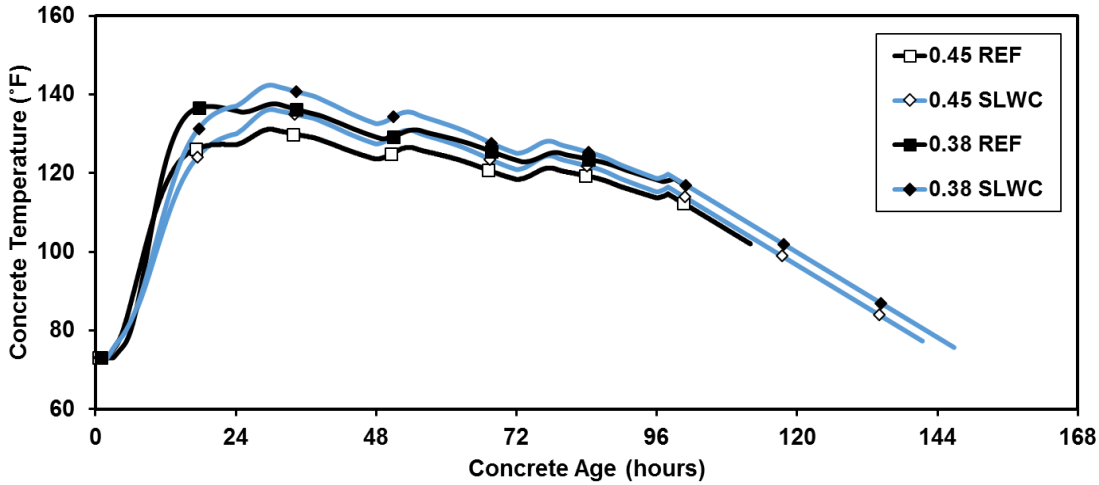

Figure 6-11: Concrete temperature profile of SLW and reference concretes

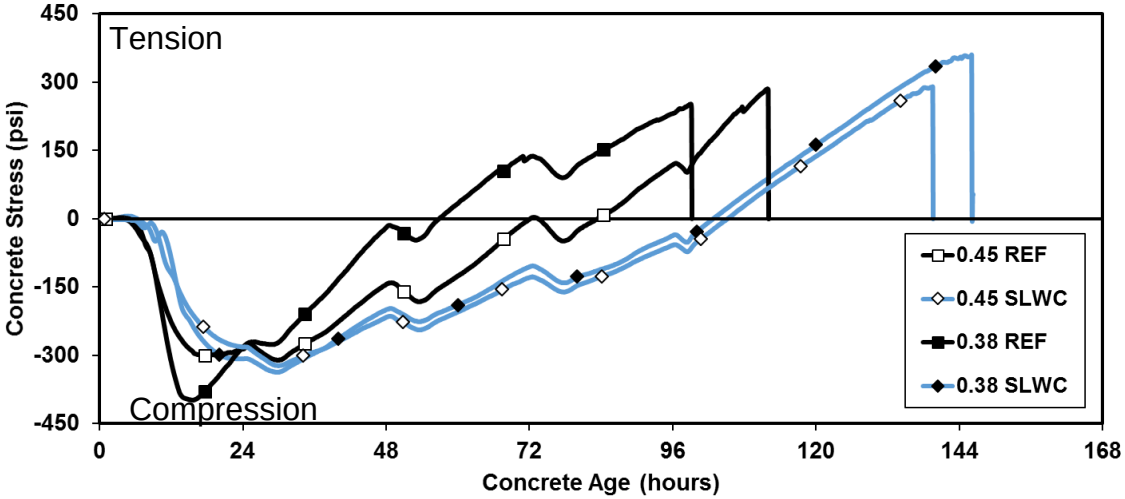

Figure 6-12: Measured restrained stress development of SLW and reference concretes

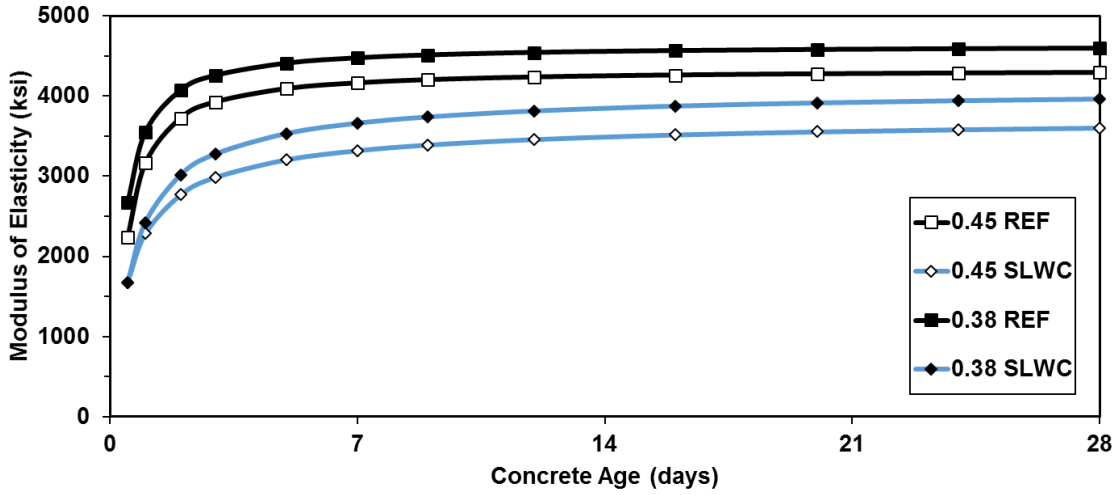

Figure 6-13: Measured modulus of elasticity of SLW and reference concretes

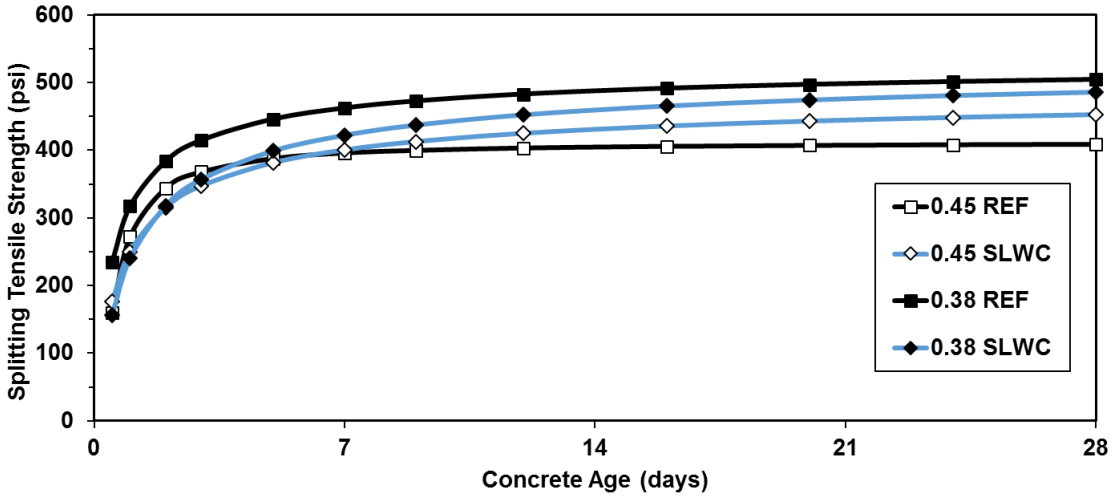

Figure 6-14: Measured splitting tensile strengths of SLW and reference concretes

6.3.4 Behavior of All-Lightweight Concretes

The concrete temperature profiles and restrained stress development for the ALW concretes for both *w/cm* concretes are compared to the response of reference concretes in Figures 6-15 and 6-16. For comparison, the modulus of elasticity and splitting tensile

strength development of both ALW and reference concretes are plotted in Figures 6-17 and 6-18.

The concrete temperatures of the ALW concrete are higher than the reference concretes by 5% and 8%, for *w/cm* = 0.45 and *w/cm* = 0.38, respectively, since all the aggregate particles are lightweight aggregates. The reduced thermal diffusivity and increased heat of hydration due to internal curing, which causes higher temperatures in ALW concretes.

The time of cracking for ALW concretes is delayed by 22 and 43 hours for *w/cm* = 0.45 and *w/cm* = 0.38, respectively, in comparison to the reference concretes. Although the ALW concretes had much lower splitting tensile strengths when compared to the reference concretes (as shown in Figure 6-18), they still had a much improved cracking tendency when compared to the reference concretes. An average reduction of 33 % in modulus of elasticity for both the *w/cm* concretes (as shown in Figure 6-17), the elimination of autogenous shrinkage related stresses for the 0.38 *w/cm* ALW concrete, and a lower coefficient of thermal expansion, all combine to delay the time to cracking for the ALW concretes when compared to reference concretes.

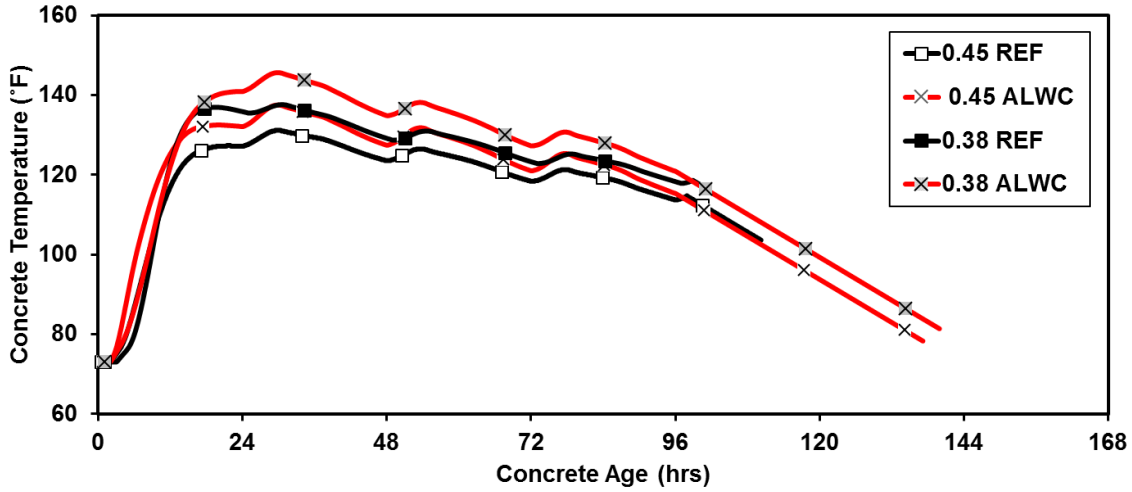

Figure 6-15: Concrete temperature profile of ALW and reference concretes

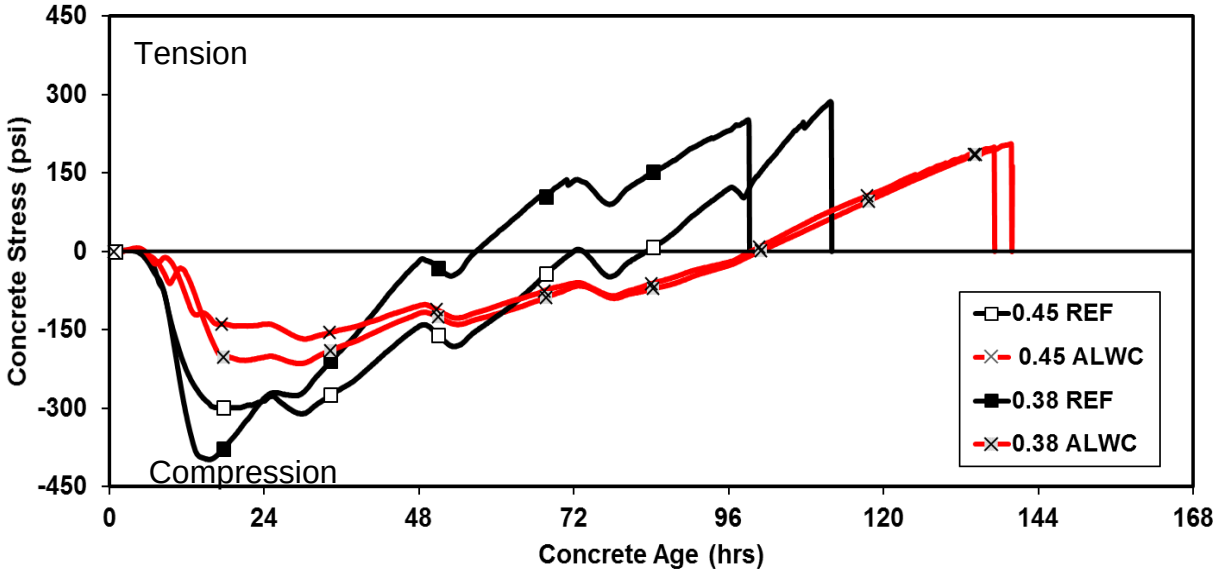

Figure 6-16: Measured restrained stress development of ALW and reference concretes

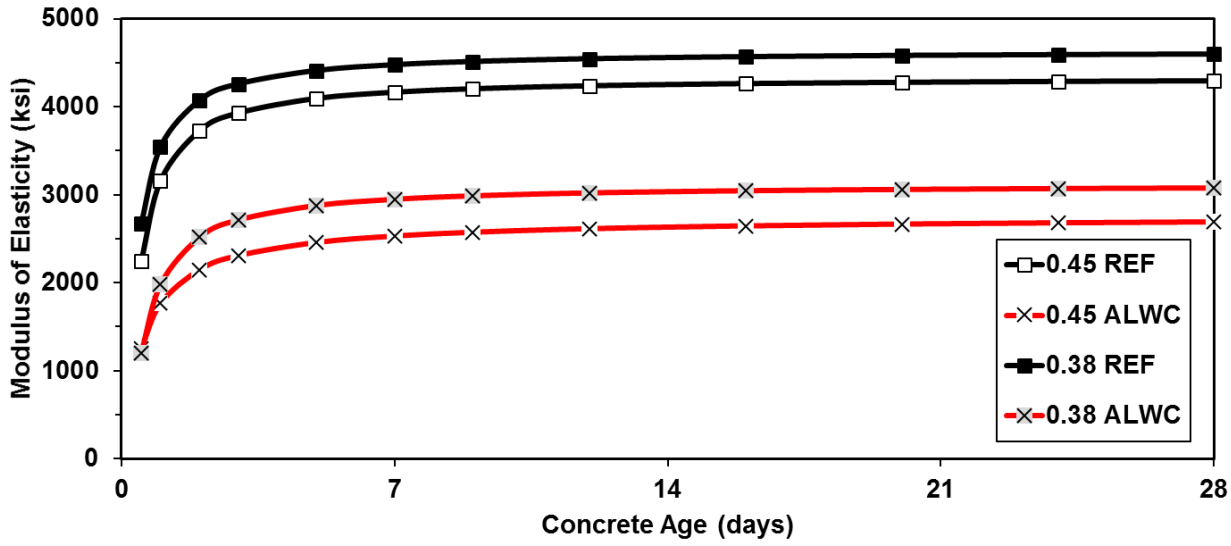

Figure 6-17: Measured modulus of elasticity of ALW and reference concretes

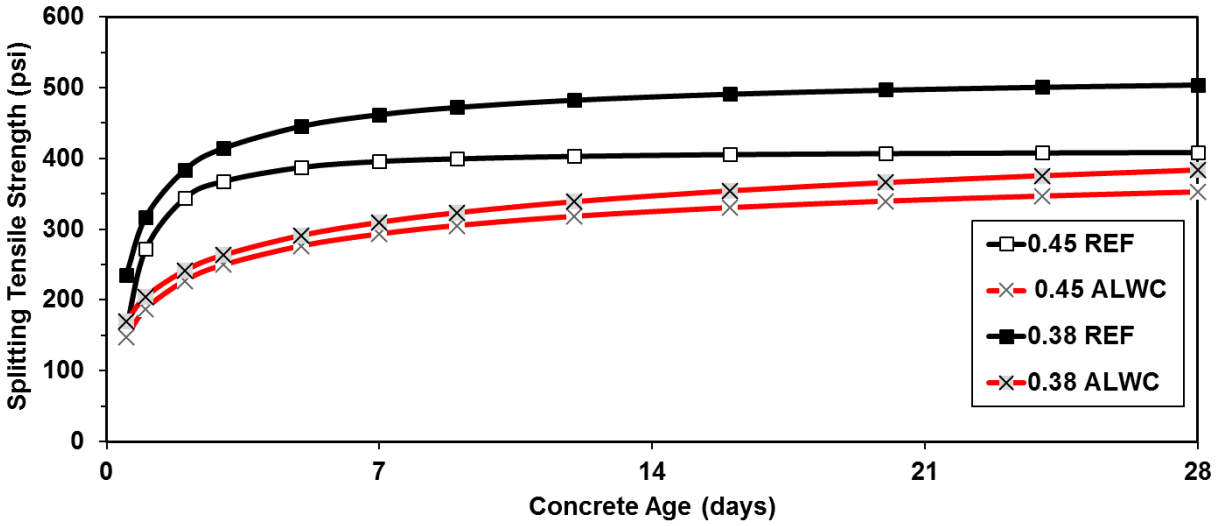

Figure 6-18: Measured splitting tensile strengths of ALW and reference concretes

6.4 EFFECT OF LIGHTWEIGHT AGGREGATE CONCRETES ON EARLY-AGE CONCRETE STRESS DEVELOPMENT

The restrained stress development and concrete temperature profiles for all concretes tested were discussed in the previous section. The maximum concrete temperature, denoted as T_{max}, reached in the rigid cracking frame for each concrete type is plotted in Figure 6-19(a) versus the approximate equilibrium density of each concrete. Similarly, in Figure 6-19(b), the time of cracking, denoted as t_c, for each concrete type as tested in the rigid cracking frame is plotted versus the approximate equilibrium density of concrete. As can be seen in Figure 6-19(a), ALW concrete has the highest maximum concrete temperature followed in order of decreasing maximum concrete temperature by the SLW, ISLW, IC, and reference concretes. The addition of LWA to concrete systematically lowers the thermal diffusivity, as shown in Figure 6-2, and subsequently increases the maximum concrete temperature. It can be observed from Figure 6-19 that despite an increase in the maximum concrete temperatures for LWA concretes in comparison to the reference concretes, all concretes made with LWA exhibit an improved crack resistance. The presence of LWA in concrete delays the time to cracking with SLWC having the latest time to cracking followed in order of decreasing time to cracking by ALW, ISLW, IC, and reference concretes. Concrete in the RCF were deliberately cooled after a period of 4 days to expedite the test performed in the laboratory, however it needs to be noted that if the concrete were not cooled then the concrete which would likely exhibit a high propensity to cracking would be concretes not containing lightweight aggregates.

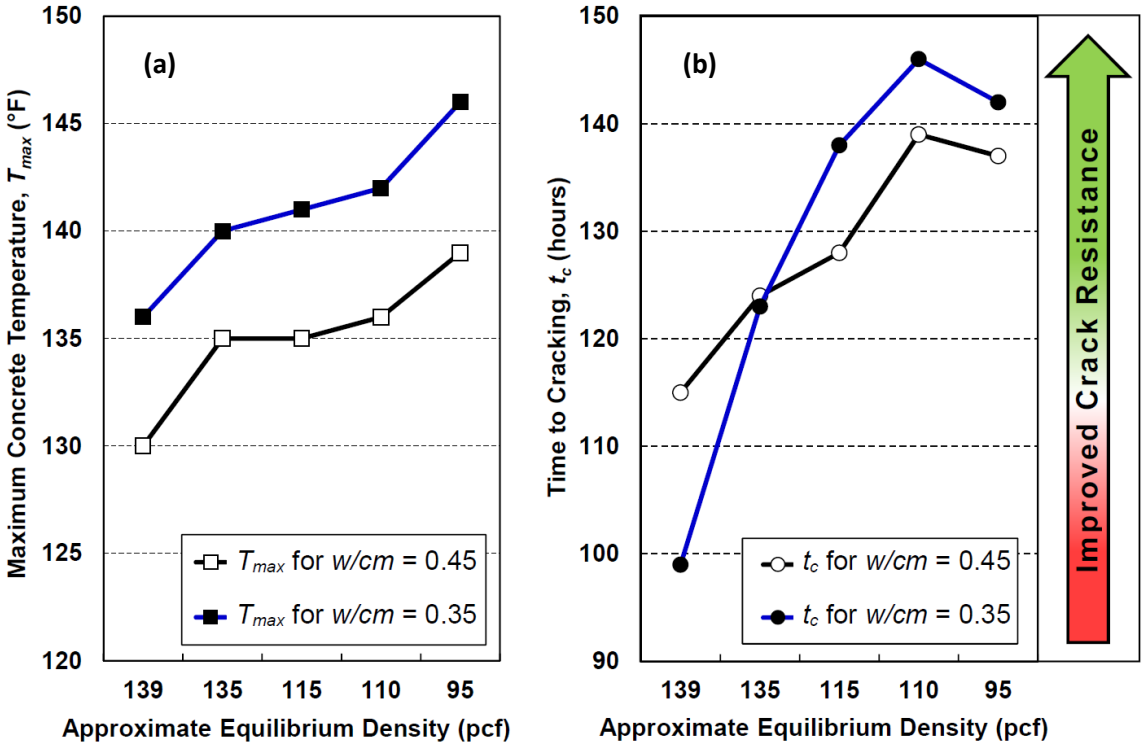

Figure 6-19: Summary of cracking tendency test results versus concrete density: a) Maximum concrete temperature and b) Time to cracking

Increasing the amount of pre-wetted LWA in concrete systematically decreases the density and subsequently the modulus of elasticity of the concrete. The only exception being ISLWC, which had a very low modulus of elasticity and this, is attributed to a lower compressive strength observed in both groups of ISLW concrete specimens. In addition, for both groups of concrete, the CTE decreases with an increasing proportion of pre-wetted LWA, as shown in Figure 6-1. Furthermore, autogenous shrinkage related stresses are eliminated in the 0.38 *w/cm* lightweight aggregate concretes, due to internal curing provided by the pre-wetted LWAs. Similar decrease in autogenous shrinkage related stresses have been reported by others (Byard and Schindler 2010; Lura et al. 2003).

It can thus be concluded that although an increasing amount of LWA in concrete will increase the maximum concrete temperature, the increasing use of LWA will reduce the modulus of elasticity, reduce the coefficient of thermal expansion, and eliminate autogenous shrinkage effects, which all result in an overall improvement in resistance to early-age cracking. As shown in Figure 6-19, sand-lightweight concrete provided the best overall resistance to early-age cracking. The all-lightweight concrete did not perform as well as the sand-lightweight concrete, and this is attributed to its reduced splitting tensile strength when compared to the sand-lightweight concrete.

6.5 MEASURED MODULUS OF ELASTICITY COMPARED TO ACI 318 AND AASHTO LRFD ESTIMATES

Equation 3-7 (ACI 318 2014) and 3-8 (AASHTO LRFD 2016) can be used to estimate the concrete modulus of elasticity using a known compressive strength. The concrete equilibrium density was used to estimate the modulus of elasticity for both ACI 318 (2014) and AASHTO LRFD (2016). The estimated modulus of elasticity according to ACI 318 (2014) and AASHTO LRFD (2016) is compared with the measured modulus of elasticity at 0.5, 1, 2, 3, 7, and 28 days in Figure 5-20 and 5-21, respectively.

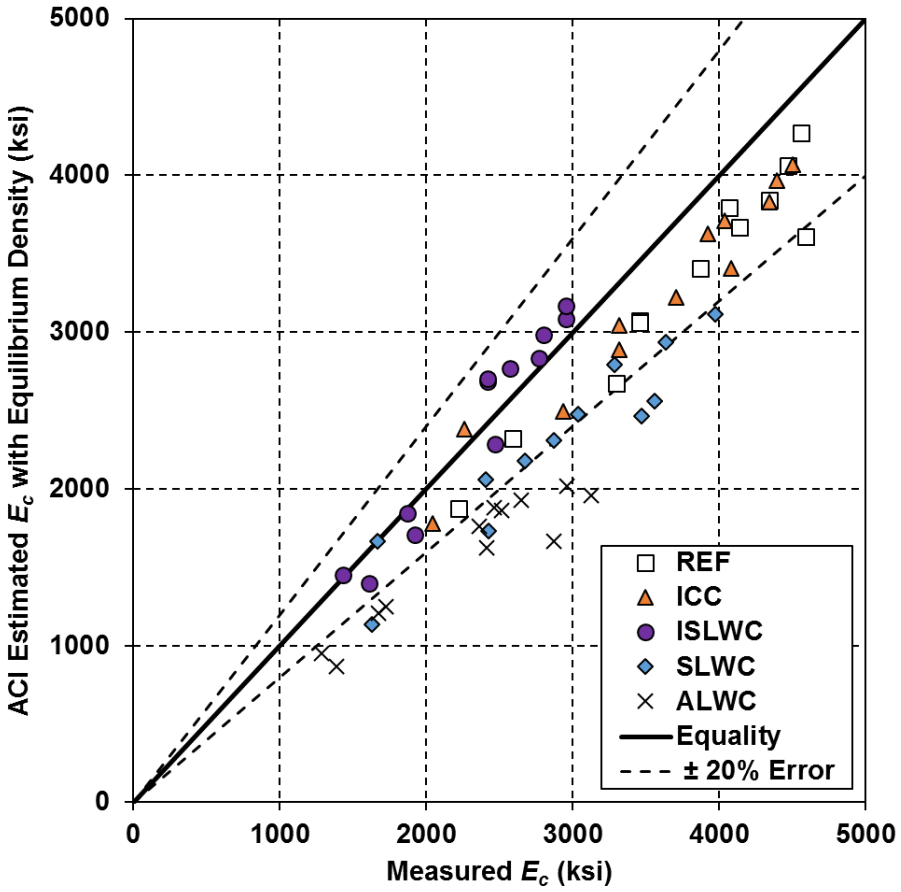

Figure 6-20: Measured versus ACI 318 (2014) predicted modulus of elasticity

From Figure 6-20, it can be observed that the ACI 318 (2014) modulus of elasticity formulation provides accurate results for the reference, IC, and ISLW concretes, because most of the data points fall within the ± 20 % error zone. However, many of the results for the SLW and ALW concretes fall below the – 20 % error line; therefore, ACI 318 (2014) tends to underestimate the modulus of elasticity for the SLW and ALW concretes tested in this study.

From Figure 6-21, it can be observed that the AASHTO LRFD (2016) modulus of elasticity formulation provides accurate results for the reference, IC, and ISLW concretes, because most of the data fall within the ± 20 % error zone. However, many of the results for the

SLW and ALW concretes fall below the – 20 % error line; therefore, AASHTO LRFD (2016) tends to underestimate the modulus of elasticity for the SLW and ALW concretes tested in this study.

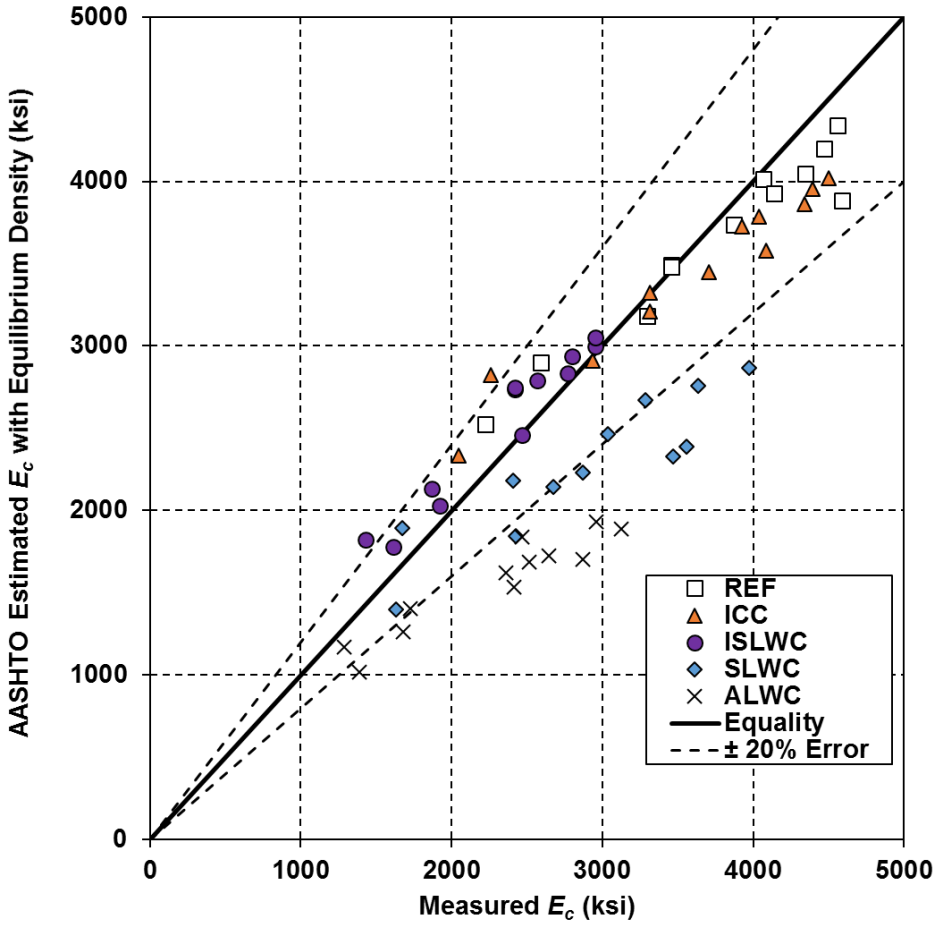

Figure 6-21: Measured versus AASHTO LRFD (2016) predicted modulus of elasticity

The unbiased estimate of the standard deviation of the absolute error, S_j, can be determined as shown in Equation 6-1 (Ayyub and McCuen 2011). The average unbiased estimate of the standard deviation of the absolute error for the modulus of elasticity when using the ACI 318 (2014) and AASHTO LRFD (2016) equations is presented in Table 6-1. It can be seen from the results shown in Table 5-1 that the ACI 318 and AASHTO

LRFD expressions predict the modulus of elasticity well for high-density concretes (i.e. REF, ICC, and ISLWC), but produce a high S_j for concretes having lower densities (i.e. SLW and ALW concretes). Based on the average S_j values reported in Table 6-1, it can be concluded that the ACI 318 (2014) and AASHTO LRFD (2016) expressions predict the modulus of elasticity with similar accuracy.

$$S_j = \sqrt{\frac{1}{n-1}\sum_{i}^{n}\Delta_i^2} \qquad \text{(Equation 5-1)}$$

Where,

S_j = unbiased estimate of the standard deviation (units of property),

n = number of data points (unitless), and

Δ = absolute error (units of property).

Table 6-1: Unbiased estimate of standard deviation of absolute error for the modulus of elasticity estimation models

Modulus of Elasticity Estimation Model	**S_j for E_c Estimate (ksi)**					
	REF	**ICC**	**ISLWC**	**SLWC**	**ALWC**	**Average**
ACI 318: Equation 2-7	525	450	205	715	815	545
AASHTO LRFD: Equation 2-8	310	380	235	805	870	520

6.6 SPLITTING TENSILE STRENGTH BEHAVIOR COMPARED TO ACI ESTIMATES

The ACI 207.2R (2007) and ACI 207.1R (2012) splitting tensile strength equations were used to estimate the measured splitting tensile strength from measured compressive strength test results. The measured splitting tensile strengths at various ages are

compared to the estimates obtained from the ACI 207.2R (2007) and ACI 207.1R (2012) equations in Figures 5-22 and 5-23, respectively.

From Figure 6-22, it can be observed that ACI 207.2R (2007) provides reasonably accurate estimates of the splitting tensile strength for the reference and IC concretes, because most of the data points fall within the ± 20 % error zone. However, many of the results for the ISLW, SLW and ALW concretes fall above the + 20 % error line; therefore, ACI 207.2R (2007) tends to overestimate the splitting tensile strength for the ISLW, SLW and ALW concretes tested in this study.

From Figure 6-23 it can be observed that ACI 207.1R (2012) provides reasonably accurate estimates of the splitting tensile strength for the reference and IC concretes, because most of the data points fall within the ± 20 % error zone. However, the majority of the results for the ISLW, SLW, and ALW concretes fall above the + 20 % error line; therefore, ACI 207.1R (2012) overestimates the splitting tensile strength for the ISLW, SLW, and ALW concretes tested in this study.

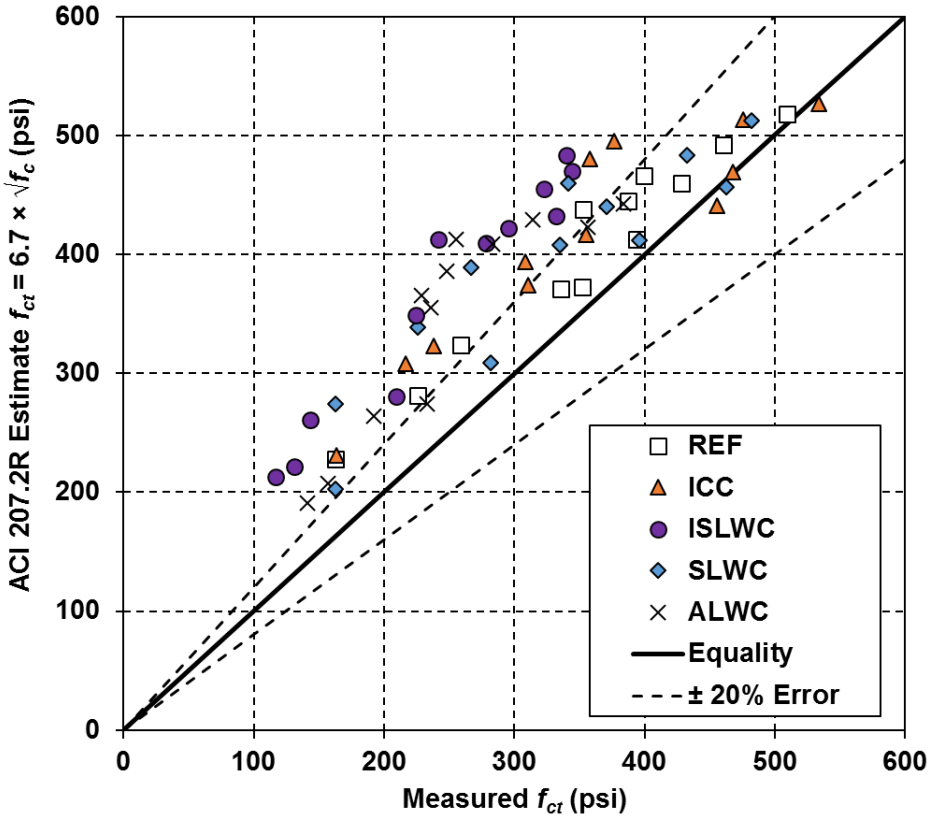

Figure 6-22: Measured versus ACI 207.2R (2007) predicted splitting tensile strength

The unbiased estimate of the standard deviation of absolute error, S_j, for the splitting tensile strength when using the ACI 207.2R (2007) and ACI 207.1R (2012) equations is presented in Table 6-2. It can be seen from the results shown in Table 5-2 that both ACI 207.2R (2007) and ACI 207.1R (2012) equations provide similar estimates of the splitting tensile strengths of the concretes.

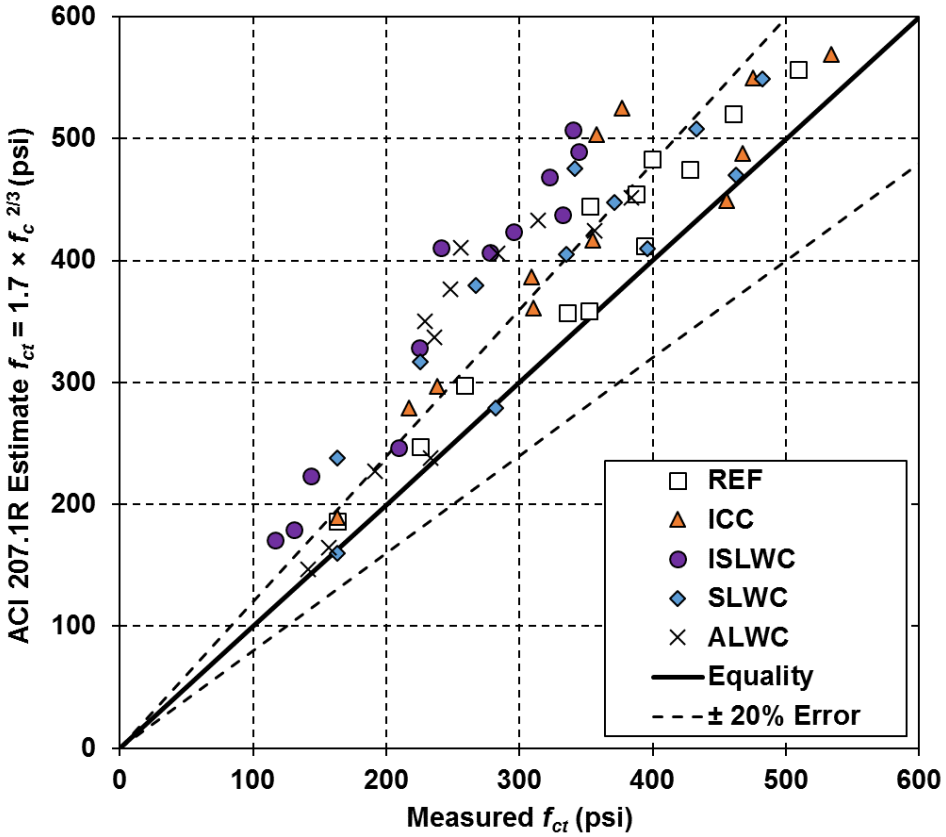

Figure 6-23: Measured versus ACI 207.1R (2012) predicted splitting tensile strength

Table 6-2: Unbiased estimate of standard deviation of absolute error for the splitting tensile strength estimation models

Splitting Tensile Strength Estimation Model	S_j for f_{ct} Estimate (psi)					
	REF	ICC	ISLWC	SLWC	ALWC	Average
ACI 207.2R: Equation 3-3	55	80	135	80	110	90
ACI 207.1R: Equation 3-4	55	80	130	80	105	90

6.7 EVALUATION OF MEASURED LIGHTWEIGHT MODIFICATION FACTORS FOR SPLITTING TENSILE STRENGTH

Green and Graybeal (2013) recommended the use of lightweight modification (λ) factor to estimate the splitting tensile strength as discussed in Section 3.1.4.2. This *λ*-factor can be computed in two ways (Green and Graybeal 2013):

1. If the splitting tensile strength is known, the *λ*-factor can be computed using Equation 6-2.

$$\lambda = \frac{4.7 \times f_{st}''}{\sqrt{f_c''}} \leq 1.0 \qquad \text{(Equation 6-2)}$$

Where,

λ = lightweight modification factor,

f_{st}'' = splitting tensile strength (ksi), and

f''_c = compressive strength (ksi).

2. If splitting tensile strength is unknown, then the *λ*-factor can be computed with Equation 6-3.

$$0.75 \leq \lambda = 7.5 \times w_c'' \leq 1.0 \qquad \text{(Equation 6-3)}$$

Where,

w''_c = concrete equilibrium density (kcf).

The lambda factor can also be computed from ACI 318 (2014) as well. The lambda factor can be computed as follows:

$$\lambda = \frac{f_{st}}{6.7\times\sqrt{f_c}} \leq 1.0 \qquad \text{(Equation 6-4)}$$

Where,

λ = lightweight modification factor,

f_{st} = splitting tensile strength (psi), and

f_c = compressive strength (psi).

The average λ-factors obtained using Equations 6-2, 6-3 and 6-4 for SLW, ISLW, and ALW concretes are presented in Table 6-3. Since the equilibrium density of the reference and IC concretes are 135 pcf or greater, they are considered normalweight concretes and are thus not included in Table 6-3. It can be observed that for SLW and ALW concretes, the λ-factor calculated by using the measured compressive and splitting tensile strengths (Equation 6-2) are similar to those obtained by using equilibrium densities (Equation 6-3). However, the λ-factor obtained from Equation 6-3 for ISLW concrete is much higher than the value obtained from using the measured compressive and splitting tensile strengths. This is partly due to the unexpected lower compressive and splitting tensile strengths observed in the ISLW concretes. Based on these observations, it can be concluded that the λ-factor calculated by using equilibrium density as shown in Equation 6-3, can be used to accurately estimate the splitting tensile strength of the SLW and ALW concretes tested in this study. It can also be observed from Table 6-3 that the lambda factor for ISLWC obtained from Equation 6-4 is lower than that obtained from Equation 6-3 which uses only the equilibrium density of the concrete. Thus care should be taken

when using the lambda factor for ISLWC, since the values only form the equilibrium density is not conservative and experimental testing of the concrete to determine the lambda factor is recommended.

Table 6-3: Average lightweight modification factor (λ-value) by mixture type

Calculation Method	**Lightweight Modification Factor**		
	ISLWC	**SLWC**	**ALWC**
λ-factor from Equation 6-2	0.65	0.82	0.74
λ-factor from Equation 6-3	0.90	0.83	0.75
λ-factor from Equation 6-4	0.66	0.81	0.75

Chapter 7

PART 1: CONCLUSIONS

7.1 SUMMARY

In this study, the effect of using lightweight aggregate on the early-age cracking tendency of mass concrete was evaluated. Two groups of concrete mixtures with a water-to-cementitious materials ratio (*w/cm*) of 0.38 and 0.45 were tested. Each group of concretes contained five mixtures: a reference normalweight concrete, internally cured (IC) concrete, inverse sand-lightweight (ISLW) concrete, sand-lightweight (SLW) concrete, and all-lightweight (ALW) concrete. Ten concretes were thus produced under laboratory conditions and evaluated in this study. The IC concrete is similar to normalweight concrete, except that a portion of fine aggregates was replaced with lightweight fine aggregates. The amount of lightweight aggregate was determined to ensure that the autogenous shrinkage was eliminated and the equilibrium density was greater than 135 pcf, which classifies the IC concrete as normalweight concrete according to AASHTO LRFD (2016). ISLW concrete contained normalweight coarse aggregates and lightweight fine aggregates, whereas the SLW concrete contained normalweight fine aggregate and lightweight coarse aggregate. The ALW concrete contained lightweight fine and coarse aggregates. In order to be representative of mass concrete, Class F fly ash at a 30% (by mass) cement replacement level was used in all mixtures.

The cracking tendency of the concretes were measured in a rigid cracking frame (RCF), using a unique temperature profile to simulate mass concrete placement under fall

environmental conditions. For the lower *w/cm* concrete mixtures, the development of stress due to autogenous shrinkage were recorded under isothermal conditions. A free-shrinkage frame (FSF) was used to assess the unrestrained free shrinkage of the concretes. The time-depended development of mechanical properties was determined by performing compressive, splitting tensile, and modulus of elasticity tests at 0.5, 1, 2, 3, 7, and 28 days. The cylinders used to test the time-depended development of mechanical properties were match cured to the temperature of the RCF specimens. Semi-adiabatic calorimetry was used to characterize the release of heat of hydration from each mixture. The thermal diffusivity of each concrete was also tested to characterize the impact of lightweight aggregate on the development of concrete temperatures. The coefficient of thermal expansion of the hardened concrete was also assessed with a test setup similar to that required by AASHTO T 336 (2009).

7.2 CONCLUSIONS

7.2.1 Effect of Using Lightweight Aggregates on Concrete Properties

From this research, the following conclusions can be made regarding the effects of lightweight aggregate on concrete properties:

- The compressive strength development for the reference, IC, and SLW concretes were similar. However, the compressive strengths of the ALW and ISLW concretes were approximately 10 to 15 % lower when compared to the reference concretes.
- The splitting tensile strength development for the reference, IC, and SLW concretes were similar. However, the splitting tensile strengths of the ISLW and

ALW concretes were approximately 20 to 30 % lower when compared to the reference concretes.

- Increasing the amount of lightweight aggregate systematically decreased the concrete density, thereby also reducing the modulus of elasticity of concrete. When considering the with-in test variability, the modulus of elasticity development for the reference and IC concretes were similar. The modulus of elasticity values were lower on average by 12 %, 33 %, and 33 % for SLW, ISLW, and ALW concretes, respectively, when compared to the reference concretes.
- Increasing the amount of lightweight aggregate in concrete systematically decreased the concrete coefficient of thermal expansion (CTE). The average CTE values were reduced by 5 %, 10 %, 10 %, and 30 % for IC, ISLW, SLW, and ALW concretes, respectively when compared to the reference concretes.
- Concretes with increasing proportion of LWAs exhibit lower thermal diffusivity values, with an average thermal diffusivity reduction of 5 %, 10 %, 30 %, and 50 % for IC, ISLW, SLW, ALW concretes, respectively when compared to the reference concretes.
- The ACI 318 (2014) and AASHTO LRFD (2016) modulus of elasticity formulations provide accurate estimates for the reference, IC, and ISLW concretes tested in this study. However, both ACI 318 (2014) and AASHTO LRFD (2016) tend to underestimate the modulus of elasticity for the SLW and ALW concretes tested in this study.
- The ACI 207.2R (2007) and ACI 207.1R (2012) splitting tensile strength formulations provide reasonably accurate estimates for the reference and IC

concretes tested in this project. However, both ACI 207.2R (2007) and ACI 207.1R (2012) tend to overestimate the splitting tensile strength for the ISLW, SLW, and ALW concretes tested in this study.

- The lightweight modification factor (λ-factor), calculated by using the equilibrium density as proposed by Green and Graybeal (2013), can be used to accurately estimate the splitting tensile strength of the SLW and ALW concretes tested in this study.

7.2.2 Early-Age Concrete Behavior

From this research, the following conclusions can be made about the effect of using lightweight aggregate on the effect of cracking tendency and autogenous shrinkage of concrete:

1. Concretes containing an increased proportion of LWAs experienced higher concrete temperatures when compared to the reference concretes. ALW concrete had the highest maximum concrete temperature followed in order of decreasing maximum concrete temperature by the SLW, ISLW, IC, and reference concretes. This behavior is attributed to the lower thermal diffusivity and increased heat of hydration present in concretes containing LWAs. Care should be taken when using LWA concrete in mass concrete to make sure that the threshold for DEF to occur is not exceeded.
2. As the *w/cm* of the concrete decreased, the peak concrete temperatures increased, which is due to the presence of more cementitious material in low *w/cm* concretes.

3. The presence of LWA in concrete delayed the time to cracking, with SLW concrete providing the best overall resistance to early-age cracking. The time to cracking for all concretes containing pre-wetted lightweight aggregates was greater than the time to cracking of the normalweight concretes.
4. For the concretes with *w/cm* = 0.38, the presence of pre-wetted lightweight aggregate eliminated autogenous shrinkage and its related stresses. The use of lightweight aggregates in concrete with low *w/cm* is beneficial to control early-age cracking, because it helps to mitigate autogenous shrinkage and lower the modulus of elasticity of the higher strength concrete.
5. Although an increasing amount of LWA in the concrete will increase the maximum concrete temperature in mass concrete applications, the increasing use of LWA will reduce the modulus of elasticity, reduce the coefficient of thermal expansion, and eliminate autogenous shrinkage effects, which all contribute to improve the resistance to early-age cracking.

PART II: DETERMINATION OF ALLOWABLE TEMPERATURE DIFFERENCE LIMITS FOR CONCRETES CONTAINING LWA

Chapter 8

PART II: INTRODUCTION

8.1 BACKGROUND

Mass concrete is defined by ACI 207.1R (2012) as “any volume of concrete with dimensions large enough to require that measures be taken to cope with the generation of heat from hydration of the cement and attendant volume change to minimize cracking”. Today, mass concrete includes dams, bridge elements as shown in Figure 8-1, mat foundations, etc.

With increasing construction of mass concrete structures, especially in the infrastructure sector, it is necessary to prevent early-age cracking in mass concrete structures. Cracking in concrete occurs when the tensile stresses exceed the tensile strength of the material (Mehta and Monteiro 2013). ‘Early age’ is commonly defined as the time after setting in which the properties of concrete are rapidly changing and for most concrete mixtures it occurs within seven days of placement (ACI 231 2010). At early ages, the tensile strength of concrete is low, hence, it is more susceptible to early-age cracking. Early-age cracking will compromise the intended design and service life of a concrete structure by providing pathways for the ingress of deleterious substances (Bentz and Weiss 2011).

Figure 8-1: Mass concrete column under construction (Courtesy: PCA 2007)

Based on the definition of mass concrete, there are three different, but closely related, issues associated with mass concrete: size, heat of hydration, and cracking. With regard to size, most state mass concrete specifications designate mass concrete as concrete with a least dimension that is equal to or greater than 4 feet. During hydration of the cementious materials, the entrapped heat causes the mass concrete element's core temperature to rise significantly. Two common types of distress can occur due to a major temperature increase. The first of these—known as thermal cracking—is primarily attributed to a large difference between the core concrete temperature and external concrete temperature. Thermal cracking can reduce the service lifetime of the structure. Figure 8-2 is an example of thermal cracking and shows a concrete core from a footing where the insulation blew off in cold weather conditions. The second type of distress is known as delayed ettringite formation (DEF). DEF is an internal sulfate attack and occurs

when the maximum temperature in concrete exceeds 160°F, and causes expansive stresses in the hardened concrete (Taylor et al. 2001).

Internal curing technologies have become popular in the concrete construction industry and hold promise for producing concrete with increased resistance to early-age cracking and enhanced durability. The American Concrete Institute (ACI) defined internal curing (IC) as the “process by which the hydration of cement continues because of the availability of internal water that is not part of the mixing water” (ACI CT 2016). In internally cured concretes, the maintenance of high moisture content by incorporating pre-wetted absorptive materials, usually lightweight aggregates (LWAs), in the mixture during batching ensures increased hydration (Holt 2001). The increased hydration results in higher early-age strengths of the hardened concrete, thus improving the early-age mechanical properties of the concrete (Mehta and Monteiro 2013).

Figure 8-2: Cored concrete from footing when the insulation blew off during cold weather conditions (Courtesy: CTL Group)

8.2 RESEARCH SIGNIFICANCE

During the construction of the Benicia-Martinez bridge, concretes incorporating lightweight aggregates were determined to have higher maximum core temperatures and higher maximum concrete temperature differences than their normalweight concrete counterparts (Maggenti 2007). This phenomenon indirectly led to a conclusion that higher concrete temperature differences would lead to higher early-age concrete stresses resulting in early-age cracking of mass concrete (Maggenti 2007). Also, research surveys conducted in 2014, concluded that seven of the states with mass concrete specifications limit the maximum concrete temperature difference to 20 °C (35 °F), and two states limit the maximum in-place temperature to 71 °C (160 °F) (Jahren et al. 2014). The reasons behind these restrictions on maximum core temperatures and temperature differences are to avoid DEF and early age thermal cracking, respectively. However, conclusions from previous research (Byard and Schindler 2010) has shown that maximum core

temperatures and temperature differences alone do not contribute to thermal cracking in the concrete, and in fact, thermal cracking in concrete is a culmination of many factors such as splitting tensile strength, modulus of elasticity, creep (relaxation), coefficient of thermal expansion (CTE), and temperature differences of the concrete.

8.3 RESEARCH OBJECTIVES

The focus of this part of this dissertation is to determine the early-age behavior of concrete incorporating lightweight aggregates in mass concrete applications. This investigation is based on a numerical study supplemented with data from experimental work to evaluate the effects of incorporating LWA in mass concrete structures. The objectives of the research presented in this part are as follows:

- Evaluate the maximum concrete temperature differences, early-age stresses, early-age cracking-risk of normalweight concrete and concrete containing LWAs.
- Develop a simplified and improved model to calculate allowable temperature limits in concrete containing LWAs.

8.4 RESEARCH APPROACH

ConcreteWorks is a mass concrete thermal analysis software package developed at UT Austin. ConcreteWorks takes into account the concrete hydration parameters such as specific heat, thermal conductivity, as well as the bridge geometry, mixture proportions, concrete compressive strength, placement temperature, placement date, city, wind speed, and percent cloud cover. All of these parameters are used to generate a unique temperature profile that each concrete mixture would undergo due to its own heat of hydration if it were to be placed in a mass concrete structure (Riding 2007). In this study, ConcreteWorks was used to evaluate the development of concrete core and edge

temperatures, concrete temperature differences, early-age concrete stresses and early-age concrete cracking risk for a time duration of seven days, starting from time of placement. A detailed discussion regarding ConcreteWorks is presented in Section 10.8.

In addition, the time-dependent development of mechanical properties such as concrete compressive strength, splitting tensile strength, and modulus of elasticity of the specimens were evaluated using 6 × 12 in. cylinders. The testing and evaluation of the mechanical properties are covered in Section 6.1. Semi-adiabatic calorimetry was used to characterize the heat of hydration of each concrete as discussed in Section 4.4.1. The coefficient of thermal expansion of each concrete was determined as per AASHTO T336 (2009).

Two groups of concrete mixtures with different *w/cm*: 0.45 and 0.38 were tested. Each group comprised of four different types of concrete, containing normalweight and lightweight aggregates. The four concretes were: reference concrete (REF), internally cured concrete (ICC), sand-lightweight concrete (SLWC) and all-lightweight concrete (ALWC). Three different concrete cross-sectional sizes namely: 4 × 4 ft, 8 × 8 ft, and 12 × 12 ft were chosen for conducting the numerical investigation. In order to be representative of mass concrete, Class F fly ash at a 30% (by mass) cement replacement level was used in all mixtures.

8.5 OUTLINE OF PART II OF DISSERTATION

This part of this dissertation comprises of six chapters. A literature review containing the early-age thermal effects specific to mass concrete, internal curing, lightweight aggregates and their beneficial effects on concrete are summarized in Chapter 9. The experimental work including the mixture proportions, raw concrete materials, and heat of

hydration are examined in Chapter 10. Results of this study, which includes the maximum core and edge temperatures, temperature differences, early-age stresses and mechanical properties of the concrete are discussed in Chapter 11. A discussion and synthesis of the results are presented in Chapter 12. A simplified and improved method to estimate the allowable concrete temperature difference limit is presented in Chapter 13. Summary, conclusions, and recommendations for future study are presented in Chapter 14.

Chapter 9

PART II: LITERATURE REVIEW

In this chapter, the published literature pertaining to mass concrete construction is reviewed. The results of a literature review of thermal effects specific to mass concrete including early-age thermal stress development, compliance models for calculating early-age concrete stresses, causes and effects of delayed ettringite formation, internal curing, and improvement of concrete properties due to incorporation of LWA are presented in this chapter.

9.1 THERMAL CRACKING

9.1.1 Thermal Strain Development

The reaction between cement and fly ash with water is an exothermic reaction, resulting in the dissipation of large quantities of heat (Neville 2011). In a mass concrete element, during the hydration process of cementious materials, concrete transforms itself from a plastic state to a hardened state and the subsequent volume changes produce a strain on the concrete element (Mehta and Monteiro 2013). The resistance of the concrete element to volume changes is defined as restraint. There are two types of restraint, internal and external restraint.

After initial set in the concrete, the temperature in the interior of a mass concrete element increases considerably higher than the edges of the concrete element. When the edges of the mass concrete element is exposed to air (ambient temperature), the edges cool at a faster rate when compared to the interior of the concrete element. This results in a large thermal gradient between the exterior and the interior of the concrete element resulting in an uneven thermal strain distribution across the cross section of the element. The concrete core restrains the contraction of the cooling edge, and this is known as internal restraint. This concept is illustrated in Figure 9-1. Generally, a larger cross section results in a larger temperature difference (Gajda and Vangeem 2002).

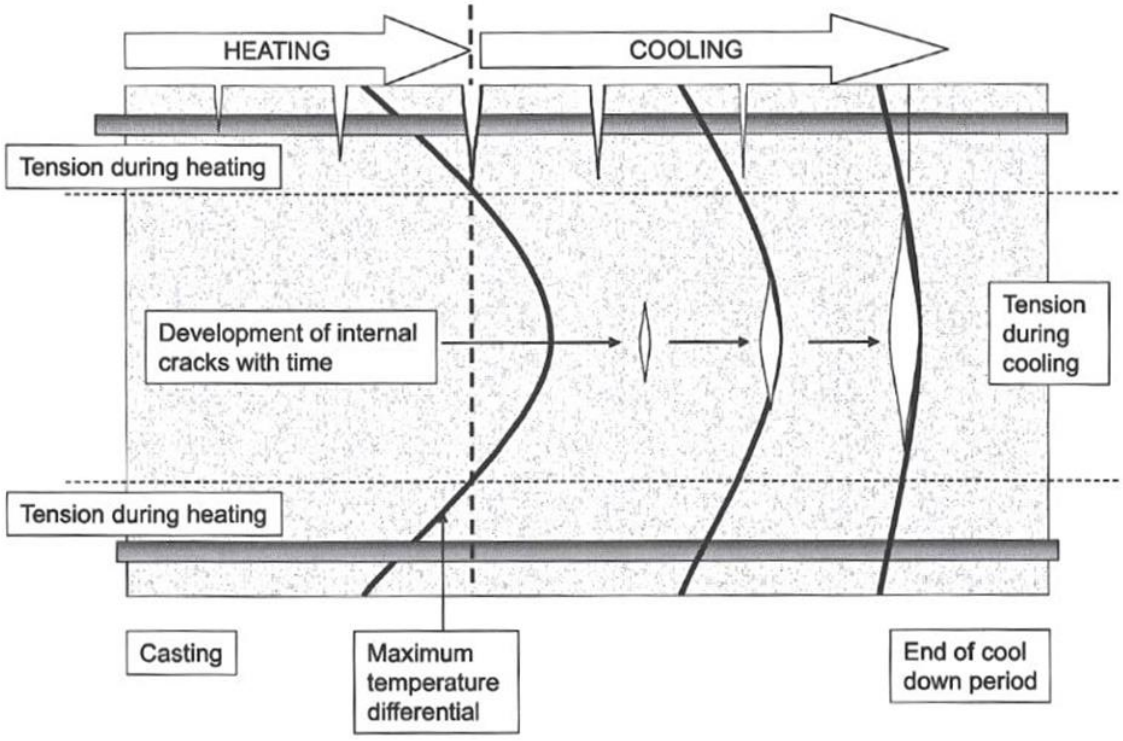

Figure 9-1: Development of cracks in a mass concrete element due to temperature differences assuming only internal restraint (Bamforth 2007)

External restraint occurs when the concrete volume changes are resisted by structural members external to the mass concrete element. After the concrete reaches its maximum temperature, it begins to cool, and subsequently contract in volume. When the volume change is resisted by external elements, tensile stresses develop in the concrete leading to cracking at early-ages. An example of external restraint would be a previously placed adjacent concrete element or other restraining boundary condition (Rostasy et al. 1998). In Figure 9-2 it can be observed that the presence of the pre-existing slab restrains the expansion or contraction of the wall resulting in high tensile stresses (in the wall) and subsequently leads to the formation of tensile thermal cracks across the cross section. Thermal cracking is observed in concrete barriers in Figure 9-3.

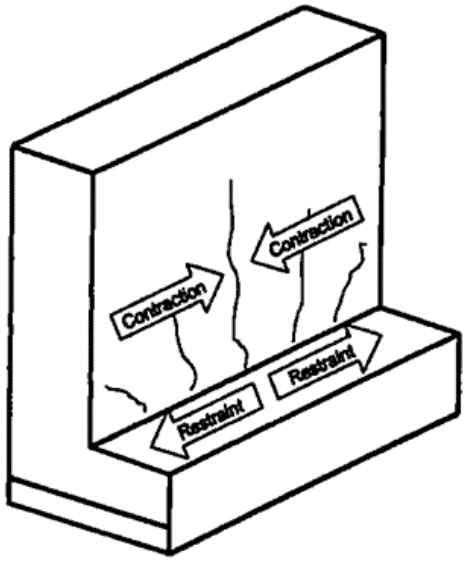

Figure 9-2: Restraint of a concrete member by adjacent elements (Bamforth 2007)

Figure 9-3: Thermal cracking in concrete barrier walls (Bjontegaard 2013)

9.1.2 Causes and Effects of Thermal Cracking in Concrete.

The development of thermal stress in concrete can be determined from Equation 9-1. (Emborg and Bernander 1994). The development of thermal stress is explained in detail in Section 2.1.

$$\sigma = CTE \times \Delta T \times (E_c) \times K_r \qquad \text{(Equation 9-1)}$$

where,

σ is the thermal stress (psi),

CTE is the coefficient of thermal expansion of concrete (in./in./˚F),

ΔT is the difference in temperature = $T_{zero\text{-}stress}$ - T_{min} (˚F),

E_c is the creep-adjusted modulus of elasticity of the concrete (ksi),

K_r is the internal/external restraint factor,

$T_{zero\text{-}stress}$ is the temperature at zero stress in the concrete (˚F), and

T_{min} is the minimum temperature recorded by the concrete member (˚F).

Thermal cracking in concrete reduces the durability and service life of the structure. They also provide pathways for the exchange of deleterious chemicals such as chlorides, which can cause corrosion thus affecting the durability of the concrete structure (Neville 2011). Thus, thermal cracking must be prevented at early ages to improve the long term durability of the concrete structure.

Four primary factors influence the thermal stress development, as shown in Equation 9-1. The first variable is the restraint factor (K_r). For mass concrete applications, Bamforth (2007) assumed the restraint factor between 0.36 and 0.42, since restraint is difficult to quantify for young hardening concrete. The assumed value corresponds to a reasonable assumption for typical mass concrete structures (ACI 207.2R 2007). ACI 207.2R (2007) and Bamforth (2007) provide guidelines to determine the restraint factors for various structures based on shape, cross-section size, age of the concrete, and boundary conditions.

The second factor is the coefficient of thermal expansion (CTE) of the hardened concrete. The CTE is primarily controlled by the coarse aggregate composition (Neville 2011). Aggregates having larger CTE values would cause a higher concrete volume change due to expansion or contraction when compared to aggregates having lower CTE values (Mehta and Monterio 2013). The most common coarse aggregate types and their respective CTEs are displayed in Figure 9-4.

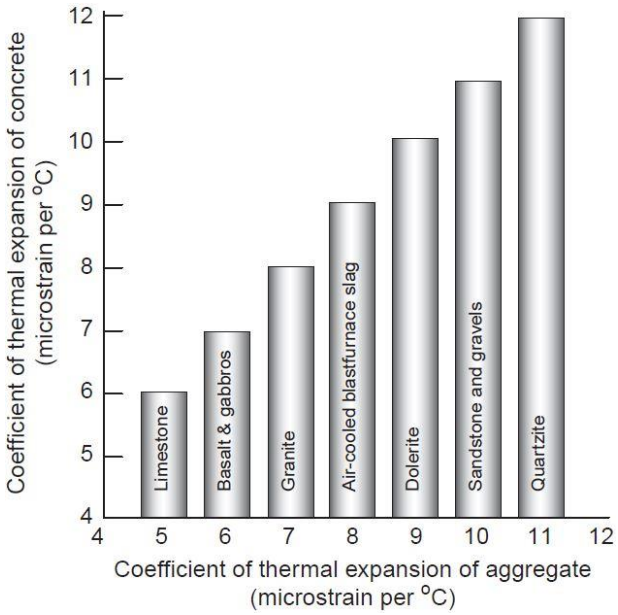

Figure 9-4: Effect of aggregate type on concrete coefficient of thermal expansion ($\Delta°F = 1.8 \times \Delta°C$) (Mehta and Monteiro 2013)

The third variable is the creep adjusted modulus of elasticity (E_c). Various Equations are available for computing the creep-adjusted modulus of elasticity (Bamforth 2007; Bazant and Baweja 2000; ACI 207.1R 2012). For example, Bamforth and Price (1995) recommended a creep modification factor of 0.65, for creep and shrinkage, after taking into account temperature differences across a concrete cross section at early ages.

The last variable, temperature difference (ΔT) is the difference in temperature at various locations of the concrete structure. As mentioned previously, the temperature differences between the edge and the interior of the concrete structure is generally high in mass concrete applications. Based on the tensile strain capacity, Table 9-2 can be used to determine the limiting temperature differential in concrete containing various types of coarse aggregate and differing degrees of restraint (Bamforth and Price 1995).

Table 9-1: Temperature difference limits based on assumed values of CTE and tensile strain capacity (adapted from Bamforth and Price 1995) ($\Delta°F=1.8\times\Delta°C$)

Aggregate Type	Gravel	Granite	Limestone
Coefficient of Thermal Expansion ($\mu\varepsilon$/°C)	12.0	10.0	8.0
Tensile Strain Capacity ($\mu\varepsilon$)	70	80	90
Limiting temperature change for different restraint factors (°C):			
R = 1.0	7	10	16
R = 0.75	10	13	19
R = 0.50	15	20	32
R = 0.36	**20**	28	39
R = 0.25	29	40	64

From Table 9-1 it can be observed that the limiting temperature difference of 36°F (20°C), calculated with a restraint factor of 0.36 is adopted as the recommended temperature difference limit for mass concrete applications (Gajda and Vangeem 2002).

9.1.3 Models for Early-Age Concrete Properties

Equation 9-1 provides a method of computing thermal stresses in concrete at a particular instant of time. However, stresses in concrete vary over a large time duration, hence it would be beneficial to develop the time-dependent model to assess the stresses in concrete. In order to quantify the effect of all the primary factors influencing stresses in concrete, it is important to model the concrete strength and stiffness. Bazant and Baweja (2000) developed a model for the prediction of concrete stresses taking into account the effects of creep, shrinkage, and temperature. This model is known as the B3 model, and is covered in more detail in the remainder of this section.

9.1.3.1 Modeling concrete strength and modulus of elasticity at early ages.

Compressive strength is computed using the following Equation (Bazant and Baweja 2000)

$$f_c(t) = \left(\frac{t}{a+bt}\right) \times f_c\,(28) \qquad \text{(Equation 9-2)}$$

Where,

$f_c\,(t)$ = concrete compressive strength at any time t (psi),

t = age of the concrete (days),

a = 4.0 for moist-cured concrete with Type I cement (days),

b = 0.85 for moist-cured concrete with Type I cement (unitless), and

$f_c\,(28)$ = concrete compressive strength at 28 days (psi).

The splitting tensile strength must be used for mass concrete applications (Raphael 1984). Splitting tensile strength of concrete can be estimated from a known compressive strength, as shown, in Equation 9-3 (Raphael 1984).

$$f_{st}(t) = 1.7 \times f_c(t)^{2/3} \qquad \text{(Equation 9-3)}$$

Where,

$f_t\,(t)$ = concrete tensile strength at time t (psi), and

$f_c\,(t)$ = concrete compressive strength at time t (psi).

AASHTO LRFD (2016) provides Equation 9-4 to estimate the modulus of elasticity from the known equilibrium density and compressive strength of concrete.

$$E''_c(t) = 120000\,(f''_c(t))^{0.33}(w''_c)^{2.0} \qquad \text{(Equation 9-4)}$$

Where,

$E''_c(t)$ = concrete modulus of elasticity (ksi),

w''_c = concrete unit weight (kcf), and

$f''_c(t)$ = concrete compressive strength (ksi).

After computing the compressive strength and modulus of elasticity of concrete, the creep coefficient can be calculated.

9.1.3.2 Modeling of creep effects

The Bazant Baweja B3 model was designed to predict the effects of creep and shrinkage in concrete elements (Bazant and Baweja 2000). The various parameters in this model is summarised in ACI 209 (2008). From the B3 model a creep coefficient can be determined to compute the effects of creep in concrete, and the creep coefficient can be calculated as shown by Equation 9-5.

$$\Phi(t, t_o) = E(t_o)J(t, t_o) - 1 \qquad \text{(Equation 9-5)}$$

Where,

$\Phi(t,t_o)$ = creep coefficient (unitless),

$J(t,t_o)$ = compliance (1/psi),

$E(t_o)$ = modulus of elasticity at the age of concrete loading (psi),

t = age of concrete (days), and

t_o = age of concrete loading (days).

Creep can also be calculated using a compliance function. However, elastic effects must be subtracted from compliance to obtain the time-dependent response. The compliance function present in the B3 Model is shown in Equation 9-6.

$$J(t, t_o) = q_1 + C_o(t, t_o) + C_d(t, t_o, t_c) \quad \text{(Equation 9-6)}$$

Where,

q_1 = instantaneous strain due to unit stress (1/psi),

$C_o(t,t_o)$ = compliance function for basic creep (1/psi),

$C_d(t,t_o,t_c)$ = compliance function for drying creep (1/psi), and

t_c = age drying began (end of moist curing) (days).

The B3 model underestimates the effects of creep and shrinkage for concrete at early ages (Byard 2011). Therefore, a model with improved early-age stress predictions was developed by Byard and Schindler (2015), and is known as the Modified B3 Model. The Modified B3 Model incorporates the existing B3 Model and in addition has two extra parameters which better quantify the effects of creep on concrete at early ages (Byard and Schindler 2015).

9.2 DELAYED ETTRINGITE FORMATION

Delayed ettringite formation (DEF), also known as secondary ettringite formation, is an internal sulfate attack which causes an expansion in the concrete due to the formation of ettringite. A detailed description of DEF is provided in Section 2.2.1.

It was determined that when the concrete temperatures exceeded 158°F (70°C), concrete members containing only Portland cement are susceptible to DEF and this can cause long term damage to the load-bearing capacity of the concrete structure (ACI 201

2016). The most widely accepted temperature limit for mass concrete structures in the United States is 158°F (71°C) (ACI 201 2016). This limit can be increased to 185°F (85°C), if sufficient amount of supplementary cementious materials are present in the concrete mixture (ACI 201 2016). Table 9-2 provides the recommended maximum temperature limits for mitigating DEF in concretes exposed to high temperatures at early-ages (ACI 201 2016).

Table 9-2: Maximum recommended temperature limits for concretes exposed to high temperatures at early ages (adopted from ACI 201 2016)

Maximum Concrete Temperature,	**Prevention Required**
T ≤ 158°F	No prevention required
158°F < T ≤ 185°F	Use one of the following approaches to minimize the risk of expansion: 1. Portland cement meeting requirements of ASTM C150 moderate or high sulfate-resisting and low-alkali cement with a fineness value less than or equal to 430 m2/kg 2. Portland cement with a 1-day mortar strength (ASTM C109) less than or equal to 2850 psi 3. Any ASTM C150 portland cement in combination with the following proportions of pozzolan or slag cement: a) Greater than or equal to 25 percent fly ash meeting the requirements of ASTM C618 for Class F fly ash b) Greater than or equal to 35 percent fly ash meeting the requirements of ASTM C618 for Class C fly ash c) Greater than or equal to 35 percent slag cement meeting the requirements of ASTM C989 d) Greater than or equal to 5 percent silica fume (meeting ASTM C1240) in combination with at least 25 percent slag cement e) Greater than or equal to 5 percent silica fume (meeting ASTM C1240) in combination with at least 20 percent Class F fly ash f) Greater than or equal to 10 percent metakaolin meeting ASTM C618 4. An ASTM C595/C595M or ASTM C1157/C1157M blended hydraulic cement with the same pozzolan or slag cement content in Item 3
T > 185°F	The internal concrete temperature should not exceed 185°F (85°C) under any circumstances.

9.3 INTERNAL CURING

Man-made lightweight aggregates (LWAs) such as expanded shale, slate and clay have been used to promote internal curing in concrete (Bremner and Ries 2009). Pre-wetted LWAs have the capability of absorbing large amounts of water during the pre-wetting process, and when added to concrete, can desorb the water into the concrete during the hydration process of cementious materials (Lura et al. 2003). A partial replacement of fine normalweight aggregate with fine lightweight aggregate promotes internal curing and this concept is illustrated in Figure 9-5.

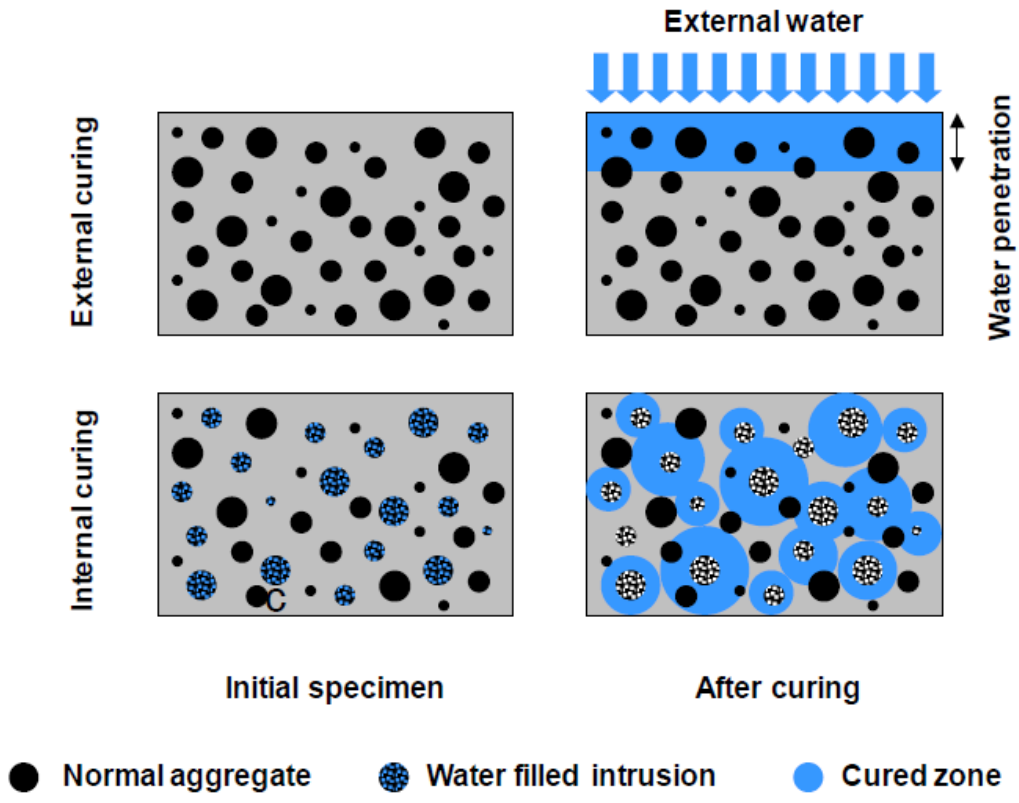

Figure 9-5: Mechanism of external and internal curing in concrete (Bentz and Weiss 2011)

The addition of pre-wetted LWA relieves stresses in concrete due to autogenous shrinkage, especially in concretes containing low *w/cm*. This is achieved by desorbing the water from the aggregate particles into the hydrated cement-paste matrix and relieving some or all of the capillary stresses (Holt 2001). Additional benefits of adding pre-wetted LWA to concrete include higher degree of hydration, reduced modulus of elasticity, and coefficient of thermal expansion of concrete (Byard, Schindler, and Barnes 2012). A detailed summary of internal curing is provided in Section 2.4.

9.4 EFFECTS OF USING LIGHTWEIGHT AGGREGATES IN CONCRETE

Adding lightweight aggregates to concrete improves the overall concrete resistance to early-age cracking. Table 9-3 presents the effect of adding LWA to concrete on the various concrete properties. A detailed description is presented in Section 2.5.

Table 9-3: The effect of different concrete properties when LWA is added to concrete

Property	Addition of LWA on early-age concrete stresses
Autogenous Shrinkage	Decrease (Henkensiefken et al. 2009; Byard and Schindler 2010)
Coefficient of Thermal Expansion	Decrease (Neville 2011; Byard and Schindler 2010)
Modulus of Elasticity	Decrease (Bentz and Weiss 2011; Byard and Schindler 2010)
Splitting Tensile Strength	Similar for sad-lightweight concrete, decreases for all-lightweight concrete (Byard and Schindler 2010)
Relaxation (Creep)	Increase (Cusson and Hoogevan 2007; Byard and Schindler 2015)

Chapter 10

PART II: EXPERIMENTAL WORK

10.1 EXPERIMENTAL PROGRAM

The early-age temperature, stress development and cracking risk was evaluated for four different concrete types: reference concrete (REF), internally-cured concrete (ICC), sand-lightweight concrete (SLWC), and all-lightweight concrete (ALWC). In addition, the effect of each concrete type was modeled for three different concrete cross-section sizes; 4 × 4 ft, 8 × 8 ft, and 12 × 12 ft. Two different groups of concrete mixtures with *w/cm* of 0.45 and 0.38 were tested. Semi-adiabatic calorimetry (SAC) was used to determine the heat of hydration for each concrete type. Mechanical properties such as compressive strength, splitting tensile strength, and modulus of elasticity of each concrete type were evaluated using 6 × 12 in. cylinders in accordance to ASTM standards. Numerical simulation using ConcreteWorks software was performed on three rectangular shaped piers having the cross-section sizes mentioned before, to model the temperatures, stresses and cracking risk for all the concretes. The time of placement, ambient weather conditions, cross-section sizes, and materials used in the concrete mixture proportion for this study were chosen to closely represent the construction of the Benicia-Martinez bridge in California. This was to ensure the validity of the temperature rise reported in the lightweight mass concrete elements (Maggenti 2007).

10.2 LIGHTWEIGHT AGGREGATE PRECONDITIONING

Water-filled plastic barrels were used for moisture conditioning of the lightweight aggregates. The lightweight aggregates pre-conditioning procedure is explained in detail in Section 3.2.3.

The relative density testing of the coarse and fine lightweight aggregates was conducted according to ASTM C127 (2014) and ASTM C128 (2014), respectively. The absorption tests for the lightweight aggregates were performed according to ASTM C1761 (2015). This method is usually known as the “paper towel method” and commercial grade paper towels are used to determine the surface-dry condition of the LWAs. The aggregate type, source, particle size, relative density, pre-wetted absorption, and fineness modulus results are shown in Table 10-1. The aggregate gradations can be seen in Appendix A. When LWAs are exposed to moisture not all the pores in the LWAs get filled, because a small portion of pores are never filled despite years of immersion in water (Bremnar and Ries 2009). Therefore, the relative density calculations presented in Table 10-1 are for the aggregates in pre-wetted surface-dry condition after an immersion period of 7 days.

Table 10-1: Lightweight aggregate source, type, and properties

Item	**Shale Lightweight Aggregate**	
Source	Norlite Aggregates (Albany, NY)	
Type of LWA	Fine Aggregate	Coarse Aggregate
Particle size	0 to #4	#4 to ¾ in.
Relative density (SD[§])	1.67	1.35
Pre-wetted absorption *	20%	18%
Fineness modulus	3.3	NA

Note: * Measured water absorption after soaking in water for 7 days.

[§] Relative density at surface-dry state after 7 days of soaking in water.

10.3 MIXTURE PROPORTIONS

Two groups of *w/cm* mixture proportion were evaluated in this study. Each mixture proportion comprised of four concrete types, and they consisted of normal-weight concrete, known as reference concrete (REF), internally-cured concrete (ICC), sand-lightweight concrete (SLWC) and all-lightweight concrete (ALWC). The mixture proportion for all the concretes with the *w/cm* of 0.45 and 0.38 is provided in Table 10-2 and 10-3, respectively. The reference concrete was proportioned to represent a typical mass concrete mixture used in south eastern U.S. The reference concrete comprised of normalweight coarse and fine aggregates. Internally-cured concrete was proportioned by replacing a small portion of normalweight fine aggregate with lightweight fine aggregate. ICC was proportioned to be categorized as normalweight concrete according to AASHTO LRFD (2016), therefore, the equilibrium density of ICC was greater than 135 pcf. The equilibrium density was computed using ASTM C567 (2014). Sand-lightweight concrete comprised of coarse lightweight aggregates and river sand, whereas all-lightweight concrete comprised of coarse and fine lightweight aggregates. The naming convention is similar to the convention described in Section 3.3.

Table 10-2: Proportions and properties for all *w/cm* = 0.45 mixtures

Item	REF 0.45	ICC 0.45	SLWC 0.45	ALWC 0.45
Water Content (lb/yd^3)	263	263	263	263
Cement Content (lb/yd^3)	410	410	410	410
Class F Fly Ash Content (lb/yd^3)	175	175	175	175
SSD Normalweight Coarse Aggregate (lb/yd^3)	1740	1740	0	0
SD Lightweight Coarse Aggregate (lb/yd^3)	0	0	910	857
SSD Normalweight Fine Aggregate (lb/yd^3)	1220	1000	1190	0
SD Lightweight Fine Aggregate (lb/yd^3)	0	140	0	820
Water-Reducing Admixture (oz/yd^3)	16.0	14.0	0.0	0.0
Mid-Range Water-Reducing Admixture (oz/yd^3)	0.0	0.0	22.0	18.0
Rheology-Controlling Admixture (oz/yd^3)	0.0	0.0	0.0	32.0
Air-Entraining Admixture (oz/yd^3)	1.0	1.0	3.5	3.5
Target Total Air Content (%)	5.0	5.0	5.0	5.0
Water-cementious materials (*w/cm*)	0.45	0.45	0.45	0.45

Table 10-3: Proportions and properties for all *w/cm* = 0.38 mixtures

Item	REF 0.38	ICC 0.38	SLWC 0.38	ALWC 0.38
Water Content (lb/yd^3)	243	243	243	243
Cement Content (lb/yd^3)	435	435	435	435
Class F Fly Ash Content (lb/yd^3)	195	195	195	195
SSD Normalweight Coarse Aggregate (lb/yd^3)	1740	1740	0	0
SD Lightweight Coarse Aggregate (lb/yd^3)	0	0	910	857
SSD Normalweight Fine Aggregate (lb/yd^3)	1220	1000	1190	0
SD Lightweight Fine Aggregate (lb/yd^3)	0	140	0	820
Water-Reducing Admixture (oz/yd^3)	20.0	20.0	0.0	0.0
Mid-Range Water-Reducing Admixture (oz/yd^3)	0.0	0.0	28.0	26.0
Rheology-Controlling Admixture (oz/yd^3)	0.0	0.0	0.0	34.0
Air-Entraining Admixture (oz/yd^3)	1.0	1.0	3.5	3.5
Target Total Air Content (%)	5.0	5.0	5.0	5.0
Water-cementious materials (*w/cm*)	0.38	0.38	0.38	0.38

The target slump and total-air content for all the mixtures were 4±1 in. and 5.5±1.5%, respectively, which are typical values for mass concrete construction in the southeastern U.S. In this study, the measured equilibrium density was within ±1 pcf of the calculated density after correcting for the measured total air content.

10.4 OTHER RAW CONCRETE MATERIALS

10.4.1 Portland Cement

Type I Portland cement was used in all the concrete mixtures relevant to this study. The chemical composition and fineness of this cement are shown in Table 10-4.

Table 10-4: Portland cement chemical composition and fineness

C_3S	C_2S	C_3A	C_4AF	Free CaO	SO_3	MgO	Blaine Fineness
60.3 %	18.2 %	5.4 %	11.3 %	0.9 %	2.6 %	1.3 %	351 (m^2/kg)

10.4.2 Fly Ash

The fly ash used in this study was Class F fly ash and was obtained from Boral Material Technologies. The chemical composition of this fly ash is listed in Table 10-5.

Table 10-5: Fly ash chemical composition

SiO_2	Al_2O_3	Fe_2O_3	CaO	MgO	SO_3	K_2O	Na_2O	Total Alkalies
55.7 %	27.9%	6.5 %	1.2 %	0.7 %	0.1 %	2.5%	0.3 %	2.0%

10.4.3 Normalweight Coarse and Fine Aggregates

The normalweight coarse aggregate for this project was ASTM C33 No. 67 siliceous river gravel. The normalweight fine aggregate was siliceous river sand. Both the aggregate types were obtained from Auburn, Alabama. The aggregates were sampled and ASTM

C136 (2014) sieve analysis was performed to determine the gradations. The specific gravity, absorption capacity, and fineness modulus of both the aggregate types are shown in Table 10-6.

Table 10-6: Properties of normalweight coarse and fine aggregate

Property	Coarse Aggregate	Fine Aggregate
Absorption Capacity (%)	0.16	0.34
Specific gravity	2.63	2.64
Fineness modulus	-	3.00

10.4.4 Chemical Admixtures

Chemical admixtures were used to obtain the desired slump and total-air content for each concrete mixture. All the admixtures were supplied by the BASF Corporation. The dosages are provided in Table 10-2 and 10-3.

10.5 HEAT OF HYDRATION

The reaction of cement, fly ash with water is an exothermic reaction, resulting in a temperature rise in the concrete specimen. Semi-adiabatic calorimetry was used to determine the hydration parameters for temperature modeling.

The semi-adiabatic calorimeter (SAC) test equipment used during this project was supplied from Digital Site Systems, Pittsburg, Pennsylvania. The SAC setup comprised of a 55- gallon drum and a 6 × 12 in. cylinder setup. The concrete temperature, external air temperature, and the heat loss through the calorimeter walls are recorded by probes present in the test equipment. Initial calibration using heated water is performed to record the heat loss through the calorimeter.

The concrete heat of hydration parameters tau (τ), beta (β), ultimate degree of hydration (α_u) parameters were computed from semi-adiabatic calorimetry tests performed according to recommendations from the RILEM technical committee 119 (RILEM 119 1998). A detailed description of this procedure is presented in Section 3.4.1.

10.6 MECHANICAL PROPERTIES

For each concrete type, 24 6 × 12 in. cylinders were cast as per ASTM C192 (2014). The cylinders were tested for compressive strength (ASTM C39), splitting tensile strength (ASTM C496), and modulus of elasticity (ASTM C469) at 0.5, 1, 2, 3, 7, and 28 days. All mechanical property testing met the precision and bias conditions of their respective ASTM standards.

10.7 COEFFICIENT OF THERMAL EXPANSION

The coefficient of thermal expansion (CTE) for each concrete type was measured as per AASHTO T336 (2009). A 6 × 7 in. concrete cylinder is placed in a frame that is submerged in water. Spring-loaded LVDTs mounted on the frame are placed in contact with the concrete cylinder. The temperature of the water bath is varied between 50°F to 122°F, and the ensuing change in length of concrete cylinder is measured. From the resulting displacements and temperature changes, the CTE of the concrete can be calculated. A detailed description of the procedure is provided in Section 3.4.6.

10.8 CONCRETEWORKS

ConcreteWorks is an early-age concrete temperature development and thermal stress analysis software developed to aid engineers to predict concrete behavior and durability. ConcreteWorks was developed by the Concrete Durability Center at the University of Texas. The software is capable of analyzing various environmental, construction, and concrete mixture proportioning parameters in specific types of concrete elements. The available output results for the program include predictions of the maximum concrete temperature over time, maximum temperature differences, compressive strength development, early-age stresses, splitting tensile stremgth, and cracking risk potential with respect to time (Riding 2007; Poole et al. 2006). Tables 10-7 and 10-8 gives a brief overview of the input and output categories of ConcreteWorks (Riding et al. 2017).

Table 10-7: ConcreteWorks input categories (adapted from Riding et al. 2017)

Input Category	**Specific Inputs**
General	• Time, date, and location of concrete placement. • Duration of thermal analysis (1-14 days)
Shape	• Element shape
Dimensions	• Dimensions specific to element shape
Mixture Proportions	• Batch weights and properties of all raw materials in concrete • Additional properties include the detailed aggregate gradation properties, coarseness factor, etc.
Material Properties	• Chemical composition, hydration properties of cementious materials • Type of aggregates used and corresponding CTEs
Mechanical Properties	• Maturity function, equivalent age, and early age creep inputs
Construction	• Placement temperature, formwork type, method and duration of curing
Environment	• Ambient weather data
Corrosion	• Details about reinforcing steel used, barrier protection

Table 10-8: ConcreteWorks output categories (adapted from Riding et al. 2017)

Mass Concrete Member Type	Chloride Service Life	Thermal Cracking Risk	Temperature Prediction	Stress/Strength Development
Rectangular Column	X	X	X	X
Rectangular Footing	X	X	X	X
Partially Submerged Rectangular Footing	X	X	X	X
Rectangular Bent Cap	X	X	X	X
T-Shaped Bent Cap	X		X	X
Circular Column	X		X	X
Drilled Shaft	X		X	X

The predicted temperature profiles for any element size is a useful feature and can be used to determine the temperature difference between the core and the edge of a concrete element. The temperature difference can also be viewed in tandem with concrete cracking risk, which enables the user to determine if the particular type of concrete is susceptible to early-age cracking (Riding et al. 2017). Another output result of ConcreteWorks is the early-age stresses that develop across the cross section, which is obtained by performing a finite-difference analysis. ConcreteWorks utilizes the Linear Logarithmic Model (LLM) for modeling creep. The LLM can model the basic creep behavior in young concrete with a good correlation to experimental data (Larson 2003).

Figure 10-1 is an example which shows the ConcreteWorks's output summary and temperature difference/cracking risk plot at early-ages (Eiland 2016). The concrete element used was a rectangular footing placed in Alabama.

Figure 10-1: ConcreteWorks output summary (top) and temperature difference/cracking risk profile (bottom) (Eiland 2016)

In figure 10-1 (top), the maximum temperature and maximum temperature differences are marked in red. The maximum temperature and temperature difference limits for mass concrete elements in ConcreteWorks are 158°F and 35°F, respectively

(Concrete Durability Center 2005). These values match the TXDOT 2004 specification, however the maximum temperature limit has been raised from 158°F to 160°F in the Texas Standard Specification for highway and bridge construction (2014).

In figure 10-1 (bottom), the cracking risk profile is shown for the particular type of concrete used at early-ages. The cracking risk or stress-to-strength ratio is color coded and allows for quick evaluation of potential cracking or durability issues associated with the concrete. Table 10-9 shows the definition of colors used. From Table 10-9 and Figure 10-1 it can be observed that the cracking probability index for the given example is high.

Table 10-9: ConcreteWorks cracking risk (adapted from Concrete Durability Center 2005)

Color	Cracking Probability	Tensile Stress-Strength Ratio C_r
Green	Low	$C_r < 0.60$
Yellow	Medium	$0.60 \leq C_r < 0.67$
Orange	High	$0.67 \leq C_r < 0.72$
Red	Very High	$C_r \geq 0.72$

Three different rectangular cross-section sizes, i.e. 4 × 4 ft, 8 × 8 ft, and 12 × 12 ft, were chosen in this study for evaluating the temperature rise, stresses and cracking risk of concretes containing normalweight and lightweight aggregates. For rectangular columns, ConcreteWorks models a two-dimensional horizontal cross section as shown in Figure 10-2 (a) (Riding et al. 2017). The rectangular columns along with formwork are modeled using symmetry in both directions as shown in Figure 10-2 (b). ConcreteWorks allows for removal of formwork and curing of concrete post formwork removal. This feature enables one to model the temperature differences present during the formwork

removal process, which may induce thermal shocks in the concrete. A typical concrete formwork removal process is shown in Figure 10-3.

The varying input values for ConcreteWorks used for this study are defined in Appendix B. As mentioned previously, the time of casting, the formwork used, and the formwork removal time were chosen closely to represent the construction of the Benicia-Martinez bridge in California (Maggenti 2007). Since the bridge was constructed during the months of December to January, a date of January 15th was chosen to simulate the construction process. The time of casting was chosen to be 8:00 am which represents a reasonable start time for winter construction. The other construction inputs chosen were the wooden forms for form type and the 'wet curing blanket' option for insulation purposes (after formwork removal). The formwork was removed after a duration of 96 hours and a 15-minute interval was accounted for the removal time. The environmental inputs are already pre-programmed in ConcreteWorks and the software allows the user to choose a location, which was chosen as San Francisco for this study. For all other factors, default inputs were chosen.

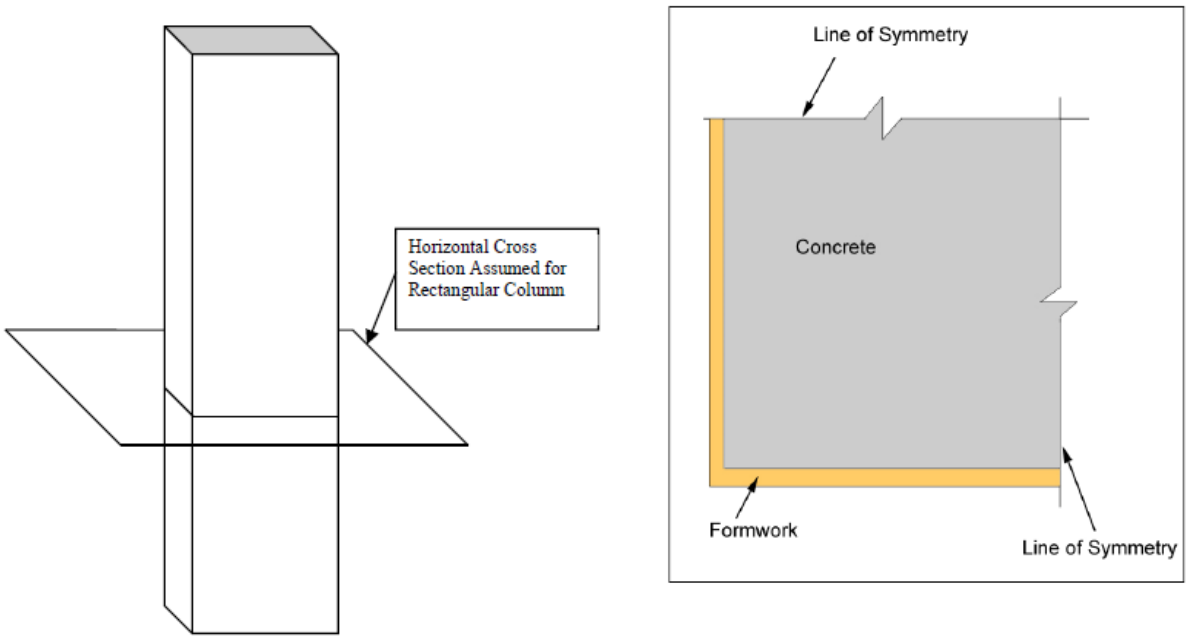

(a) (b)

Figure 10-2: (a) Horizontal cross section of rectangular column assumed in ConcreteWorks (b) Rectangular column model used in ConcreteWorks

Figure 10-3: Rectangular column formwork removal (Riding et al. 2017)

10.9 OTHER FRESH QUALITY CONTROL TESTS

The concrete was mixed as per ASTM C192 (2014) under standard laboratory conditions. The slump, temperature, and the density were measured as per ASTM C143 (2014), ASTM C1064 (2014), and ASTM C138 (2014), respectively for every batch of concrete. The total air content was determined using the pressure method as per ASTM C231 (2014) for normalweight concretes. The volumetric method as per ASTM C173 (2014) was used to determine the total air content for concretes incorporating lightweight aggregates.

Chapter 11

PART II: EXPERIMENTAL RESULTS

The results from the numerical investigation performed for this study are presented in this chapter. A detailed discussion and analysis of results are presented in Chapter 12. The results presented include:

- Combined mixture gradations,
- Fresh concrete properties,
- Time-dependent mechanical properties,
- Thermal properties,
- Concrete temperatures,
- Concrete stresses, and
- Cracking risk of concrete

11.1 CONCRETES WITH *W/CM* = 0.45

11.1.1 Combined Mixture Gradations

Four concrete mixtures with a *w/cm* of 0.45 and with three of them containing lightweight aggregates were produced and tested. The combined gradations of these concretes are plotted on a 0.45-power curve, as shown in Figure 5-1 in. Their workability factors for all the 0.45 *w/cm* concretes are presented in Figure 5-2 in Part I.

11.1.2 Fresh Concrete Properties

The fresh concrete properties such as the slump, total air content, temperature, and density were measured for each concrete mixture and are presented in Table 5-1. The

calculated equilibrium densities in accordance with ASTM C567 (2014) are also presented in Table 5-1.

11.1.3 Time-Dependent Development of Concrete Mechanical Properties

The time-dependent development of compressive strength, splitting tensile strength, and modulus of elasticity were tested for each concrete mixture. A total of 24 cylinders were used in the testing process for each concrete type. The measured values were averaged for two cylinders and are presented in Appendix C. A regression analysis was performed as per ASTM C1074 (2014), which recommends the use of an exponential function. Best-fit curves were determined for the measured values and are plotted in Figures 5-7 to 5-9.

11.1.4 Thermal Properties

The calculated equilibrium density, coefficient of thermal expansion, and thermal diffusivity are summarized in Table 5-2

11.1.5 Concrete Temperature Development

11.1.5.1 Core Temperatures

The simulated core temperatures for all 0.45 *w/cm* concretes belonging to three different cross-section sizes are presented in Figures 11-1 to 11-3. The DEF limit which is fixed at 185°F (ACI 201 2016) is also shown.

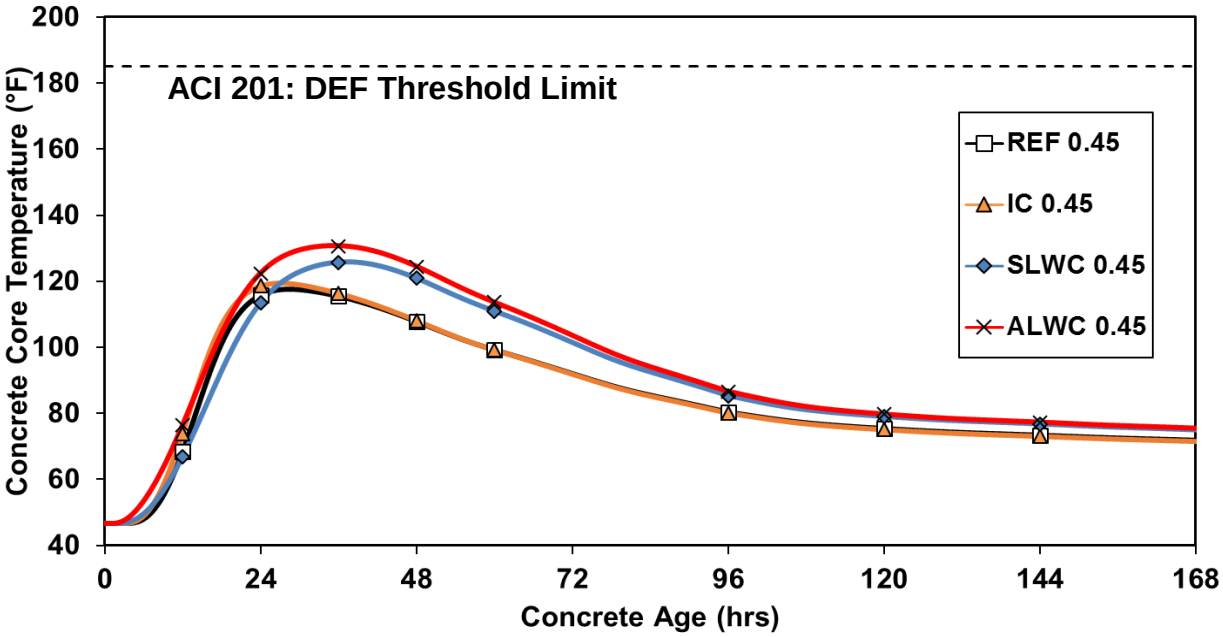

Figure 11-1: Maximum core temperatures for 4× 4 ft cross-section size column for all 0.45 *w/cm* concrete

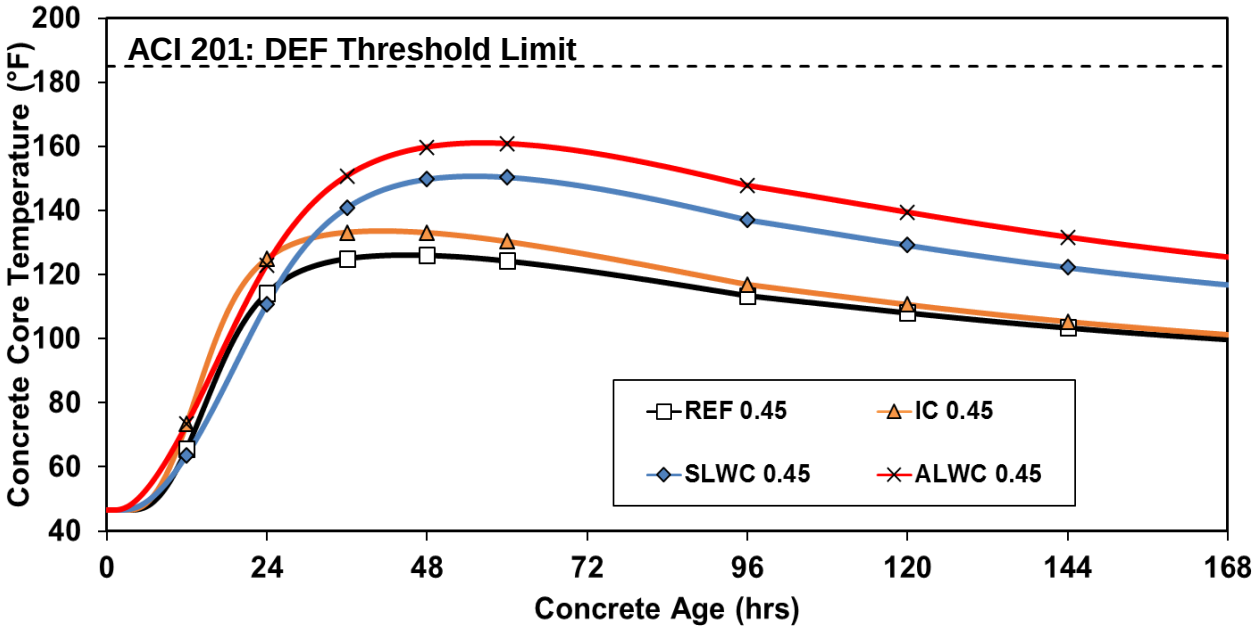

Figure 11-2: Maximum core temperature for 8 × 8 ft cross-section size column for all 0.45 *w/cm* concretes

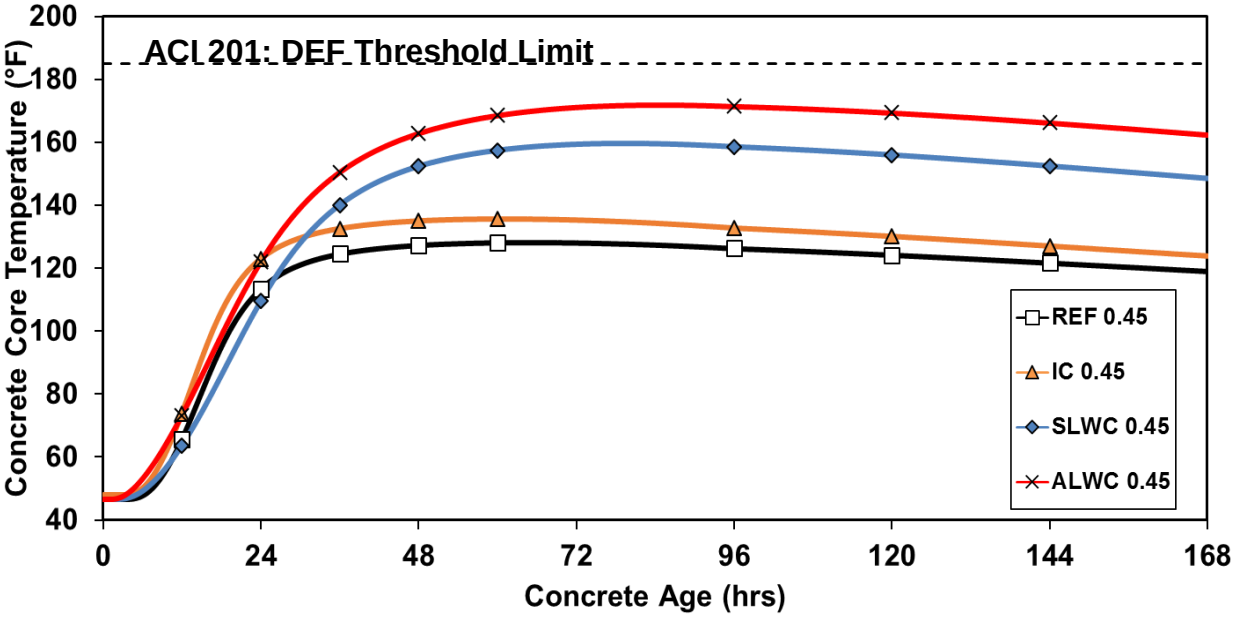

Figure 11-3: Maximum core temperature for 12 × 12 ft cross-section size column for all 0.45 *w/cm* concretes

11.1.5.2 Edge Temperatures

The simulated edge temperatures for all the concretes belonging to the three different cross-section sizes are presented in Figures 11-4 to 11-6.

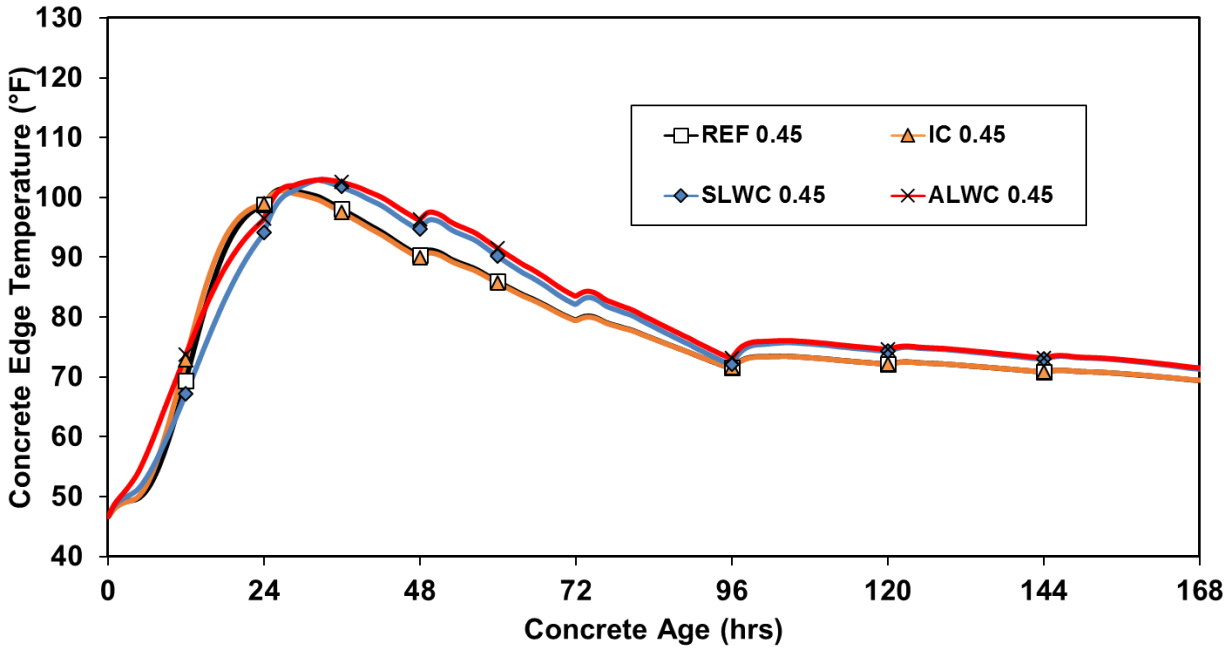

Figure 11-4: Edge Temperature development of 4 × 4 ft cross-section for all 0.45 *w/cm* concretes

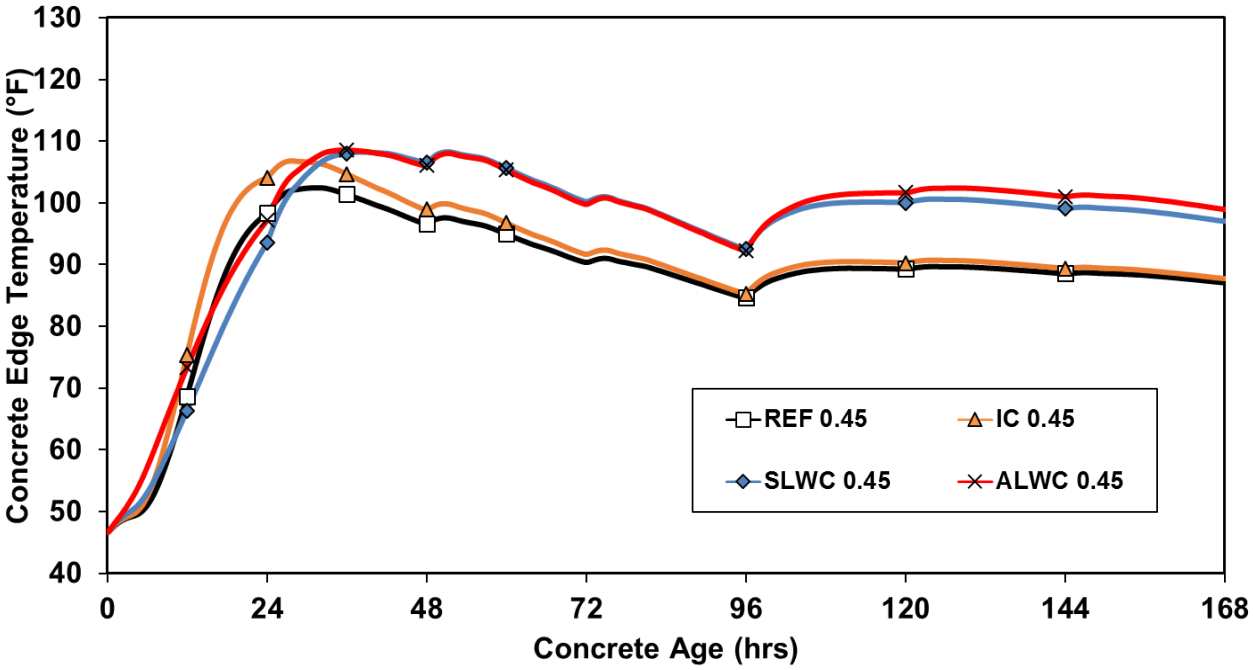

Figure 11-5: Temperature development at the edge of 8 × 8 ft cross-section size column for all 0.45 *w/cm* concretes

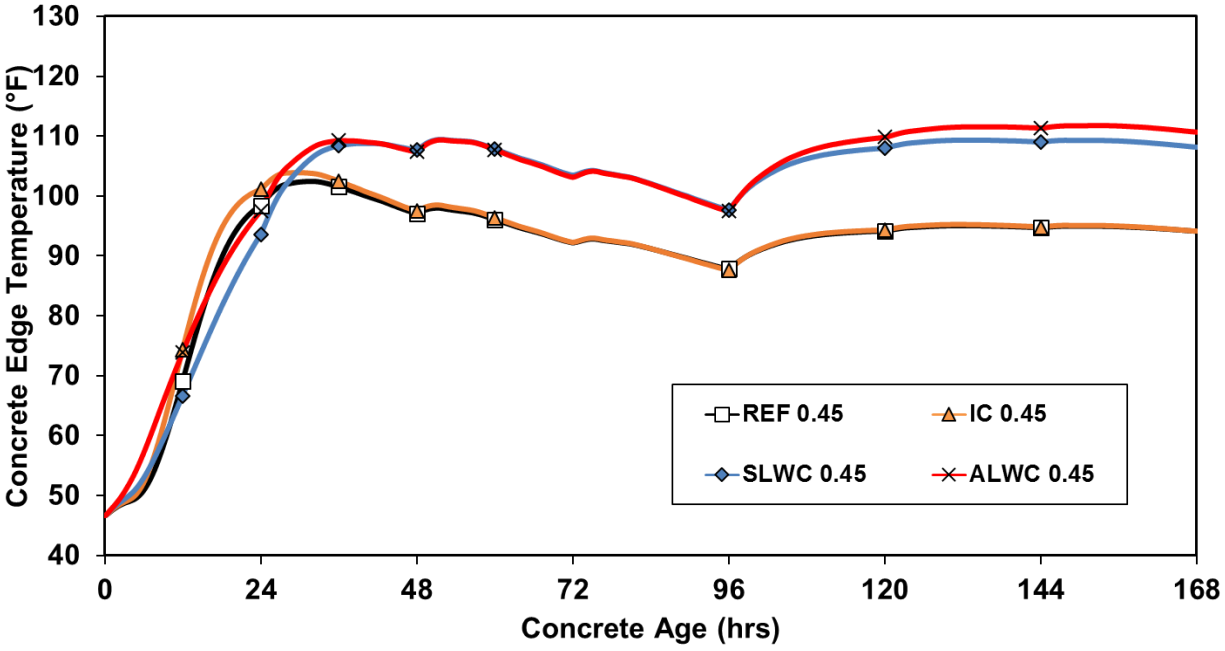

Figure 11-6: Temperature development at the edge of 12 × 12 ft cross-section size column for all 0.45 *w/cm* concretes

11.1.5.3 Concrete Temperature Differences

The simulated concrete temperature differences for all the concretes belonging to the three different cross-section sizes are presented in Figures 11-7 to 11-9. The maximum temperature difference is calculated as the temperature difference between the midpoint on edge and the core of the structure. The maximum temperature difference limit fixed at 35°F (ACI 301 2016) is also shown. Figure 11-10 indicates the temperature differences for reference concrete for a 12 × 12 ft cross section between the core, midpoint on edge and core, corner. It can be observed that the temperatures of the corner are cooler than the midpoint on edges. Thus the corners cool faster than the midpoint on the edges. Therefore the temperature differences between the core, midpoint on edge is lower than the temperature difference between core and corner.

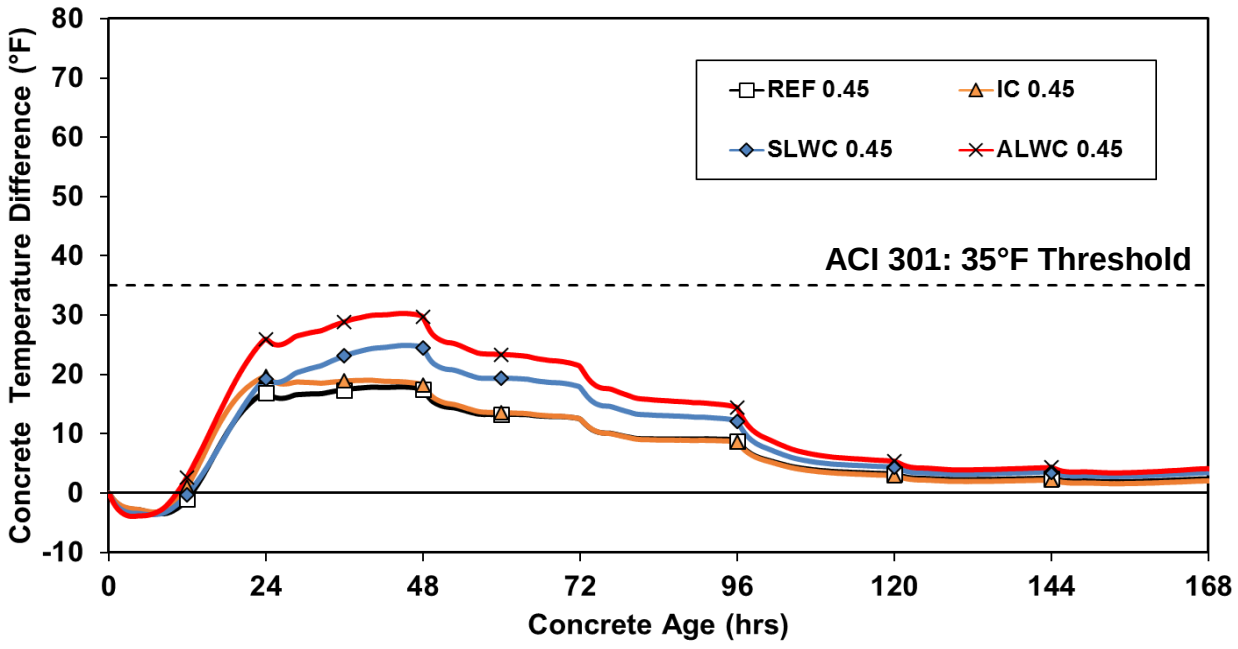

Figure 11-7: Maximum temperature difference for 4 × 4 ft cross-section size column for all 0.45 *w/cm* concretes

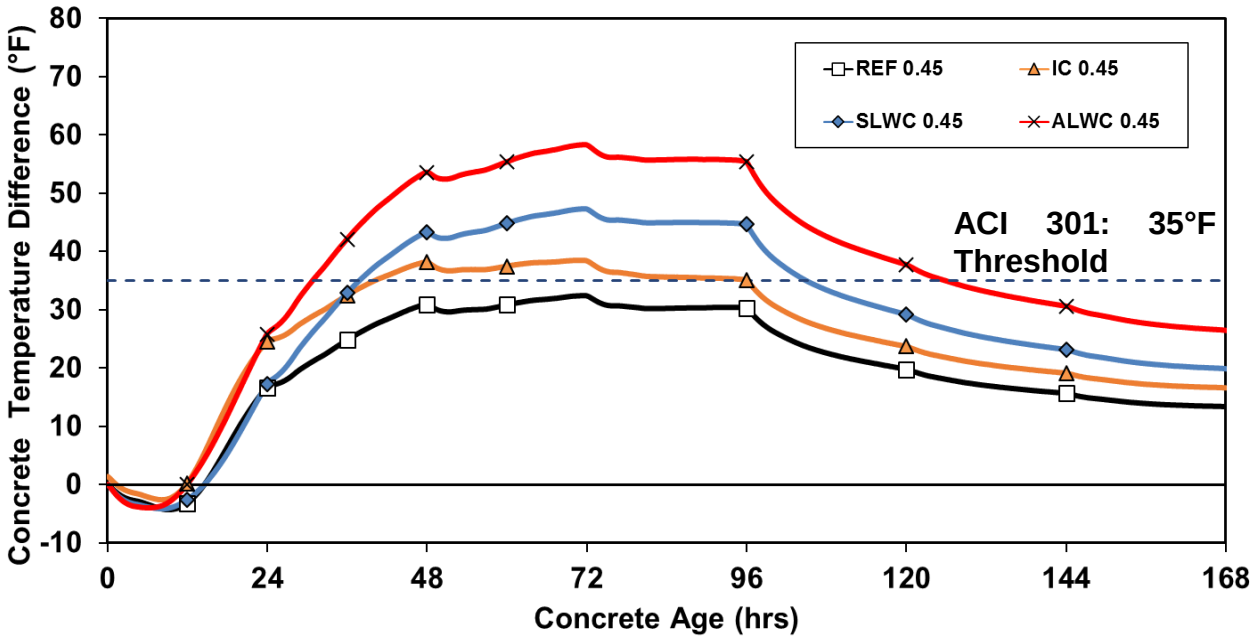

Figure 11-8: Maximum temperature difference for 8 × 8 ft cross section size column for all 0.45 *w/cm* concretes

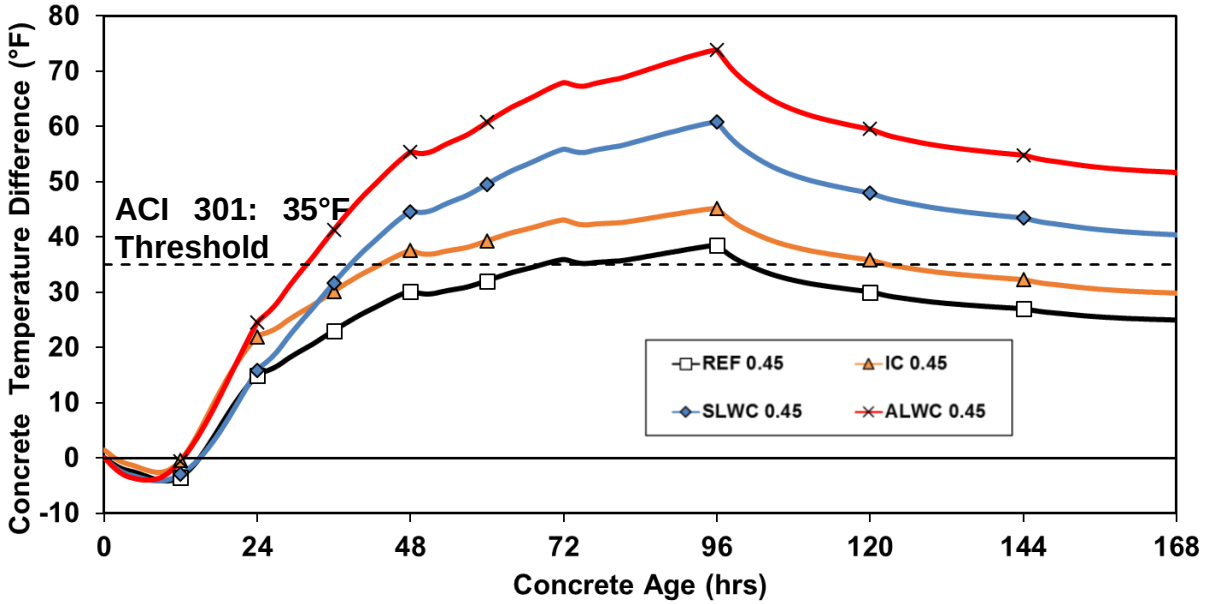

Figure 11-9: Maximum temperature difference for 12 × 12 ft cross-section size column for all 0.45 *w/cm* concretes

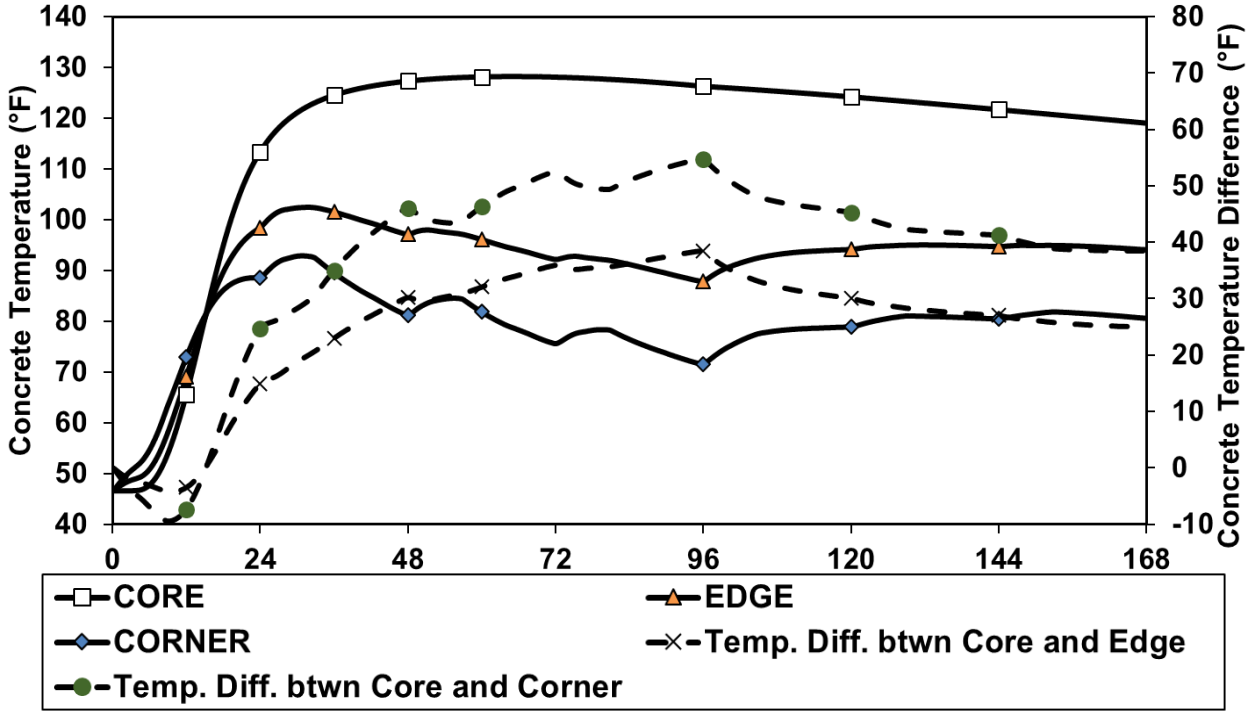

Figure 11-10: Maximum temperature difference present between core, edge and core, corner (of reference concrete) for 12 × 12 ft cross section size column

11.1.6 Concrete Stress Development

The concrete stresses development across the cross section for a 12 × 12 ft size column is shown in Figure 11-11. It can be observed from Figure 11-11 that the thermal stresses at early-ages are a maximum near the edges, and lower at core of the cross section. Hence, the following figures, Figure 11-12 to 11-14 only show the maximum thermal stresses at edge of section for all concrete types for the three cross section sizes.

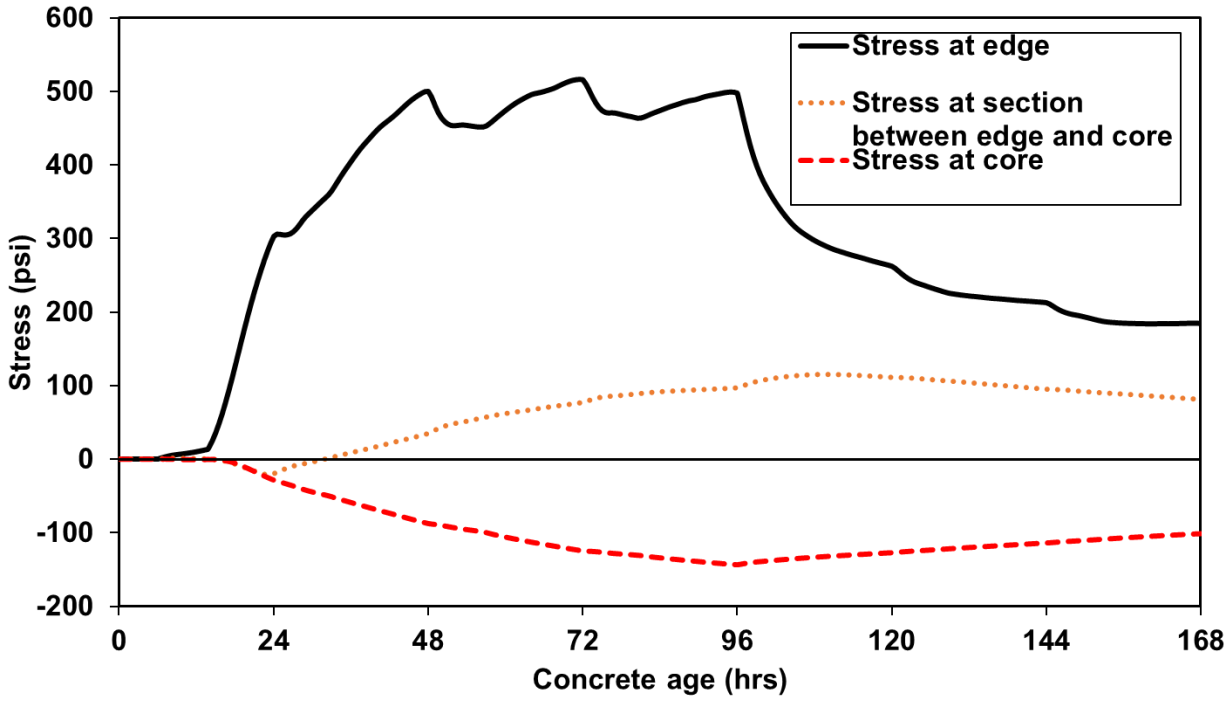

Figure 11-11: Maximum stresses across cross section for 12 × 12 ft size column

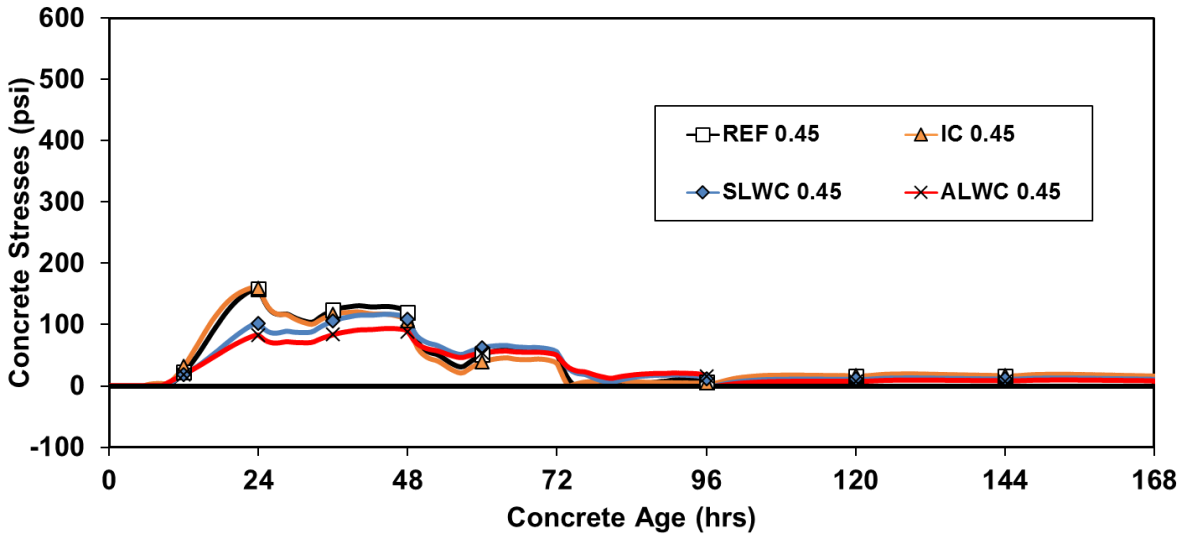

Figure 11-12: Maximum stresses for 4 × 4 ft cross-section size column for all 0.45 *w/cm* concretes

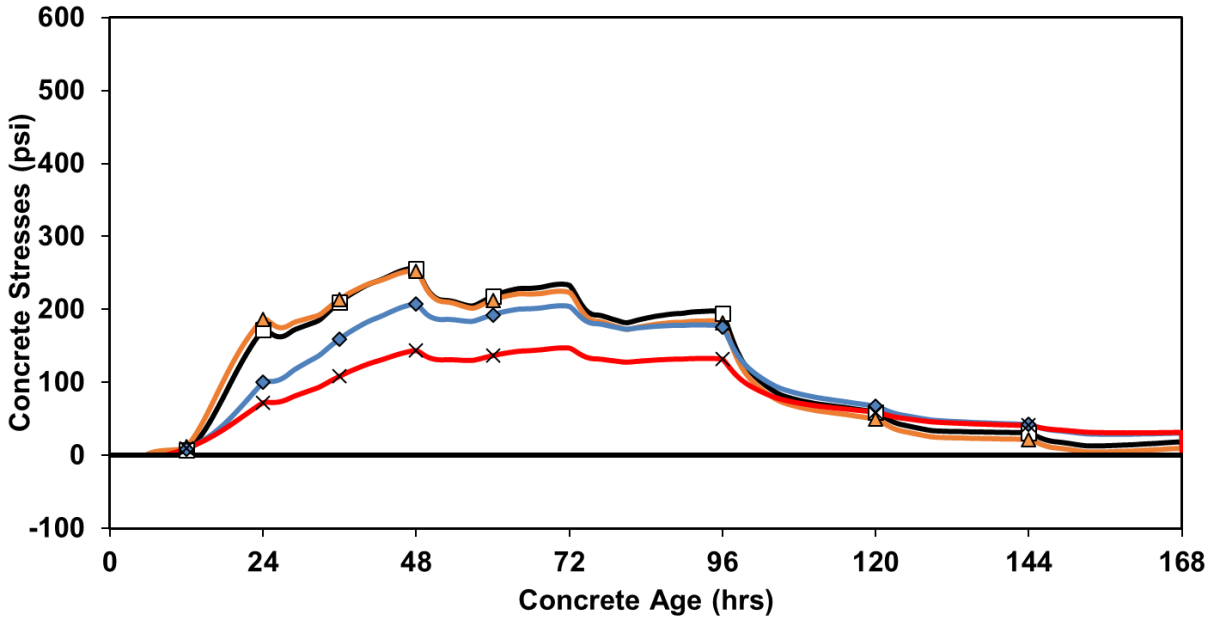

Figure 11-13: Maximum stresses for 8 × 8 ft cross-section size column for all 0.45 *w/cm* concretes

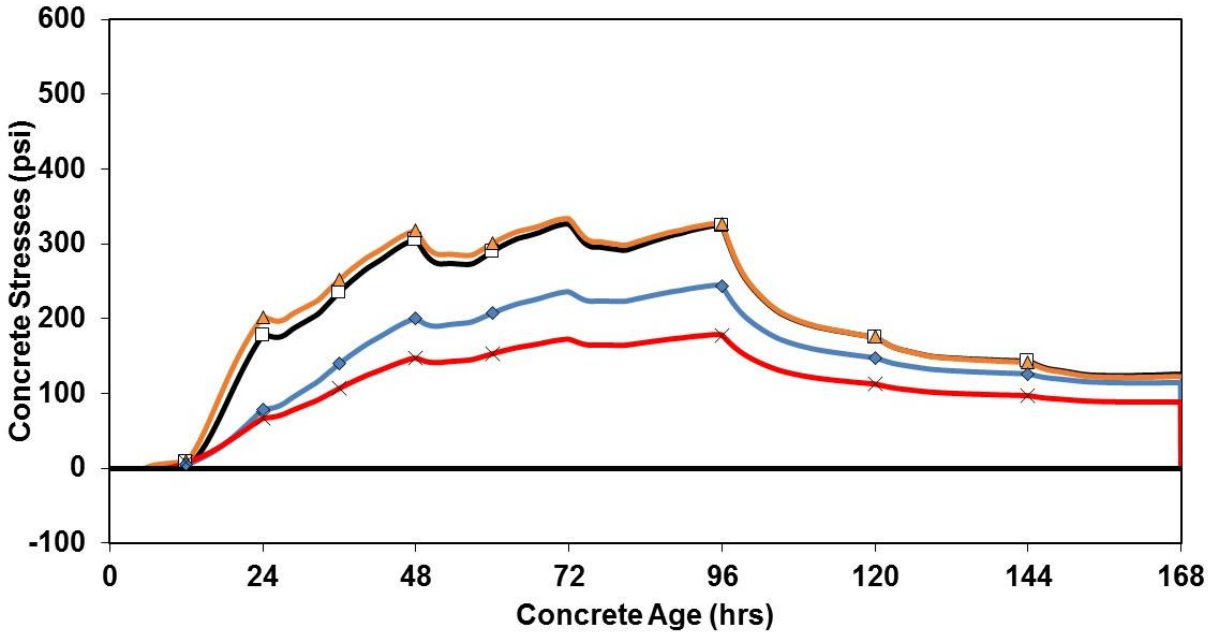

Figure 11-14: Maximum stresses for 12 × 12 ft cross-section size column for all 0.45 *w/cm* concretes

11.1.7 Concrete Cracking Risk

The concrete cracking risk is defined as the tensile stress-to-splitting-tensile-strength ratio in concrete. The tensile strength is defined in terms of the splitting tensile strength. The development of the cracking risk during early-ages is presented in Figures 11-15 to 11-17. If the value of the cracking risk exceeds 0.72, it is then categorized as very high early-age cracking risk (Riding et al. 2014).

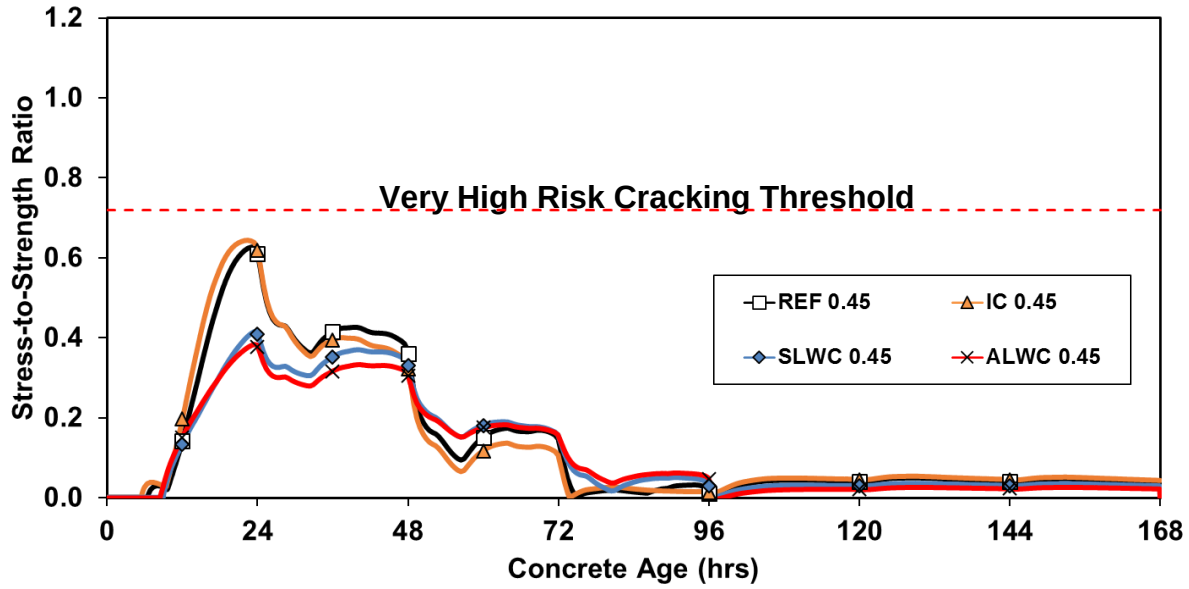

Figure 11-15: Concrete cracking risk for 4 × 4 ft cross-section size column for all 0.45 *w/cm* concretes

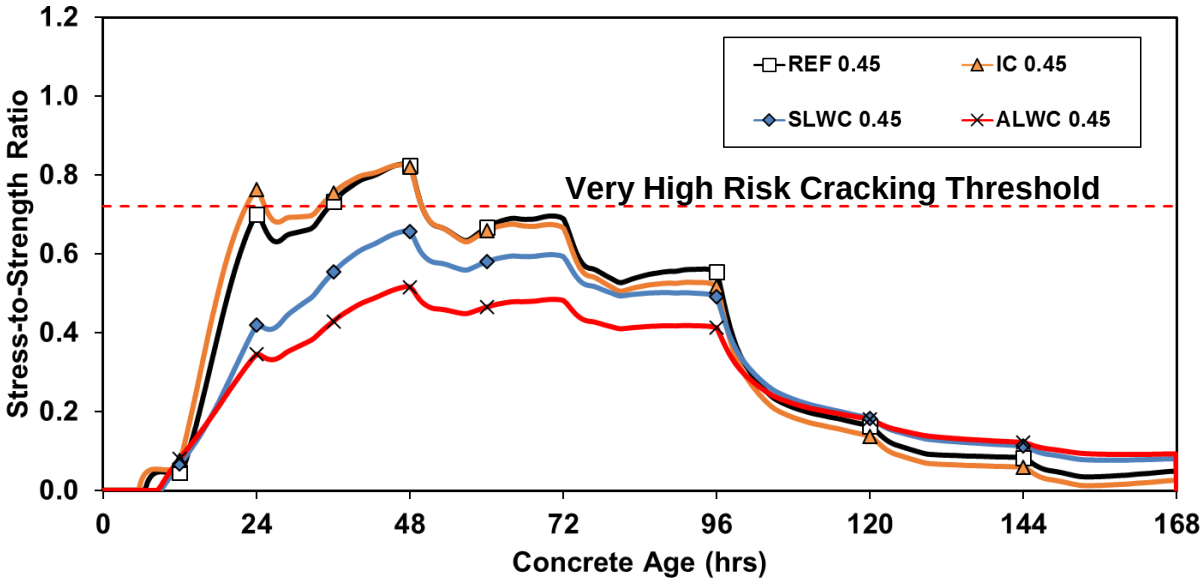

Figure 11-16: Concrete cracking risk for 8 × 8 ft cross section size column for all 0.45 *w/cm* concrete

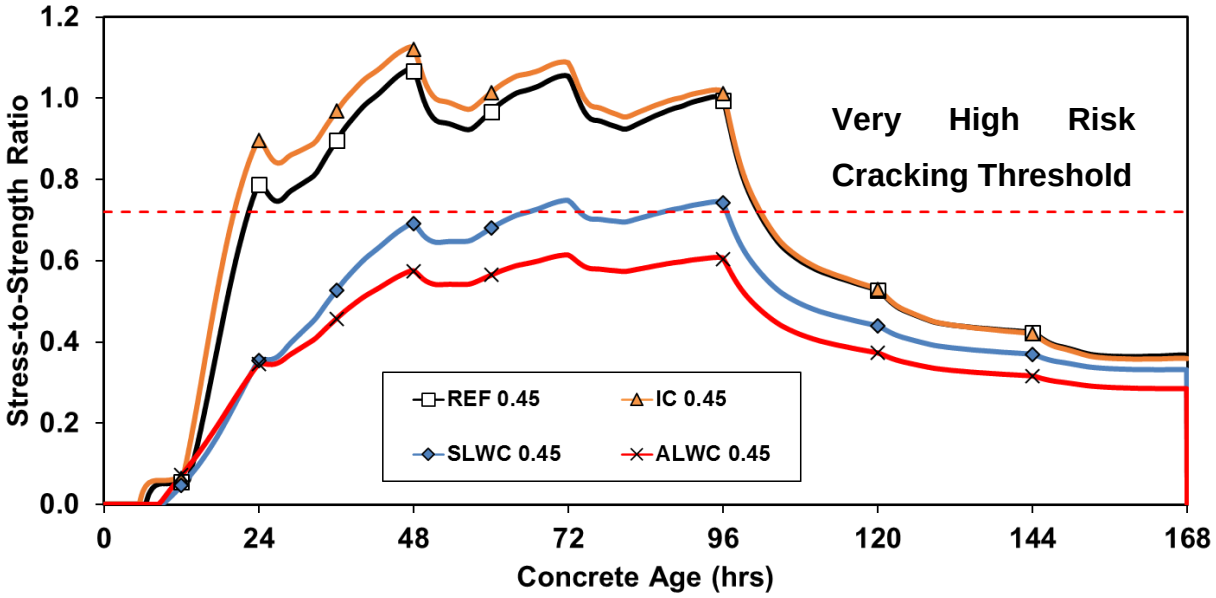

Figure 11-17: Concrete cracking risk for 12 × 12 ft cross-section size column for all 0.45 *w/cm* concretes

11.2 CONCRETES WITH *W/CM* = 0.38

11.2.1 Combined Mixture Gradations

Four concrete mixtures with a *w/cm* of 0.38 and with three of them containing lightweight aggregates were produced and tested. The combined gradations of these concretes are plotted on a 0.45- power curve, as shown in Figure 5-10. Their workability factors are presented in Figure 5-11.

11.2.2 Fresh Concrete Properties

The fresh concrete properties such as the slump, total air content, temperature, and density were measured for each concrete type and are presented in Table 5-4. The

calculated equilibrium densities in accordance with ASTM C567 (2014) are also presented in Table 5-4.

11.2.3 Time-Dependent Development of Concrete Mechanical Properties

The time-dependent development of compressive strength, splitting tensile strength, and modulus of elasticity were tested for each concrete mixture. A total of 24 cylinders were used in the testing process for each concrete type. The measured values were averaged for two cylinders and are presented in Appendix C. A regression analysis was performed as per ASTM C1074 (2014), which recommends the use of an exponential function. Best-fit curves were determined for the measured values and are plotted in Figures 5-17 to 5-19.

11.2.4 Thermal Properties

The calculated equilibrium density, coefficient of thermal expansion, and thermal diffusivity are summarized in Table 5-2 in Part I.

11.2.5 Concrete Temperature Development

11.2.5.1 Core Temperatures

The simulated core temperatures for all 0.38 *w/cm* concretes belonging to the three different cross-section sizes are presented in Figures 11-18 to 11-20. The DEF limit which is fixed at 185°F (ACI 201 2016) is also shown.

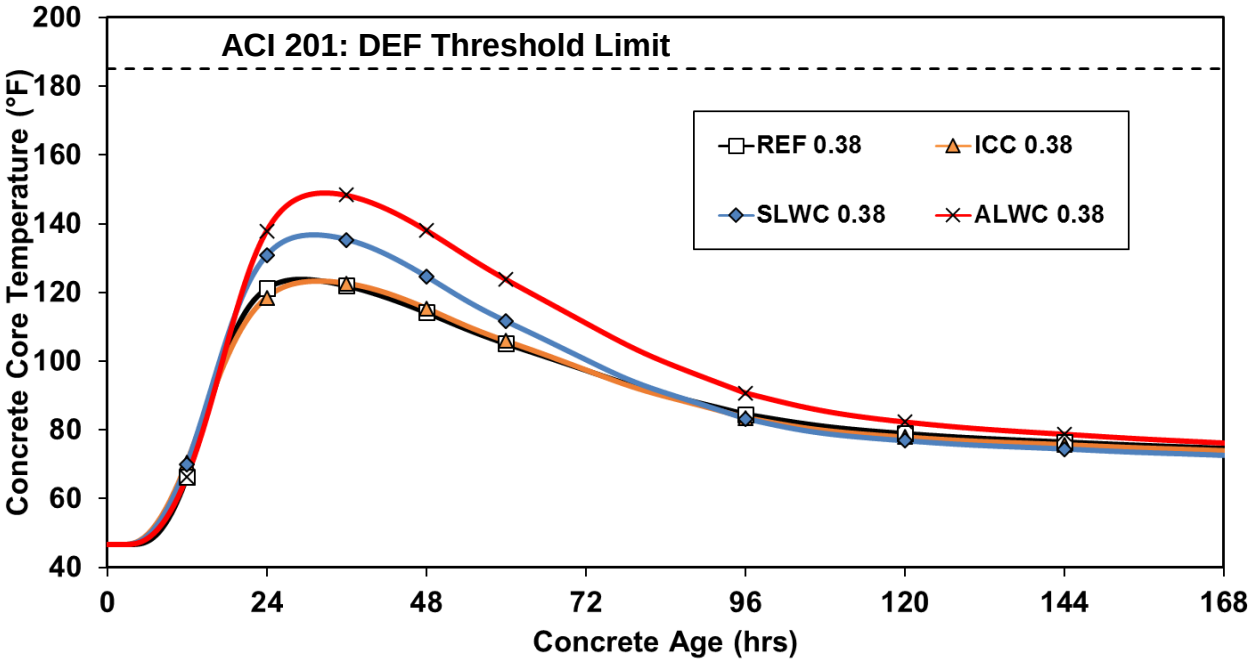

Figure 11-18: Maximum core temperatures for 4× 4 ft cross-section size column for all 0.38 *w/cm* concretes

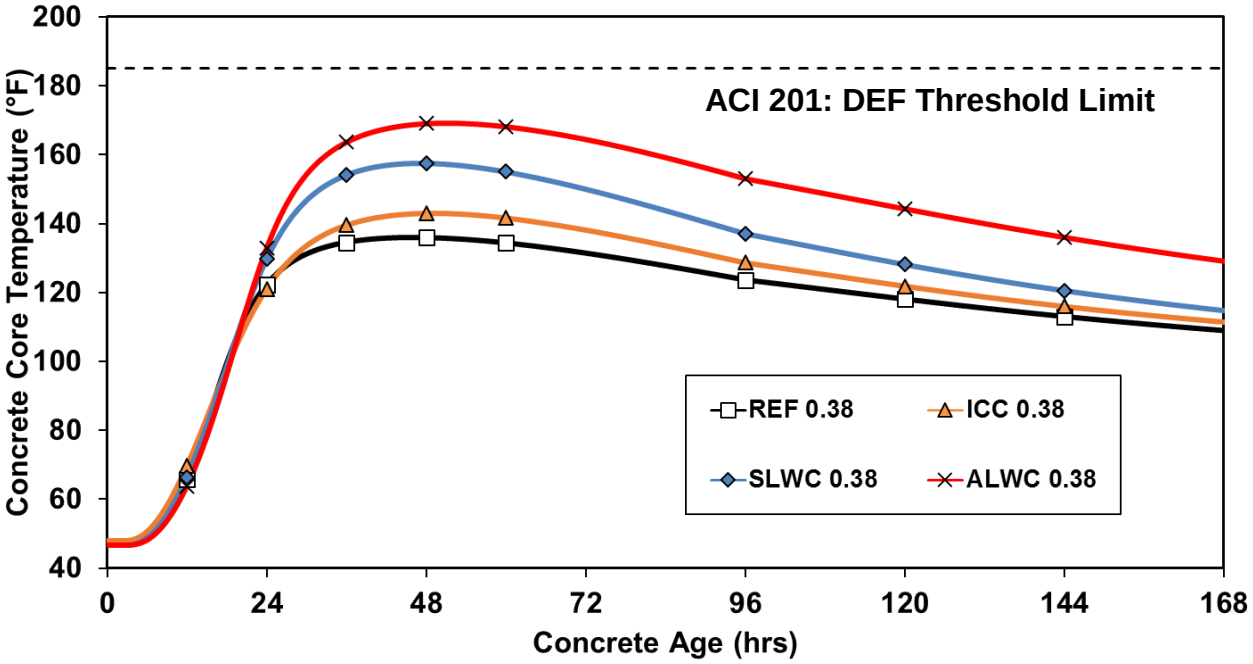

Figure 11-19: Maximum core temperatures for 8 × 8 ft cross-section size column for all 0.38 w/cm concretes

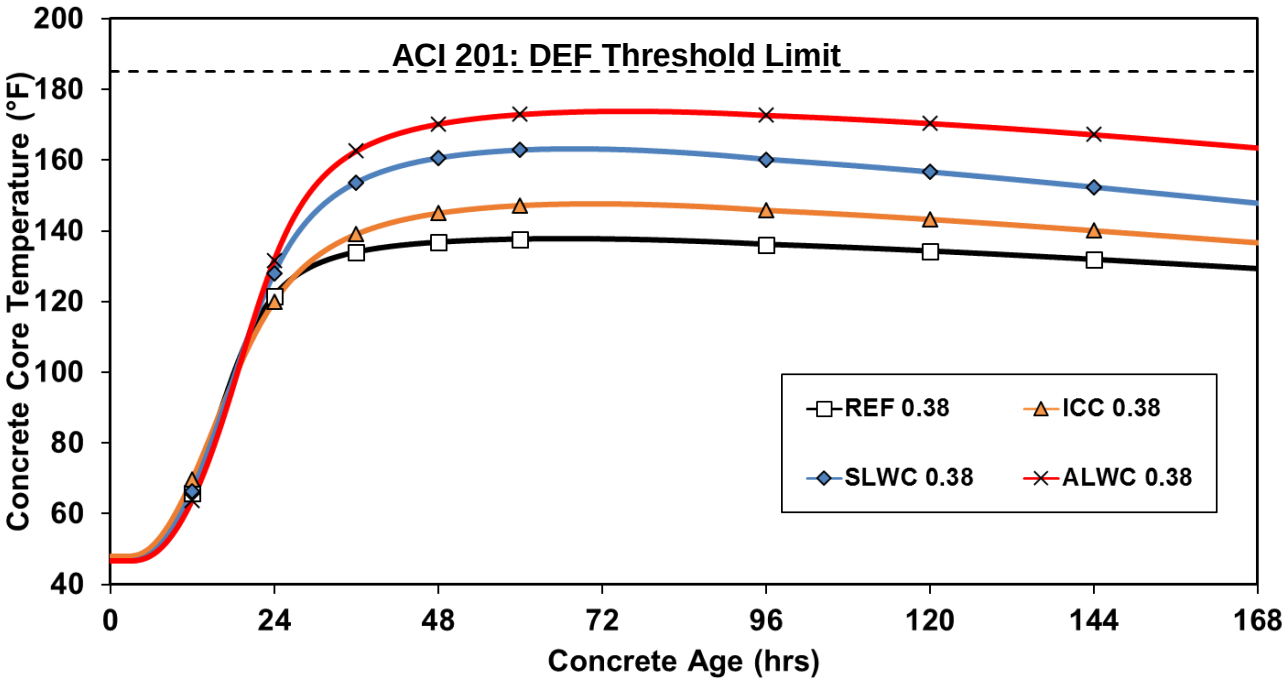

Figure 11-20: Maximum core temperatures for 12× 12 ft cross-section size column for all 0.38 *w/cm* concretes

11.2.5.2 Edge Temperatures

The simulated edge temperatures for all the concretes belonging to the three different cross-section sizes are presented in Figures 11-21 to 11-23.

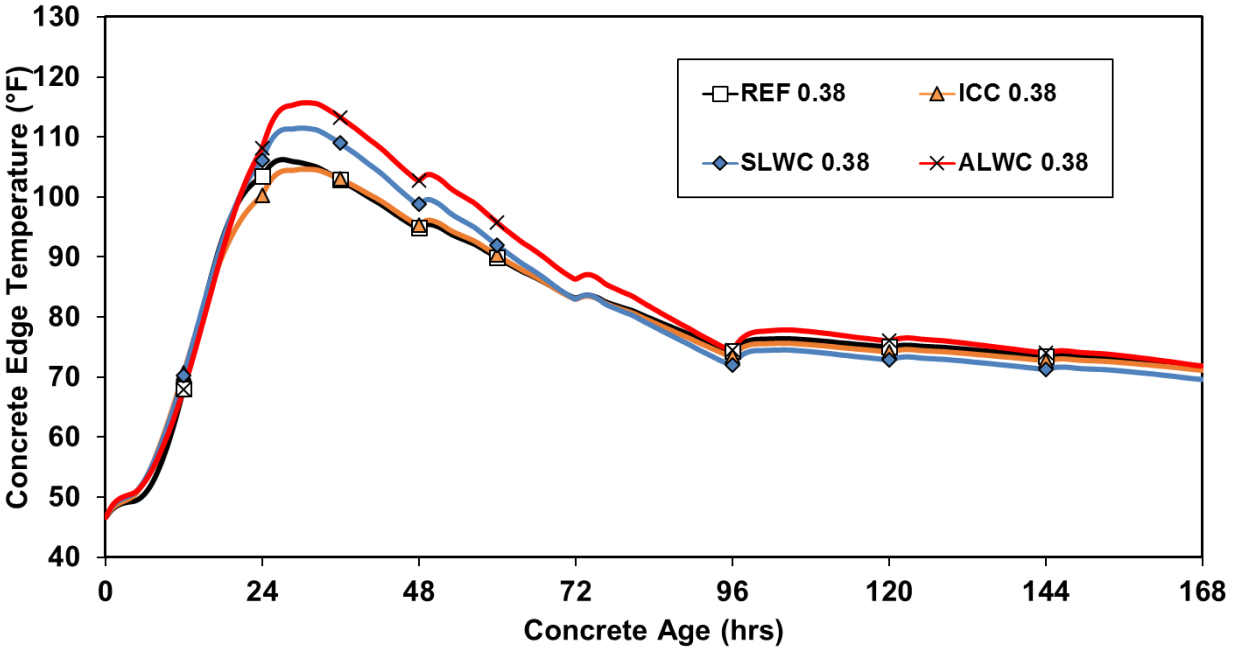

Figure 11-21: Temperature development at the edge of 4 × 4 ft cross-section size column for all 0.38 *w/cm* concretes

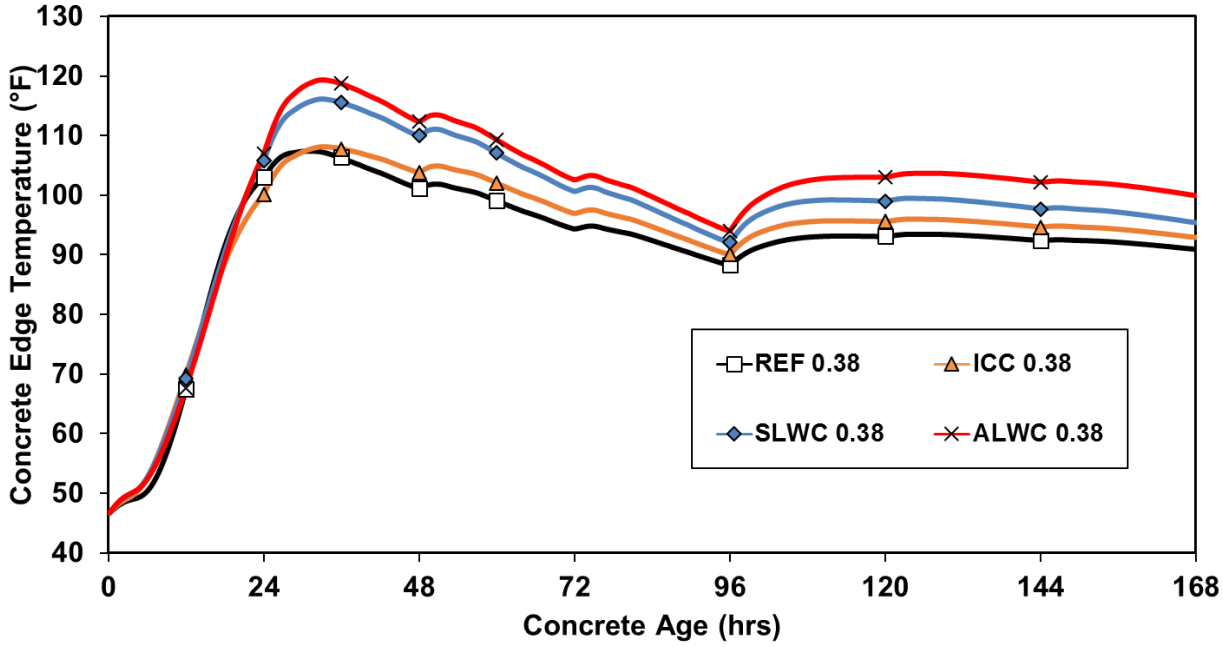

Figure 11-22: Temperature development at the edge of 8×8 ft cross section size column for all 0.38 w/cm concretes

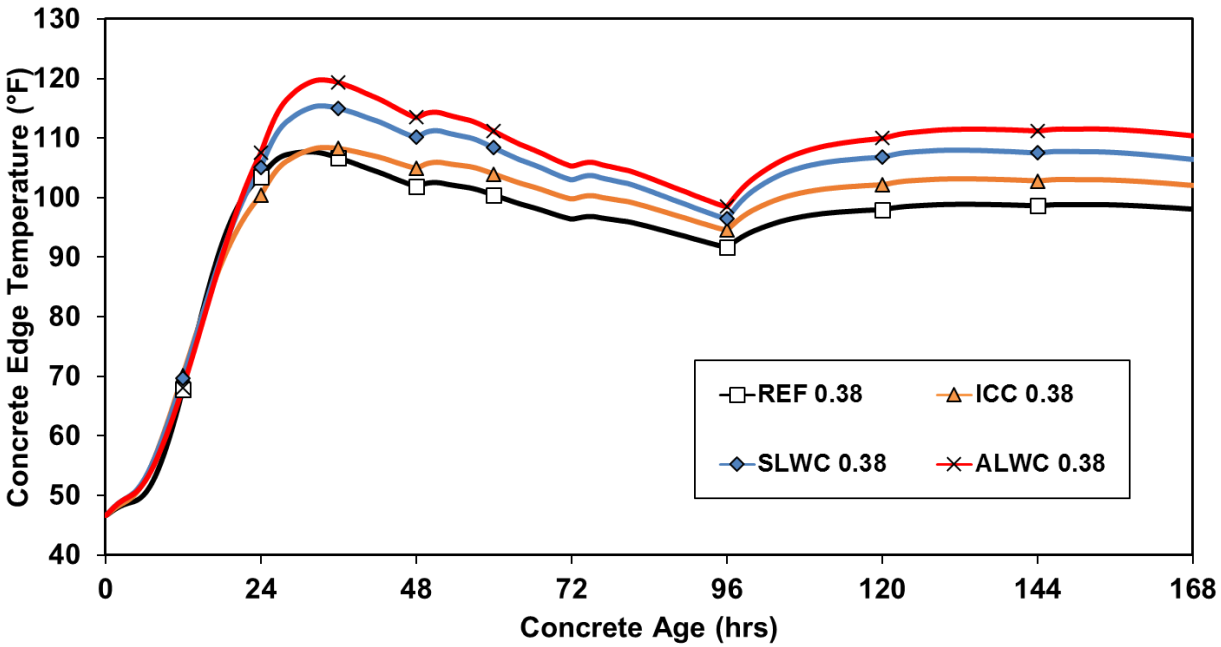

Figure 11-23: Temperature development at the edge of 12 × 12 ft cross-section size column for all 0.38 *w/cm* concretes

11.2.5.3 Concrete Temperature Differences

The simulated concrete temperature differences for all the concretes belonging to the three different cross-section sizes are presented in Figures 11-24 to 11-26. The maximum temperature difference limit fixed at 35°F (ACI 301 2016) is also shown.

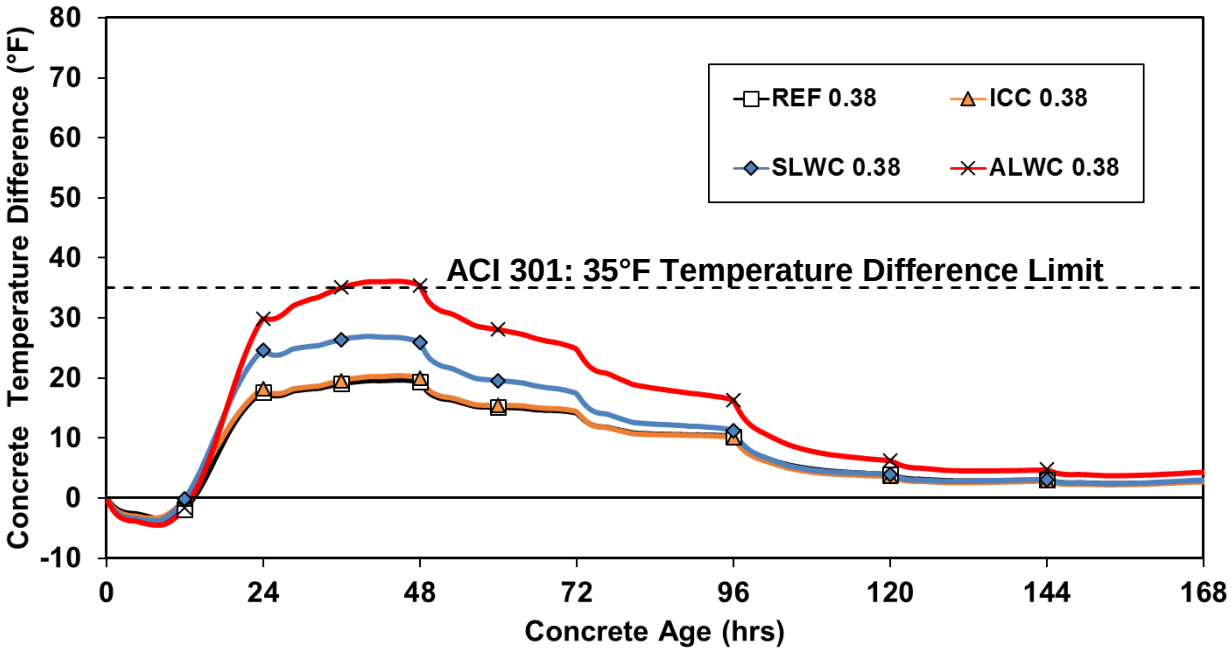

Figure 11-24: Maximum temperature difference for 4 × 4 ft cross-section size column for all 0.38 *w/cm* concretes

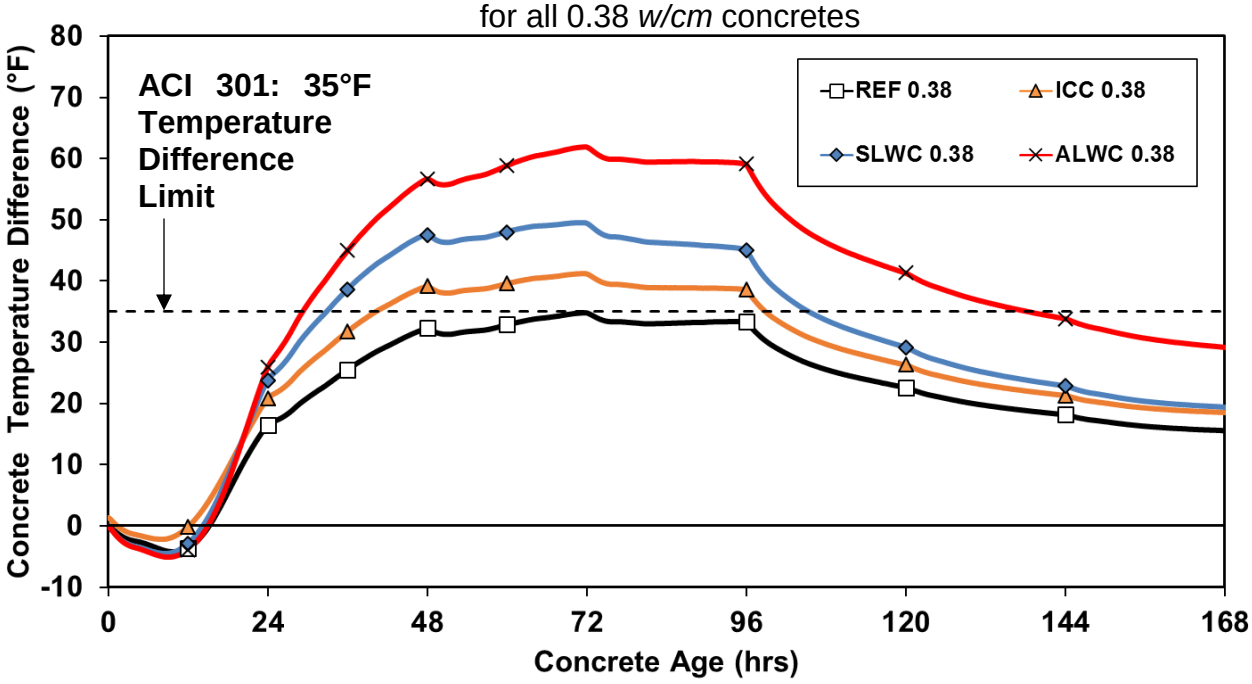

Figure 11-25: Maximum temperature difference for 8 × 8 ft cross section size column for all 0.38 *w/cm* concretes

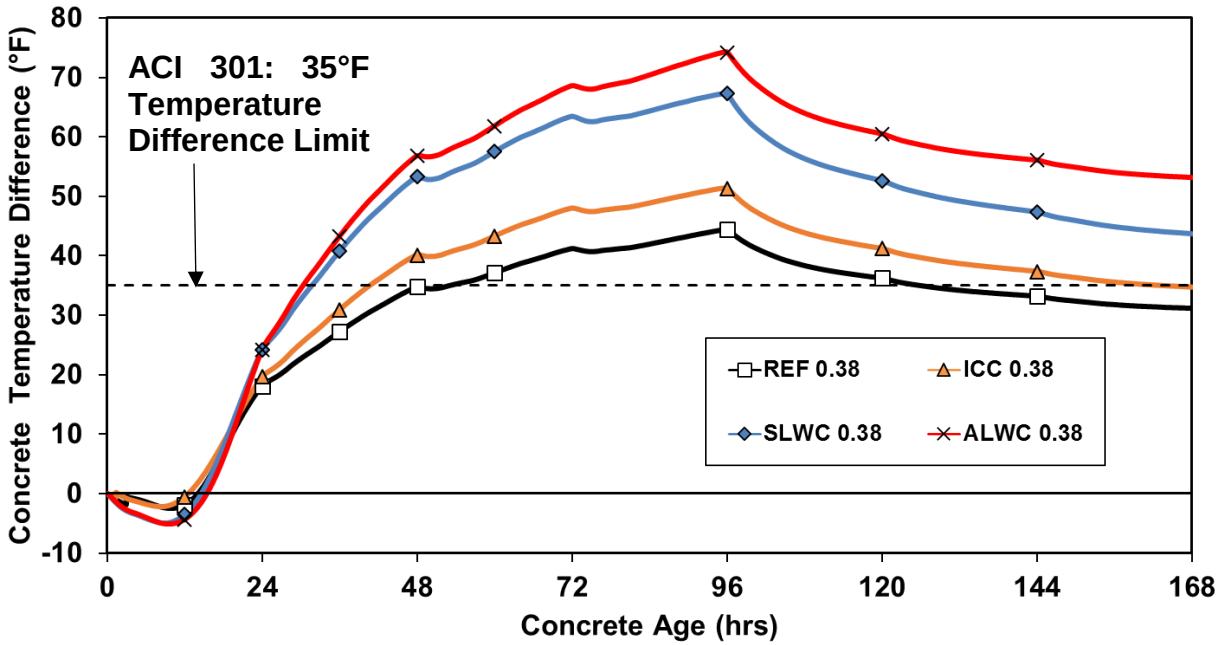

Figure 11-26: Maximum temperature difference for 12 × 12 ft cross section size column for all 0.38 *w/cm* concretes

11.2.6 Concrete Stress Development

The concrete stress development for all the 0.38 w/cm concretes for the three column cross-section sizes are shown in Figure 11-27 to 11-29.

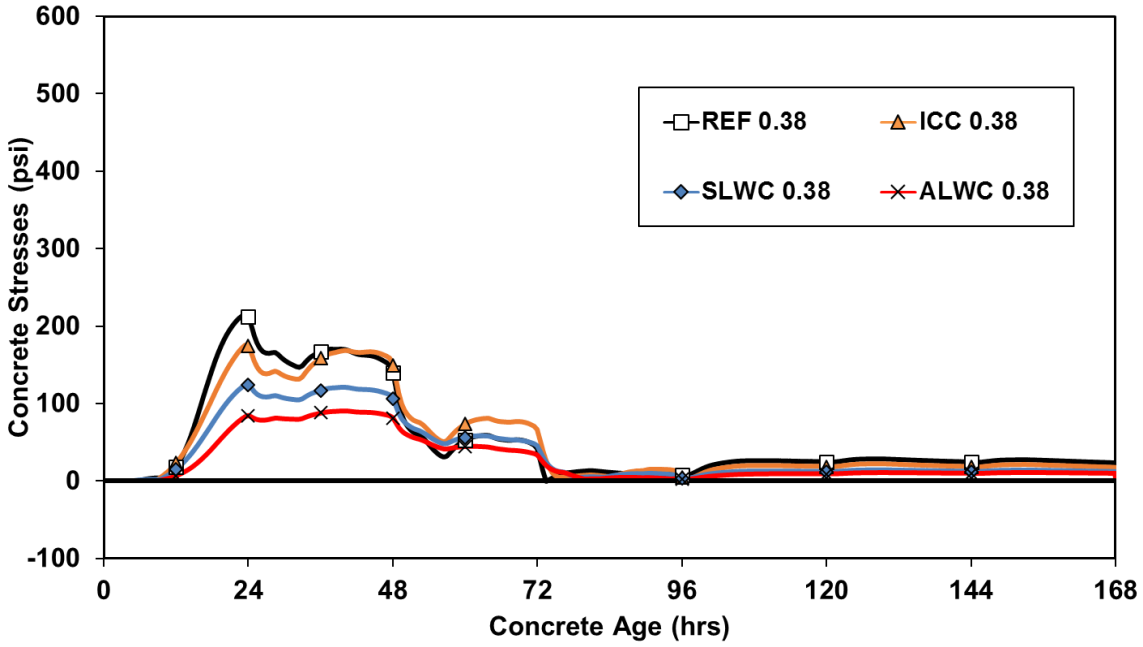

Figure 11-27: Maximum stresses for 4 × 4 ft cross-section size column for all 0.38 *w/cm* concretes

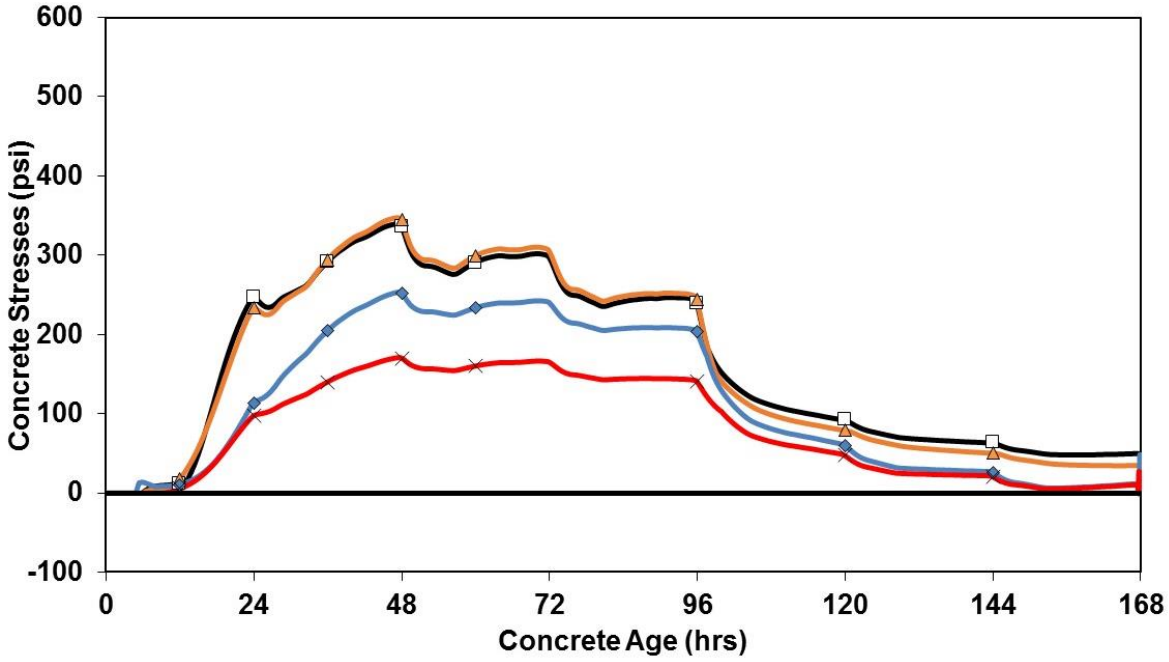

Figure 11-28: Maximum stresses for 8 × 8 ft cross-section size column for all 0.38 *w/cm* concretes

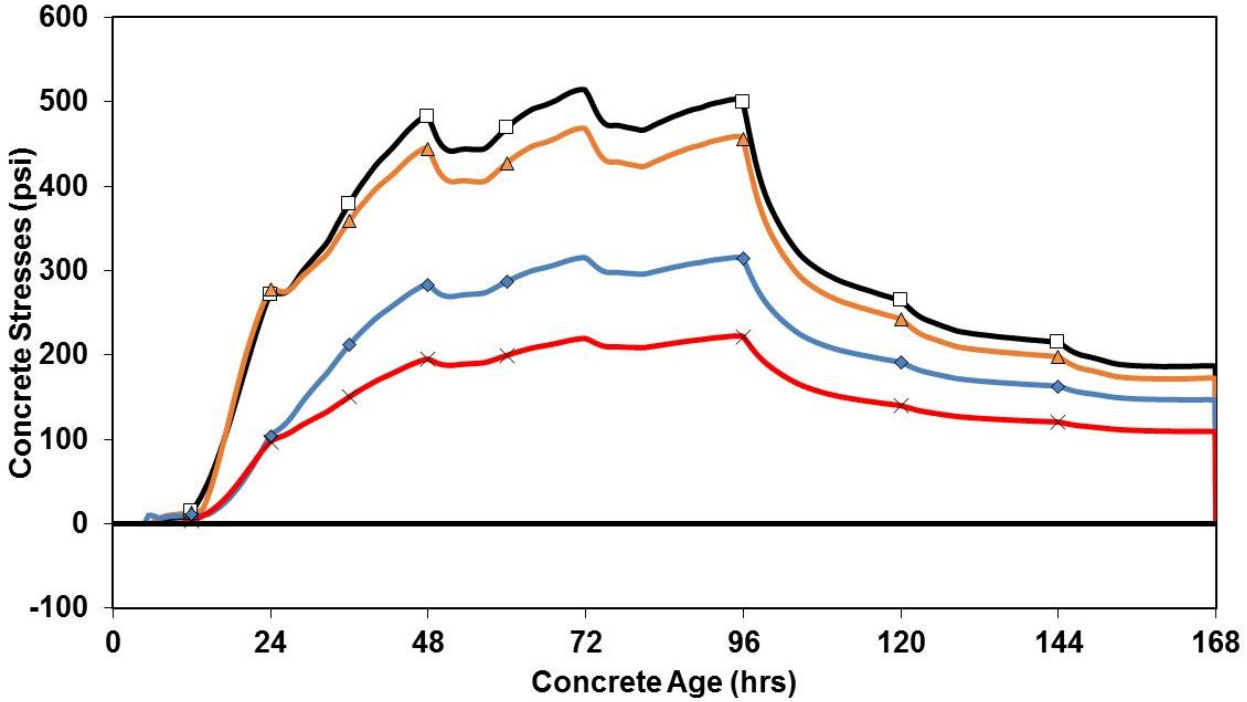

Figure 11-29: Maximum stresses for 12 × 12 ft cross-section size column for all 0.38 *w/cm* concretes

11.2.7 Concrete Cracking Risk

The concrete cracking risk is defined as the stress-to-strength ratio in concrete. The development of the cracking risk during early-ages is presented in Figures 11-30 to 11-32. If the value of the cracking risk exceeds 0.72, it is then categorized as very high early-age cracking risk (Riding et al. 2014).

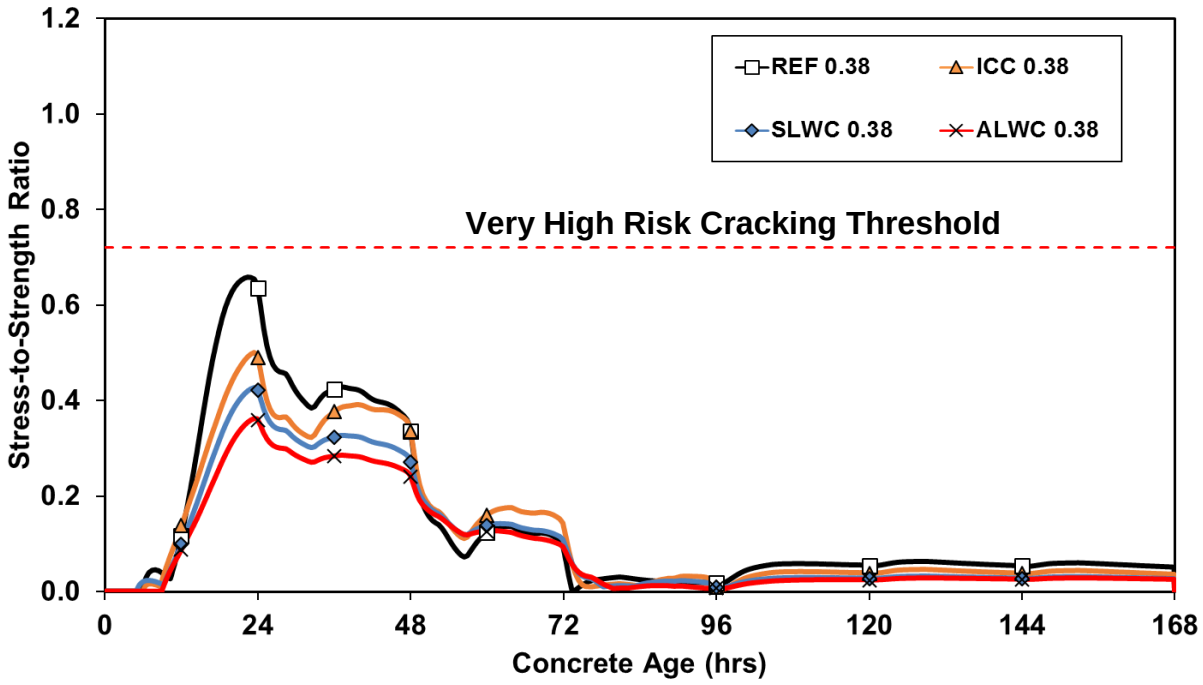

Figure 11-30: Concrete cracking risk for 4 × 4 ft cross-section size column for all 0.38 *w/cm* concretes

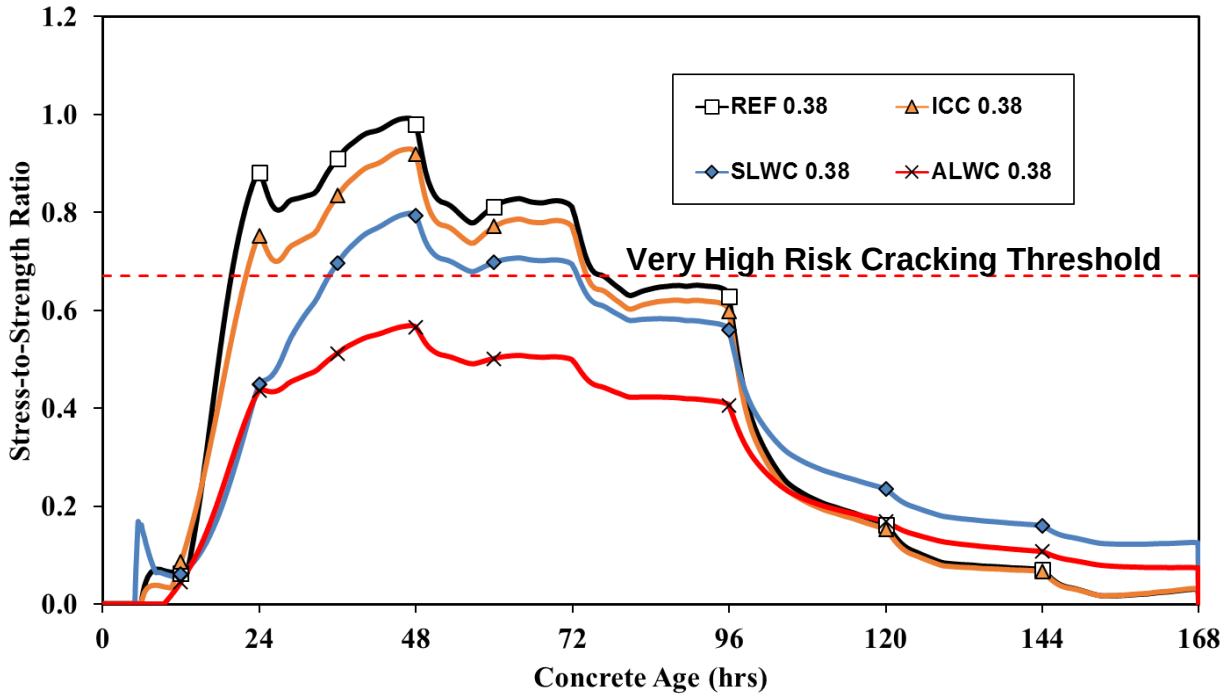

Figure 11-31: Concrete cracking risk for 8 × 8 ft cross-section size column for all 0.38 *w/cm* concretes

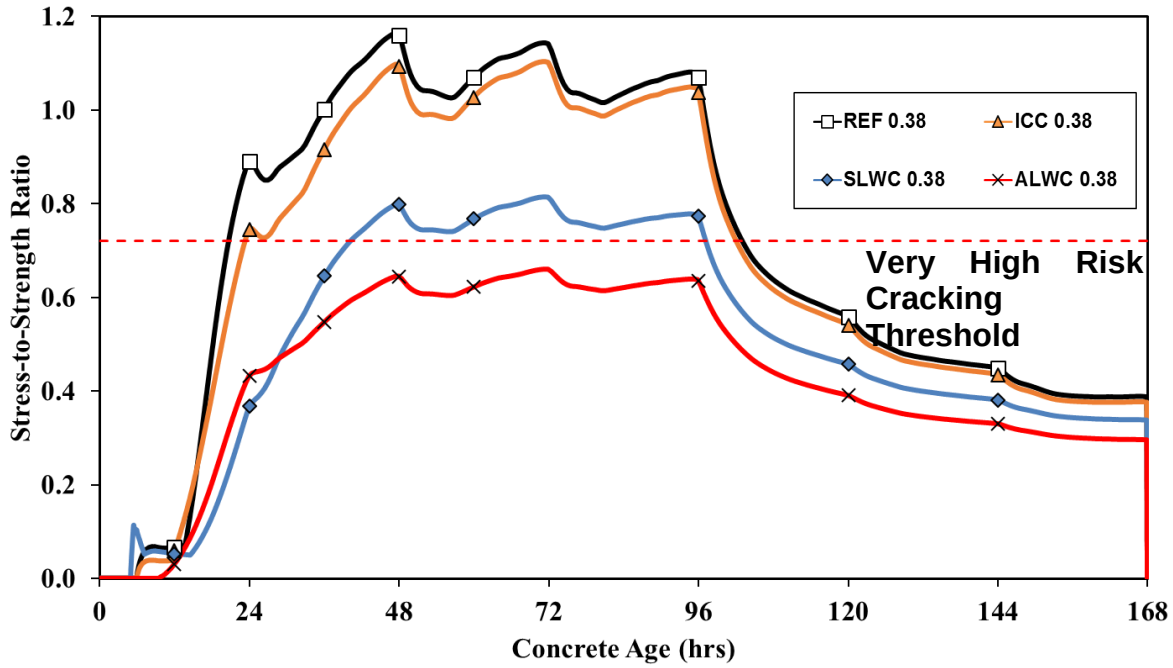

Figure 11-32: Concrete cracking risk for 12 × 12 ft cross-section size column for all 0.38 *w/cm* concretes

Chapter 12

PART II: DISCUSSION OF RESULTS

A detailed analysis and discussion of the numerical investigation are presented in this chapter. The changes in concrete properties due to the presence of lightweight aggregates are evaluated in Section 12.1. In Section 12.2, the effect of LWA on the concrete core temperature, edge temperature and temperature difference is assessed. Next, the effects of LWA on the concrete stresses and cracking risk are evaluated.

12.1 EFFECT OF LIGHTWEIGHT AGGREGATE ON CONCRETE PROPERTIES

The effect of lightweight aggregate on the concrete properties such as compressive strength, splitting tensile strength, modulus of elasticity, thermal diffusivity, and the coefficient of thermal expansion is presented in Section 6-1.

12.2 EFFECT OF LWA ON CONCRETE TEMPERATURES

12.2.1 Concrete Core Temperatures

The development of concrete core temperatures simulated with ConcreteWorks in mass concrete elements of different sizes for concrete mixtures with *w/cm* = 0.45 and 0.38 are presented in Figures 11-1 to 11-3 and 11-18 to 11-20, respectively. For both groups of *w/cm* concretes it can be observed that the core temperature are the highest for the 12 × 12 ft cross-section size followed in order of decreasing temperatures by 8 × 8 ft and 4 × 4 ft. The maximum core temperature is higher for the lower *w/cm* concretes, since more cementious content are present in these concretes. Also, the concrete core temperature is the highest for the ALW concretes, followed in the order of decreasing temperature by

SLW, IC, and the reference concrete. It can be observed from Figures 11-1 to 11-3 and 11-18 to 11-20 that the higher amount of LWAs in the concrete, the higher the core concrete temperature. This is due to the decreased thermal diffusivity (from Figure 5-2) and decreased density of concretes containing LWA. Thus, the concrete core temperatures increase due to addition of LWA to concrete. The maximum core temperatures for all the concretes along with the cross-section sizes are summarized in Figure 12-1. Table 12-1 shows the maximum core temperatures. Since the maximum core temperatures may exceed the DEF limit for certain cross-section sizes and concrete compositions, care should be taken when using LWA concrete in mass concrete construction to ensure that the in-place concrete temperature does not exceed the DEF threshold.

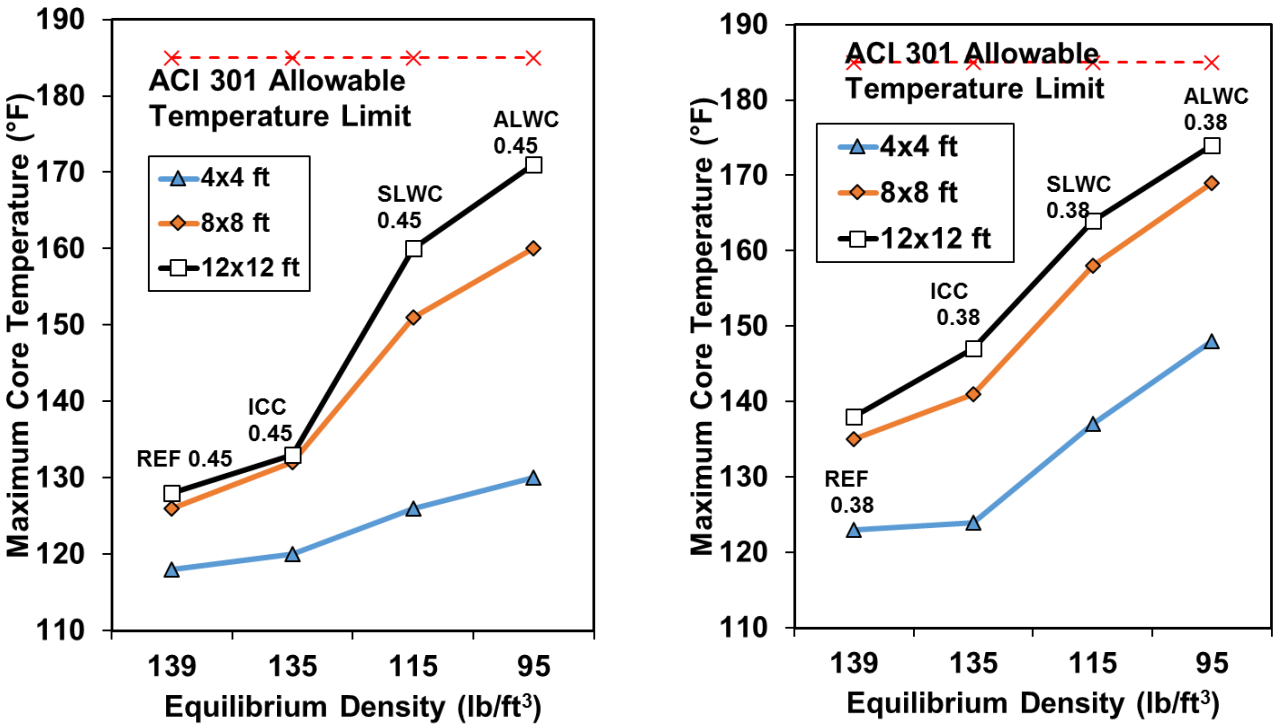

Figure 12-1: Maximum core concrete temperatures for all *w/cm* concretes

Table 12-1: Summary of maximum core temperatures for all concretes

Concrete Type	Maximum Core Temperatures (°F)		
	4 × 4 ft	8 × 8 ft	12 × 12 ft
REF 0.45	118	126	128
ICC 0.45	120	133	135
SLWC 0.45	126	151	159
ALWC 0.45	130	161	171
REF 0.38	123	135	138
ICC 0.38	124	141	147
SLWC 0.38	137	159	163
ALWC 0.38	148	168	174

12.2.2 Concrete Edge Temperatures

The development of concrete edge temperatures for concrete mixtures with *w/cm* = 0.45 and 0.38 are presented in Figures 11-4 to 11-6 and 11-21 to 11-23, respectively. Table 12-2 shows the maximum edge temperatures for all the cross-section sizes. For both groups of *w/cm* concretes, it can be observed that the edge temperatures are similar for the 12 × 12, 8 × 8 ft and 4 × 4 ft cross-section sizes. Also, with an increase in LWA in the concretes, the edge temperatures increase. For example: for the 0.38 *w/cm* concretes, for all cross-section sizes, ALWC has the highest edge temperature followed in order of decreasing temperatures by SLWC, ICC, and REF concrete. From the Figures 11-4 to 11-6 and 11-21 to 11-23, it can be observed that the edge temperatures of concrete increase after the formwork has been removed at 96 hrs. The reason is due to a higher R value (approximately between 5 and 7, Neville (2011)) of the insulated blankets in comparison to the R value (approximately equal to 3, Folliard et al. (2017)) of the wooden forms.

The concrete edge temperature is influenced by the prevailing ambient weather conditions such as, ambient temperature, relative humidity, percent cloud cover, and formwork type, etc. Since the environmental conditions and formwork type are similar for all concrete types, the edge temperatures for all concrete cross-section sizes are similar. It can be observed that lower the *w/cm* in the concrete, the higher the edge concrete temperature. This is in part due to the increased amount of cementious materials in the concrete. Thus, the concrete edge temperatures increase due to a decrease in *w/cm* of the concrete and increase with an addition of LWA in concrete. However, they are similar

for different cross-section sizes when exposed to similar environmental and formwork conditions.

Table 12-2: Summary of maximum edge temperatures for all concretes

Concrete Type	Maximum Edge Temperatures (°F)		
	4 × 4 ft	8 × 8 ft	12 × 12 ft
REF 0.45	101	102	102
ICC 0.45	101	105	106
SLWC 0.45	103	108	109
ALWC 0.45	103	109	112
REF 0.38	105	107	107
ICC 0.38	106	108	108
SLWC 0.38	111	115	115
ALWC 0.38	115	119	119

12.2.3 Concrete Temperature Differences

The development of concrete temperature differences for concrete mixtures with *w/cm* = 0.45 and 0.38 are presented in Figures 11-7 to 11-9 and 11-24 to 11-26, respectively. Table 12-3 shows the maximum concrete temperature differences for all the cross-section sizes. It can be observed that the concrete temperature differences are the highest for the 12 × 12 ft followed by 8 × 8 ft and 4 × 4 ft cross-section size. Under similar environmental and formwork conditions, the larger cross-section size leads to greater temperature differences.

The concrete temperature difference is maximum for the ALW concrete, followed in the order of decreasing temperature difference by SLW, IC, and reference concrete. From Figure 12-2 one may conclude that temperature differences increase with a decrease in concrete density. Although the results indicate that the temperature differences increase with increased use of LWA, the cracking risk of these concretes will

not be necessarily higher and should be determined by a stress analysis using Equation 9-4. By using Equation 9-4, the impact of different CTE, creep-adjusted modulus of elasticity, and the temperature differences on cracking risk can be determined. A stress analysis will be used in the following section to assess the impact of using LWA on the thermal cracking risk.

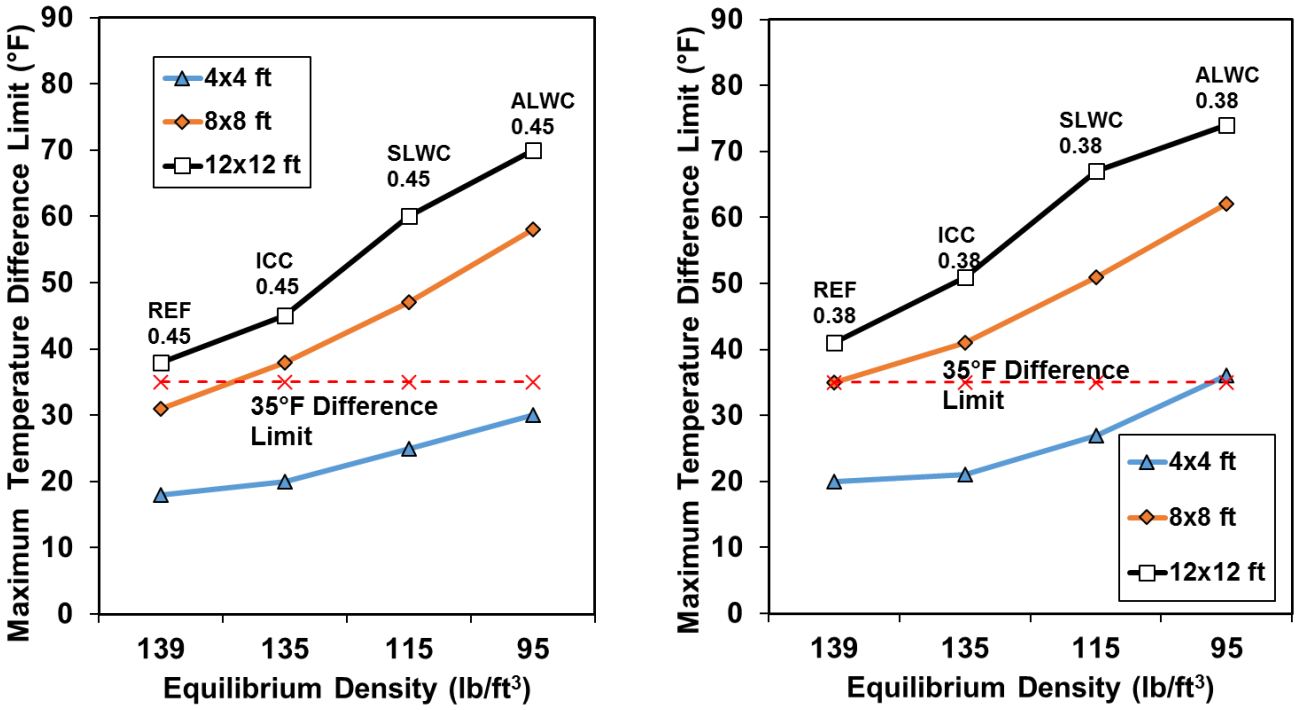

Figure 12-2: Maximum concrete temperature differences for all *w/cm* concretes

Table 12-3: Summary of maximum temperature differences for all concretes

Concrete Type	Maximum Temperature Differences (°F)		
	4 × 4 ft	8 × 8 ft	12 × 12 ft
REF 0.45	17	30	38
ICC 0.45	20	38	45
SLWC 0.45	25	47	60
ALWC 0.45	30	58	70
REF 0.38	19	35	45
ICC 0.38	21	41	51
SLWC 0.38	27	50	67
ALWC 0.38	36	62	75

12.3 EFFECT OF LWA ON CONCRETE STRESSES AND CRACKING RISK

12.3.1 Calculated Concrete Stresses

The early-age concrete tensile stresses were computed from ConcreteWorks at all points along the cross section for all concrete types and cross-section sizes. The development of concrete stresses for concrete mixtures with *w/cm* = 0.45 and 0.38 are presented in Figures 11-12 to 11-14 and 11-27 to 11-29, respectively. Table 12-4 provides the maximum concrete stresses for both groups of *w/cm* concretes. Figure 11-11 shows the development of the reference concrete stresses along the cross section for a 12 × 12 size column. It can be seen that the stresses are a maximum at the edges and decrease in magnitude as one moves towards the core of the cross section. Also, for all concrete types and cross-section sizes, the thermal stresses are maximum at the edges and decrease in magnitude as one moves towards the core. Thus, despite increased temperature differences observed at the corner when compared with the temperature differences at midpoint on edge (from Figure 11-10), the stresses are maximum at the midpoint on edges and not the corners. This is due to the much reduced restraint present

at the corners in comparison to the midpoint along the edges (Hedlund 2000). Since the midpoint along the edges are more restrained than the corners, the stresses at midpoint along the edge are higher than at the corners. Since the thermal stresses are maximum at the midpoint along the edges, only these stresses are considered for discussion in the following sections. Figure 12-3 shows the distribution of maximum concrete stresses at a time period of 96 hours for a 12 × 12 ft 0.38 *w/cm* reference concrete cross-section. From Figure 12-3 it can be observed that the maximum stresses occur along the midpoint on edges, and the stresses decrease in magnitude as one moves towards the core of the cross-section. Thus, the midpoint along the edges are identified as the critical location along the cross section. From Figures 11-12 to 11-14 and 11-27 to 11-29, for all concretes it can be observed that the concrete stresses at the critical location are maximum for a 12 × 12 ft cross-section size followed by the 8 × 8 ft and 4 × 4 ft cross-section size. The temperature differences between the core and the edges increase as the cross-section size increases; therefore the, concrete stresses at the critical location increase as the cross-section size increases.

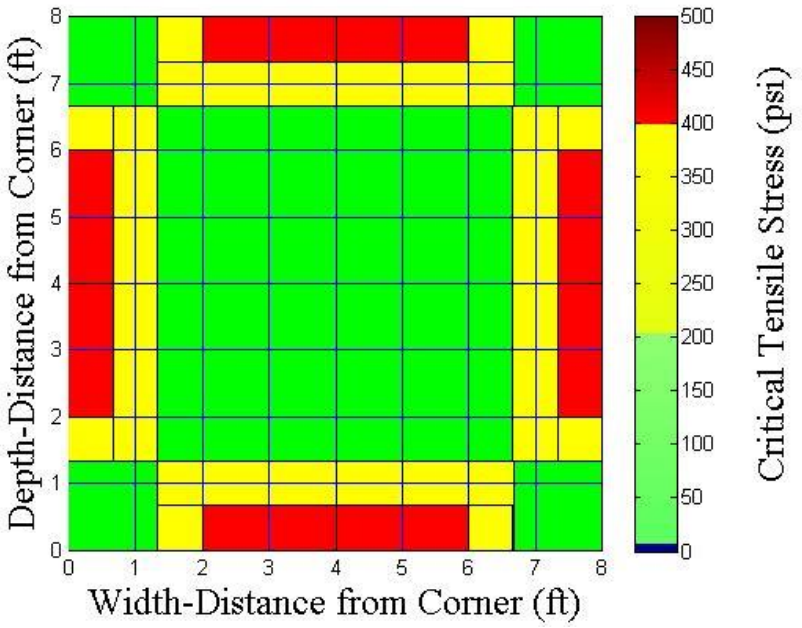

Figure 12-3: Maximum stresses occurring at 96 hrs for reference concrete for a 0.38 *w/cm* 12 x 12 ft cross section

Also, it can be observed that the concrete stresses for the 0.45 *w/cm* concretes at the critical location are the highest for the reference and IC concretes, followed in the order of decreasing stresses by SLW and ALW concretes. Also, for the 0.38 *w/cm* concretes, the concrete stresses are the highest for reference concretes, followed in order of decreasing stresses by ICC, SLW, and ALW concretes. For lower *w/cm* concretes, the stresses due to autogenous shrinkage are eliminated with the addition of LWAs, as observed in Section 6.4. Thus at lower *w/cm,* inclusion of LWAs reduce the early-age stresses present in concrete as shown in Table 12-4. Thus it can be seen that despite increased temperature differences observed in concretes containing higher proportions of LWA, the concrete stresses are lower due to the decreased modulus of elasticity (from Figure 5-9 and 5-19), coefficient of thermal expansion (from Figure 6-1), and increased creep (relaxation) of the concrete containing LWA (Byard and Schindler 2015).

Table 12-4: Summary of maximum tensile stresses for all concretes

Type of Concrete	Maximum Tensile Stresses at Critical Location		
	4 × 4 ft	**8 × 8 ft**	**12 × 12 ft**
REF 0.45	140	260	375
ICC 0.45	140	250	375
SLWC 0.45	105	205	280
ALWC 0.45	80	150	205
REF 0.38	205	350	515
ICC 0.38	175	350	495
SLWC 0.38	135	260	330
ALWC 0.38	90	175	235

12.3.2 Calculated Cracking Risk

In ConcreteWorks the cracking risk classification of a concrete member is based on the calculated tensile stress-to-tensile strength ratio as explained by Riding et al. (2014). The concrete tensile stress-to-tensile strength ratio calculated in the software is assigned a cracking probability classification using a probability density function. The cracking probability density function was obtained from the distribution of the tensile stress-to-splitting tensile strength at cracking from experimental data. At stress-to-strength ratios above 0.72, the cracking risk is classified as being in the very high cracking risk zone (Riding et al. 2014).

The development of concrete stresses for concrete mixtures with *w/cm* = 0.45 and 0.38 are presented in Figures 11-15 to 11-17 and 11-30 to 11-32, respectively. Table 12-5 shows the maximum values of cracking risk for all the cross-section sizes. It can be seen from both sets of figures that the concrete cracking-risk increases with increasing

cross-section size. Thus larger cross-section sizes are more susceptible to early-age thermal cracking. The cracking risk is more important than the maximum critical stresses, because as shown in Figure 11-32, the maximum value of the stress-to-strength ratio for reference concrete occurs at 48 hrs; however, from Figure 11-29, one can observe that the maximum stresses for the same concrete and cross-section size occurs at approximately 72 hrs. Thus, in this example, the critical time for cracking occurs earlier than the maximum concrete stresses, because the tensile strength is time dependent. Therefore, the maximum stresses are not the primary concern for cracking in concrete but rather the cracking risk defined as the ratio of stress-to-strength is the most important indicator of early-age thermal cracking.

Table 12-5: Summary of maximum cracking risk for all concretes

Concrete Type	**Maximum Cracking Risk**		
	4 × 4 ft	**8 × 8 ft**	**12 × 12 ft**
REF 0.45	0.65	0.85	1.15
ICC 0.45	0.65	0.85	1.10
SLWC 0.45	0.40	0.65	0.75
ALWC 0.45	0.40	0.45	0.65
REF 0.38	0.65	0.95	1.15
ICC 0.38	0.45	0.85	1.10
SLWC 0.38	0.40	0.75	0.80
ALWC 0.38	0.35	0.60	0.70

Also, it can be observed from Figures 11-15 to 11-17 and 11-30 to 11-32 that the concrete cracking-risk decreases with the increased addition of LWA in the concrete. In fact, ALW concretes used in all cross-section sizes maintain a lower cracking risk in all cases. Thus, despite the greatest temperature differences observed in ALW concretes, the cracking risk of ALW concretes is the lowest when compared to the other concretes.

This is attributed to the ALWC having a reduced modulus of elasticity, reduced coefficient of thermal expansion, and an increased creep (relaxation).

It has been shown that although concretes containing LWA will develop increased temperature differences, their thermal cracking risk is reduced relative to reference concrete. The use of a 35°F temperature difference limit for concrete incorporating LWA is thus inappropriate. In order to mitigate early-age thermal cracking, an accurate stress analysis should be performed to account for all the factors that impact thermal cracking. This stress analysis is important since concerns have been raised regarding the cracking risk associated with concretes containing LWA (Maggenti 2007). Maggenti (2007) concluded that the temperature differences and core temperature of LWA concretes (specifically SLW and ALW concretes) were higher than reference concretes, which is in agreement with the above analysis. However, it can be concluded that cracking risk does not increase, but rather decreases, with decreasing density due to the addition of LWA in the mixture. Gajda and Vangeem (2002) and Bamforth (2007) suggested an increase of the 35°F temperature difference limit, based on the compressive strength and CTE of the concrete. Therefore, in the next chapter the development of a simplified formulation to estimate the impact of tensile strength, CTE, modulus of elasticity, and creep will be explored.

Chapter 13

PART II: DEVELOPMENT OF A METHOD TO DETERMINE THE TEMPERATURE DIFFERENCE LIMIT TO CONTROL THERMAL CRACKING

This chapter provides recommendations towards developing a thermal cracking specification to account for concretes made with different types of coarse and fine aggregate, including LWA. Temperature difference limits will be developed by using established ACI (ACI 318 2014) and AASHTO (AASHTO LRFD 2016) expressions for some concrete properties. Finally, guidelines for maximum concrete temperature differences limits for different types of concretes will be provided to control thermal cracking.

13.1 ALLOWABLE CONCRETE TEMPERATURE DIFFERENCE LIMIT

13.1.1 Simplified Modeling of Early-age Concrete Stress Development

From the previous sections, it was concluded that using a constant 35°F temperature difference limit for concrete containing LWA was overly conservative. It is also important to specify a time-dependent temperature difference limit for concretes containing LWA to provide an incentive for a contractor to use LWA to reduce early-age thermal cracking. In this section, an age-dependent temperature difference limit is developed using established relationships for concrete properties with Equation 8-1. The approach involves predicting the concrete tensile strength development and concrete creep (relaxation) effects at early-ages, in order to develop an age-dependent allowable temperature difference limit.

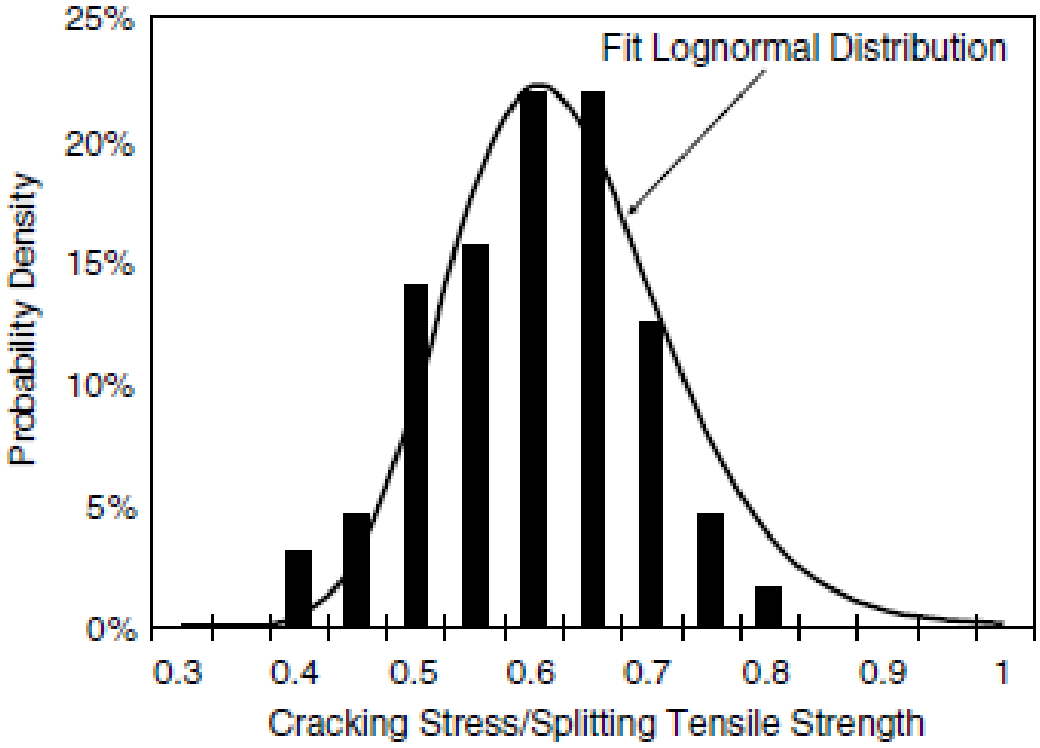

Figure 13-1: Cracking probability categories for stress-to-strength ratio using ACI 207.1R (2012) for splitting tensile strength (Riding et al. 2014)

Riding et al. (2014) used the stress-to-splitting strength as a failure criterion for thermal cracking of concrete. Based on the results of 64 rigid cracking frame tests and measured tensile strengths, a log normal fit of cracking stress-to-splitting tensile strengths for concretes (with the splitting tensile strength computed using ACI 207.1R (2012) expression), was developed and is shown in Figure 13-1. From the results, Riding et al. developed four cracking probability categories for stress to estimated splitting tensile strength. For specimens whose stress to splitting tensile strength exceeded 0.72, it was categorized as very high risk of cracking. In the case of the rigid cracking frame (RCF) tests on concretes summarized in Part I, the ratio of stress-to-strength at cracking ranged

from 0.67 to 0.80, as shown in Table 13-1, with an average value of 0.72. Thus, in this study, it is recommended to define that cracking occurs when the ratio of stresses in the concrete structure to the splitting-tensile strength of the structure exceeds a value of 0.72.

Table 13-1 Stress-to-strength ratio for various types of concretes

Concrete Type	Stress-to-Strength Ratio
REF 0.45	0.67
ICC 0.45	0.69
SLWC 0.45	0.74
ALWC 0.45	0.70
REF 0.38	0.67
ICC 0.38	0.80
SLWC 0.38	0.80
ALWC 0.38	0.67
AVERAGE	**0.72**

The stresses observed at the time of cracking is less than the measured splitting tensile strength. This is because of differences in the loading rate, test specimen size, and type of loading of the concrete specimen (Riding et al. 2014). For example, the rate of loading is lower in the RCF and a lower rate of loading produces lower apparent strengths (Neville 2011). The splitting tensile strength specimens are loaded to failure in less than five minutes, whereas the duration of the RCF tests, cover a period of approximately 4 to 6 days (Meadows 2007; Byard 2011). The tensile stresses are spread over a larger area (6×6×49 in.) in the case of the RCF than the cylinders (12 × 6 in.), hence there is a higher probability of finding flaws in the larger specimen, which makes it more susceptible to fail at a lower apparent strength (also known as size effects (Neville

2011)). In addition, the concrete cylinders undergo a splitting tension test which is an indirect tensile strength test, whereas the concrete in the RCF is subjected to direct tension. The ratio of cracking frame stress at failure to the splitting-tensile strength at the same time is generally between 40 and 80 percent (Riding et al.2014).

In order to meet the objective of developing a simplified method to compute the allowable temperature difference limits for concrete, the time-dependent parts of the thermal cracking equation, shown in Equation 13-1, 13-2, and 13-3 were developed using the appropriate models from published literature mentioned previously in Section 8.1.

$$0.72\ f_{st}(t) \geq \sigma_t(t) \qquad \text{(Equation 13-1)}$$

$$0.72\ f_{st}(t) \geqslant \sigma_t(t) = CTE \times R \times K(t) \times E_c(t) \times \Delta T_{max}(t) \qquad \text{(Equation 13-2)}$$

$$\Delta T_{max}(t) \leq \frac{0.72 f_{st}(t)}{CTE \times R \times K(t) \times E_c(t)} \qquad \text{(Equation 13-3)}$$

where,

$\sigma_t(t)$ = mean stresses due to early-age concrete volume changes at time 't' (psi),

$\Delta T_{max}(t)$ = allowable concrete temperature difference as a function of time (°F),

$f_{st}(t)$ = mean concrete tensile strength as a function of time (psi),

$E_c(t)$ = mean concrete modulus of elasticity as a function of time (psi),

$K(t)$ = creep modification factor as a function of time (unitless),

CTE = concrete coefficient of thermal expansion (in./in./°F), and

R = Restraint factor (0 = unrestrained; 1 = full restraint) (unitless)

The concrete stresses are influenced by many variables as shown in Equation 13-2. All the values mentioned in Equations 13-2 and 13-3 refer to the mean values. Mean

values are used because thermal cracking is a serviceability issue and not an ultimate limit state. The modulus of elasticity of concrete is utilized in the computation of early-age stresses in concrete, which can be estimated from the concrete compressive strength.

In order to determine the splitting-tensile strength of concrete, the concrete compressive strength can be computed, because these properties are related. Equation 13-4 shows the compressive strength expression used in the B3 Model (Bazant and Baweja 2000; ACI 209 (2008)). The later age (91 day) compressive strengths of concretes containing supplementary cementious materials (SCMs) such as fly ash, are higher than concretes not containing SCMs (provided the other constituents are similar) (Mehta and Monteiro 2013). However, this model does not account for the strength variations due to the inclusion of SCMs. The original compressive strength equation did not take into account maturity (equivalent age), however, in this study it is taken into account, and will be used to compute the cracking risk.

Also, Equation 13-4 is a standard Equation in ACI 207.1R (2012) and ACI 209 (2008), and since the objective of this study is to provide a simplified method to compute the maximum allowable temperature difference limits for mass concretes, it was simpler and easier to use Equation 13-4 for all concretes without introducing modifiers.

$$f_c(t) = \left(\frac{t}{a + bt}\right) \times f_c\,(28) \qquad \text{(Equation 13-4)}$$

where,

$f_c\,(t)$ = concrete compressive strength at time t (psi),

t = equivalent age of the concrete (days),

a = 4.0 for moist-cured concrete with Type I cement (days),

b = 0.85 for moist-cured concrete with Type I cement (unitless), and

$f_c(28)$ = concrete compressive strength at 28 days (psi).

The compressive strength of concrete can be computed using Equation 13-4, if the concrete compressive strength at 28 days is known. The mean compressive strength of a concrete member is typically higher than the specified 28 day compressive strength. ACI 214 (2011) provides guidance to compute the mean concrete compressive strength as a function of the specified 28 day strength, as shown in Table 13-2.

Table 13-2: Calculation of actual concrete compressive strength (ACI 214 2011)

Required Mean Compressive Strength	Specified Compressive Strength
$f_{cm} = f'_c + 1{,}000$ psi	when $f'_c < 3{,}000$ psi
$f_{cm} = f'_c + 1{,}200$ psi	when $f'_c \geq 3{,}000$ psi and $f'_c \leq 5{,}000$ psi
$f_{cm} = 1.10\, f'_c + 700$ psi	when $f'_c > 5{,}000$ psi

Raphael's splitting tensile strength expression (1984) shown in Equation 13-5 is used for estimating the splitting tensile strength of concrete from the concrete compressive strength. The expression is included in ACI 207.1R (2012) and it was developed for mass concrete structures.

$$f_{st}(t) = 1.7 \times f_c(t)^{2/3} \quad \text{(Equation 13-5)}$$

Where,

$f_t(t)$ = concrete tensile strength at time t (psi), and

$f_c(t)$ = concrete compressive strength at time t (psi).

Graybeal and Greene (2013) recommended the use of Equation 13-6 for estimating the splitting tensile strength of concrete—including concrete made with LWA—

from the concrete compressive strength. The lambda values for SLWC and ALWC are determined from the unit weight, as shown in Equation 13-7.

$$f''_{st}(t) = \frac{\lambda \times \sqrt{f''_c(t)}}{4.7} \quad \text{(Equation 13-6)}$$

$$0.75 \leq \lambda = 7.5 w''_c \leq 1.0 \quad \text{(Equation 13-7)}$$

Where,

w''_c = concrete equilibrium density (kcf),

$f''_{st}(t)$ = concrete tensile strength (ksi), and

$f''_c(t)$ = concrete compressive strength (ksi).

The concrete modulus of elasticity can also be calculated as a function of the concrete compressive strength. ACI 318 (2014) provides guidance on how to compute the concrete modulus of elasticity, as shown in Equation 13-8.

$$E_c(t) = 33(w_c)^{1.5}\sqrt{f_c(t)} \quad \text{(Equation 13-8)}$$

Where,

$E_c(t)$ = concrete modulus of elasticity (psi),

w_c = concrete unit weight (pcf), and

$f_c(t)$ = concrete compressive strength at any time t (psi).

The concrete modulus of elasticity can be calculated as a function of the concrete compressive strength. AASHTO LRFD (2016) is used to calculate the mean concrete modulus of elasticity, as shown in Equation 13-9.

$$E''_c(t) = 120000\,(f''_c(t))^{0.33}(w''_c)^{2.0} \qquad \text{(Equation 13-9)}$$

Where,

$E''_c(t)$ = concrete modulus of elasticity (ksi),

w''_c = concrete unit weight (kcf), and

$f''_c(t)$ = concrete compressive strength (ksi).

Equation 13-10 contains the creep coefficient Equation used in the B3 Model (Bazant and Baweja 2000).

$$\phi(t, t_o) = E(t_o)J(t, t_o) - 1 \qquad \text{(Equation 13-10)}$$

Where,

$\phi(t,t_o)$ = creep coefficient (unitless),

$J(t,t_o)$ = average compliance function (1/psi),

$E(t_o)$ = static modulus of elasticity at the age of concrete loading (psi),

t = age of concrete (days), and

t_o = age of concrete loading (days).

In the B3 model, the creep coefficient is directly calculated from the compliance function. The compliance function present in the B3 model is shown in Equation 13-11.

$$J(t, t_o) = q_1 + C_o(t, t_o) + C_d(t, t_o, t_c) \qquad \text{(Equation 13-11)}$$

where,

q_1 = instantaneous strain due to unit stress (1/psi),

$C_o(t,t_o)$ = compliance function for basic creep (1/psi),

$C_d(t,t_o,t_c)$ = compliance function for drying creep (1/psi), and

t_c = age drying began (end of moist curing) (hrs)

Also, the B3 creep coefficient can be expressed as a creep factor using Equation 13-12 (ACI 209 2008).

$$K(t) = \frac{1}{1 + \varphi(t, t_o)} \quad \text{(Equation 13-12)}$$

Where,

$\varphi(t,t_o)$ = creep coefficient (unitless), and

$K(t)$ = creep modification factor (unitless).

13.1.2 Accounting for Early-Age Creep and Restraint

Modeling creep effects in concrete is important when assessing the early-age cracking risk. While many creep models exist to model the creep effects (Bamforth 1995; Bazant and Baweja 1989), the Modified B3 Model (Byard and Schindler 2015) and Bamforth Model (Bamforth 2007) will be used in this study to quantify early-age creep effects in concrete.

The Modified B3 Model was developed by Byard and Schindler (2015) to assess the concrete stresses at early-ages, i.e. from the time of initial set to cracking of concrete. The presence of two modifiers, one accounting for increased early-age viscoelastic response and another modifier accounting for the early-age development of the modulus of elasticity response ensures that the early-age stresses in concrete are better quantified when compared to the B3 Model (Byard and Schindler 2015).

Since this study involves two groups of *w/cm* concretes, the Modified B3 Model and Bamforth Model was used to model the creep factors at early-ages for both *w/cm* concretes. Table 13-3 and Table 13-4 display the input variables used in the calculation

of the Modified B3 Model compliance values. The input values were computed from the mixture proportion tables shown in Tables 10-2 and 10-3.

Table 13-3: Summary of input values for the Modified B3 Model compliance calculations for *w/cm* = 0.45

Input	Symbol	Input Values for Various Concrete Types			
		REF 0.45	**ICC 0.45**	**SLWC 0.45**	**ALWC 0.45**
Mean 28-day compressive strength	f_{cm} *(28)*	5,200 psi	5,200 psi	5,200 psi	4,200 psi
Cementious Content	*c*	590 lb/yd^3	590 lb/yd^3	590 lb/yd^3	590 lb/yd^3
Empirical Constants	*m*	0.5	0.5	0.5	0.5
	n	1	1	1	1
Water-to-cementious materials ratio	*w/cm*	0.45	0.45	0.45	0.45
Aggregate-cement ratio	*a/c*	5.01	4.88	3.56	2.84

Table 13-4: Summary of input values for Modified B3 Model compliance calculations for *w/cm* = 0.38

Input	Symbol	Input Values for Various Concrete Types			
		REF 0.38	**ICC 0.38**	**SLWC 0.38**	**ALWC 0.38**
Mean 28-day compressive strength	f_{cm} *(28)*	6,200 psi	6,200 psi	6,200 psi	5,200 psi
Cementious Content	*c*	620 lb/yd^3	620 lb/yd^3	620 lb/yd^3	620 lb/yd^3
Empirical Constants	*m*	0.5	0.5	0.5	0.5
	n	1	1	1	1
Water-to-cementious materials ratio	*w/cm*	0.38	0.38	0.38	0.38
Aggregate-cement ratio	*a/c*	4.77	4.65	3.39	2.70

Figures 13-2 and 13-3 depict the compliance values for both groups of *w/cm* concretes using time steps of 0-24 hours, 24-48 hours, 48-72 hours, 72-120 hours and 120-168 hours.

From Figure 13-2, it can be seen that the compliance values are higher for concrete containing LWA, with ALWC having the highest compliance values followed by SLWC, ICC, and reference concrete. This is to be expected, due to the lower stiffness of LWA (Byard 2011; Neville 2011). Also, from both Figures 13-2 and 13-3, it can be concluded that concretes with *w/cm* = 0.38 have lower compliance than concretes with *w/cm* = 0.45. This could be attributed to higher quality paste in concretes with a lower *w/cm* (Byard 2011; Neville 2011).

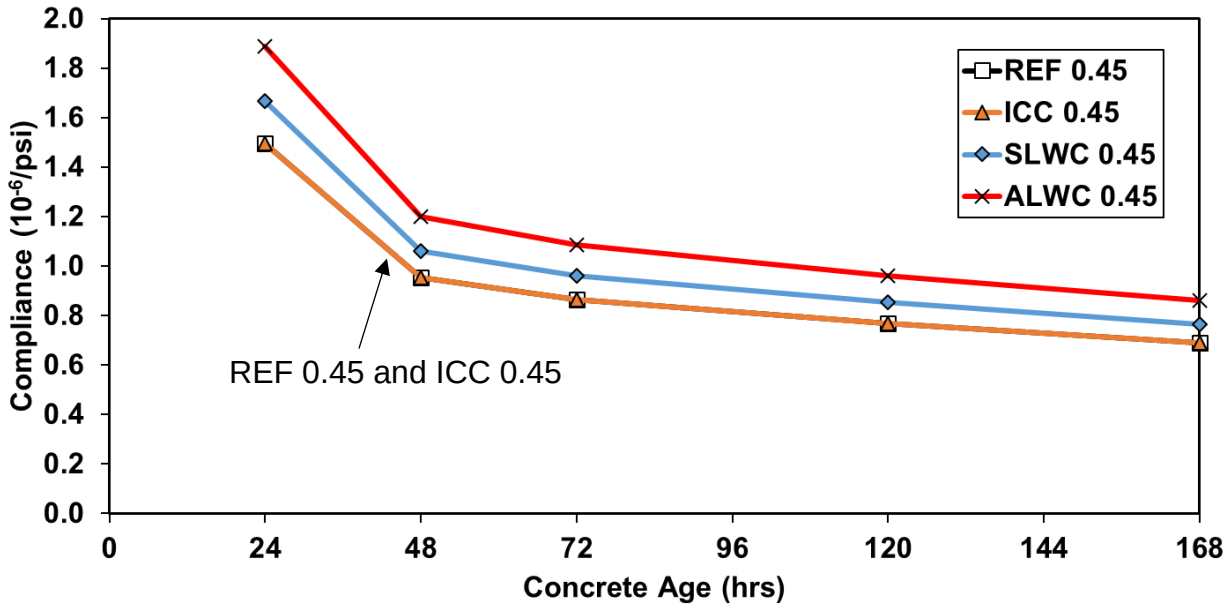

Figure 13-2: Compliance values- Modified B3 Model for all 0.45 *w/cm* concretes

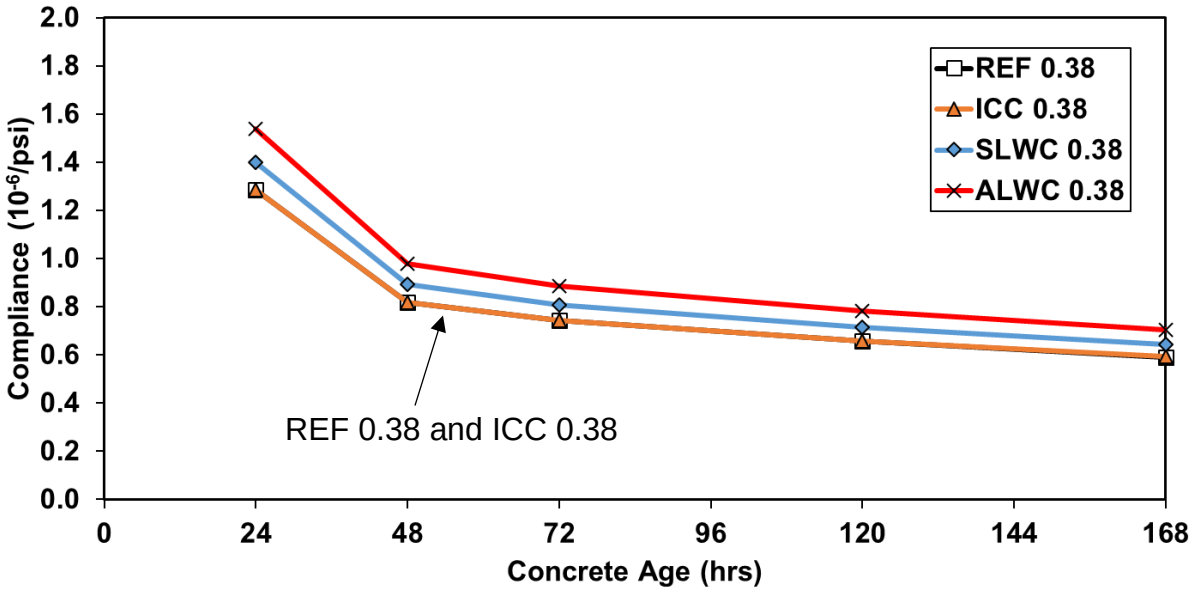

Figure 13-3: Compliance values- Modified B3 Model for all 0.38 *w/cm* concretes

13.1.2.1 Creep Factor of Concrete

The development of creep factor at early-ages for all 0.45 *w/cm* and 0.38 *w/cm* concretes can be computed from the compliance and using Equations 13-10 and 13-12 and shown in Figure 13-4 and 13-5, respectively. From both these figures, it can be seen that the creep factor is higher for the reference concretes (similar for ICC), followed by SLWC and ALWC. It is also clear that concretes with *w/cm* = 0.38 have slightly higher creep factors in comparison to concretes with *w/cm* = 0.45. The Bamforth Model (2007) which assumes a constant value of 0.65 for creep factor is also shown in Figures 13-4 and 13-5. Since the Bamforth Model creep factor value is simpler to use and is higher (conservative stress estimate) than the calculated Modified B3 Model creep factor, it will be used for computing the allowable concrete temperature difference limits.

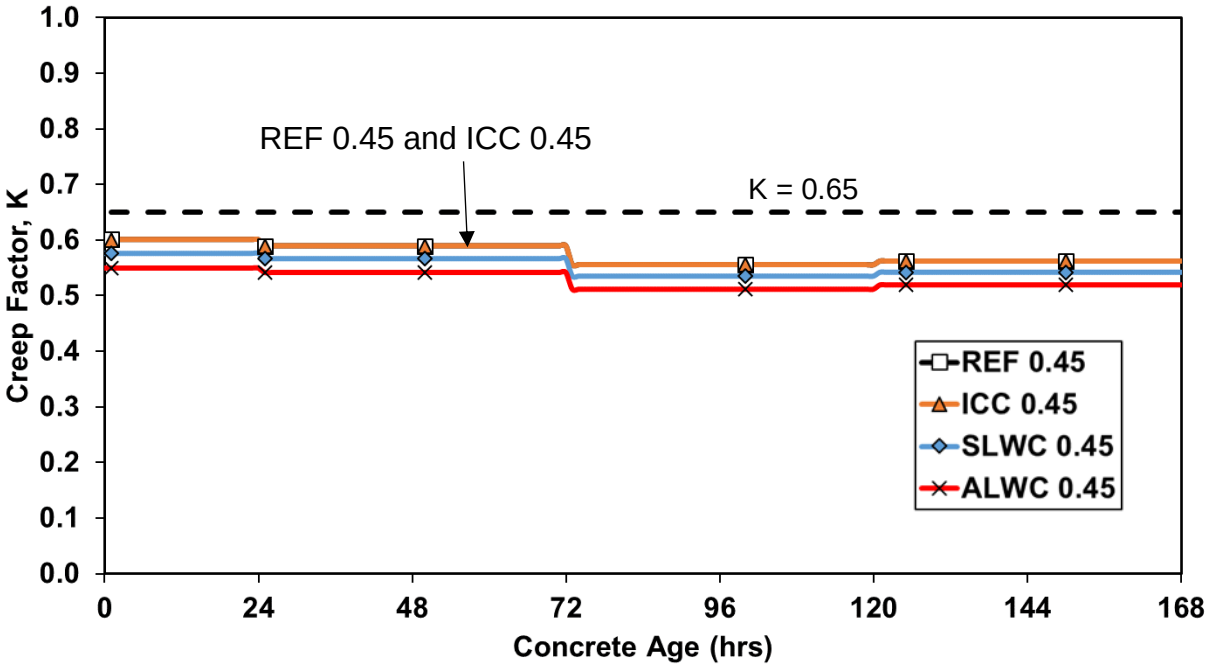

Figure 13-4: Creep factors- Modified B3 and Bamforth Model for 0.45 *w/cm* concretes

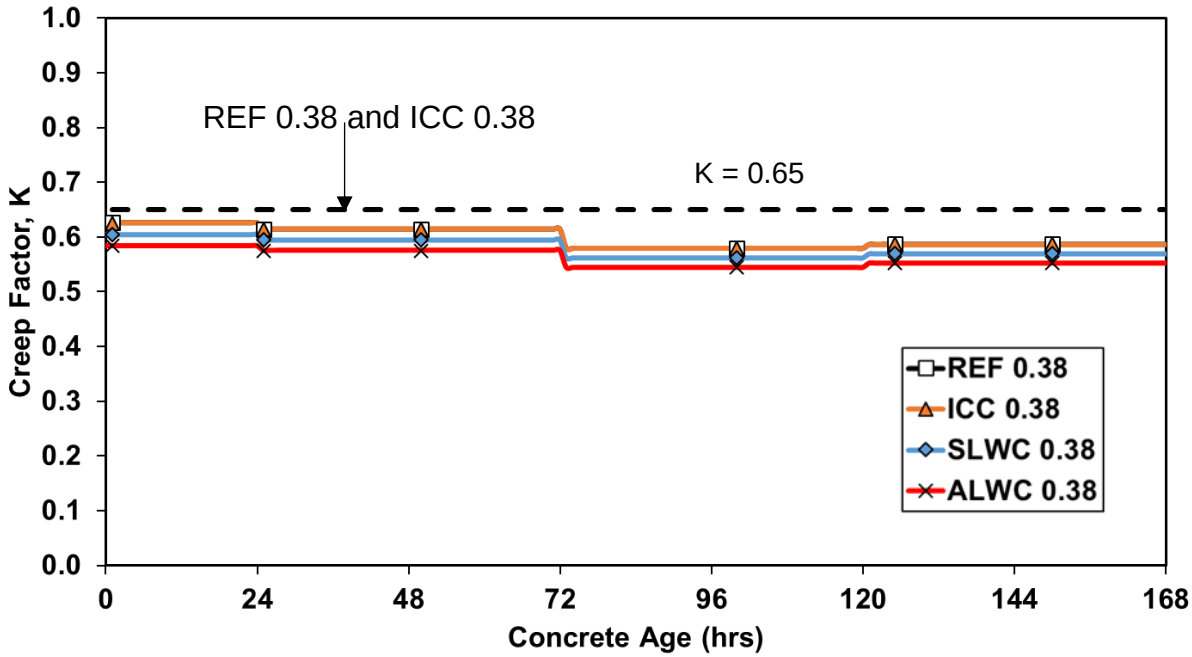

Figure 13-5: Creep factors- Modified B3 and Bamforth Model for 0.38 *w/cm* concretes

13.1.2.2 Restraint Factor

Internal restraint is a result of differential temperature changes within a concrete structure as explained in Section 9.1. Bamforth (2007) recommended a value of 0.42 for internal restraint from research conducted on large mass concrete structures. BS 8110 (1997) recommended a value of 0.36, however this was considered as a low value and was changed to 0.42 (Bamforth 2007). An appropriate restraint factor will be identified based on the ConcreteWorks stress analysis in Section 13.1.3.

13.1.3 Determining the Allowable Concrete Temperature Difference Limit Based on the ConcreteWorks Analysis

The allowable temperature limits can be obtained from the AASHTO (2016) expression of modulus of elasticity (Equation 13-9) and Green and Graybeal (2013) expression of splitting tensile strength (Equation 13-6). The allowable temperature difference limits derived from these expressions will be known as the AASHTO allowable temperature limits.

The ACI (2014) expressions for splitting tensile strength (Equation 13-7) and modulus of elasticity (Equation 13-8) will be used to derive the ACI allowable temperature difference limits for concrete.

In this section both the AASHTO and ACI allowable temperature difference limits are determined and compared. The AASHTO and ACI Equations are calibrated using ConcreteWorks cracking risk values and the temperature difference predicted from this software. Varying cross-section sizes in increments of 0.5 ft starting from 4×4 ft were simulated in ConcreteWorks to determine the early-age cracking risk of all concretes. The

minimum cross-section size that has a cracking risk value approaching 0.72 (very high cracking risk) was determined for each concrete. The AASHTO and ACI equations were then suitably calibrated by changing the internal restraint factor to match with the ConcreteWorks high cracking risk value. This was done for all concretes and the minimum cross-section sizes for all concretes are presented in Table 13-5. The equilibrium densities and CTE of the concretes are provided in Table 13-6.

The restraint factor was set to 0.60 during the calibration study and was found to be provide the best results for all types of concrete. The calibration for the restraint factor was based on the temperature difference limits obtained from ConcreteWorks. The temperature difference limit from the AASHTO (2017) expression was used to determine the restraint factor. The temperature difference limit from the AASHTO (2017) expression coincides with the temperature difference limit, at 72 hrs which is the maximum concrete risk, from ConcreteWorks for a restraint factor of 0.60. An example with different restraint factors and the corresponding temperature difference limits is shown in Figure 13-15. Thus this value was chosen for the temperature difference limit for the ACI 318 (2017) expression as well. As discussed in section 13.1.2.2 Bamforth (2007) recommended a value of 0.42 for internal restraint. The value of 0.60 used in this study is thus conservative and is recommended for determining the allowable concrete temperature differential for concrete.

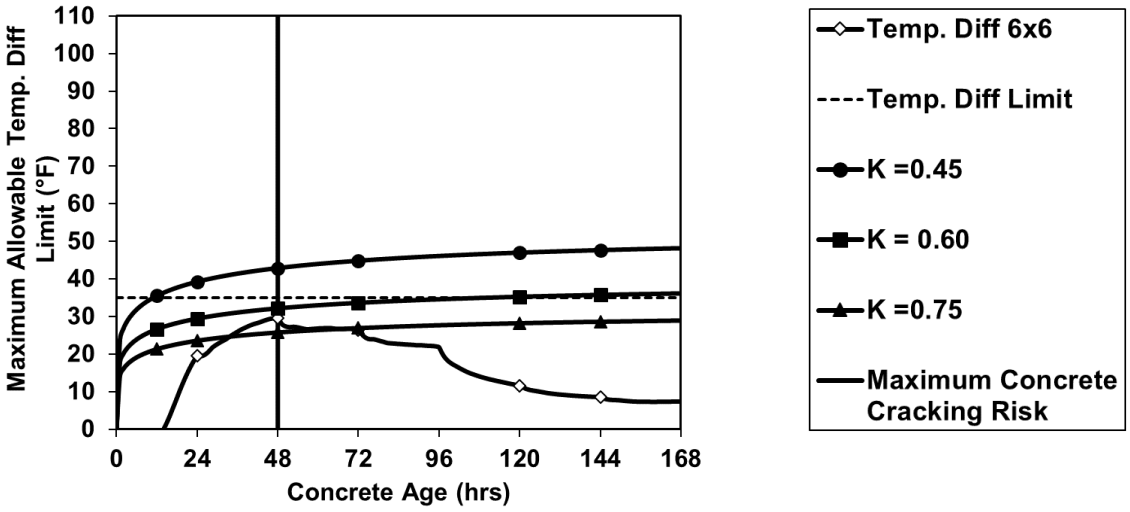

Figure 13-5: Allowable Temperature Limits for different restraint factors using the AASHTO (2016) expression for REF 0.45 concrete with 6×6 ft cross section size.

Table 13-5: Minimum cross-section sizes and time at cracking for 0.45 *w/cm* and 0.38 *w/cm* concretes

Concrete Type	Minimum Cross-section Size (ft)	Time when Maximum Cracking Risk Occurs (hrs)	Maximum Cracking Risk
REF 0.45	6×6	48	0.72
ICC 0.45	6.5×6.5	48	0.72
SLWC 0.45	10.5×10.5	96	0.72
ALWC 0.45	13x13	96	0.72
REF 0.38	5.5×5.5	48	0.72
ICC 0.38	6×6	48	0.72
SLWC 0.38	9×9	72	0.72
ALWC 0.38	10.5×10.5	96	0.72

Table 13-6: CTE and equilibrium density values for 0.45 *w/cm* and 0.38 *w/cm* concretes

Concrete Type	Coarse Aggregate Type	Fine Aggregate Type	Equilibrium Density (pcf)	CTE of Concrete (in./in./°F)
REF 0.45	River Gravel	River Sand	139	5.80×10^{-6}
ICC 0.45	River Gravel	River Sand/Expanded Shale	136	5.70×10^{-6}
SLWC 0.45	Expanded Shale	River Sand	115	5.20×10^{-6}
ALWC 0.45	Expanded Shale	Expanded Shale	95	4.10×10^{-6}
REF 0.38	River Gravel	River Sand	139	6.10×10^{-6}
ICC 0.38	River Gravel	River Sand/Expanded Shale	136	5.90×10^{-6}
SLWC 0.38	Expanded Shale	River Sand	115	5.30×10^{-6}
ALWC 0.38	Expanded Shale	Expanded Shale	95	4.10×10^{-6}

Each result from the Figures 13-6 to 13-13, was determined with ConcreteWorks to represent the minimum cross-section size above which the cracking risk would be very high. For example, in the case of REF 0.45 shown in Figure 13-6, the minimum concrete cross-section size above which the concrete cracking risk would be high is 6 × 6 ft. Thus, any REF 0.45 concrete with a larger cross-section size would be at a very high risk of thermal cracking. Similarly, for ALWC 0.45, the minimum cross-section size where the ALWC 0.45 concrete would be at a very high risk of thermal cracking is 13×13 ft. Thus, from the temperature figures provided in Figures 13-6 to 13-13 that show the cross-

section size and the recorded temperature difference data for each concrete mixture, it is possible to determine how close the computed temperature difference limit is to that modeled with ConcreteWorks at a very high cracking risk. While this method is not considered as a substitute for a stress analysis, it can provide an initial assessment as to whether a particular structure can be susceptible to early-age cracking.

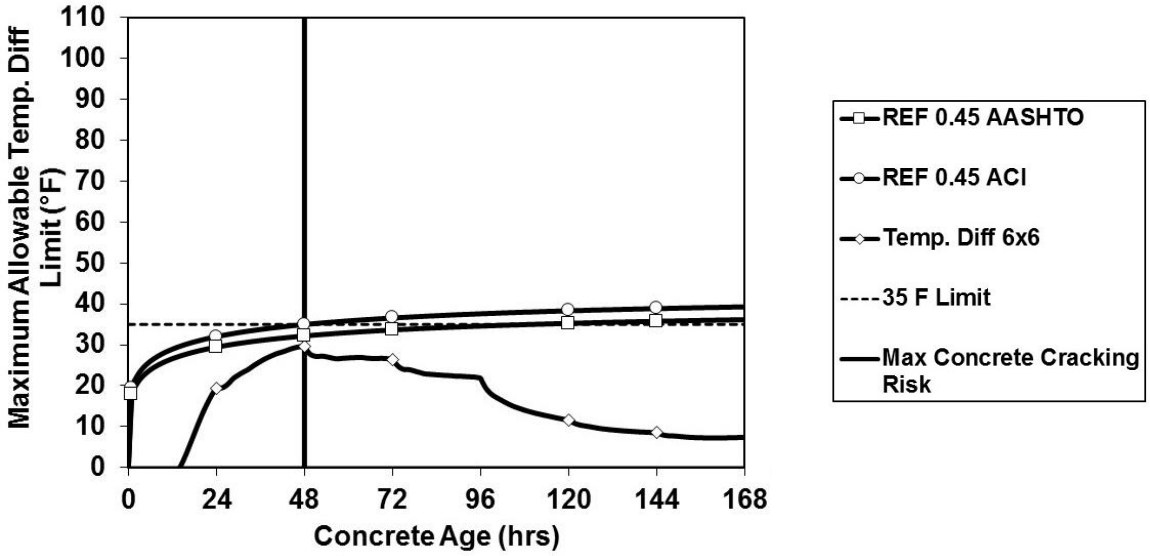

Figure 13-6: REF 0.45 with 6 × 6 ft Cross-section Size Column Temperature Differences versus Allowable Temperature Limit

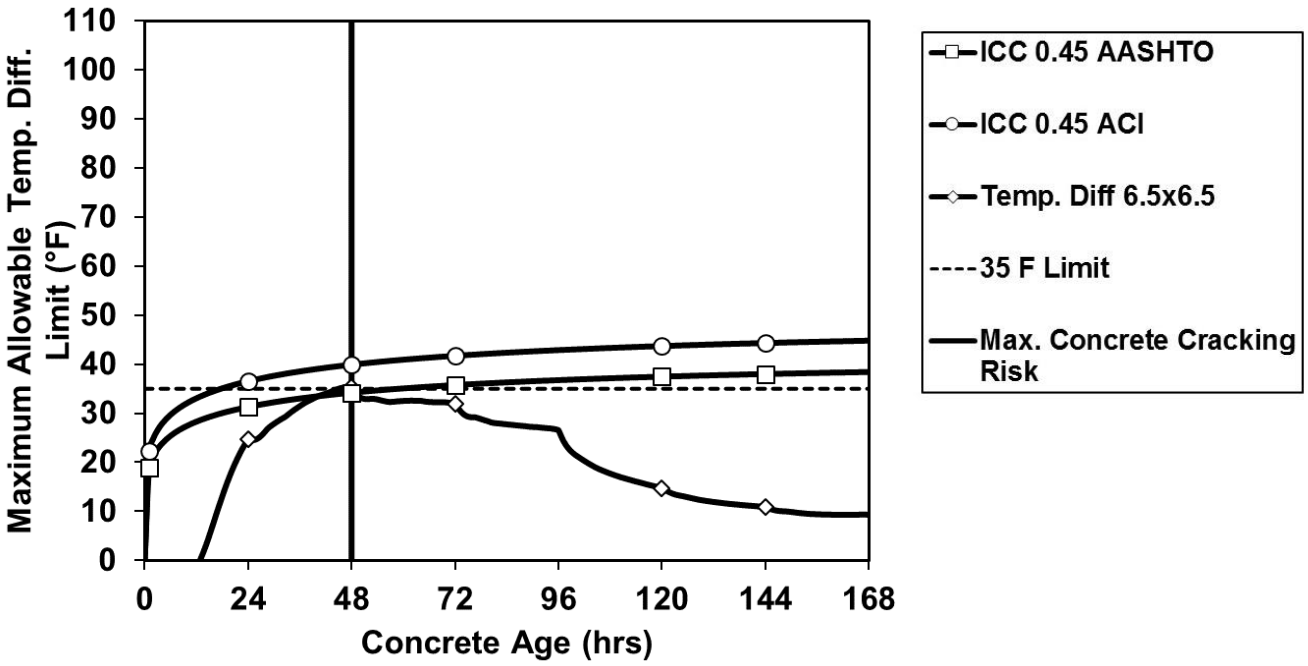

Figure 13-7: ICC 0.45 with 6.5 × 6.5 ft Cross-section Size Column Temperature Differences versus Allowable Temperature Limits

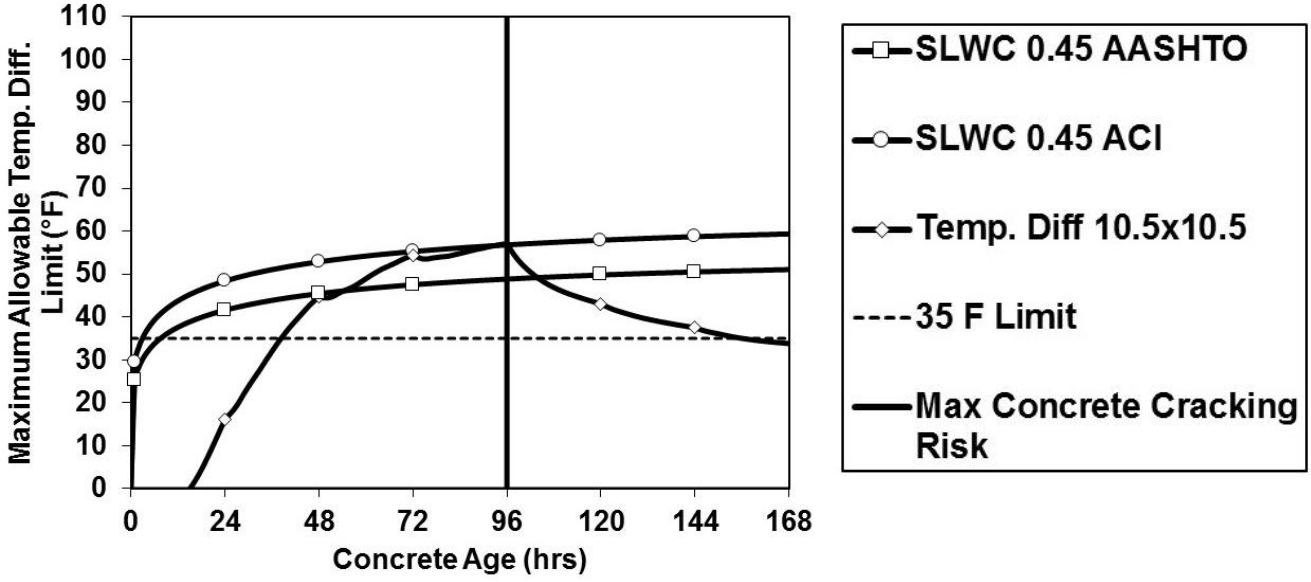

Figure 13-8: SLWC 0.45 – 10.5×10.5 ft Cross-section Size Column Temperature Differences versus Allowable Temperature Limits

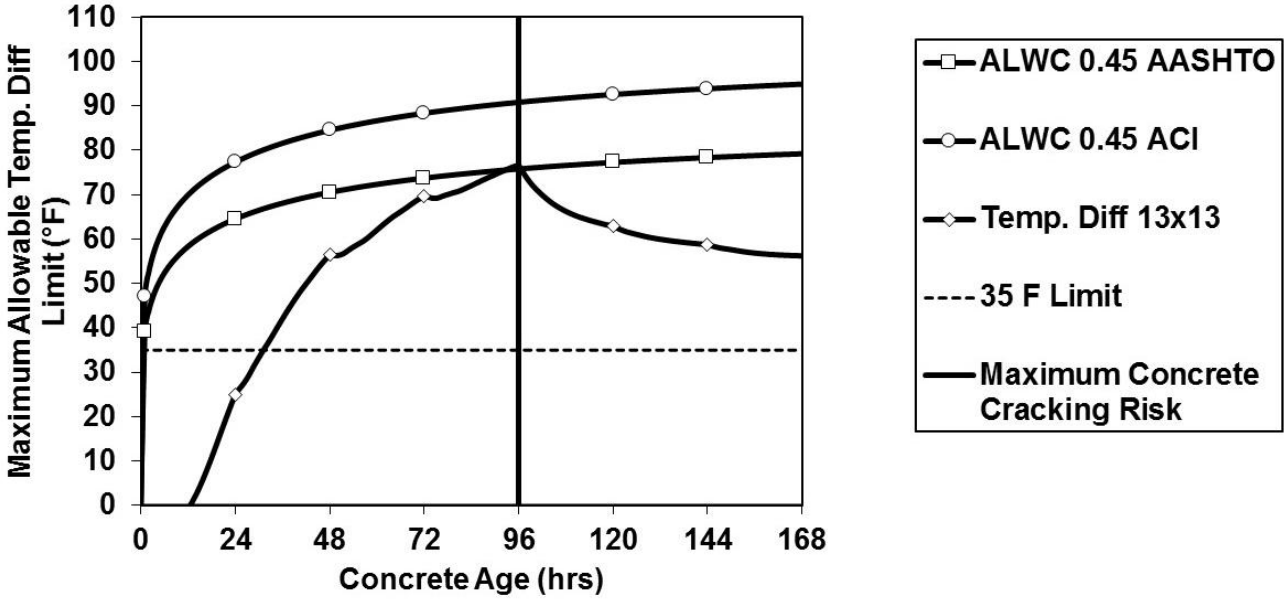

Figure 13-9: ALWC 0.45 with 13×13 ft Cross-section Size Column Temperature Differences versus Allowable Temperature Limits

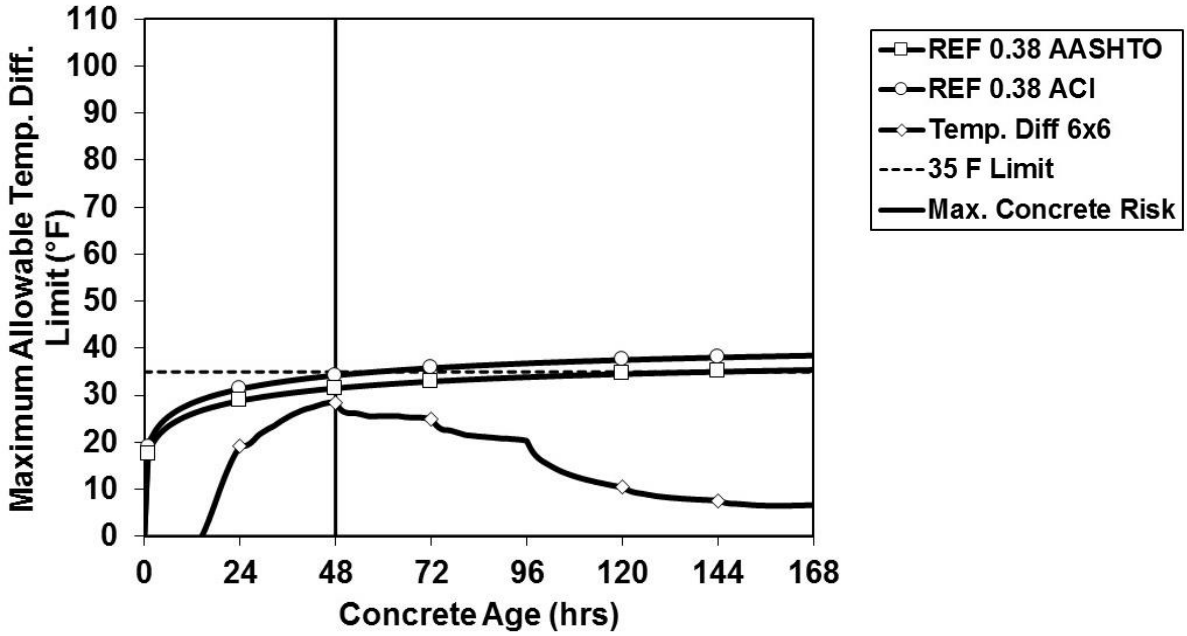

Figure 13-10: REF 0.38 – 6×6 ft Cross-section Size Column Temperature Differences versus Allowable Temperature Limits

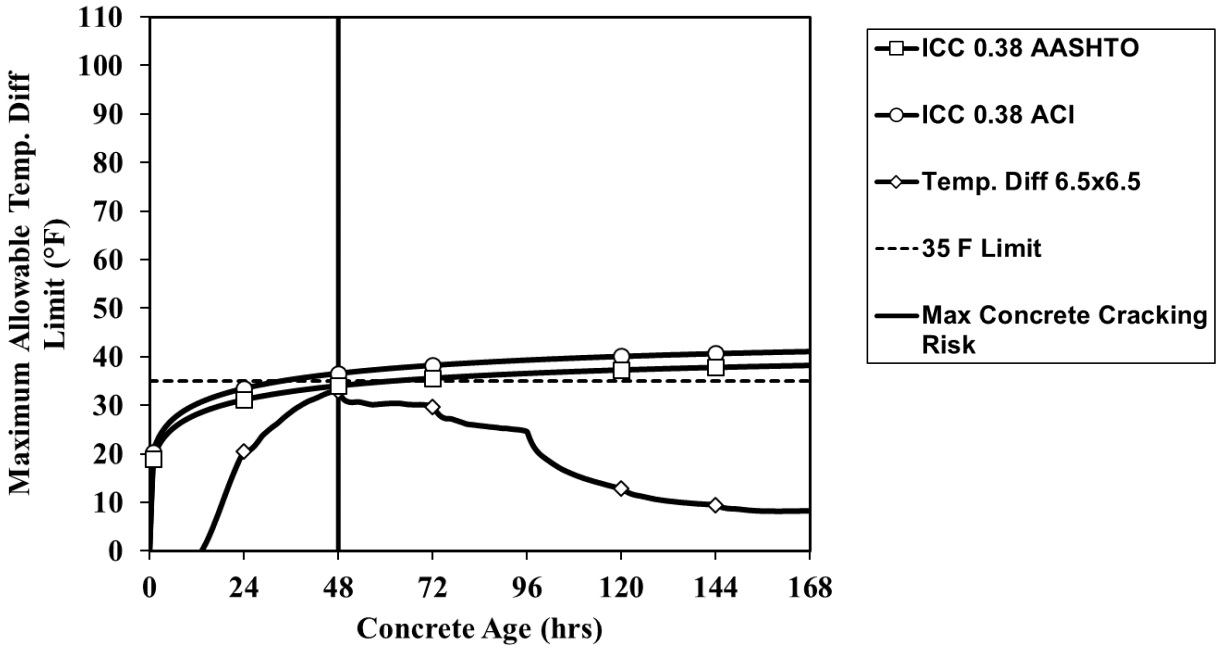

Figure 13-11: ICC 0.38 – 6.5×6.5 ft Cross-section Size Column Temperature Differences versus Allowable Temperature Limits

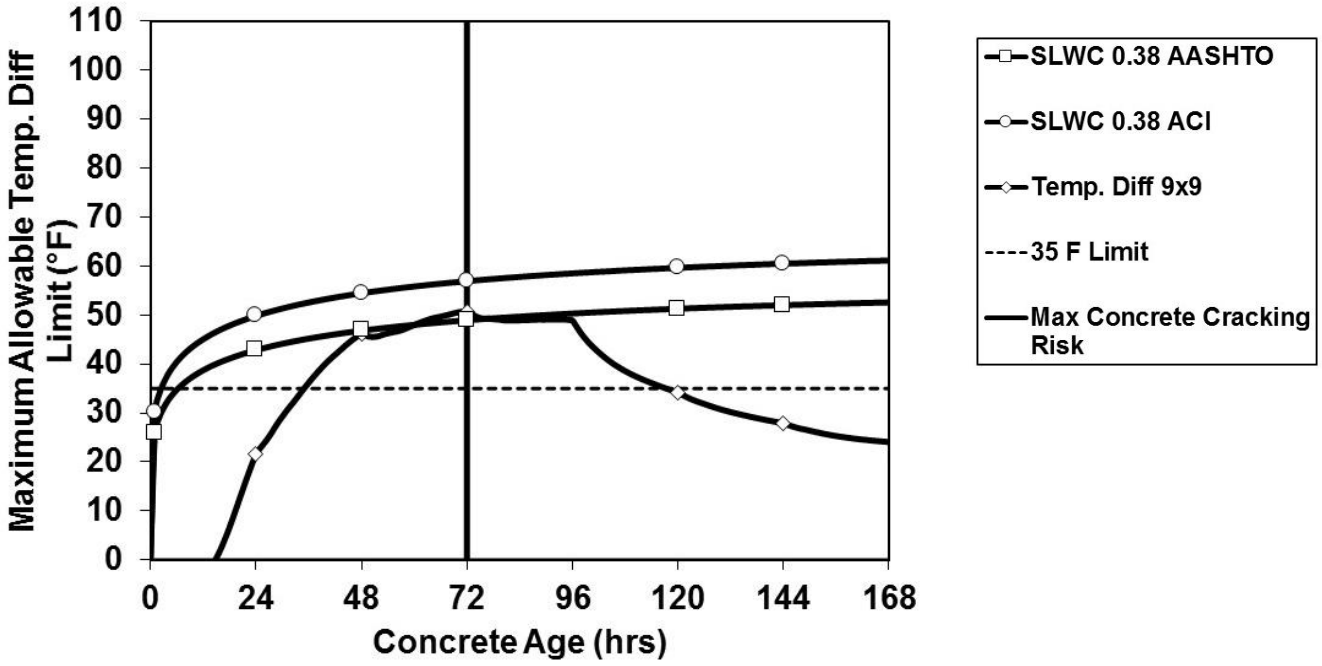

Figure 13-12: SLWC 0.38 – 9×9 ft Cross-section Size Column Temperature Differences versus Allowable Temperature Limits

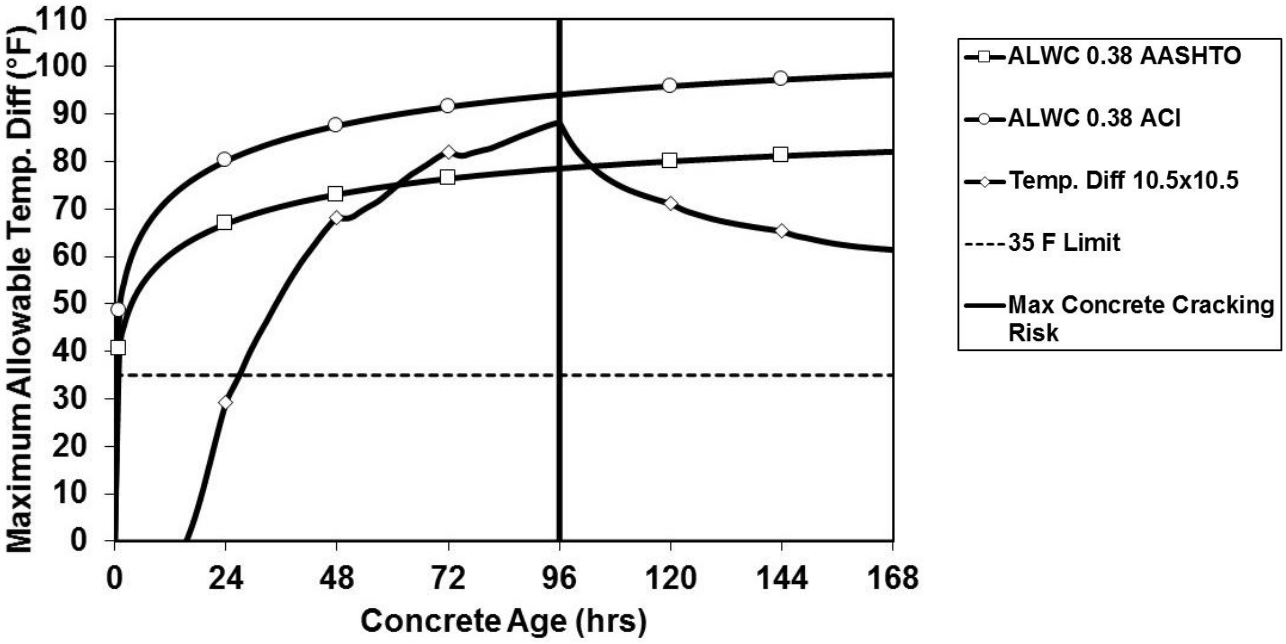

Figure 13-13: ALWC 0.38 – 10.5×10.5 ft Cross-section Size Column Temperature Differences versus Allowable Temperature Limits

An overall summary of the temperature difference limits obtained from ConcreteWorks and ACI 318 (2014), AASHTO LRFD (2012) expressions for all concretes are shown in Figures 13-14 (a) and 13-14 (b).

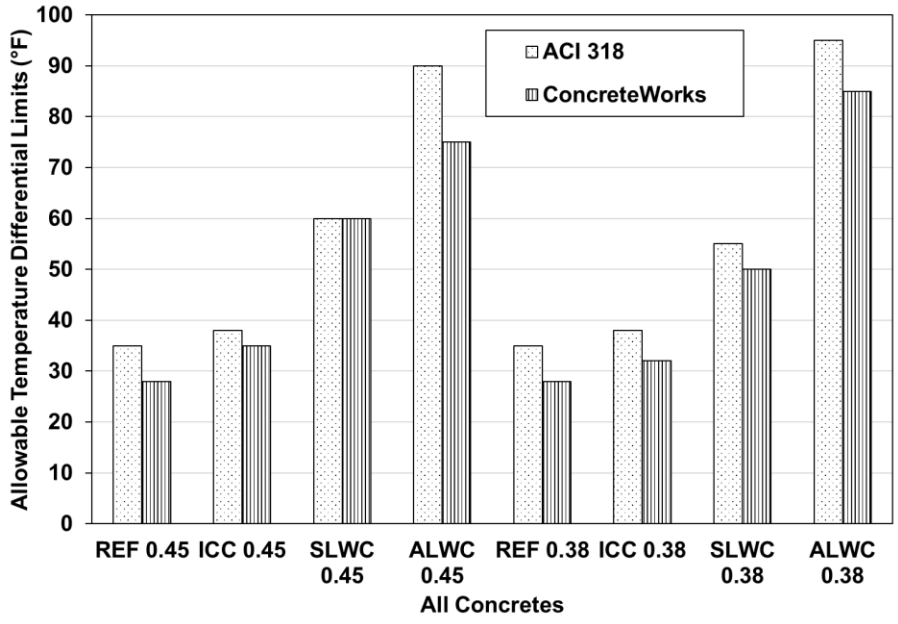

Figure 13-14 (a): Allowable Temperature Limits vs ACI 318 (2014) expression for all concretes

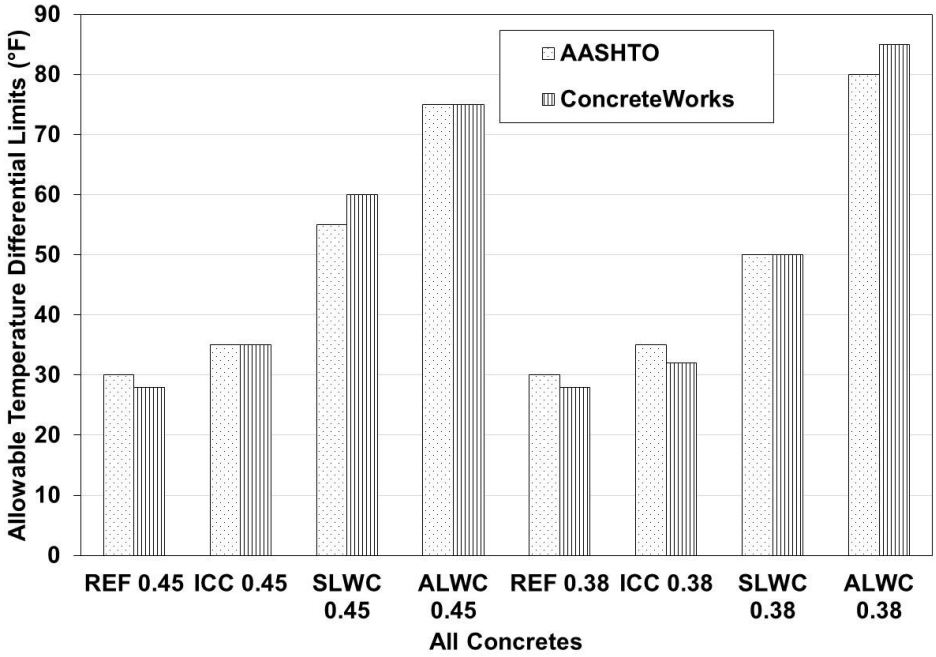

Figure 13-14 (b): Allowable Temperature Limits vs AASHTO LRFD (2012) expression for all concretes

From Figures 13-6 to 13-13, it can be observed that for SLWC and ALWC, the ACI allowable temperature limits are slightly higher than the AASHTO allowable temperature limits. The lower AASHTO temperature limit for SLWC and ALWC is due to the lightweight modification factor in the Graybeal and Green (2013) expression.

From Figures 13-6 to 13-7 and 13-10 to 13-11, it can be observed that after 24 to 48 hours for all the reference and IC concretes, the ACI and AASHTO allowable temperature limits exceed the 35°F temperature difference limit. While from Figures 13-8 to 13-9 and 13-12 to 13-13 it can be seen that for SLWC and ALWC, the respective ACI and AASHTO allowable temperature limits are much higher than the 35 °F temperature limit. Thus, a constant 35°F concrete temperature difference limit for all concretes is inappropriate. A combination of reduced modulus of elasticity, coefficient of thermal expansion, and creep factor, for concrete made with LWA in comparison with normalweight concretes ensures that the ACI and AASHTO allowable temperature difference limits for all concretes are higher than the constant 35°F temperature differential.

The allowable temperature limits for 0.38 *w/cm* concretes are slightly higher than the 0.45 *w/cm* concretes. This may be attributed to an increase in concrete compressive strength for 0.38 *w/cm* concretes.

For concretes containing lightweight aggregates, the AASHTO allowable temperature difference limit is more conservative (lower) when compared with the ACI allowable temperature limits. In order to develop a simple allowable temperature difference limit for all concretes, the AASHTO 0.45 *w/cm* concrete allowable temperature difference limits will be used in Section 13.1.4. This is reasonable, because a specified

design strength of 4,000 psi is typically used for mass concrete which can be achieved with a *w/cm* of 0.45.

In summary, the allowable temperature difference limits obtained from AASHTO and 0.45 *w/cm* concretes are conservative (lower bound). This leads to the conclusion that the use of AASHTO 0.45 *w/cm* concrete temperature difference limits are more applicable and representative of early-age concrete behavior than using a constant 35°F temperature difference limit for all concretes.

13.1.4 Development of Maximum Concrete Temperature Difference Limit

The AASHTO age-dependent allowable concrete temperature difference limit versus age for normalweight concrete containing river gravel and natural river sand is shown in Table 13-8. The table was developed for normalweight concrete (REF 0.45), with a restraint factor of 0.60, a creep factor of 0.65, a CTE of 5.8 microstrain/°F, an equilibrium density of 139 pcf and a specified concrete compressive strength of 4000 psi. The total air content in the concrete is approximately equal to 5 percent. This explains the slight reduction in equilibrium density when compared to the standard density value of density of 145 pcf for normalweight concrete.

Table 13-7: Allowable maximum temperature differences for control concrete

Concrete Age, *t* (hours)	**Maximum Allowable Temperature Difference, $\Delta T_{max}(t)$ (°F)**
12	27
24	29
36	31
48	32
60	33
72	33
84	34
96	34
108	35
120	35
132	36
144	36
156	36
168	37

The allowable temperature limits for normalweight concrete in Table 13-7 can be computed or modified with Equation 13-3 provided all input are known. The limits mentioned in Table 13-7 can be adjusted proportionally to account for any concrete type, including those containing LWA. For example, concretes containing LWA have a lower CTE, thus the allowable concrete temperature limits will be increased when using SLWC and ALWC. In order to modify the temperature difference limits in Table 13-7 for concretes containing LWA, the modification factors defined in Sections 13.1.2.1 to 13.1.2.3 are recommended.

The concrete temperature difference limit values from Table 13-7 can be altered according to Equation 13-13

$$\Delta T_{max,modified}(t) = F_{CTE} \times F_E \times F_{ST} \times \Delta T_{max}(t) \quad \text{(Equation 13-13)}$$

where,

$\Delta T_{max,modified}(t)$ = modified allowed maximum temperature difference limit (°F),

F_{CTE} = concrete CTE modification factor (unitless),

F_{ST} = concrete splitting tensile strength modification factor (unitless),

F_E = concrete modulus of elasticity modification factor (unitless), and

$\Delta T_{max}(t)$ = allowable maximum temperature difference limit as a function of concrete age (°F) (listed in Table 12-8).

13.1.4.1 Modification Factor for CTE

The modification factor for CTE is shown in Equation 13-14.

$$F_{CTE} = \frac{5.8 \times 10^{-6}}{CTE_{measured}} \quad \text{(Equation 13-14)}$$

Where,

F_{CTE} = concrete CTE modification factor (unitless), and

$CTE_{measured}$ = measured concrete CTE (in./in./°F).

13.1.4.2 Modification Factor for Modulus of Elastcity

The modification factor for modulus of elasticity is shown in Equation 13-15. The modulus of elasticity is proportional to the square of the equilibrium density, from the Greene and Graybeal (2013) expression, shown in Equation 13-9. Hence the modification factor for

modulus of elasticity comprises of the square of the equilibrium density, as shown in Equation 13-15.

$$F_E = (\frac{0.139}{w_{measured}})^2 \quad \text{(Equation 13-15)}$$

Where,

F_E = concrete CTE modification factor (unitless), and

w_{actual} = measured concrete equilibrium density (kcf).

13.1.2.3 Modification Factor for Splitting Tensile Strength

The modification factor for splitting tensile strength is shown in Equation 13-16 and 13-17. The splitting tensile strength for concrete containing lightweight aggregate is modified using a lambda factor (Green and Graybeal 2013). This expression was found to be suitable for SLWC and ALWC mixtures from Section 6.5. Thus the modification factor for splitting tensile strength contains this expression, as shown in Equation 13-16.

$$F_{ST} = \lambda \quad \text{(Equation 13-16)}$$

$$0.75 \leq \lambda = 7.5 \times w'_c \leq 1.0 \quad \text{(Equation 13-17)}$$

Where,

F_{ST} = concrete splitting tensile strength modification factor (unitless),

w'_c = concrete equilibrium density (kcf), and

λ = lightweight modification factor (= 1.0 for normalweight concretes) (unitless).

Thus, the values from Table 13-7, and with the aid of Equation 13-12 can be used to determine the allowable temperature difference limit in all concretes including those containing LWA. Equation 13-12 may also be used for concretes containing different coarse and fine aggregate types. An example is provided in the following section.

Example: Determine the maximum temperature difference limit for ALWC at 24, 48, 72, 96, 120, and 168 hrs, if the equilibrium density of ALWC is 95 pcf , specified design strength of 4000 psi, and the CTE of ALWC is 4.0 με/°F.

Solution: From Table 13-7, the maximum allowable temperature difference limit for reference concrete at 72 hrs is 36°F. The lightweight modification factor for this concrete would be equal to 0.75. Using the modification factors mentioned from Equation 13-12 to 13-17, the maximum allowable temperature difference limit for ALWC at 72 hrs is (from Equation 13-17)

$$\Delta T_{max,modified}(t) = F_{CTE} \times F_E \times F_{ST} \times \Delta T_{max}(t)$$

$$\Delta T_{max,modified}(t) = \frac{5.8 \times 10^{-6}}{4 \times 10^{-6}} \times \left(\frac{139}{95}\right)^2 \times 0.75 \times 33 = 77°F$$

Similarly, the maximum allowable temperature difference limit at 24, 48, 96, and 120 hrs is 66°F, 73°F, 77°F, and 87°F respectively. A plot containing these values is shown in Figure 13-15.

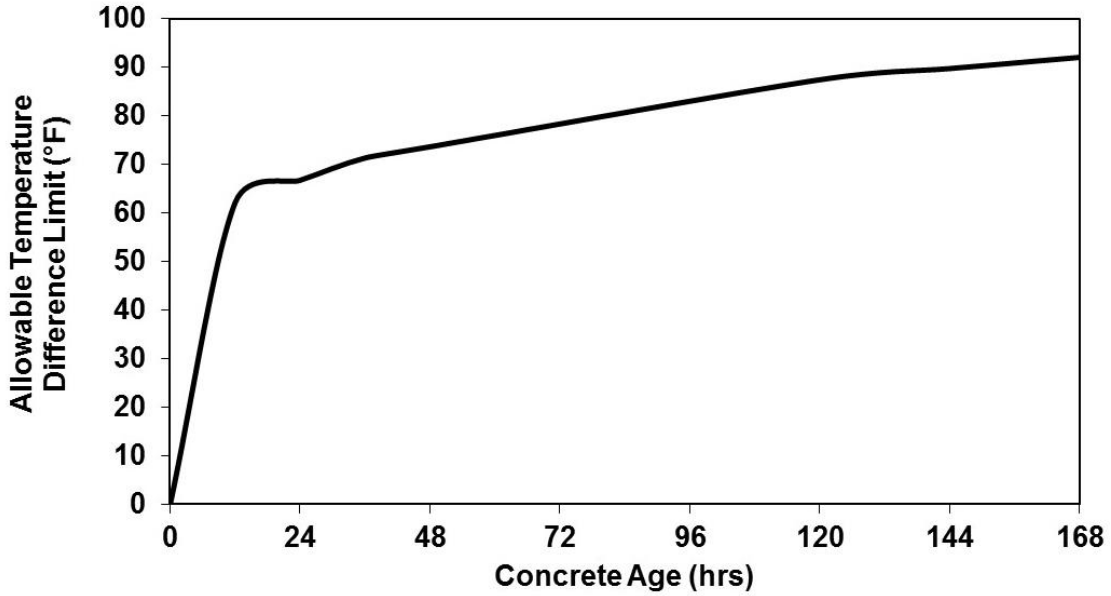

Figure 13-16: ALWC allowable temperature difference limits

The maximum temperature difference limits for concretes containing LWA can easily be obtained from any concrete values if the CTE and equilibrium density of the LWA concretes are known. The concrete CTE can be assessed by testing concrete samples with AASHTO T336 (2009). Similarly, the approximate equilibrium density of concrete can be obtained from Equation 13-18 (ASTM C567).

$$w_c = w_{oc} + 0.003 \qquad \text{(Equation 13-18)}$$

where,

w_c is the calculated equilibrium density (kcf), and

w_{oc} is the oven dry density (kcf).

The concrete CTE and equilibrium density is very dependent on the coarse and fine aggregate types (Mehta and Monteiro 2013). It is recommended to test the concrete CTE and evaluate the concrete equilibrium density prior to construction. However, if the CTE and equilibrium density values are not available, default values of concrete CTE and

equilibrium density based on the coarse aggregate or fine aggregate type may be used from research and published literature (Neville 2011; Schindler et al. 2010).

Examples of default values of concrete CTE and equilibrium density consisting of various aggregate (including lightweight aggregate) is provided in Table 13-8. A plot containing the allowable temperature limits for concretes with a specified compressive strength of 4,000 psi and containing various types of aggregates are shown in Figure 13-16.

Table 13-8: Default CTE and equilibrium density values for concretes made with various coarse and fine aggregate types

Type of Concrete	**Coarse Aggregate Type**	**Fine Aggregate Type**	**Concrete CTE (in./in./°F)**	**Equilibrium Density (pcf)**	**Reference**
Normalweight Concrete	Limestone	River Sand	3.4 to 4.1 × 10^{-6}	143	Neville and Brooks (1987)
ICC	River Gravel	River Sand/Fine Lightweight Aggregate (Clay)	5.8 × 10^{-6}	136	Byard and Schindler (2010)
SLWC	Slate	River Sand	5.6 × 10^{-6}	113	
SLWC	Shale	River Sand	5.1 × 10^{-6}	111	
SLWC	Clay	River Sand	5.2 × 10^{-6}	110	
ALWC	Slate	Slate	4.3 × 10^{-6}	95	
ALWC	Shale	Shale	4.1 × 10^{-6}	91	
ALWC	Clay	Clay	4.0 × 10^{-6}	87	

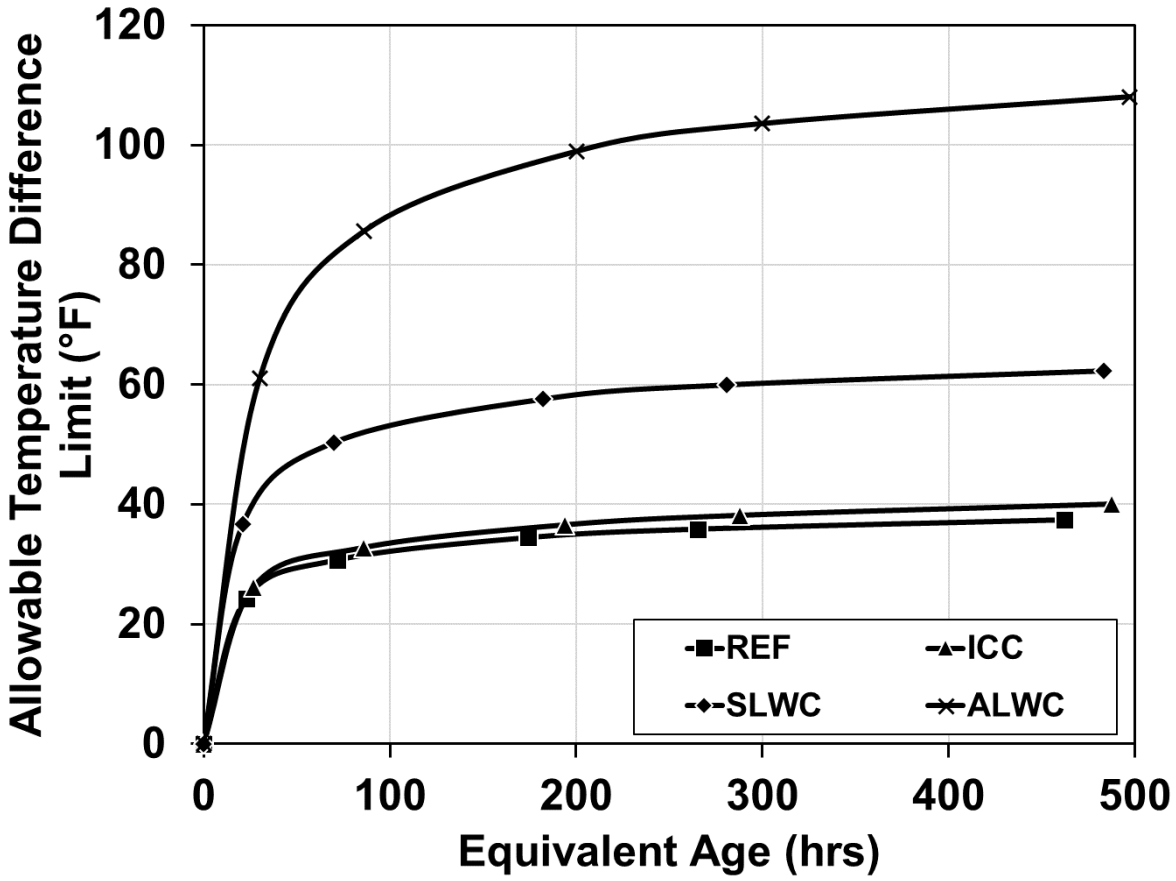

Figure 13-16: Allowable temperature difference limits for various types of concrete vs equivalent ages of concrete

It can be observed from Figure 13-16 that the allowable temperature difference limit changes according to the type of aggregate type, allowing a higher value for all-lightweight concretes when compared with river gravel concretes. The equivalent ages for each concrete was computed and the compressive strength was derived from the ACI expression. The splitting tensile strength and modulus of elasticity was derived from the compressive strength. Thus, Table 13-7 when used in conjunction with the modification

factors mentioned previously can be used to calculate the allowable temperature differences for all types of concretes if the CTE and equilibrium densities are known.

To account for all the conditions, a tiered temperature difference specification is proposed based on work by Gross (2017) and is shown in Table 13-9. The table would provide researchers and engineers a method to calculate the maximum concrete temperature differences when the concrete CTE is known or unknown. From Table 13-9 if the CTE and equilibrium density of the concrete is not known, then the allowable temperature difference limit for concretes is restricted to a conservative value of 35°F.

Table 13-9: Tiered maximum temperature difference limit for a mass concrete specification (Gross 2017)

Tier	Requirement	Specification
I	CTE of concrete is tested according to AASHTO T336, equilibrium density of concrete is tested according to ASTM C567	Use ***known*** CTE value and equilibrium density to calculate ***age-dependent ΔT limit*** in accordance with Table 13-7 and modified with Equation 13-13
II	Coarse aggregate/Fine aggregate of concrete is known, but concrete CTE and equilibrium density has not been tested	Use ***default*** CTE and equilibrium density value from published literature (Table 13-8) to calculate ***age-dependent ΔT limit*** in accordance with Table 13-7 and modified with Equation 13-13
III	Coarse/ Fine aggregate type of concrete is unknown	Use maximum ΔT limit of ***35 °F***

Chapter 14

PART II: SUMMARY, AND CONCLUSIONS

14.1 Summary of Work

In this study, two groups of concrete with *w/cm*: 0.45 and 0.38 were tested. Each group of concrete contained four different types of concrete namely, reference concrete, internally cured concrete (ICC), sand-lightweight concrete (SLWC), and all-lightweight concrete (ALWC). Three column cross-section sizes 4×4 ft, 8×8 ft, and 12 ×12 ft were chosen and a numerical investigation using ConcreteWorks software, supplemented with data from experimental work, was conducted to evaluate the maximum concrete temperatures, concrete temperature differences, early-age thermal stresses, and early-age concrete cracking risk. Each column size was analyzed for both groups of concretes. The mechanical properties of the concretes were evaluated at 0.5, 1, 2, 3, 7, and 28 days. The coefficient of thermal expansion was evaluated in accordance with AASHTO T336 (2009) for this study. Also, the semi-adiabatic calorimetry methods were employed to determine hydration and thermal properties of the concrete, such as the ultimate degree of hydration, thermal diffusivity etc. The concrete allowable temperature difference limit was calculated using a simplified model developed using time-dependent mechanical properties for both groups of concretes. A simplified model using the thermal cracking equation shown in Equation 9-1 was modified to produce an age-dependent allowable concrete temperature difference limit for reference concretes. Appropriate modification factors were used to adjust the age-dependent allowable temperature difference limit for concretes containing varying coarse or fine aggregate types. Finally, a set of guidelines, focusing on the allowable temperature limit for concretes containing LWA was presented.

14.2 Conclusions

- The maximum core concrete temperatures increased with an increasing proportion of LWA. For both groups of *w/cm* concretes, the maximum core temperatures was the highest for ALWC followed by, in order of decreasing temperatures, SLWC, ICC, and reference concretes. Also, the maximum core temperatures increased with an increase in cross-section size.
- The maximum edge temperatures were similar for all cross-section sizes. However, the maximum edge temperatures increased with an increasing proportion of LWA and with a decrease in *w/cm*.
- The maximum concrete temperature differences increased with an increase in cross section size. Also, the maximum temperature differences increased with a decreasing density of concrete, with ALWC having the highest temperature difference followed by the SLWC, ICC and reference concretes.
- Early-age concrete stresses increased with an increase in cross-section size. Also, early-age stresses were higher for 0.38 *w/cm* concretes when compared with the 0.45 *w/cm* concretes.
- Despite increased temperature differences observed in ALWC, the early-age concrete stresses were lower for ALWC, followed by the SLWC, ICC and reference concretes. Thus an increase in the proportion of LWA in the concrete mixture resulted in lower early-age concrete stresses.
- Concretes containing LWA had a lower cracking risk when compared with normalweight concretes. For both *w/cm* concretes, ALWC had the lowest cracking risk followed by SLWC, ICC and reference concretes.

- The concrete allowable temperature difference limit was calculated using a simplified model developed using time-dependent mechanical properties for normalweight concretes and those containing LWA and is provided in the form of in Table in 14-1. A tiered specification (see Table 13-10) which includes allowable temperature difference limits for reference concretes, can be used in conjunction with modification factors, to determine the allowable concrete temperature difference limits for concretes containing various coarse and fine lightweight/normalweight aggregates. A default table (see Table 13-7) is also provided which provides CTE and equilibrium density from known research and published literature. The simplified model derived with the help of Table 14-1 and the modification factors was considered to be conservative for all concretes in determining the allowable concrete temperature difference limits for concretes containing LWA.

Table 14-1: Allowable Maximum Temperature Differences for River Gravel Concrete

Concrete Age, *t* (hours)	**Maximum Allowable Temperature Difference, $\Delta T_{max}(t)$ (°F)**
12	27
24	29
36	31
48	32
60	33
72	33
84	34
96	34
108	35
120	35
132	36
144	36
156	36
168	37

CHAPTER 15

OVERALL DISSERTATION SUMMARY, CONCLUSIONS, AND RECOMMENDATIONS

15.1 Summary of Work

Early-age cracking of mass concrete has been acknowledged to be a severe problem that may reduce durability and service life of a structure. In this study, the early-age behavior of concrete incorporating lightweight aggregates was evaluated. This was done in two parts 1) assessing the early-age stress and mechanical property development, and 2) numerical investigation of the cracking risk using ConcreteWorks software and development of a simplified equation to determine the maximum temperature difference limit for concretes.

For part one of this study, normalweight concrete, internally cured concrete (ICC), sand-lightweight concrete (SLWC), inverse sand-lightweight concrete (ISLWC), and all-lightweight concrete (ALWC) were made in the laboratory and their early-age behavior was evaluated. Two different *w/cm*, 0.45 and 0.38 were used, for all the concretes, thus in total 10 concrete mixtures were tested. Internally cured concrete mixtures were similar to the normalweight concretes except that a small fraction of fine aggregates were replaced with normalweight aggregates. The amount of lightweight aggregate added to the ICC mixture was selected to obtain a concrete with an equilibrium density of 135 pcf, thereby categorizing the internally cured concrete as normalweight concrete, as per

AASHTO LRFD Bridge Design Specifications (2007). The thermal properties of each concrete was assessed using semi-adiabatic calorimetry. Following which, each concrete mixture was placed in the rigid cracking frame and free-shrinkage frame and cured with a unique temperature profile simulating fall placement conditions in the south eastern parts of the United States. In addition, for each concrete mixture, 24 cylinders were cast and tested for compressive strength, splitting tensile strength, and modulus of elasticity to assess the development of mechanical properties over time. The coefficient of thermal expansion was also evaluated with a test setup similar to that required by AASHTO T336 (2009).

For part two, a numerical investigation using ConcreteWorks was performed to evaluate the early-age concrete temperatures, temperature differences, stresses, and cracking risk. Two groups of concrete mixtures with *w/cm* = 0.45 and 0.38 with each group containing four types of concrete, reference concrete, internally cured concrete, sand-lightweight concrete, and all-lightweight concrete were used for the numerical simulation. Three different cross-section sizes of 4×4 ft, 8×8 ft, and 12×12 ft were chosen for conducting the numerical investigation. The compliance, creep factors and maximum temperature difference limits were computed for each concrete mixture. Finally, a simplified equation was provided to compute the maximum temperature difference limit for various types of concrete.

15.2 Conclusions

Part 1 of this study focused on the early-age stress development and cracking tendency of concrete containing lightweight aggregate in mass concrete applications. The research presented in part one supports the following conclusions:

- The compressive strength development for the reference, IC, and SLW concretes were similar. However, the compressive strengths of the ALW and ISLW concretes were approximately 10 to 15 % lower when compared to the reference concretes.

- The splitting tensile strength development for the reference, IC, and SLW concretes were similar. However, the splitting tensile strengths of the ISLW and ALW concretes were approximately 20 to 30 % lower when compared to the reference concretes.

- Increasing the amount of lightweight aggregate systematically decreased the concrete density, thereby also reducing the modulus of elasticity of concrete. When considering the with-in test variability, the modulus of elasticity development for the reference and IC concretes were similar. The modulus of elasticity values were lower on average by 12 %, 33 %, and 33 % for SLW, ISLW, and ALW concretes, respectively, when compared to the reference concretes.

- Increasing the amount of lightweight aggregate in concrete systematically decreased the concrete coefficient of thermal expansion (CTE). The average CTE values were reduced by 5 %, 10 %, 10 %, and 30 % for IC, ISLW, SLW, and ALW concretes, respectively when compared to the reference concretes.

- Concretes with increasing proportion of LWAs exhibit lower thermal diffusivity values, with an average thermal diffusivity reduction of 5 %, 10 %, 30 %, and 50 % for IC, ISLW, SLW, ALW concretes, respectively when compared to the reference concretes.

- The ACI 318 (2014) and AASHTO LRFD (2016) modulus of elasticity formulations provide accurate estimates for the reference, IC, and ISLW concretes tested in this project. However, both ACI 318 (2014) and AASHTO LRFD (2016) tend to underestimate the modulus of elasticity for the SLW and ALW concretes tested in this project.

- The ACI 207.2R (2007) and ACI 207.1R (2012) splitting tensile strength formulations provide reasonably accurate estimates for the reference and IC concretes tested in this project. However, both ACI 207.2R (2007) and ACI 207.1R (2012) tend to overestimate the splitting tensile strength for the ISLW, SLW, and ALW concretes tested in this project.

- The lightweight modification factor (λ-factor), calculated by using the equilibrium density as proposed by Green and Graybeal (2013), can be used to accurately estimate the splitting tensile strength of the SLW and ALW concretes tested in this project.

- Concretes containing an increased proportion of LWAs experienced higher concrete temperatures when compared to the reference concretes. ALW concrete had the highest maximum concrete temperature followed in order of decreasing maximum concrete temperature by the SLW, ISLW, IC, and reference concretes. This behavior is attributed to the lower thermal diffusivity and increased heat of hydration present in concretes containing LWAs. Care should be taken when using LWA concrete in mass concrete to make sure that the threshold for DEF to occur is not exceeded.

- As the *w/cm* of the concrete decreased, the peak concrete temperatures increased, which is due to the presence of more cementitious material in low *w/cm* concretes.

- The presence of LWA in concrete delayed the time to cracking, with SLW concrete providing the best overall resistance to early-age cracking. The time to cracking for all concretes containing pre-wetted lightweight aggregates was greater than the time to cracking of the normalweight concretes.

- For the concretes with *w/cm* = 0.38, the presence of pre-wetted lightweight aggregate eliminated autogenous shrinkage and its related stresses. The use of lightweight aggregates in concrete with low *w/cm* is beneficial to control early-age cracking, because it helps to mitigate autogenous shrinkage and lower the modulus of elasticity of the higher strength concrete.

- Although an increasing amount of LWA in the concrete will increase the maximum concrete temperature in mass concrete applications, the increasing use of LWA will reduce the modulus of elasticity, reduce the coefficient of thermal expansion, and eliminate autogenous shrinkage effects, which all contribute to improve the resistance to early-age cracking.

The focus of part two was to investigate the early-age concrete temperatures, temperature differences, stresses, and cracking risk of concretes containing lightweight aggregates and providing a simplified equation to compute the allowable temperature difference limits in concrete containing LWA. The research presented in part two supports the following conclusions:

- The maximum core concrete temperatures increased with an increasing proportion of LWA. For both groups of *w/cm* concretes, the maximum core temperatures was the highest for ALWC followed by, in order of decreasing temperatures, SLWC, ICC, and reference concretes. Also, the maximum core temperatures increased with an increase in cross-section size.
- The maximum edge temperatures were similar for all cross-section sizes. However, the maximum edge temperatures increased with an increasing proportion of LWA and with a decrease in *w/cm*.
- The maximum concrete temperature differences increased with an increase in cross section size. Also, the maximum temperature differences increased with a decreasing density of concrete, with ALWC having the highest temperature difference followed by the SLWC, ICC and reference concretes.
- Early-age concrete stresses increased with an increase in cross-section size. Also, early-age stresses were higher for 0.38 *w/cm* concretes when compared with the 0.45 *w/cm* concretes.
- Despite increased temperature differences observed in ALWC, the early-age concrete stresses were lower for ALWC, followed by the SLWC, ICC and reference concretes. Thus an increase in the proportion of LWA in the concrete mixture resulted in lower early-age concrete stresses.
- Concretes containing LWA had a lower cracking risk when compared with normalweight concretes. For both *w/cm* concretes, ALWC had the lowest cracking risk followed by SLWC, ICC and reference concretes.

- A simplified model using the thermal cracking equation, and modifying factors was developed to compute the allowable concrete temperature difference for normalweight concretes and those containing LWA and is provided as shown in Table 14-1. A tiered specification (see Table 13-10), which includes allowable temperature difference limits for reference concretes can be used in conjunction with modification factors, to determine the allowable concrete temperature difference limits for concretes containing various coarse and fine lightweight/normalweight aggregates. A default table (see Table 14-1) is also provided which provides CTE and equilibrium density from known research and published literature. The simplified model derived from of Table 14-1 and the modification factors was considered to be conservative for all concretes in determining the allowable concrete temperature difference limits for concretes containing LWA.

15.3 Recommendations for Future Research

The following recommendations are offered for future research:

1. The compressive strength, splitting tensile strength, and modulus of elasticity results of the ISLW concrete were lower in comparison to SLW concrete, despite their densities being reasonably similar. This may be related to the specific fine lightweight aggregates, particle packing, or the combined gradation of aggregates used in this project. However, since this result was unexpected, it is recommended to determine how to proportion ISLW and SLW concrete with the same *w/cm* to achieve similar mechanical properties.

2. Due to the resources available, the thermal properties of the lightweight aggregates were back calculated from semi-adiabatic calorimetry and were not directly measured. When modeling the temperature development in mass concrete elements, it is recommended that the thermal properties of the concrete be determined using standardized ASTM test methods.

3. The effect of lightweight aggregate on drying shrinkage was not evaluated in this study. Study of drying shrinkage will aid in the evaluation of long-term effects of lightweight aggregate on drying shrinkage.

4. The early-age and long-term performance of similar full-scale mass concrete elements constructed with normalweight and sand-lightweight concrete should be collected and compared.

5. The CTE and equilibrium density of certain coarse and fine lightweight aggregates are scarce in literature. Therefore if possible, an extensive database should be created which contains the CTE and equilibrium density of commonly used coarse and fine lightweight aggregates in concrete.

6. Autogenous shrinkage related stresses in concrete containing LWA is zero. However, ConcreteWorks does not model the effects of zero autogenous shrinkage stresses in concrete containing LWA. Thus if the autogenous stresses due to the inclusion of LWA can be quantified using appropriate modeling techniques it can result in more accurate predictions of concrete stresses and early-age concrete cracking risk.

REFERENCES

AASHTO 2016. *LRFD Bridge Design Specifications 7th Edition with 2016 interim revisions*. American Association of State Highway and Transportation Officials, Washington DC.

AASHTO T336. 2009. *Standard Method of Test for Coefficient of Thermal Expansion of Hydraulic Cement Concrete.* Washington D.C.: American Association of State Highway and Transportation Officials.

ACI 201. 2016. *Guide to Durable Concrete*. American Concrete Institute. Farmington Hills, MI.

ACI Committee 207.1R 2012. *Report on Guide to Mass Concrete*. American Concrete Institute, Farmington Hills, MI.

ACI Committee 207.2R 2007. *Report on Guide to Thermal and Volume Change Effects on Cracking of Mass Concrete*. American Concrete Institute, Farmington Hills, MI.

ACI 209. 2008. *Guide for Modeling and Calculating Shrinkage and Creep in Hardened Concrete*. American Concrete Institute. Farmington Hills, MI.

ACI Committee 213. 2013. *Guide for Structural Lightweight-Aggregate Concrete*. American Concrete Institute, Farmington Hills, MI.

ACI Committee 231. 2010. *Report on Early-Age Cracking: Causes, Measurement and Mitigation* American Concrete Institute, Farmington Hills, MI.

ACI Committee 301. 2016. *Specifications for Structural Concrete*. American Concrete Institute, Farmington Hills, MI.

ACI Committee 318. 2014. *Building Code Requirements for Structural Concrete and Commentary.* American Concrete Institute. Farmington Hills, MI.

ACI CT-16. 2016. *Concrete Terminology- An ACI Standard*. American Concrete Institute, Farmington Hills, MI.

Atrushi, D. 2003. *Tensile and Compressive Creep of Early Age Concrete: Testing and Modelling*. Doctoral Dissertation, NTNU Trondheim, Norway.

Ayyub, B.M. and R.H. McCuen. 2011. *Probability, Statistics, and Reliability for Engineers and Scientists*. CRC Press, 3rd Edition, Boca Rotan, FL.

Bamforth, P.B. 1981. *Large Pours*. Letters to the editor, Concrete, Concrete and Cement Association, London.

Bamforth, P.B., and W.F. Price. 1995. Concreting Deep Lifts and Large Volume Pours. Construction Industry Research and Information Association.

Bamforth, P.B. 2007. *Early-age thermal crack control in concrete*. Ciria.

Bažant, Z.P. 1982. *Mathematical Models for Creep and Shrinkage of Concrete Structures*. Creep and Shrinkage in Concrete Structures (ed. Bažant and Wittmann), John Wiley & Sons, New York, NY, pp. 163-256.

Bazant, Z.P. and S. Baweja. 2000. Creep and Shrinkage Prediction Model for Analysis and Design of Concrete Structures: Model B3. *Adam Neville Symposium: Creep and Shrinkage – Structural Design Effects*. American Concrete Institute. Farmington Hills, MI. 1-83.

Bentz, D.P., and W.J. Weiss. 2011. *Internal Curing: A 2010 State-of-the- Art Review*. Publication NISTIRR 7765. NIST, U.S. Department of Commerce.

Bentz, D.P., P. Lura, and J.W. Roberts. 2005. *Mixture proportioning for internal curing*. Concrete International, Vol. 27, No. 2, pp. 35-40.

Bjøntegaard, Ø. 1999. *Thermal Dilation and Autogenous Deformation as Driving Forces to Self-Induced Stresses in High Performance Concrete*. Doctoral Thesis. Norwegian University of Science and Technology, Division of Structural Engineering, Norway.

Bremner, T., and J. Ries. 2009. *Stephen J. Hayde: Father of the Lightweight Concrete Industry*. Concrete International, Vol.31, No.8, pp. 35-38.

Byard B.E., and A.K. Schindler. 2010. *Cracking Tendency of Lightweight Concrete*. Research Report Submitted to the Expanded Shale, Clay, and Slate Institute. Highway Research Centre, Auburn, AL

Byard B.E., A.K. Schindler, and R.W. Barnes. 2012. Early-age cracking tendency and ultimate degree of hydration of internally cured concrete. *ASCE Journal of Materials in Civil Engineering*, Vol. 24, No. 8, pp. 1025-1033.

Byard B.E. 2011. *Early-age Properties of Lightweight Aggregate Concrete*. Doctoral Dissertation. Auburn University, Auburn, AL.

Byard, B.E. and A.K. Schindler. 2015. Modeling early-age stress development of restrained concrete. *Materials and Structures* 48, no. 1-2: 435-450.

Carino, N.J. 1991. The Maturity Method. *Handbook on Non-Destructive Testing of Concrete* (Ed.by V.M. Malhotra and N.J. Carino), C.R.C. Press, Boca Rotan, FL, pp. 101-147

Castro, J., L. Keiser., M. Golias., and W. Weiss. 2011. Absorption and Desorption of Fine Lightweight Aggregate for Applications to Internally Cured Concrete Mixtures. *Cement and Concrete Composites*, Vol. 33, No. 10, pp. 1001-08.

Chandra, S., and L. Berntsson. 2002. *Lightweight Aggregate Concrete*. 1st Edition, William Andrew, NY.

Clarke, J.L. 1993. *Structural Lightweight Aggregate Concrete*. CRC Press, Boca Rotan, FL.

Concrete Durability Center. 2005. Concrete Works Version 2.0 User's Manual. Sponsored by Texas Department of Transportation: Project 0-4563.

Cusson, D., and T. Hoogeveen. 2007. An experimental approach for the analysis of early-age behaviour of high-performance concrete structures under restrained shrinkage. *Cement and Concrete Research*, Vol.37, No.2, pp. 200-209.

Delatte, N., D. Crowl., E. Mack., and J. Cleary. 2008. Evaluating High Absorptive Materials to Improve Internal Curing of Concrete. In ACI Special Publication 256, *Internal Curing of High-Performance Concretes*, (ed. D. Bentz and B. Mohr), Farmington Hills, MI.

Eiland, A. 2016. *Development of Specifications for ALDOT Mass Concrete Construction* Master's thesis. Auburn University. Auburn, AL.

Emborg, M.1989. *Thermal Stresses in Concrete at Early Ages*. Doctoral Dissertation. Luleå University of Technology, Luleå, Sweden.

Emborg, M., and S. Bernander. 1994. Thermal Stresses Computed by a Method for Manual Calculations. *In RILEM Proceedings 25, Thermal Cracking in Concrete at Early Age*, (ed.by R.Springenschmid) E&FN Spon, London, pp.321–328.

FitzGibbon, M.E.1976. *Large pours for reinforced concrete structures*. Concrete, Concrete and Cement Association, Vol 10, No. 3, pp. 41, London.

Folliard, K.J., R. Barborak., T. Drimalas., L. Du., S. Garber., J. Ideker., T. Ley., S. Williams., M.G. Juenger., B. Fournier., and M.D.A. Thomas. 2006. *Preventing ASR/DEF in New Concrete: Final Report.* Center for Transportation Research, University of Texas at Austin.

Freieslben Hansen, P., and E. J. Pederson.1977. *Maturity Computer for Controlling Curing and Hardening of Concrete.* Nordisk Betong, V.1, No.19, pp. 21-25.

Gajda, J. 2007. *Mass Concrete for Buildings and Bridges*. Portland Cement Association, Skokie, IL.

Gajda, J. and M. Vangeem. 2002. Controlling Temperatures in Mass Concrete. Concrete International: 59-62.

Greene, G., and B.A. Graybeal. 2013. Synthesis and Evaluation of Lightweight Concrete Research Relevant to the AASHTO LRFD Bridge Design Specifications: Potential Revisions for Definition and Mechanical Properties. *Publication FHWA –HRT-13-030*. FHWA, U.S Department of Transportation.

Gross, E.2017. *Development of a Mass Concrete Specification for Use in ALDOT Bridge Construction.* Master's thesis. Auburn University. Auburn, AL.

Hedlund, H. 2000. *Hardening Concrete Modelling of Non Elastic Deformations and Related Properties*. Doctoral Dissertation, LULEÅ University of Technology, Sweden, 2000.

Henkensiefken, R., D.P. Bentz., T. Nantung., and W.J. Weiss. 2009. Volume Change and Cracking in Internally Cured Mixtures Made with Saturated Lightweight

Aggregates under Sealed and Unsealed Conditions. *Cement and Concrete Composites*, Vol.31, No.7, pp. 426-437

Henkensiefken, R., T. Nantung., and W.J. Weiss. 2011. Saturated Lightweight Aggregate for Internal Curing in Low w/c Mixtures: Monitoring Water Movement Using X-ray Absorption. *Strain*, Vol 47, Issue 1, pp.1-10.

Holm, T.A. and J. Ries. 2007. *ESCSI's Reference Manual for the Properties and Applications of Expanded Shale, Clay and Slate Lightweight Aggregate.* ESCSI.

Holt, E. *Early Age Autogenous Shrinkage of Concrete*. 2001. Doctoral Thesis. The University of Washington in Seattle.

Jahren, T. C., J. L. Li., J. J Shaw, and K. Wang. 2014. *Iowa Mass Concrete for Bridge Foundations Study – Phase II.* Publication Iowa DOT In-Trans Project 10-384. Institute for Transportation, Ames, IA.

Kim, S.G. 2010. *Effect of Heat Generation from Cement Hydration on Mass Concrete Placement*. Master's Thesis, Iowa State University, Ames, Iowa.

Klieger, P. 1957. Early High Strength Concrete for Prestressing. *Proceedings World Conference on Prestressed Concrete*, San Francisco, pp. A5-1 to A5-14.

Larson, M. 2003. *Thermal crack estimation in early age concrete: models and methods for practical application*. Doctoral Dissertation, LULEÅ University of Technology, Sweden.

Livingston, R.A., C. Ormsby., A.M. Made., M.S. Ceary., N. McMorris., and P.G. Finnerty. 2006. *Field Survey of Delayed Ettringite Formation-Related Damage in Concrete Bridges in the State of Maryland*. American Concrete Journal, Special Publication 234, pp. 251-268.

Lura, P., O.M. Jensen., and K. Breugel.2003.Autogenous shrinkage in high-performance cement paste: an evaluation of basic mechanisms. *Cement and Concrete Research*, Vol. 33, Issue 2, pp. 223-32.

Maggenti, R. 2007.From Passive to Active Thermal Control. *Concrete International*, V.29, No.11, pp. 24-30.

Mangold, M. 1998. Methods for Experimental Determination of Thermal Stresses and Crack Sensitivity in the Laboratory. In RILEM Report 15, *Prevention of Thermal Cracking in Concrete at Early Ages* (ed. R. Springenschmidt), London, E & FN Spon, pp. 26-40.

Meadows, J.L. 2007. *Early-Age Cracking of Mass Concrete Structures*. Master of Science Thesis, Auburn University.

Mehta, P. K., and P.J.M. Monteiro. 2013. *Concrete: Microstructure, Properties and Materials*. Mc Graw Hill, Inc., NY.

Mindess, S., J.F. Young, and D. Darwin. 2002. *Concrete*. 2nd Edition, Prentice Hall, Saddle River, NJ.

Morabito, P. 1998. Methods to Determine the Heat of Hydration of Concrete. In RILEM Report 15, *Prevention of Thermal Cracking in Concrete at Early ages*, (ed. R. Springenschmidt) E&FN Spon, London, pp. 1-25.

Neville, A.M. 2011. *Properties of Concrete*. Pearson Education, Inc., NJ.

Neville, A.M., and J.J. Brooks. 1987. *Concrete Technology*. Essex, UK: Longman Scientific and Technical.

Poole, J.L, K.A. Riding, R.A. Browne, and A.K. Schindler.2006. Temperature Management of Mass Concrete Structures. *Concrete Construction Magazine*.

Rao, A. 2008. *Evaluation of Early-Age Cracking Sensitivity in Bridge Deck Concrete*. Master of Science Thesis, Auburn University, AL.

Raoufi, K. 2011. *Restrained Shrinkage Cracking of Concrete: The Influence of Damage Localization*. Doctoral Dissertation, Purdue University, IN.

Raphael, J.M. 1984. *Tensile Strength of Mass Concrete*. American Concrete Institute Vol. 81, No. 17, pp. 158-165.

Riding, K.A. 2007. *Early Age Concrete Thermal Stress Measurement and Modeling*. Doctoral Dissertation. University of Texas, Austin, TX.

Riding, K., J. Poole, A.K. Schindler, M.G. Juenger, and K.J. Folliard 2014. Statistical Determination of Cracking Probability for Mass Concrete. *ASCE Journal of Materials in Civil Engineering*, Vol. 26, No. 9.

Riding, K., A.K. Schindler, P. Pesek, T. Drimalas, and K.J. Folliard 2017. *Concreteworks V3 Training/User Manual.* Centre for Transportation Research. Austin, TX.

RILEM Technical Committee 119-TCE. 1998. Testing of the Cracking Tendency of Concrete at Early Ages in the Cracking Frame Test. *In RILEM Report 15, Prevention of Thermal Cracking in Concrete at Early Ages*, ed. R. Springenschmid, London, E & FN Spon, pp. 315-339.

RILEM Technical Committee 196-ICC. 2007. Mechanisms of Internal Water Curing. *In RILEM Report 41*. *Internal Curing of Concrete* (Ed. by Kovler and Jensen). RILEM publications, Bagneux, France.

Robertson, E.C. 1988. *Thermal Properties of Rocks*. USGS Open File Report 88-441. United States Geological Survey, Reston, VA. 106 p.

Rostasy, F.E., T. Tanabe., and M. Laube. 1998. *Assessment of External Restraint*. In RILEM Report 15, *Prevention of Thermal Cracking in Concrete at Early ages*, (Ed. By R. Springinschmidt) E&FN Spon, London, pp. 149-168.

Schindler, A.K., and B.F. McCullough. 2002. The Importance of Concrete Temperature Control during Concrete Pavement Construction in Hot Weather Conditions. *Journal of the Transportation Research Board*, No. 1813, Washington, D.C., pp 3-10.

Schindler, A.K., and K.J. Folliard. 2005. Heat of Hydration Models for Cementitious Materials. *ACI Materials Journal*, Vol. 102, No. 1, pp. 24-33.

Schindler, A.K., M.L. Hughes, R.W. Barnes, and B.E. Byard. 2010. Evaluation of cracking of the US 331 bridge deck. Sponsored by Alabama DOT: Project 930-645.

Shilstone, J.M. and J.M. Shilstone, Jr. 1989. *Concrete Mixtures and Construction Needs*. Concrete International Vol. 11, No. 12, pp. 53-57.

Shilstone Sr., J.M. 1990. Concrete Mixture Optimization. *Concrete International*, Vol. 12, No. 6, pp 33-39.

Springenschmidt, R., R. Breitenbucher., and M. Mangold. 1994. Development of the Cracking Frame and Temperature-Stress Testing Machine. In RILEM Proceedings 25, *Thermal Cracking in Concrete at Early Ages*, (ed. R. Springenschmidt), London, E & FN Spon, pp. 137-45.

Sylla, H.M. 1988. Reactions in Hardened Cement Paste Caused by Heat Treatment, *Beton*, Vol. 38, pp. 488–493

Tankasala, A., A.K. Schindler, K.A. Riding. 2017. Thermal Cracking Risk of Using Lightweight Aggregate in Mass Concrete. *Journal of the Transportation Research Board*, TRR No. 2629.

Taylor, H. F.W., C. Famy, and K. L. Scrivener. 2001. Delayed Ettringite Formation. *Journal of Cement and Concrete Research*, Vol. 31, Issue 5, pp. 683-693.

Tazawa, E. 1998. Autogenous Shrinkage and Its mechanism. *Autogenous Shrinkage of Concrete* (ed. E. Tazawa), E&FN Spon, London.

Thomas, M.D.A., K. Folliard, T. Drimalas, and T. Ramlochan. *2008.* Diagnosing Delayed Ettringite Formation in Concrete Structures. *Cement and Concrete Research*, Vol. 38, No. 6, pp. 841-847.

Umehara, H., T. Uehara., T. Hsaka., and A. Sugiyama. 1994. Effect of Creep in Concrete at Early Ages on Thermal Stress. *In RILEM Proceedings 25, Thermal Cracking in Concrete at Early Ages*, (Ed. By R. Springinschmidt), E&FN Spon, London, pp. 79-87.

Weakley, R.W. 2009. *Evaluation of Semi-Adiabatic Calorimetry to Quantify Concrete Setting*. Master of Science Thesis, Auburn University, AL.

Westman, G. 1999. *Concrete Creep and Thermal Stresses*. Doctoral Dissertation. Luleå University of Technology, Luleå, Sweden.

Xu, Y., and D.D.L. Chung. 2000. Cement of High Specific Heat and High Thermal Conductivity, Obtained by Using Silane and Silica Fume as Admixtures. *Cement and Concrete Research*. Vol. 30, Issue 7, pp. 1175-1178.

Appendix A

Aggregate Gradations

Table A-1: Coarse aggregate gradation

Sieve Size	Percent Passing	
	Normalweight Coarse Aggregate Auburn, AL	Lightweight Coarse Aggregate Norlite, NY
1 in.	100.0	100.0
¾ in.	95.2	97.0
½ in.	64.3	65.4
3/8 in.	39.2	22.4
# 4	1.2	2.9
# 8	0.1	0.4
# 16	0.0	0.0

Table A-2: Fine aggregate gradation

Sieve Size	Percent Passing	
	Normalweight Fine Aggregate, Auburn, AL	Lightweight Fine aggregate, Norlite, NY
½ in.	100.0	–
3/8 in.	100.0	100.0
# 4	99.7	100.0
# 8	90.7	98.8
# 16	69.4	59.5
# 30	32.8	38.3
# 50	5.9	15.6
# 100	1.5	0.3
Pan	0.0	0.0

Appendix B

Table B1: Input Variables for all 0.45 *w/cm* concretes

Group	Input		Units	NWC	IC NWC	SLWC	ALWC
Material properties	Cement Type		-	Type I/II	Type I/II	Type I/II	Type I/II
	Blaine		kg/m^2	351	351	351	351
	Bogue values		%	Producer	Producer	Producer	Producer
	Hydration Inputs	*Beta*	-	1.308	1.255	0.803	0.657
		Tau	hours	8.82	8.28	15.718	16.96
		H_u	J/kg	351782	348135	348135	346406
		$\alpha_{ultimate}$	-	0.840	0.847	0.95	0.95
		Activation Energy, E_a	J/mol	34440	34440	34440	34440
	Coefficient of Thermal Expansion		in./in./˚F	5.8	5.7	5.1	4.1
	Concrete Thermal Conductivity		BTU-ft/hr/ft^2/˚F	1.73	1.65	1.37	1.09
	Specific heat Capacity of Aggregate		BTU/lb-F	0.18	0.18	0.17	0.16
Mechanical properties	Maturity Method		-	Equivalent Age	Equivalent Age	Equivalent Age	Equivalent Age
	E_a		J/mol	34440	34440	34440	34440
	Comp. strength	f_{cult}	psi	6500	8500	5770	5000
		β_s	-	77.0	175	64	89
		τ_s	Hours	0.36	0.36	0.57	0.65

Note: All undefined ConcreteWorks input values are default values.

Table B2: Input Variables for all 0.38 *w/cm* concretes

Group	Input		Units	NWC	IC NWC	SLWC	ALWC
Material properties	Cement Type		-	Type I/II	Type I/II	Type I/II	Type I/II
	Blaine		kg/m^2	351	351	351	351
	Bogue values		%	Producer	Producer	Producer	Producer
	Hydration Inputs	*Beta*	-	1.349	0.989	0.937	0.960
		Tau	hours	9.209	10.851	11.641	13.834
		H_u	J/kg	351780	351780	351780	351780
		$\alpha_{ultimate}$	-	0.881	0.887	0.92	0.92
		Activation Energy, E_a	J/mol	34440	34440	34440	34440
	Coefficient of Thermal Expansion		in./in./˚F	6.1	5.9	5.1	4.1
	Concrete Thermal Conductivity		BTU-ft/hr/ft^2/˚F	1.73	1.65	1.37	1.09
	Specific heat Capacity of Aggregate		BTU/lb-F	0.18	0.18	0.16	0.16
Mechanical properties	Maturity Method		-	Equivalent Age	Equivalent Age	Equivalent Age	Equivalent Age
	E_a		J/mol	36450	36450	36450	36450
	Comp. strength	f_{cult}	psi	8370	7420	7027	5670
		β_s	-	76	50	57	92
		τ_s	Hours	0.42	0.60	0.60	0.62

Note: All undefined ConcreteWorks input values are default values.

Appendix C

Mechanical Property Results

Table C-1: Match-cured compressive strength results for all concretes

Concrete	Compressive strength (psi)					
	½ day	1 day	2 days	3 days	7 days	28 days
REF 0.45	1150	2340	3090	3800	4270	4710
REF 0.38	1765	3070	4410	4830	5400	5970
ICC 0.45	1180	2320	3120	3870	4330	4900
ICC 0.38	2120	3460	5140	5470	5870	6180
ISLWC 0.45	1090	1510	2710	3730	3970	4160
ISLWC 0.38	1000	1760	3790	4620	4920	5200
SLWC 0.45	910	2120	3370	3770	4310	4640
SLWC 0.38	1670	2560	3710	4710	5210	5850
ALWC 0.45	810	1560	2820	3320	3720	3980
ALWC 0.38	960	1670	2980	3780	4100	4370

Table C-2: Match-cured splitting tensile strength results for all concretes

Concrete	Splitting Tensile Strength (psi)					
	½ day	1 day	2 days	3 days	7 days	28 days
REF 0.45	160	260	350	390	350	430
REF 0.38	230	340	390	400	460	510
ICC 0.45	160	240	310	360	460	470
ICC 0.38	220	310	360	380	480	530
ISLWC 0.45	130	140	220	280	300	330
ISLWC 0.38	120	210	240	320	340	340
SLWC 0.45	160	280	270	360	370	460
SLWC 0.38	160	230	340	340	430	480
AWC 0.45	140	190	240	250	280	360
AWC 0.38	160	230	230	260	310	380

Table C-3: Match-cured modulus of elasticity results for all concretes

Concrete	Modulus of Elasticity (ksi)					
	½ day	1 day	2 days	3 days	7 days	28 days
REF 0.45	2200	3300	3450	3900	4000	4050
REF 0.38	2600	3450	4150	4350	4500	4550
ICC 0.45	2050	2950	3300	3700	4100	3950
ICC 0.38	2250	3300	4050	4350	4400	4500
ISLWC 0.45	1450	1900	2450	2400	2550	2750
ISLWC 0.38	1600	1850	2400	2800	2950	2950
SLWC 0.45	1650	2450	2700	2850	3450	3550
SLWC 0.38	1650	2400	3050	3300	3650	4000
AWC 0.45	1400	1700	2400	2350	2500	2650
AWC 0.38	1300	1750	2900	2450	3100	2950